AN INVESTIGATION INTO ION PLATING MECHANISMS AND PARAMETERS

by

Bogdan Lucian Delcea

Dipl. Eng. (Bucharest Polytechnic Institute - Romania)

A thesis submitted to the University of Salford

for the degree of Doctor of Philosophy

Department of Aero & Mechanical Engineering

1978

P R E F A C E

The work described in this thesis was carried out in the Department of Mechnical Engineering at the University of Salford between April 1975 and December 1977.

The author wishes to declare that the contents of this thesis are his own work, no part of which has been submitted to any other University or Institution for any degree or qualification.

ACKNOWLEDGEMENTS

The author is deeply indebted to Mr. D. G. Teer for his competent supervision throughout this project.

He is also indebted to Joseph Lucas Ltd. for financially supporting this entire work.

The author's appreciation and thanks are also expressed to Mr. A.J.Kirkham for technical advice and very helpful discussions.

He is also indebted to Mr. J.France and Mr. H. Pendlebury for their constant help.

The author wishes to thank Dr. J.M.Walls from Loughborough University for carrying out the Auger Spectroscopy tests.

He wishes to express his thanks to his wife, Nona, for constant moral support and for typing this thesis.

I N D E X

List of symbols

A_{ef} = activation efficiency

d = interplanar spacing

d_f = film thickness

D_R = deposition rate

$\bar{e}$ = electron charge

e = lattice internal strain

E = energy of a particle

E_i = ion energy

E_n = neutral energy

G^o = gas atom

G^* = gas metastable

G^+ = gas positive ion

I = current intensity

I_c = cathodic current

I_e = electronic current

I_i = ionic current

I_{ef} = ionization efficiency

k = cathode dark space / mean free path ratio

ℓ = mean free path

L = cathode dark space length

$L_{hk\ell}$ = crystallite size

$M_{1,2}$ = mass of the particle

M^o = metal atom

M^+ = metal positive ion

Ne = number of electrons

Ni = number of ions

Nn = number of neutrals

$N\bar{n}\bar{e}$ = number of energetic neutrals

Nno = number of nonenergetic neutrals

N_{np} = number of particles impinging 1 cm^2 of surface in a second for the pressure 'p'

p = gas pressure

R.F. = radio frequency

Sc = cathode surface area

S_{pR} = sputtering rate

T = temperature

V = voltage

Vc = cathode voltage

W = power

θ = x - rays diffraction angle

λ = molecular free path; wave length of the x - rays

ψ = deposition rate / sputtering rate ratio.

MISSING

PAGES

NOT

AVAILABLE

S y n o p s i s

Ion plating is a fairly new and modern technique for obtaining very adhesive films on any kind of surface and substrate material. The development of electron gun evaporation sources created the possibility to deposit, with high rates, materials having high melting points like : Molybdenum, Tungsten and even Carbon.

A part of this work attempts to establish the kind of particles which are involved in ion plating, especially the energetic neutrals that have been considered not to play a major role in the coating process.
For this purpose, the ions are separated from the neutrals and their energy spectrums determined using theoretical and experimental methods. The influence of process parameters upon the energies of the ions and neutrals is also studied.

Another part of this work is a parametric study of the nucleation of ion plated thin films as compared to the straight vacuum evaporated ones. The film-substrate interface of ion plated films is also analysed and measured attempting to clarify the processes that lead to the formation of a deep graded interface.

Finally, a parametric study is carried out with the aim of producing improved film structures in a controlled manner by varying the main process parameters such as : pressure, bias voltage and ion current. The substrate temperature is also considered.
A physical model for removing the columnar structure is produced and reported.

C H A P T E R I

INTRODUCTION

The most evident change of a solid surface is achieved by coating it with another material.

The deposition method is important in determining the final properties of the coated surface. At the moment, three physical vapour deposition techniques are available:

- vacuum deposition (high or low vacuum)
- sputter deposition
- ion plating

Some other alternative deposition techniques have been developed more recently like: Ionized Cluster Beam Technology[1], Magnetron Sputtering[54], Activated Vacuum Deposition[55] etc, which are basically one of the methods mentioned above, but some facilities have been incorporated to control ionization, substrate temperature, or deposition rate.

The energy of a vacuum evaporated atom is given by:

$$E = \frac{KT}{e} \simeq 0.2 \text{ eV} \qquad (1.1)$$

for $T=2900^{o}K$

The energies of sputtered atoms are reported[2] to be 20-100 eV but our own work on the energy of the bombarding species tends to indicate that the energies of sputtered atoms are probably lower than previously thought.

For Ion Plating, the energy of the ions has been reported[2,4] to be equal to the acceleration energy, i.e.3000 eV for a - 3 kV bias voltage, and thus was explained the very good adhesion of ion plated films. However, more recent experiments proved[20] that the ionization efficiency is very low, and even lower in the case of metal atoms injected into the plasma discharge.

Experiments in this work proved that the ionization efficiency is well below 1% and that the average energy of the ions is much lower than the acceleration energy.

Even in these conditions, the ion plating depositing particles are more energetic than in any other technique.

Ions and neutrals can have full energy of the discharge, though their average energy is lower than was previously thought.

The energy domains where the three vapour deposition methods take place are represented in Figure 1.2.

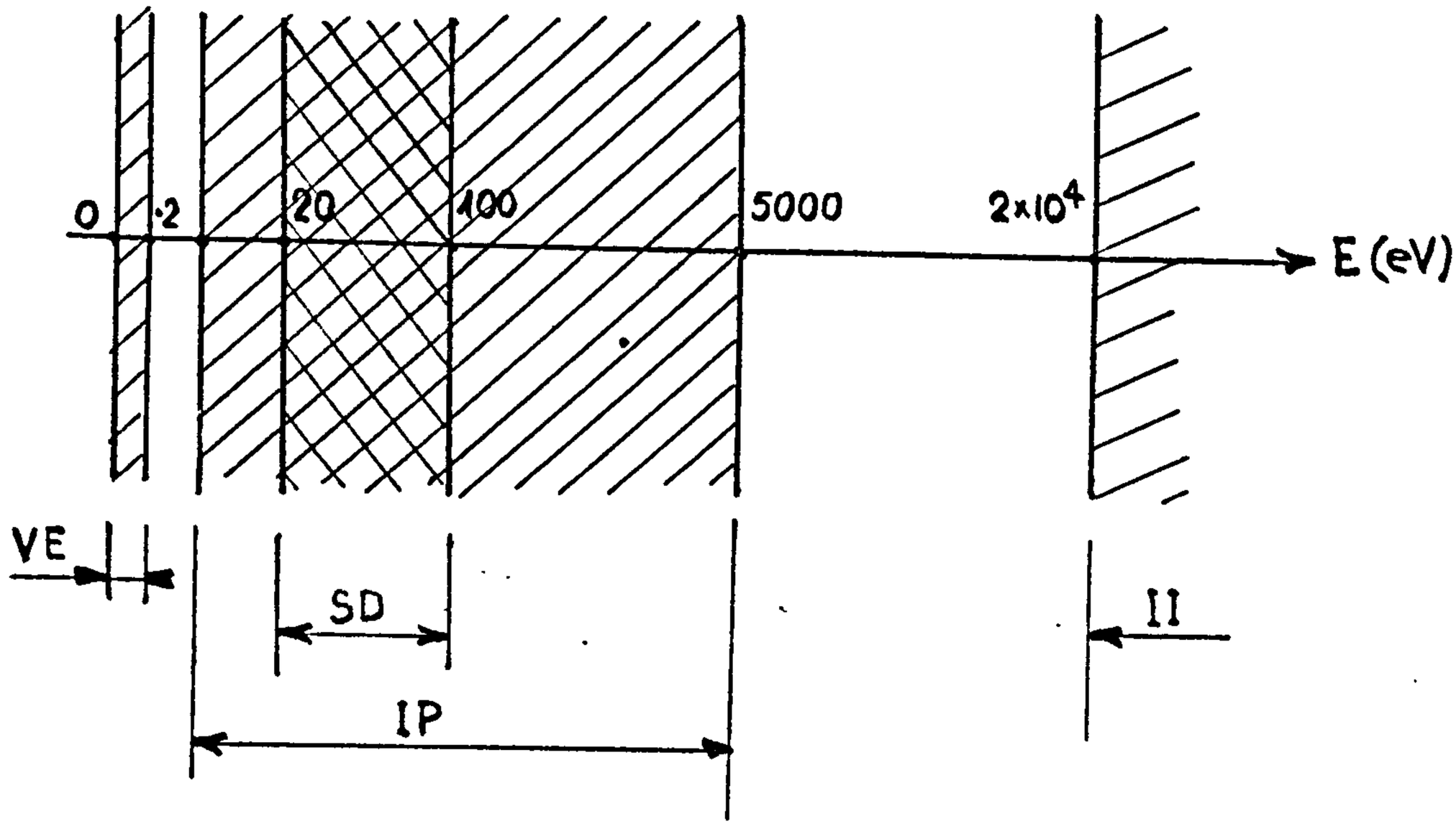

Figure 1.2.

where:

VE = Vacuum Evaporation

SD = Sputter Deposition

IP = Ion Plating

II = Ion Implantation

What makes ion plating a very desirable coating method is the achievement of a very good adhesion for any kind of film-substrate combination, and also, due to the reactive ion plating, the production of complex films like carbides, or nitrides. It has also been proved that by altering the process parameters, the structure and the physical properties of the resulting films can be changed.[51] Therefore, a parametric study of the ion plating process is necessary in order to produce reproducible and improved coatings.

Of a great importance for the adhesion of a thin film is the interface which is formed in the very early stages of nucleation and growth, since a porous interface will be weak, leading to stress concentration and therefore poor strength[3].

The types of interface have been clasified by Mattox[4] in: mechanical, monolayer to monolayer, compound, diffusion and pseudodiffusion.

Pseudodiffusion is a term which has been accepted[8] to characterize the kind of interface obtained in ion plating, which is responsible for the good adhesion of even incompatible film-substrate materials.

The early nucleation and growth must also influence the resulting morphology of the thin film.

Throwing power is a term describing the capacity to coat out of sight parts of the substrate and the influence of parameters upon it is also studied in this work.

C H A P T E R 2

ION PLATING MECHANISMS

2.1. Introduction

As shown in the previous chapter, three physical vapour deposition methods are available and to this number, electroplating could be added, which is the oldest technique and is a wet electro-chemical deposition method. A comparison of the four methods is presented in Table 2.1.1.[5] and it shows the net superiority of Ion Plating as regards the large area where it can be used, as well as the obtaining of improved film properties.

Ion Plating was defined as a plasma deposition of high energy ions.[8] The basic ion plating arrangement is a diode system with the anode, earthed and the high voltage cathode as the substrate to be coated. An argon pressure of 10-50 mTorr is set in the chamber in order to establish the glow discharge. Other gases can be used, mainly in the case of reactive ion plating when the metal vapours react with the gas to deposit as a complex compound.

The Ion Plating process is composed of two stages:

CHARACTERISTICS	ELECTROLITICAL DEPOSITION	VACUUM EVAPORATION	SPUTTER DEPOSITION	ION PLATING
FILM MATERIAL	Metals	Metals; some chemical compounds.	Metals; alloys; compounds; ceramics; polymers.	metals, alloys, chemical compounds
NATURE OF THE PROCESS	electrochemical	vacuum evaporotion and condensation (high or low vac.)	sputtering at low pressure	high energy deposition from vapour phase at low pressure
FILM QUALITY	can contain pores, voids etc.	on uniform, columnar.	dense, less porous, columnar	dense, much less porous, without voids, columnar structure removable
ADHESION	good	poor	good	excelent
KIND OF INTERFACE	contact	contact or diffusion if the substrate is heated	contact	'pseudodiffusion'
FILM UNIFORMITY	relatively uniform	not uniform	good	better
DEPOSITION RATE	moderate	high or very high with the use of electron guns	relatively low	high or very high with the use of electron guns
FILM PURITY	contains salts, gazeous inclusions	purity of the evaporant (depending on the vacuum purity)	the same	the same
FILM THICKNESS CONTROL	good	acceptable (parameters control required)	the same	the same
SUBSTRATE DIMENSIONS	limited by the dimensions of the electrolitic bath and the power supply	limited by the dimensions of the vacuum chamber	the same	the same
SUBSTRATE GEOMETRY	complex surfaces are coated non uniform	only the parts seing the source are coated	relatively uniform coating	the same
EQUIPMENT	chemical bath, power supply, control system	vacuum chamber, evaporation system	vacuum chamber, H.T. power supply (D.C. or R.F.)	vacuum chamber, H.T. power supply (D.C. or R.F.); evaporation system.

TABLE 2.1.1

a. The sputter cleaning of the substrate by ion bombardment and, as demonstrated later in this work, by energetic neutrals bombardment, a process which is continued during the second stage.

b. Deposition

During the first stage, a very clean, oxide free surface is achieved and at the same time, a highly deffective lattice is produced and this process is often referred to as "ion etching"[8]. During the ion and neutral bombardment, secondary electrons are emitted by the substrate. In the beginning, when the surface is covered with a layer of oxides, a high electronic current is drawn which adds to the ion current to give the total cathodic current. As these oxides are being removed, the secondary electronic current drops to a steady value, resulting in a steady cathodic current, moment when the sputter cleaning step is considered to be completed. The cathode voltage is usually 3-5 kV.

During the second stage which is the deposition itself, metal vapours are injected into the plasma and will deposit on the substrate as ions and high or low-energy neutrals.

All this time, the glow discharge is maintained in order to maintain a very clean surface and to remove the non-adhesive deposited particles.

A very important moment is when the interface is formed, at the very beginning of evaporation, which will affect the whole further deposited films properties (adhesion, structure, etc). At the same time, the de-

a. The sputter cleaning of the substrate by ion bombardment and, as demonstrated later in this work, by energetic neutrals bombardment, a process which is continued during the second stage.

b. Deposition

During the first stage, a very clean, oxide free surface is achieved and at the same time, a highly deffective lattice is produced and this process is often referred to as "ion etching"[8]. During the ion and neutral bombardment, secondary electrons are emitted by the substrate. In the beginning, when the surface is covered with a layer of oxides, a high electronic current is drawn which adds to the ion current to give the total cathodic current. As these oxides are being removed, the secondary electronic current drops to a steady value, resulting in a steady cathodic current, moment when the sputter cleaning step is considered to be completed. The cathode voltage is usually 3-5 kV.

During the second stage which is the deposition itself, metal vapours are injected into the plasma and will deposit on the substrate as ions and high or low-energy neutrals.

All this time, the glow discharge is maintained in order to maintain a very clean surface and to remove the non-adhesive deposited particles.

A very important moment is when the interface is formed, at the very beginning of evaporation, which will affect the whole further deposited films properties (adhesion, structure, etc). At the same time, the de-

position rate must exceed the sputtering rate in order to allow the film to grow.

2.2. Ion Plating Rig

The schematic diagram of an ion plating rig is presented in Figure 2.2.1., and Figure 2.2.2. presents an electron beam ion plating unit built at Salford University.

The basic ion plating procedure is similar for both systems.

The substrate to be coated represents the H.T. cathode and is water cooled. An earth shield is hung arround the cathode so that the discharge is confined to the substrate only, and a certain distance is required in order to avoid the masking effect on the back surface[6].

The vacuum system for both rigs is composed of a rotary pump and an oil diffusion pump with a liquid nitrogen cooled baffle valve.

For the rig presented in Figure 2.2.1., the evaporation source is a Molybdenum boat or a Tungsten filament. In this case, four boats or filaments can be mounted in the same time, in order to produce thicker films.

For the rig presented in Figure 2.2.1., a 15 kW electron gun is used to produce the evaporation. The gun is mounted in a collar, separated from the main

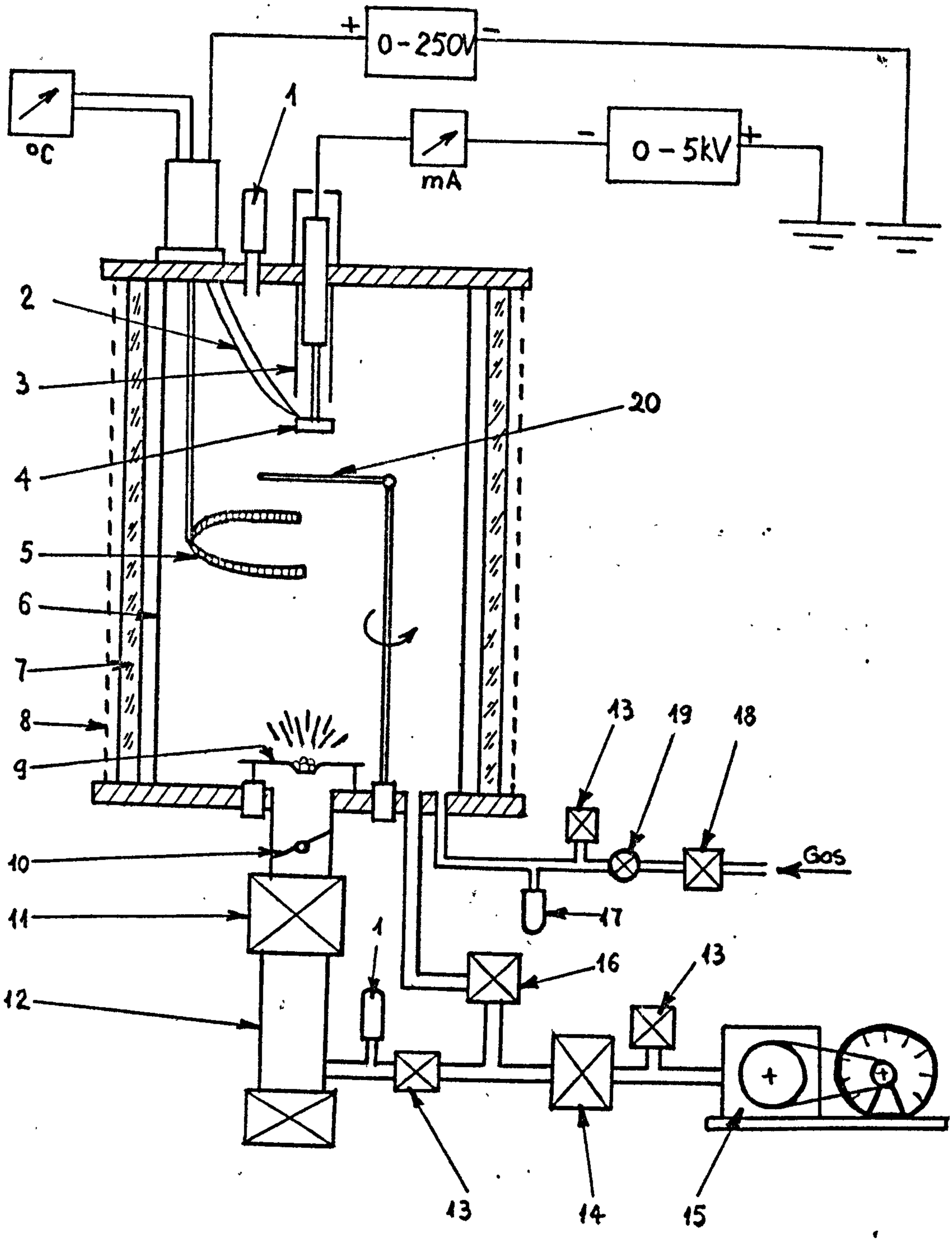

Figure 2.2.1a

ION PLATING ARRANGEMENT

Figure 2.2.1.a

Index

1. Pirane gauge
2. Thermocouple
3. Earthed shield
4. Substrate - cathode
5. Positive probe
6. Metal shield
7. Glass chamber
8. Protective shield
9. Evaporation Molybdenum boat
10. Baffle valve
11. Liquid Nitrogen trap
12. Oil diffusion pump
13. Magnetic valve
14. Foreline trap
15. Rotary pump
16. Magnetic valve
17. Penning gauge
18. Magnetic valve
19. Needle valve
20. Shutter

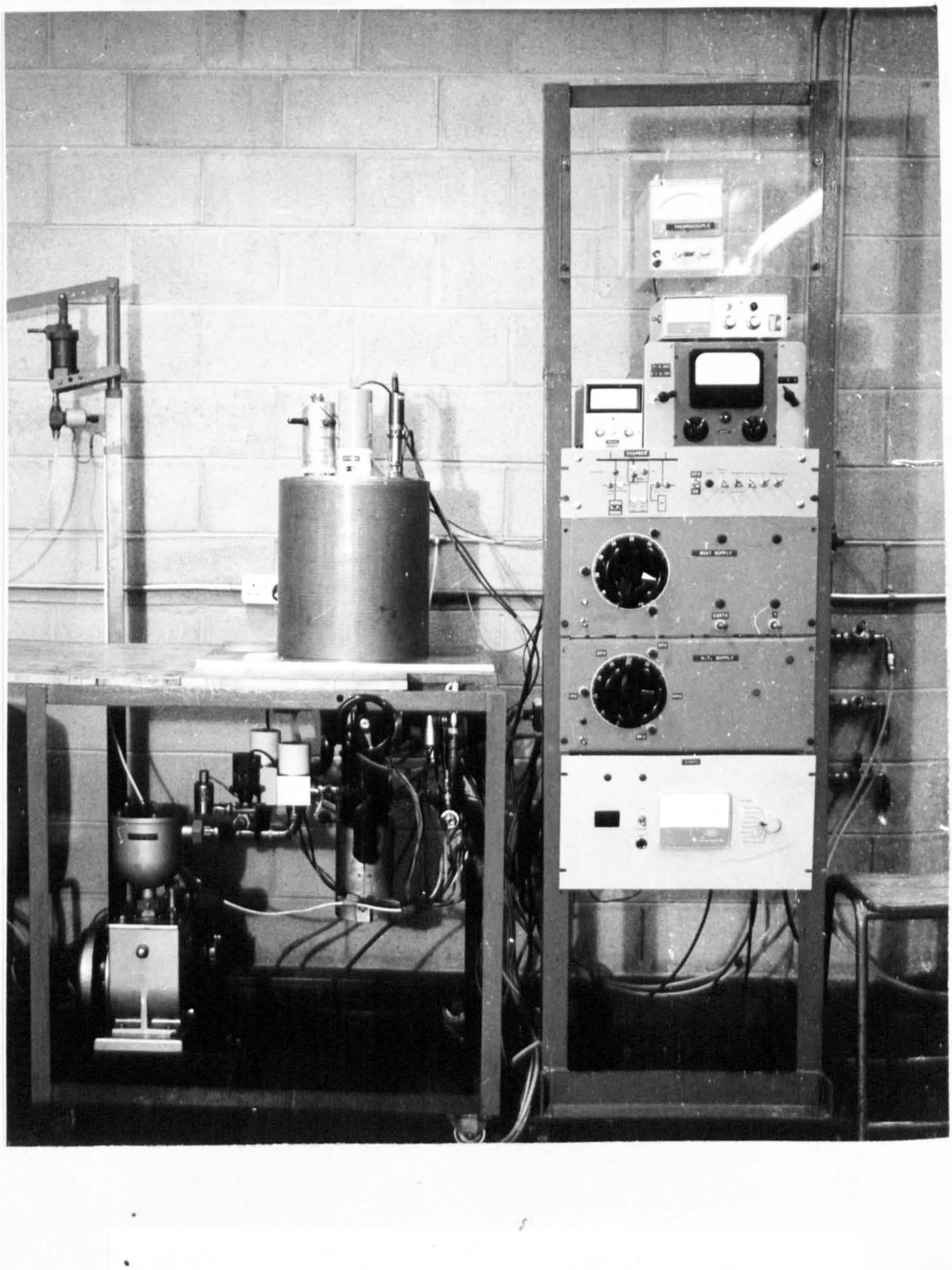

ION PLATING ARRANGEMENT

Figure 2.2.1b

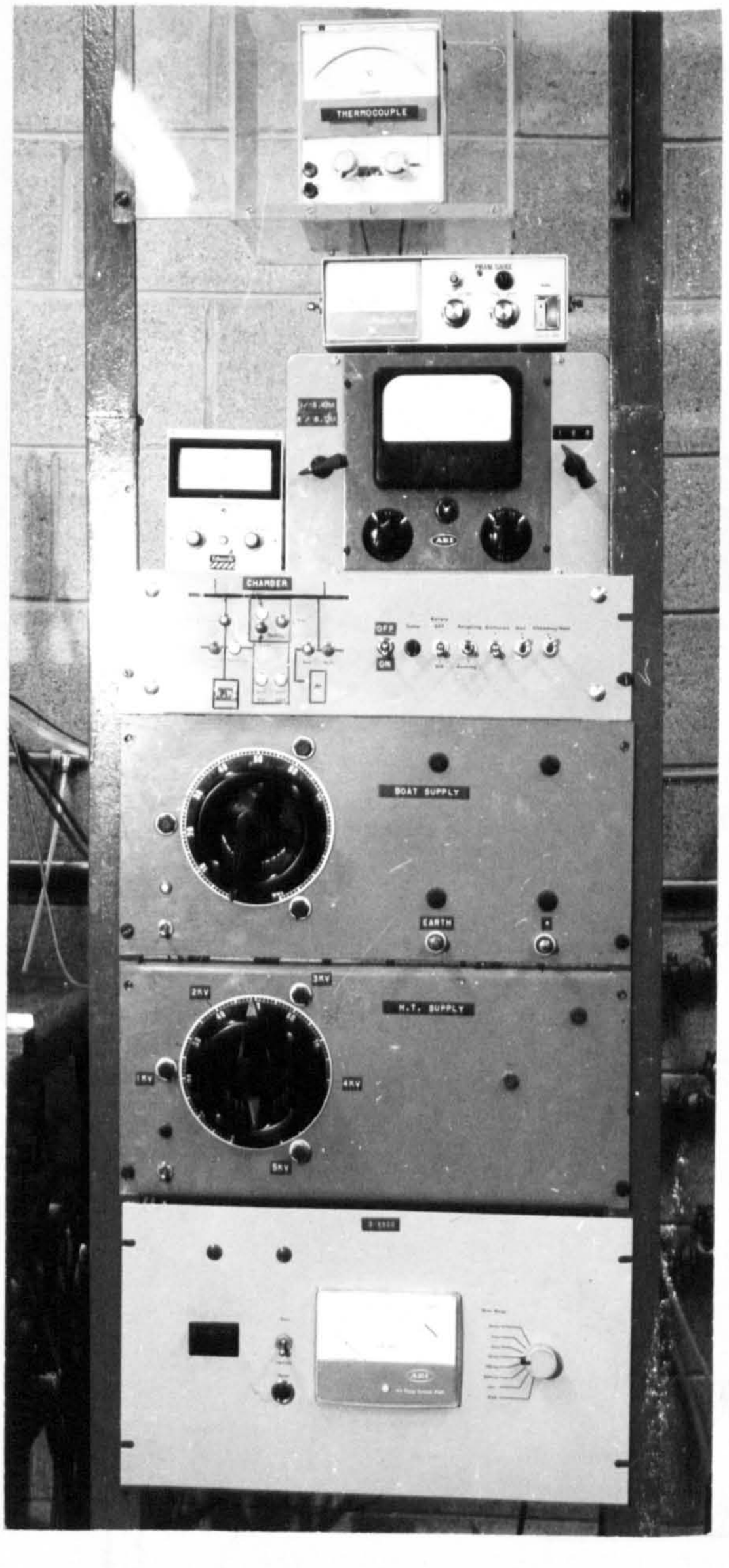

Figure 2.2.1c

The control panel

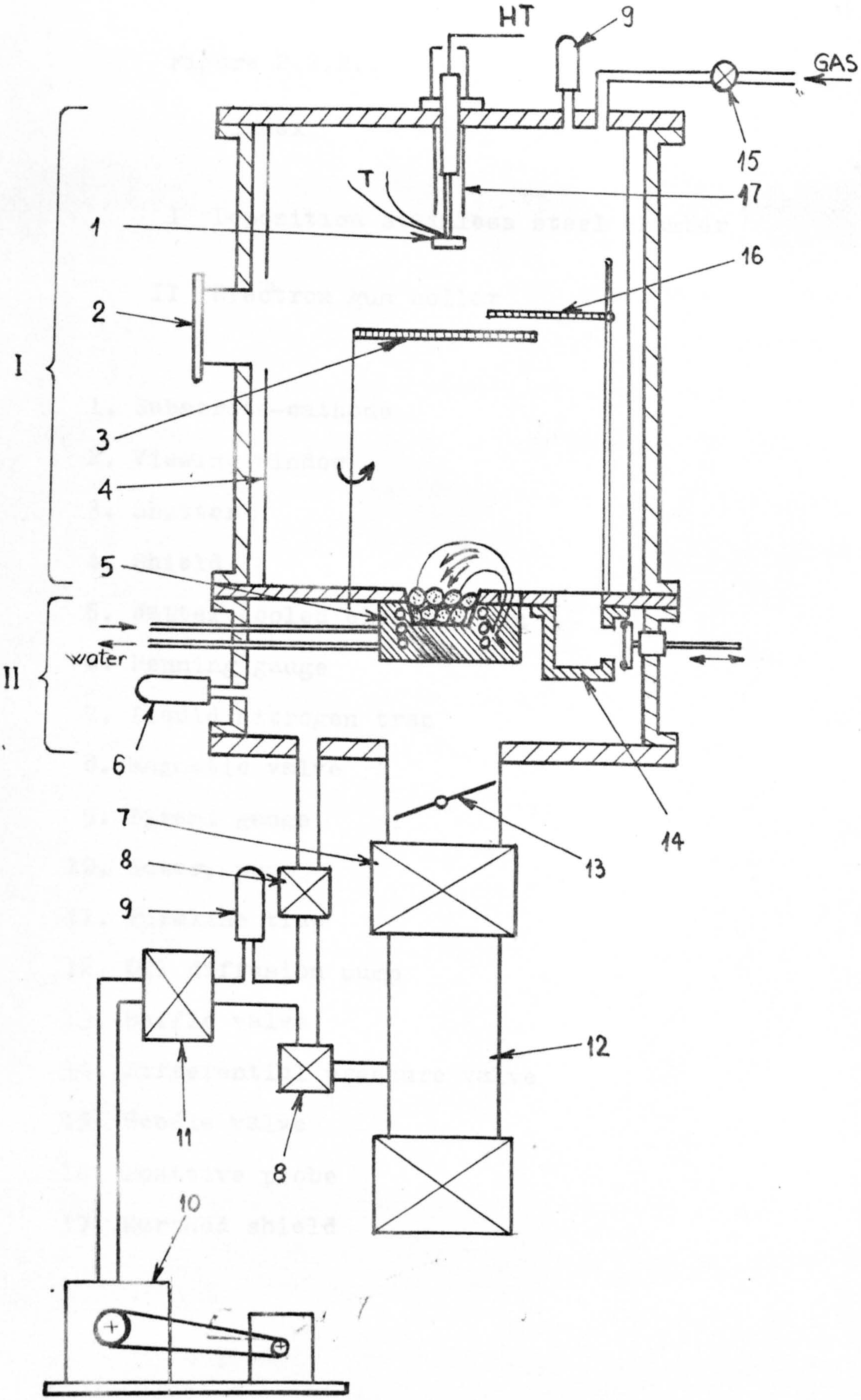

ELECTRON GUN ION PLATING RIG

Figure 2.2.2

Figure 2.2.2.

Index

I Deposition stainless steel chamber

II Electron gun collar

1. Substrate-cathode
2. Viewing window
3. Shutter
4. Shield
5. Watter cooled electron gun
6. Penning gauge
7. Liquid nitrogen trap
8. Magnetic valve
9. Pirani gauge
10. Rotary pump
11. Foreline trap
12. Oil diffusion pump
13. Baffle valve
14. Differential pressure valve
15. Needle valve
16. Positive probe
17. Earthed shield

chamber by a variable baffle valve in order to maintain the differential pressure. Inside the chamber, a pressure of 10-50 mTorr must be maintained to provide the optimum conditions for ion plating, while in the collar, where the filament assembly is mounted, a pressure of better than 10^{-4} Torr is required in order to avoid discharges between the HT parts and the earthed parts of the gun and also to extend the life of the filament. The maximum acceleration voltage of the gun is 10 kW and a maximum current of 1.5 A can be obtained. The beam can be scanned on the surface of the material to be melted so that a uniform heating is achieved. The hearth crucible is water cooled with a 7 l/h flow. The use of an electron gun provides the possibility to evaporate high melting point materials and also to have higher evaporation rates. In the same time, thicker films can be deposited conbined with an enhanced ionization,produced by the electron beam.

2.3. Ion Plating Procedure

The Ion Plating procedure has been described by many authors[6,8,20]; here is a brief presentation of the way it was performed in this work./

First, the whole system is pumped down to a pressure of 10^{-5}-10^{-6}Torr so that most of the residual gases are removed. Then, the film material is premelted in order to allow outgasing. After this, the baffle valve

between the diffusion pump and the chamber (for the system in Figure 2.2.1.),or the baffle valve between the collar and the chamber (for the system in Figure 2.2.2.) is throttled, and argon gas is let in, via a needle valve so that a pressure of 10-50 mTorr is obtained. At this moment, the glow discharge is established and allowed to strike between the earthed parts (anode) and the substrate (cathode), at a voltage of 3-5 kV and a current density of 0.5-0.8 mA/sq.cm, and thus, the first stage called - sputter cleaning - is commenced and it lasts until the total cathodic current drops to a constant value, when the substrate is considered to be clean.

Although we consider the moment when the cathodic current reaches a steady value as the end of the cleaning process, if the voltage is increased, this is followed by an increase in the value of the cathode current which will continue to drop to a new steady value, higher than the previous one, and the process will repeat with new increases in the bias voltage as shown in Figure 2.3.1.

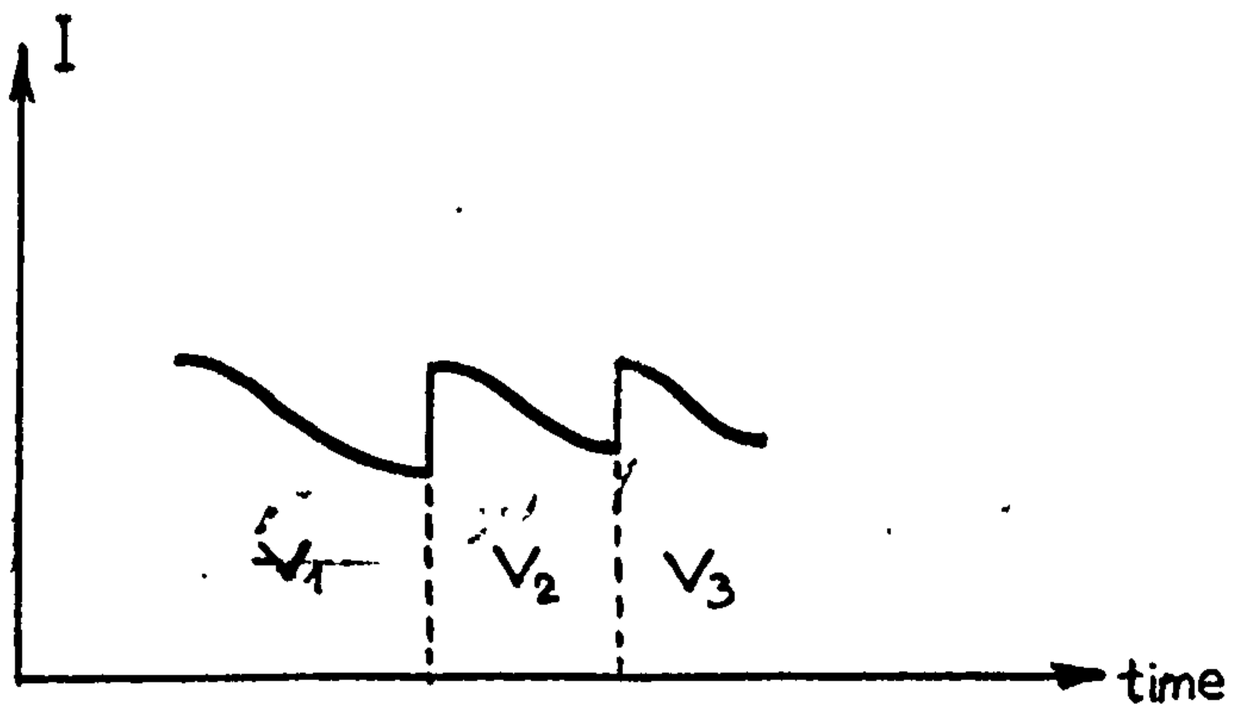

$V_1 < V_2 < V_3$.

Figure 2.3.1

This could mean that the sputtering for a given voltage does not remove all the contaminant particles, but a percentage of them, therefore a perfectly clean surface is not obtained at the end of the sputter cleaning. However, the good adhesion obtained in practice proves that even such a partial cleaning is sufficient.

After sputter cleaning, the film material is melted and evaporated and the deposition begins. During this stage, the discharge is maintained in order to maintain a perfectly clean surface and to remove the non-adhesive particles deposited on the substrate.

At the very beginning, the continuous sputtering, combined with the back scattering, will produce a mixture of substrate and film materials which will deposit as a graded interface which plays a determinant role in obtaining the very good adhesion of ion plated films.

Another condition is that the deposition rate must exceed the sputtering removal rate so that the film is allowed to grow. After obtaining the required thickness, the evaporation is stopped and the discharge quenched, the argon inlet is closed and the system is pumped down to allow the substrate to cool in a clean atmosphere thus reducing surface contamination.

The source-substrate distance could be any, but longer than the cathode dark space and is usually 8-15cm .

A very important stage in the ion plating procedure is the sputter cleaning, a term used to define

the process of continuous removal of contaminant layers on the substrate surface. In fact, sputtering means the removal of atoms or group of atoms from a solid surface subjected to energetic particles bombardment. The incident particles must have a minimum energy (sputtering threshold) in order to produce sputtering, energy which is of the order of 20-30 eV. There is also a maximum energy limit of about 50 keV above which the particle will penetrate deeply into the solid and this process is called 'implantation'. Of course, at these high energies, there will be a number of particles producing sputtering but the sputtering yield will be very low.

On the other hand, a too high sputtering rate can be damaging by removing unnecessarily too much material.

Heavier particles will have higher sputtering yields than the lighter ones.for the same incident energy.

Considering the case of 'hard spheres' collision, the transfer of energy is given by the following equation:

$$E = \frac{4M_1M_2}{(M_1+M_2)^2} E_i \qquad (2.3.2.)$$

where M_1 and M_2 are the masses of the colliding particles, E is the energy transferred to the stationary particle and E_i is the energy of the incident particle. As it can be seen, a heavier particle will transfer more energy than a lighter one having the same energy of incidence.

At the same time, the subjection to energetic bombardment induces surface defects in the substrate lattice which will help the two lattices (of the substrate and of the film) to couple together. These surface defects will also act as centres for film nucleation. The process of inducing lattice defects is often referred to as 'ion etching'. Figure 2.3.3. shows a scanning Electron Microscope picture of a copper surface etched for 35 min. at 5 kV bias voltage and 10 mTorr argon pressure. As it can be noticed, the grain structure is revealed due to different etching of grains and grain boundaries.

At the low energies typical for ion plating, inert gas atoms can be trapped in the surface and covered by film atoms during deposition, and they can either remain there or be released due to the thermal desorption (caused by the rise in temperature).

A very important process is the gas scattering when the energetic particles lose much of their energy in collisions with other particles. Also, due to gas scattering, many of the sputtered atoms are scattered back to the substrate and deposited together with the film atoms contributing to the formation of the graded interface.

It can be demonstrated that the particles less adhesive, as well as edges and sharp points are easier to sputter. In the case of non adhesive particles, the sputtering threshold will have a lower value. In the case of edges and sharp points, the electric

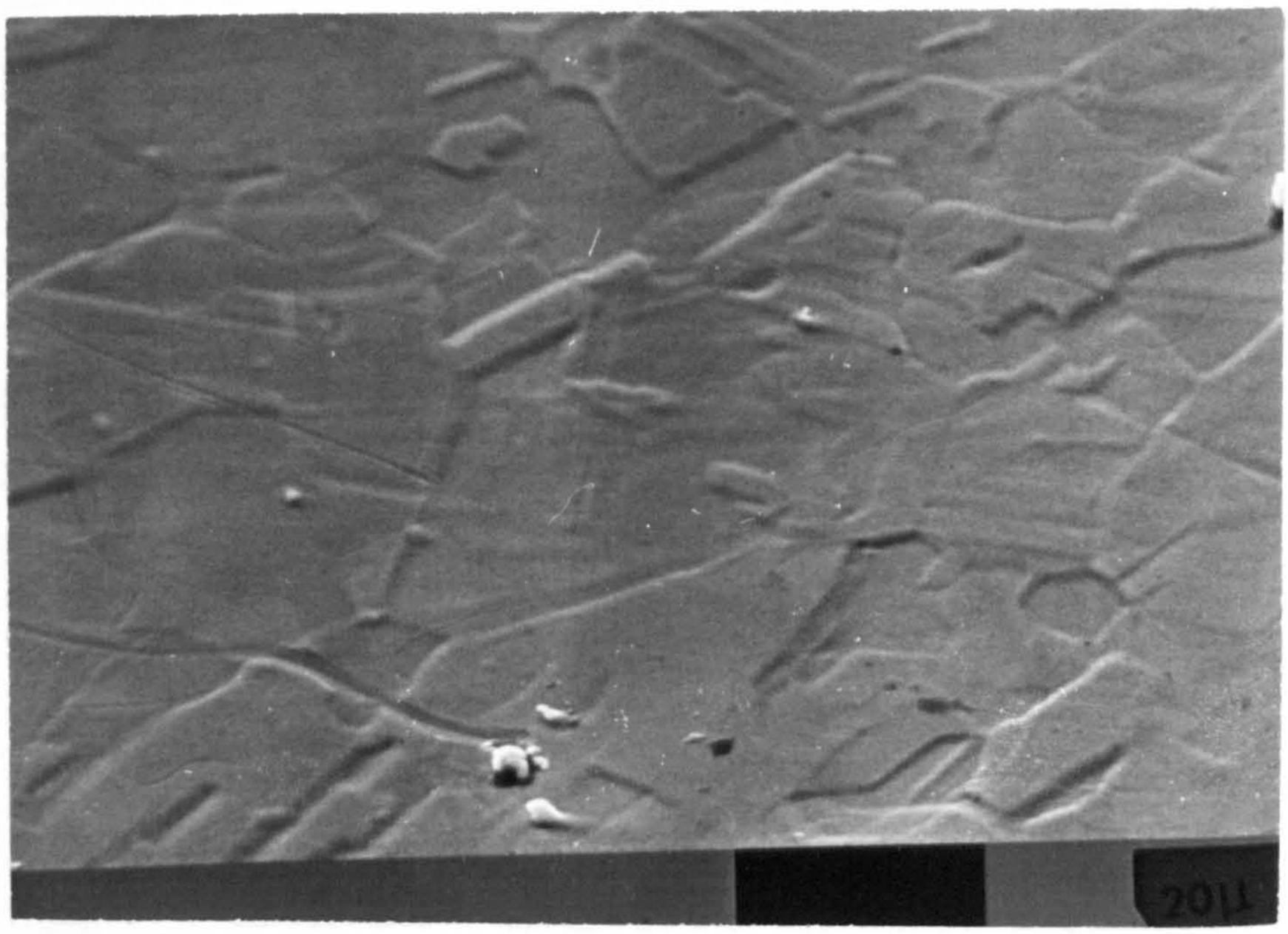

Figure 2.3.3

Copper surface - ion etched

5 kV ; 10 mTorr ; 35 minutes

field concentration will lead to higher sputtering rates. This last effect could be useful for removing the columnar structure resulting in the case of vacuum evaporated and most of the ion plated films, as shown in Figure 2.3.4.[7]

This type of film growth in peaks and valleys is created either as a replica to the surface microroughness, or by prefferential growth of crystallographic planes.

In the case when no bias voltage is applied (vacuum evaporation), a geometrical shadowing will occur in the valleys preventing the deposition, while the peaks, better exposed to the evaporant will grow. The result is a columnar structure.

If a negative bias is applied to the substrate, the ion bombardment, if sufficient, will erode the peaks by sputtering , and by forward sputtering and back scattering redeposition will fill the valleys.

There are various types of evaporation sources and they are presented in Figure 2.3.5.[8]

Some special ion sources are also available which can provide beams of metal ions for deposition.[9] A plasma evaporation source[10] can vaporize and partially ionize the film material.

The R.F. potential is normally used for coating glass, ceramic or organic insulators, but can be used for conductors as well.

Sometimes, if the insulators are exposed to the plas-

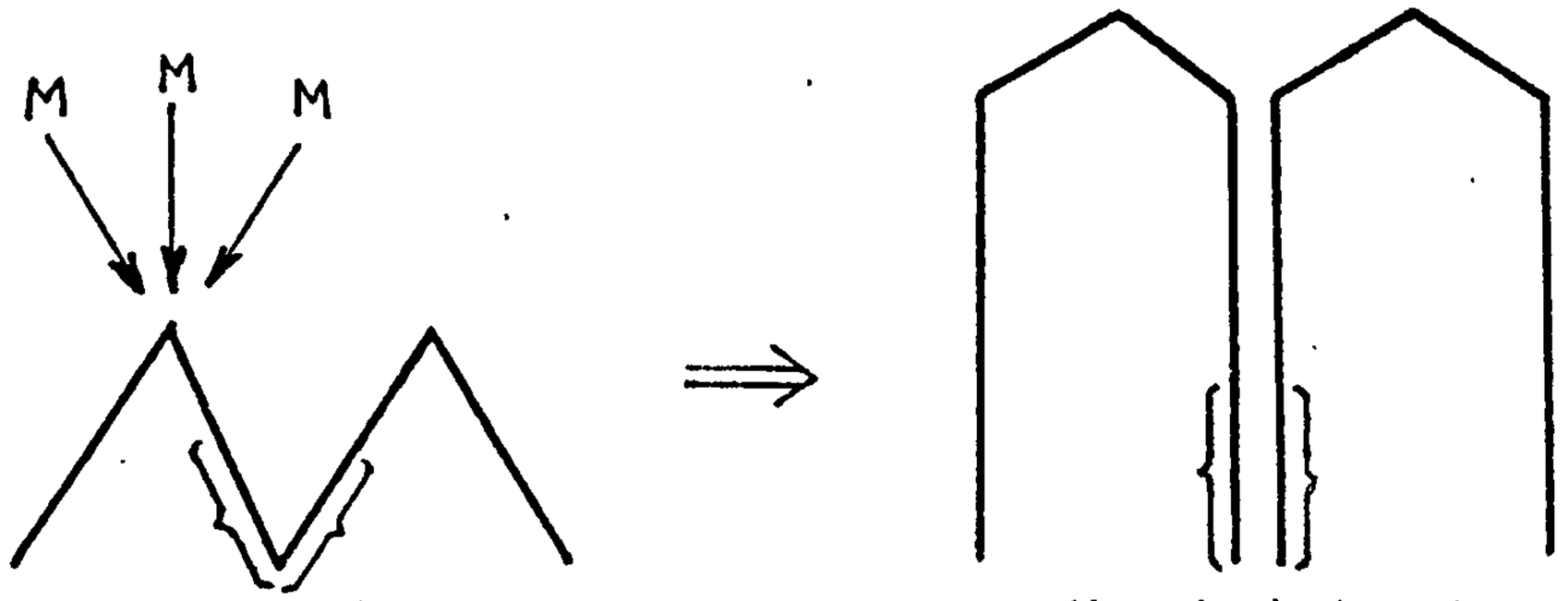

a. Columnar Structure

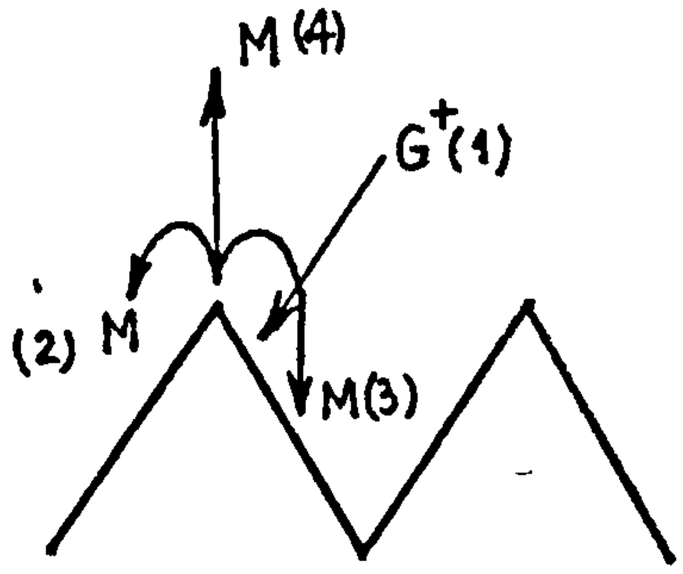

(1) Sputtering (erosion of the peak)
(2) Scattering redeposit
(3) Forword sputtering
(4) Back sputtered

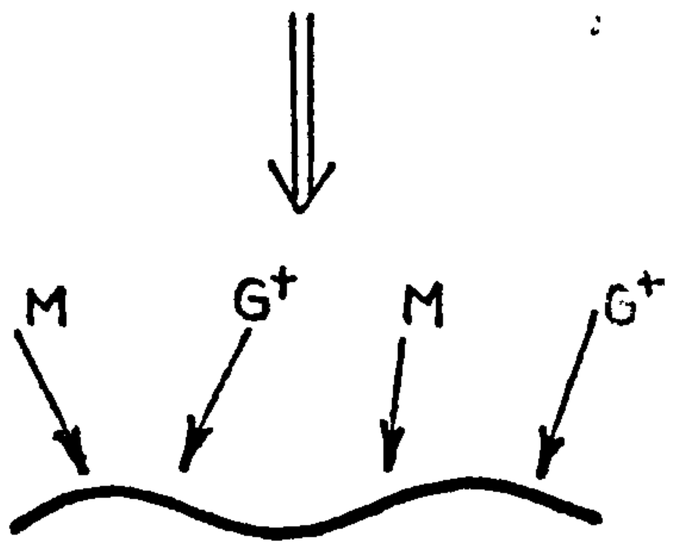

Not Columnar Structure

b.

a. No bias voltage (vacuum evaporation)
b. Bias voltage (Ion plating)

Figure 2.3.4

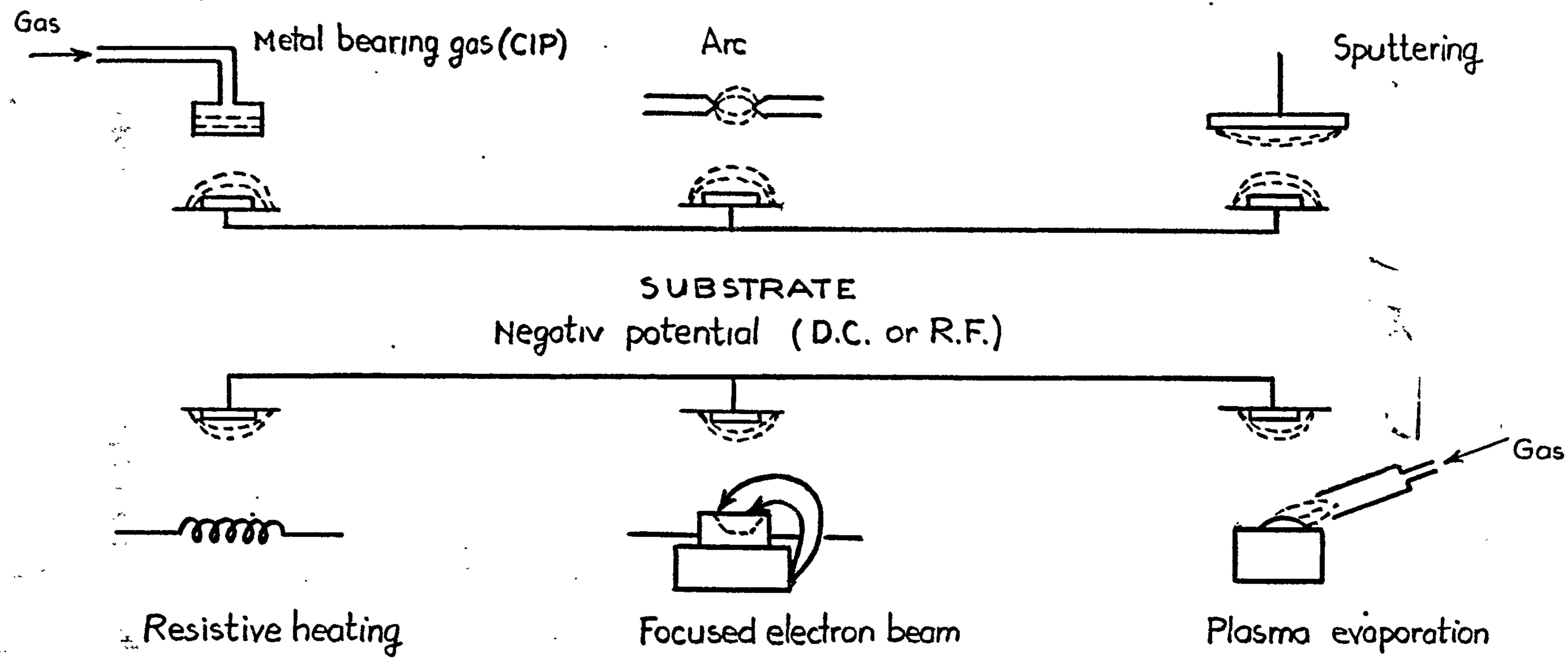

Figure 2.3.5

Evaporation Sources

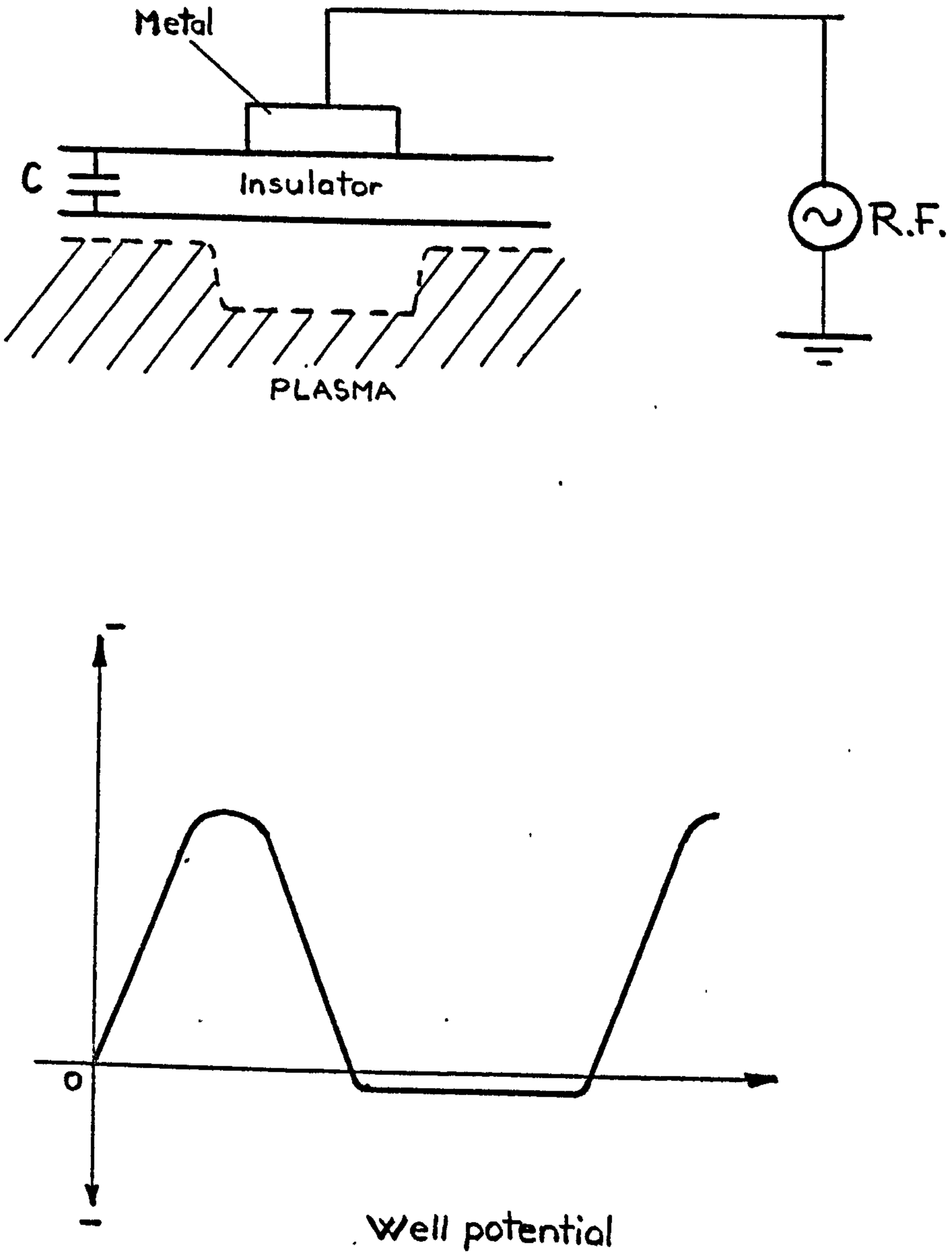

Figure 2.3.6

Electrode configuration and surface potential of insulators exposed to plasma in the case of the R.F. potential

ma due to ultraviolet radiation and also due to the 'ion scrubbing effect', the change in the surface will give better adhesion.[11]

The set-up of an R.F. substrate electrode is shown in Figure 2.3.6.[12,13]. This arrangement acts like a capacitor with the metal plate on the back acting as an electrode, and the plasma as the other electrode. When an R.F. field is applied, the surface facing the plasma will be positive and negative, alternating according to the R,F. frequency. But the electrons have higher mobility than the ions and for very high frequencies, the surface facing the plasma will attract more electrons and thus will attain a negative bias. This bias will accelerate positive ions, exposing the surface to ion bombardment.

2.4. Glow Discharge

If in a vaccum chamber containing a gas pressure of several mTorr, a D.C. voltage is applied between two electrodes at a low voltage, a uniform potential gradient is obtained across the space between the two electrodes and an extremely low current passes. Increasing the voltage, the current increases slowly and at the moment when the breakdown voltage-pressure conditions are achieved, the current increases fast followed by a drop in the potential. This is the 'nor-

mal' glow discharge and keeping the voltage constant, the current depends upon the gas pressure. A spot can be observed on the cathode surface called the 'cathode spot' over which the current density is constant. A certain colour is observed due to the sputtered material which is excited by the bombardment concomitant with the release of radiation ($h\nu$). The colour depends upon the gas and the nature of the cathode material.

Increasing the pressure (usually over 10 mTorr), the spot coveres the whole cathode area and, at constant pressure, the current becomes a function of voltage. This region is called the 'abnormal' glow discharge in which ion plating normally takes place. Figure 2.4.1. presents the I-V characteristics of a glow discharge[14].

Figure 2.4.2. a and b shows the regions of a normal glow discharge as regarding its luminosity and its electrical characteristics[14].

In the plasma region, the field value is very low, and it is composed of an equal number of electrons and ions, behaving neutral from the electrical point of view.

For a normal glow discharge, most of the potential drop occurs in the cathode dark space and most of the ionizations occur in the negative glow. If 'L' is the width of the cathode dark space, then:

$$pL \simeq \text{constant}$$

where p is the gas pressure.

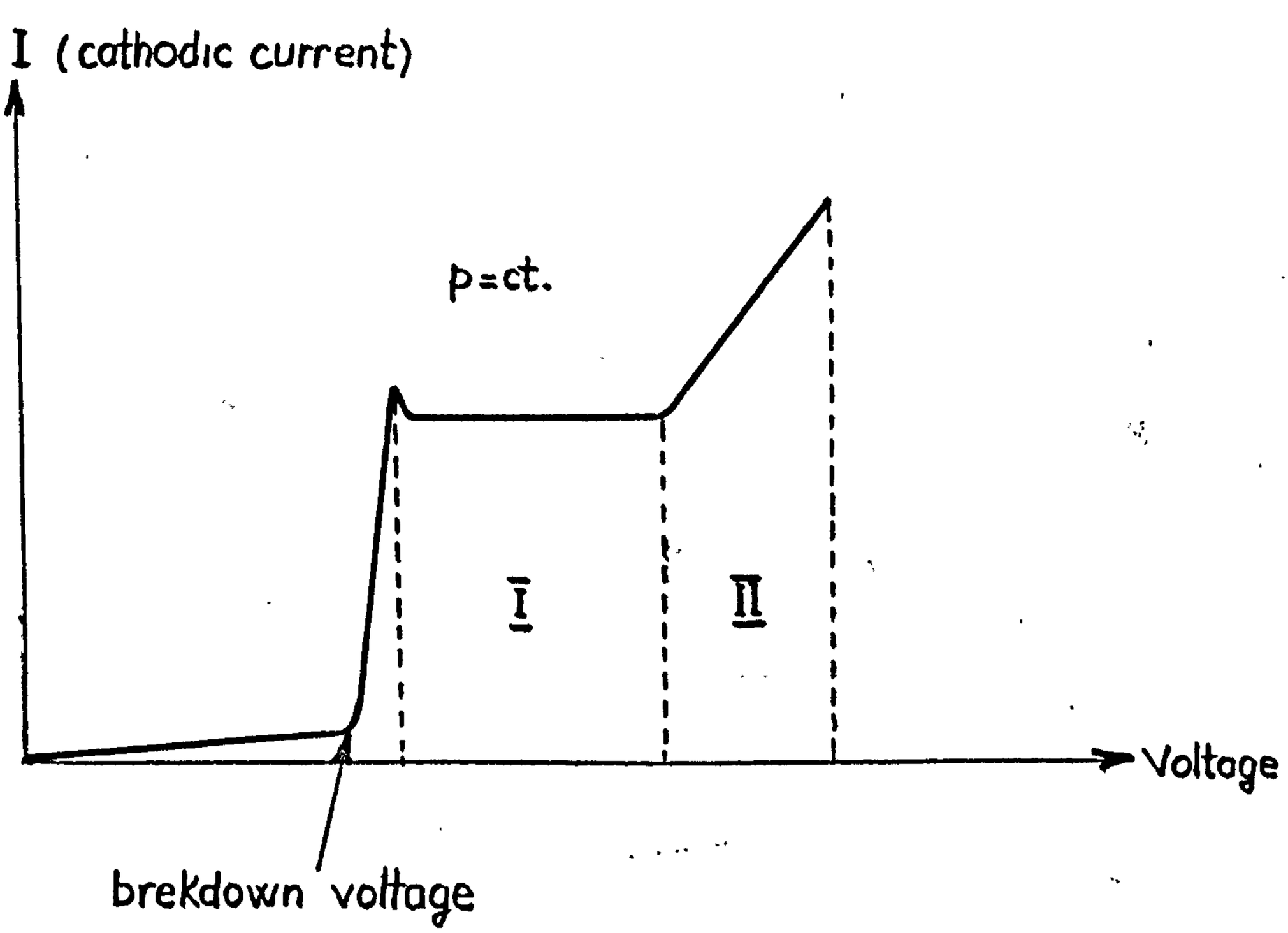

I Normal glow discharge

II Abnormal glow discharge

Figure 2.4.1

I - V characteristic of a glow discharge

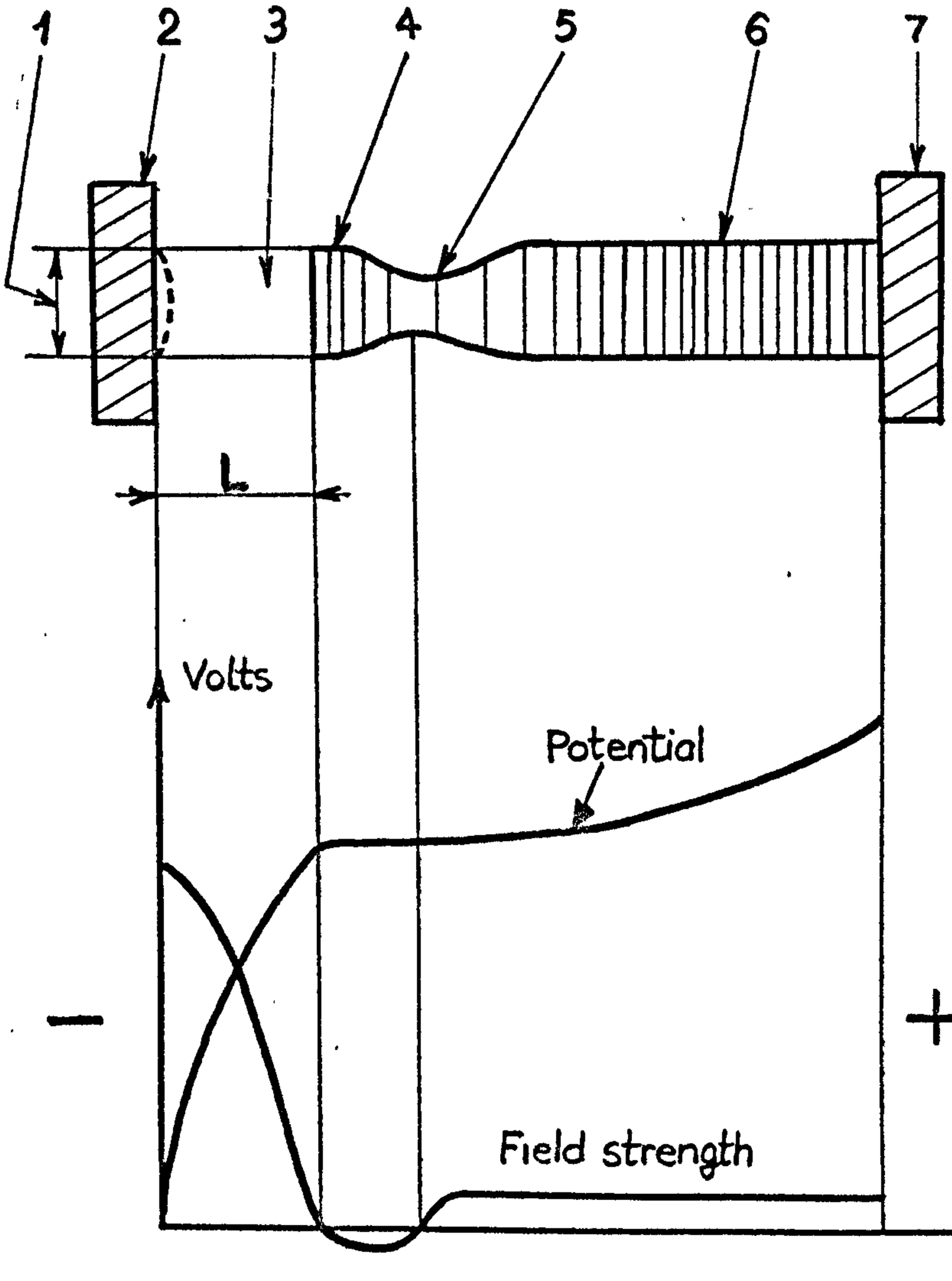

1. Cathode spot
2. Cathode
3. Cathode dark space
4. Negative glow
5. Faraday dark space
6. Positive column (plasma)
7. Anode

Figure 2.4.2

Normal glow discharge

The value of 'L' depends mostly upon pressure and very little upon the nature of the gas and temperature.

In the case of an abnormal glow discharge when ion plating process takes place, the following experiment was performed. The arrangement is shown schematically in Figure 2.4.3.

The cathode is an aluminium disk with a diameter of 10 cm and the earthed shield on the back is at approximately 3 mm distance from the cathode.
The anode is a mobile, earthed aluminium disk, having the same dimensions as the cathode. The maximum cathode-anode distance is 22 cm and the anode can be brought closer to the cathode by means of a vaccum tight lead-through.

A certain voltage and argon pressure are set in the chamber, and then the anode is moved towards the cathode and the cathodic current is measured and plotted versus distance 'D' for different voltages and 10 mtorr argon pressure in Figure 2.4.4.
When the discharge quenches, it means that the cathode-anode distance is equal to the cathode dark space. The quench happens nearly instantly and the dark space width could be determined quite accurately.
The cathode and the anode must be perfectly flat and parallel to each other in order to obtain an instant quench. Figure 2.4.5. and Figure 2.4.6. present the variation of cathode dark space 'L' with voltage and pressure. It can be noticed that there is little variation of the dark space width with the voltage,

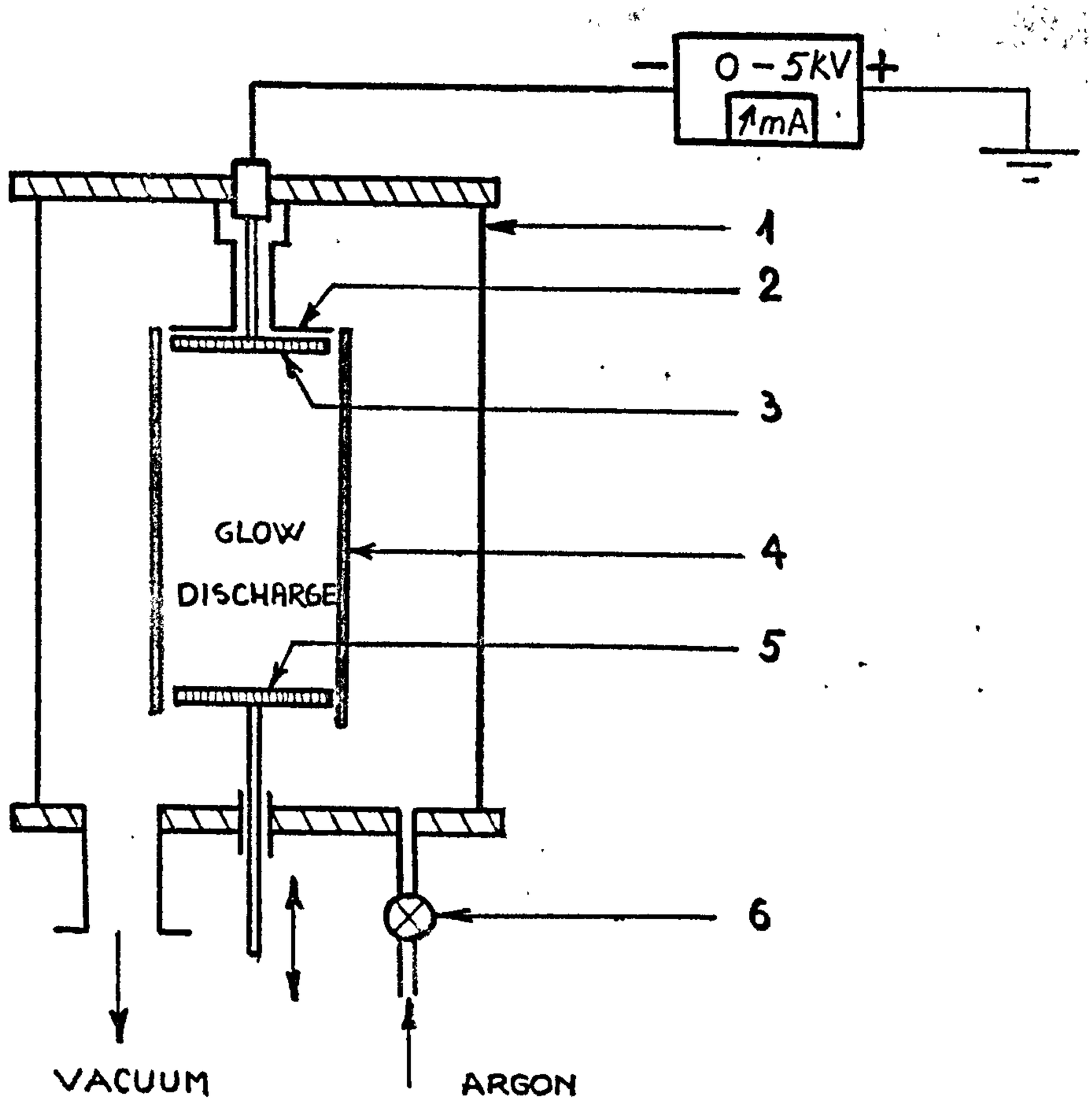

1. Vacuum chamber
2. Earthed shield
3. Cathode disk
4. Perspex tube
5. Mobile anode disk
6. Needle valve

Experimental arrangement

Figure 2.4.3

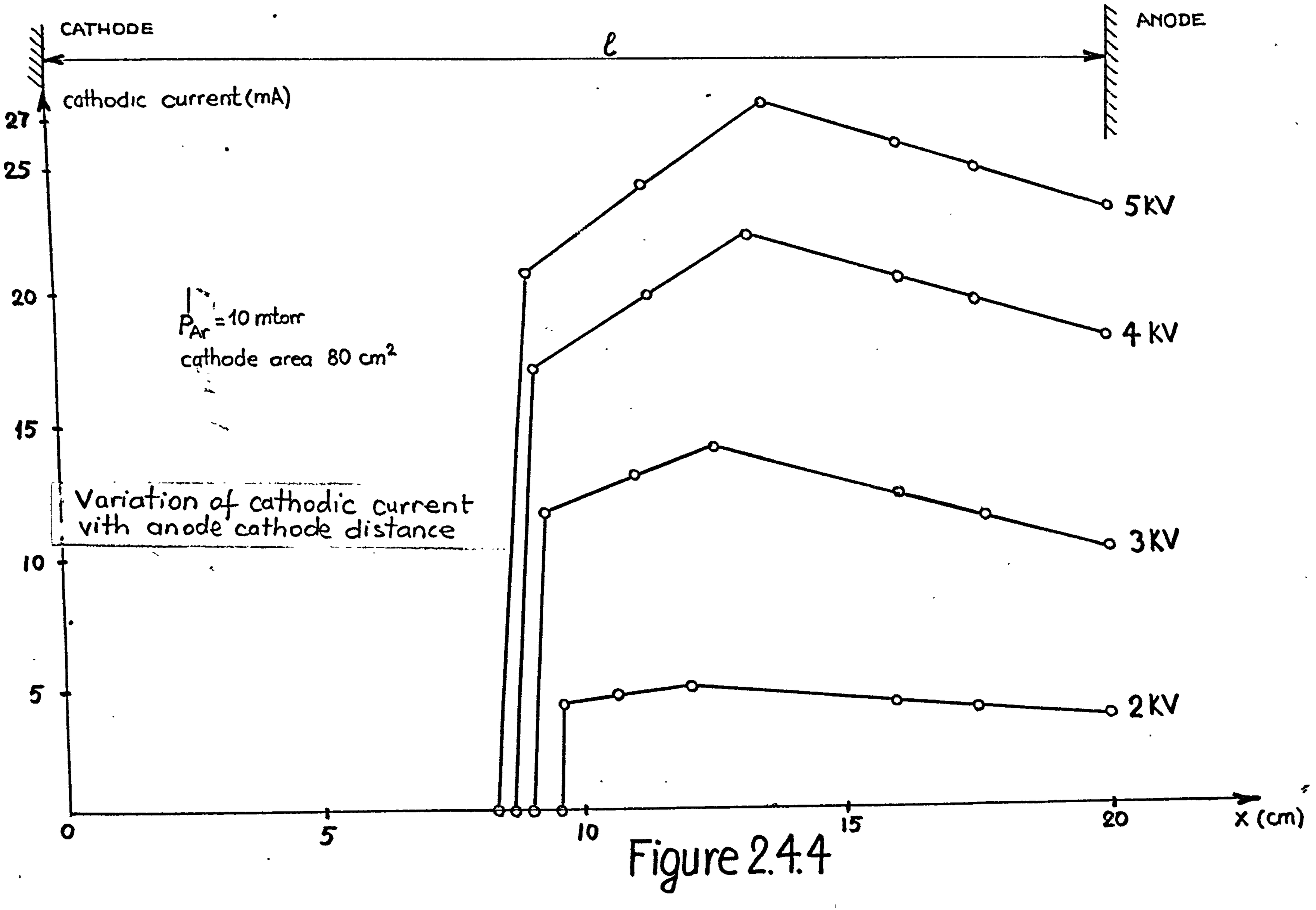
CATHODE
ANODE
ℓ
cathodic current (mA)
27
25
20
15
10
5
0
5
10
15
20
X (cm)
P_{Ar} = 10 mtorr
cathode area 80 cm²
Variation of cathodic current with anode cathode distance
5 KV
4 KV
3 KV
2 KV

Figure 2.4.4

Variation of cathode dark space with discharge parameters
L (cm)
13
10
5
0
1
2
3
4
5
quench voltage (KV)
P (mtorr)
10
15
20
25
30

Figure 2.45

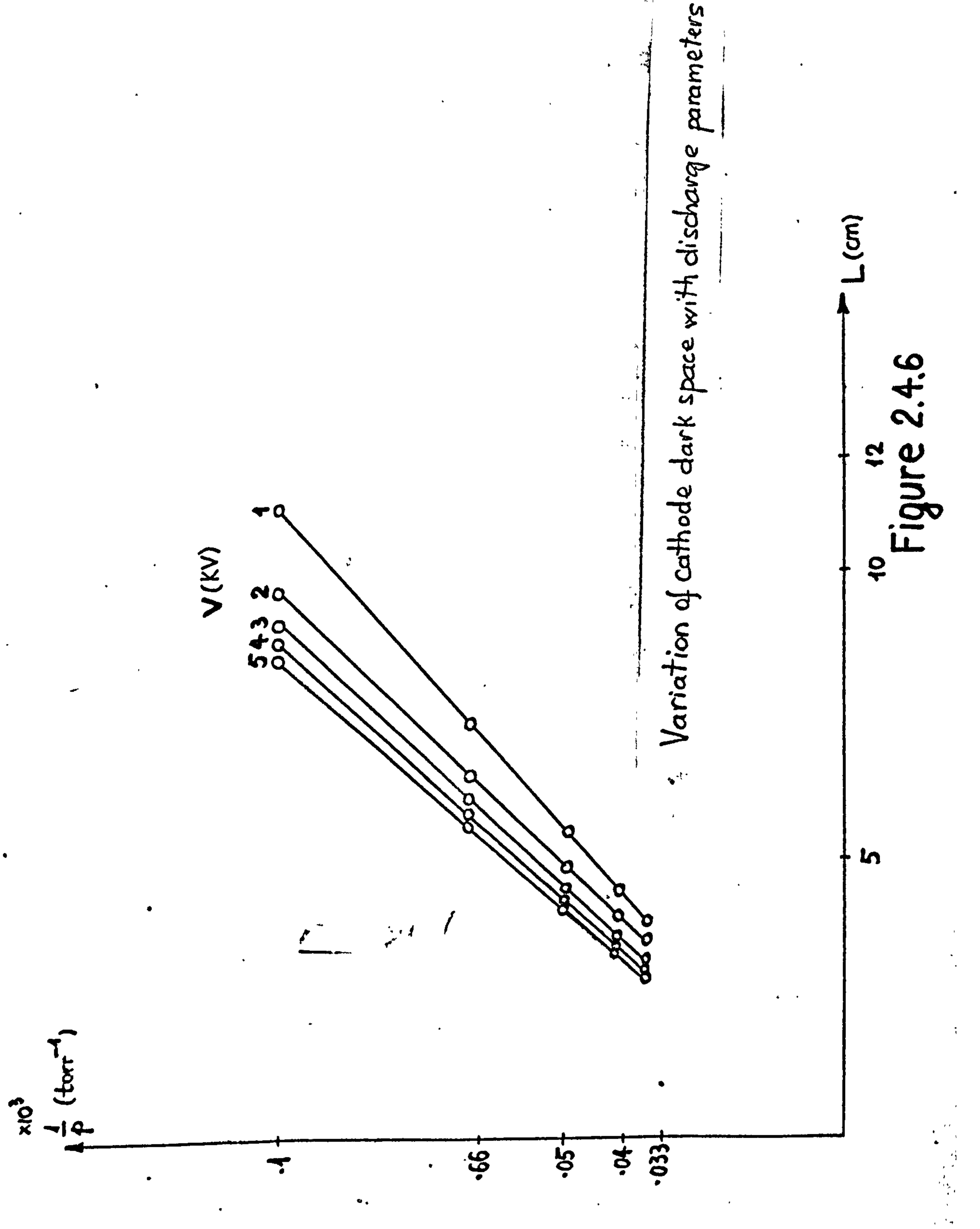
Variation of cathode dark space with discharge pamameters
V(KV)
1
2
3
4
5
L(cm)
2
4
6
8
10
12
$\frac{1}{p}$ (torr^{-1})
$\times 10^3$
.1
.066
.05
.04
.033

Figure 2.4.6

while the pressure has a large influence upon it. The increase in pressure leads to a restrain of the cathode dark space, effect which is less obvious for pressures exceeding 25 mtorr.

The increase in voltage leads to a slight decrease in the cathode dark space width.

It can also be noticed that the relation

$$pL \simeq \text{constant} \quad \text{for } V=\text{constant}$$

applies for the abnormal glow discharge as well.

From Figure 2.4.4. it results that the optimum anode-cathode distance is 12-13 cm, in order to obtain the maximum ion current. For the same p-V conditions, but with the anode at 13 cm and at 22 cm from the cathode, there is a drop in current density of 30-40% which consequently means a similar drop in the ionization efficiency.

2.5. Collisions and Ionization Mechanism

During the sputter cleaning stage of the ion plating procedure, the substrate which is the HT cathode, is subjected to a positive ion bombardment.

A theory[8] assumes that some of the gas atoms (G^o) are ionized by electron-atom collisions and accelerated across the cathode dark space until they strike the cathode surface. Travelling across the cathode dark space, some of these ions will have charge transfer collisions[15] becoming high energy neutrals. The ions and energetical neutrals striking the cathode surface can either be incorporated into the surface(on the surface or implanted into the surface), or in the case of ions, neutralized and reflected as high energy neutrals or metastables(G^*). The matastable is an excited atom which keeps this excitation for a very short poriod of time, while having a collision can ionize another neutral or in the absence of a collision loses its energy, becoming a low energy neutral and emitting a quantum ($h\nu$) of ultraviolet radiation.

The effect of substrate bombardment with high energy particles is the emission of secondary electrons ($\bar{e}$) and the sputtering of the substrate material (s^o). This sputtering material may be scattered back to the surface (due to small angle collisions with energetic neutrals) or back sputtered. The back

sputtered particles can either deposit on some parts of the system, or be ionized by ion, electron or metastable collisions and accelerated back to the cathode as positive ions (s^+).

The substrate is also exposed to an ultraviolet radiation ($h\nu$) which can affect organic and insulating surfaces[16,17,18] in the second stage of the procedure which is the deposition itself, without cutting the discharge, film atoms ar injected into the discharge. These atoms may be:

1. Scattered back to the source
2. Ionized by electron-atom collisions
3. Ionized by metastable-atom collisions
4. Transferred energy by a collision with a high energetic neutral
5. Ionized by a collision with an ion (charge transfer collision)
6. Scattered to some other parts of the system
7. Nucleate with other film atoms in the gas phase and form fine particles (clusters). These particles (~100Å) can assume a negative charge in the plasma[19].

The metal atoms and ions will behave like gas atoms and ions when entering the cathode dark space. Figure 2.5.1. presents a model of collisions and particles in a glow discharge.

Since plasma is a low field region, electrically neutral (equal number of electrons and ions), due to

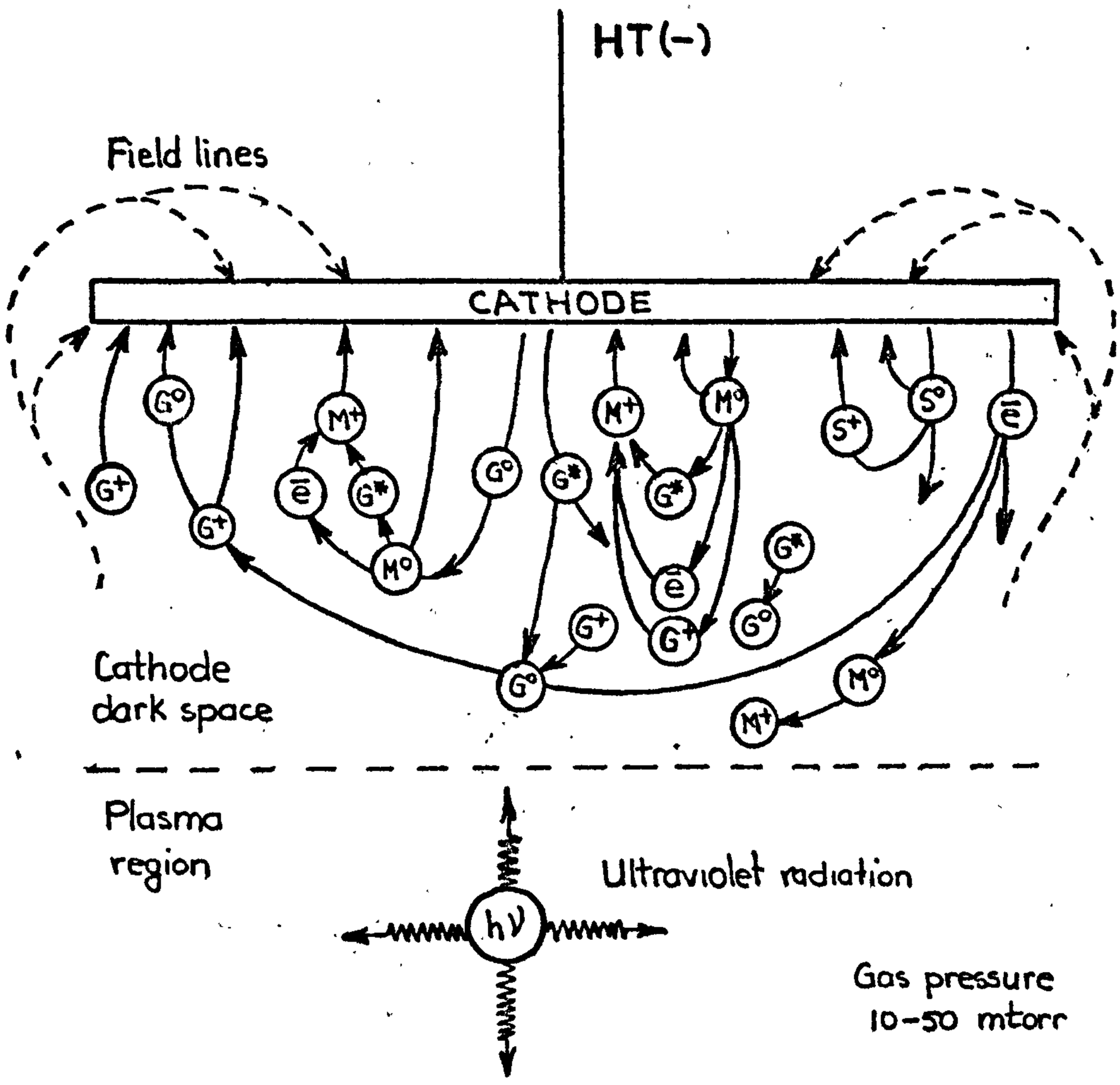

M = Coating Metal

S = Substrate Material

G = Gas

G* = Metastable

Note : The same process will take place on the back surface of the cathode due to the field lines and the scattering effect.

Ion plating Mechanisms [8]

Figure 2.5.1

the potential difference between the cathode and the anode, ions are extracted from the plasma region and accelerated across the cathode dark space. Ion-neutral and neutral-neutral collisions will take place while crossing this space, and the understanding of these collisions is very important in order to determine the nature and energy of the particles reaching the cathode.

A theoretical approach to the determination of the energy of ions in a glow dischrge was reported by Davis and Vanderslice[15] and, choosing different boundary conditions, Teer[20] obtained simpler expressions for the distribution on ions and neutrals energies for the ion plating conditions.

It was assumed that all ions originate in the negative glow, that the electric field varies linearly from the edge of the negative glow to the cathode surface and that only the charge transfer collisions can occur between an ion and a neutral, and also that neutral-neutral collisions are billiard balls type collisions (share of energy and change of direction). Of course, these assumptions lead to an error but reasonably accurate average figures can be calculated. The number of metastables is very low due to the low energies involved in the process (as proved in the further chapters) and therefore, their effect is negligible.

If the cathode dark space has a width 'L' (Figure 2.5.2) and the mean free path between two

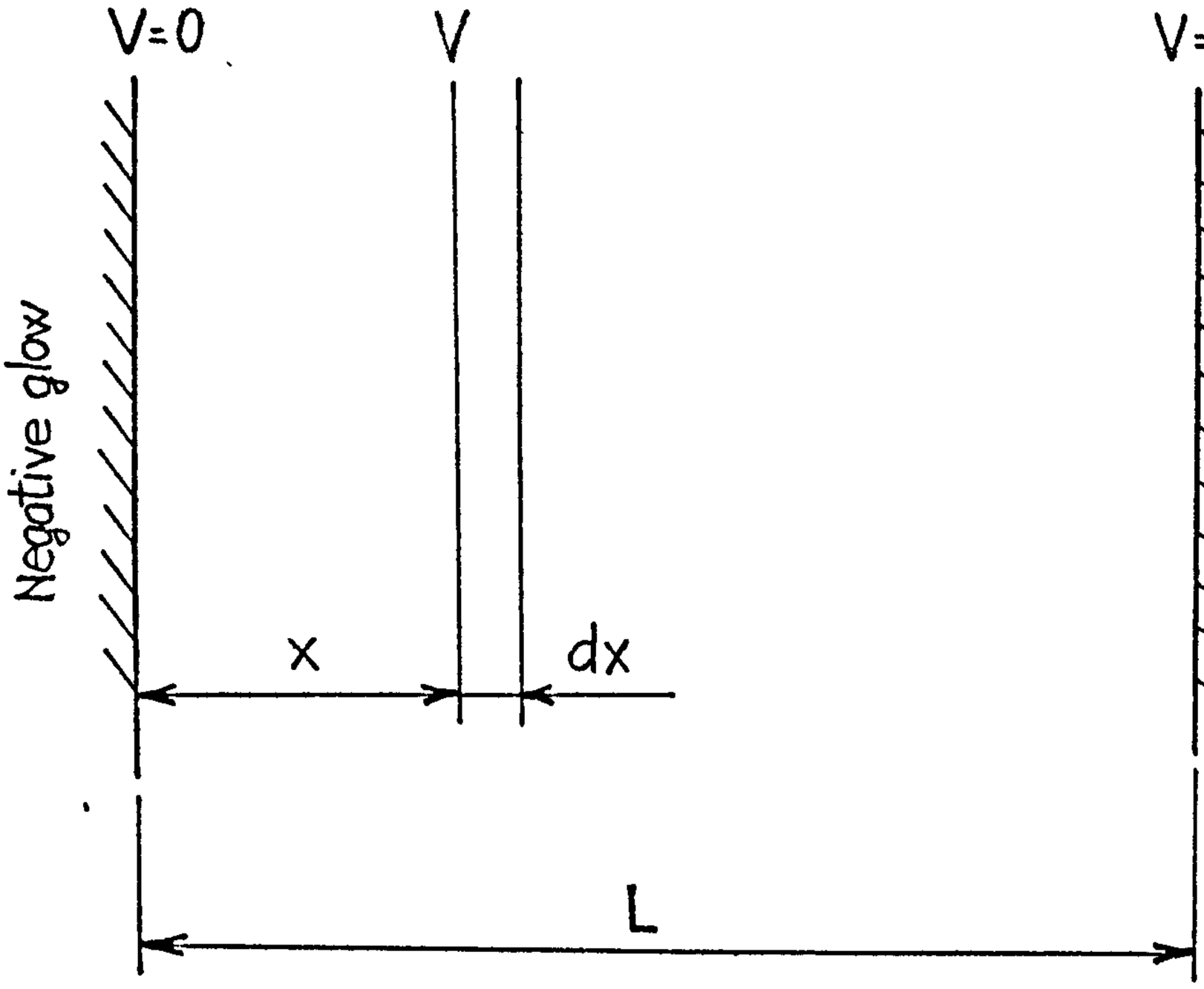

Figure 2.5.2

collisions (related to the gas pressure) is 'ℓ' and if the field strength varies linearly as it was assumed above, by applying boundary conditions, the following expression is found for the voltage variation along the dark space :

$$V = \frac{V_c}{L^2} X^2 \qquad (2.5.3.)$$

If N_i is the number of ions entering the cathode dark space, the number of collisions in the space dx, undergone by these ions, is :

$$N_i \frac{dx}{\ell} \qquad (2.5.4.)$$

and the probability of these ions to reach the cathode without further collisions is :

$$\bar{e}^{-\frac{L-X}{\ell}}$$

The number of ions reaching the cathode with the energy $(V_c - V)\ \bar{e}$ is :

$$dN = \frac{N_i}{\ell} \bar{e}^{-\frac{L-X}{\ell}} dX \qquad (2.5.5.)$$

The total energy of the ions arriving at the cathode is :

$$dE = (V_c - V)\ \bar{e}\ dN \qquad (2.5.6.)$$

Substituting and integrating an expression of this energy can be obtained :

$$E = N_i V_c \left[\frac{2\ell}{L} - \frac{2\ell^2}{L^2} + \frac{2\ell^2}{L^2} \bar{e}^{-\frac{\ell}{L}}\right] \bar{e} \qquad (2.5.7.)$$

If no collisions occurred, the total energy transported to the cathode would be equal to $N_i V_c \bar{e}$

The energy thus lost is transferred to the neutrals and their energy is:

$$E_n = N_i V_c \bar{e} - E$$

or:

$$E_n = N_i V_c \bar{e} \left[1 - \frac{2\ell}{L} + \frac{2\ell^2}{L^2} \right] \qquad (2.5.9.)$$

The term $\frac{2\ell^2}{L^2} \bar{e}^{-\frac{\ell}{L}}$ has been neglected since it has a very small value.

Assuming $\frac{\ell}{L} = \frac{1}{20}$, the total energy of the ions is $\frac{9 N_i V_c}{10}^{20}$.

Thus, it appears that the neutrals carry more energy than the ions and therefore, they can no longer be neglected as they play an important role in the ion plating process.

Using the above expressions for 3 kV bias voltage, the lowest neutral energy is approximately 7 eV and the highest about 300 eV. The average energy is around 150eV.

Experimental work in the following chapters proved that despite all the assumptions, these results are extremely accurate.

2.6. The Role of Energetic Neutrals in Obtaining Adhesive Films

Looking for an explanation for the very good adhesion of ion plated films onto any kind of substrate, Mattox[2] expressed the opinion that the clean surface and the graded interface are the main reasons, by causing a good metallurgical bond and dispersing stresses due to e.g. different thermal expansion coefficients of film and substrate.

In ion plating, the clean surface is obtained during the sputter cleaning process and at the same time, defects are induced into the substrate lattice creating very dense nucleation centres, a phenomenon often called 'ion etching'. This ion etching process has been considered to be the result of surface bombardment with high energetic ions.

The other factor leading to a good adhesion, that is the deep graded interface, is easy to explain in the case of alloying substrate-film materials, as being due to the enhanced diffusion induced by the local heating created by the bombardment with energetic particles[21].

For noncompatible materials, the explanation given was ion implantation[21]. However, even for energies of 5keV, the depth of implantation cannot be more than 50Å [22].

But the ions will lose energy in collisions with

neutrals and therefore they will reach the cathode with energies smaller than the acceleration energy, and therefore ion implantation cannot be responsible for the graded interface.

As calculated in the previous chapter and concluded by Teer[20], it appears that ion plating is the deposition of a small number of ions and a large number of neutrals their mean energy being sensibly similar and of the order of 100 - 150eV for 3kV bias voltage.

The following experiment[23] was aimed to prove the important role played by the energetic neutrals in obtaining adhesive films in the ion plating process. The apparatus is shown in Figure 2.6.1. The H.T. cathode is a fine wire mesh and the substrate is at earth potential and placed a few millimeters behind the mesh. A part of the substrate (A) was shadowed by the mesh and the other part (B) was unshadowed and subjected to direct evaporation.

The experimental conditions were:

- Mesh potential -4kV
- Substrate potential 0
- Argon gas pressure 10mtorr

The glow discharge between the earthed parts of the rig and the mesh was maintained for 50 minutes, and the current to the mesh and substrate were measured. The substrate, made of copper, which was previously ultrafinely polished, was then examined by means of an oil immersion optical microscope which indicated

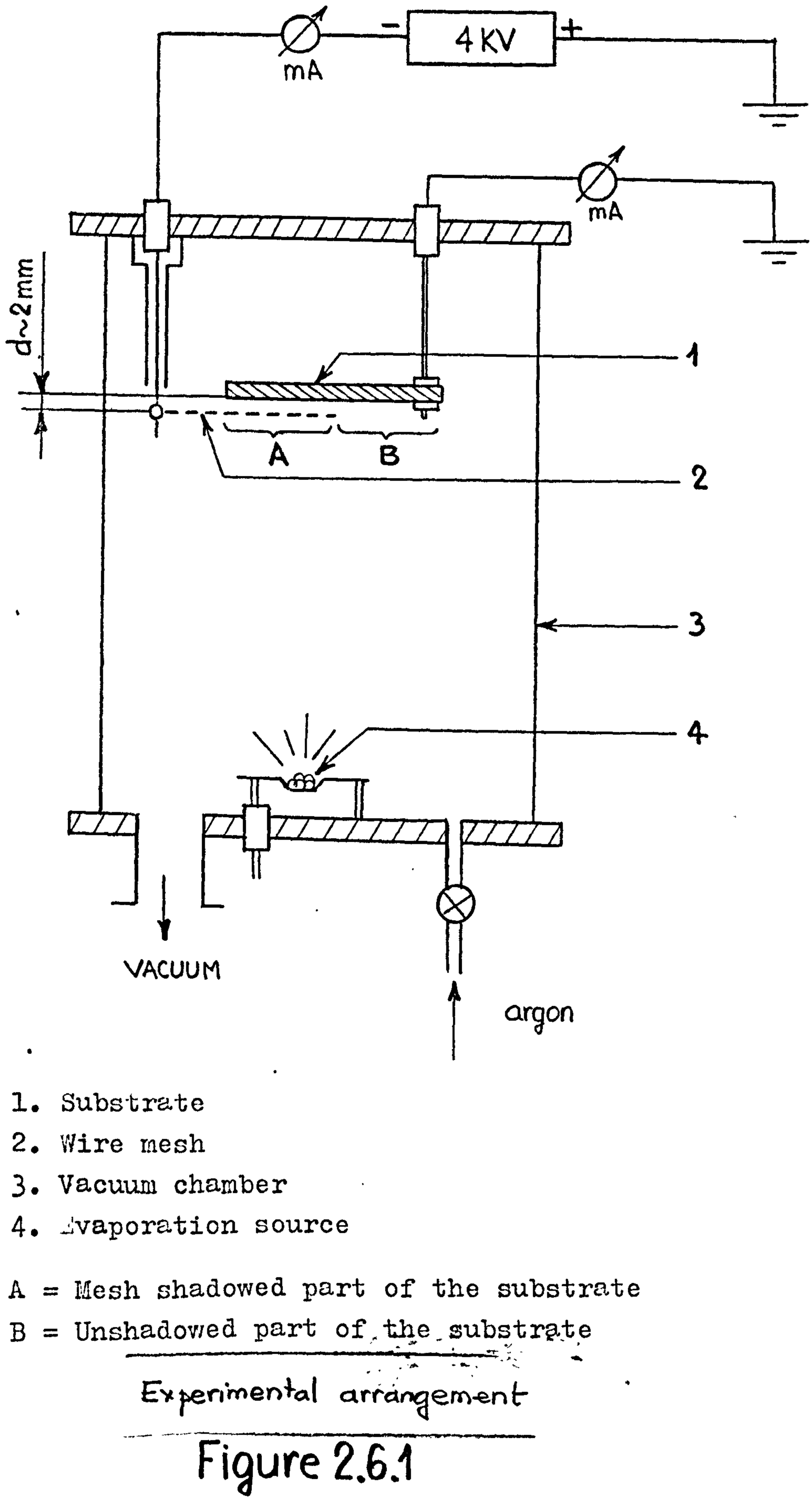

1. Substrate
2. Wire mesh
3. Vacuum chamber
4. Evaporation source

A = Mesh shadowed part of the substrate

B = Unshadowed part of the substrate

Experimental arrangement

Figure 2.6.1

that the substrate surface was deeply etched due to the bombardment as shown in Figure 2.6.2.
Durring the bombardment, the current to the mesh dropped to a steady value of 6mA. A net flow of electrons drawing a current of -0.4mA was measured to the substrate.

New substrates of copper and steel were then placed behind the mesh, and following 50 minutes of discharge at 10mtorr argon pressure and 3kV bias voltage, silver was evaporated from a molybdenum boat. The substrates were coated behind and away from the mesh. During deposition, the current to the mesh dropped to 1mA, while no current could be detected to the substrate.

The scratch tests using a modified microhardness tester and a diamond indentor, were performed on the films deposited on both regions and were then examined by means of a scanning electron microscope and the results are presented in Figure 2.6.3. and 2.6.4.

Figure 2.6.3.a shows the very good adhesion obtained for silver deposited on copper behind the mesh, and Figure 2.6.3.b shows the scratch track of the silver film deposited on the unshadowed part of the copper substrate.

Behind the mesh, the adhesion is similar to that obtained by conventional ion plating while, away from the mesh, the adhesion is very poor, similar to that of vacuum evaporated films.

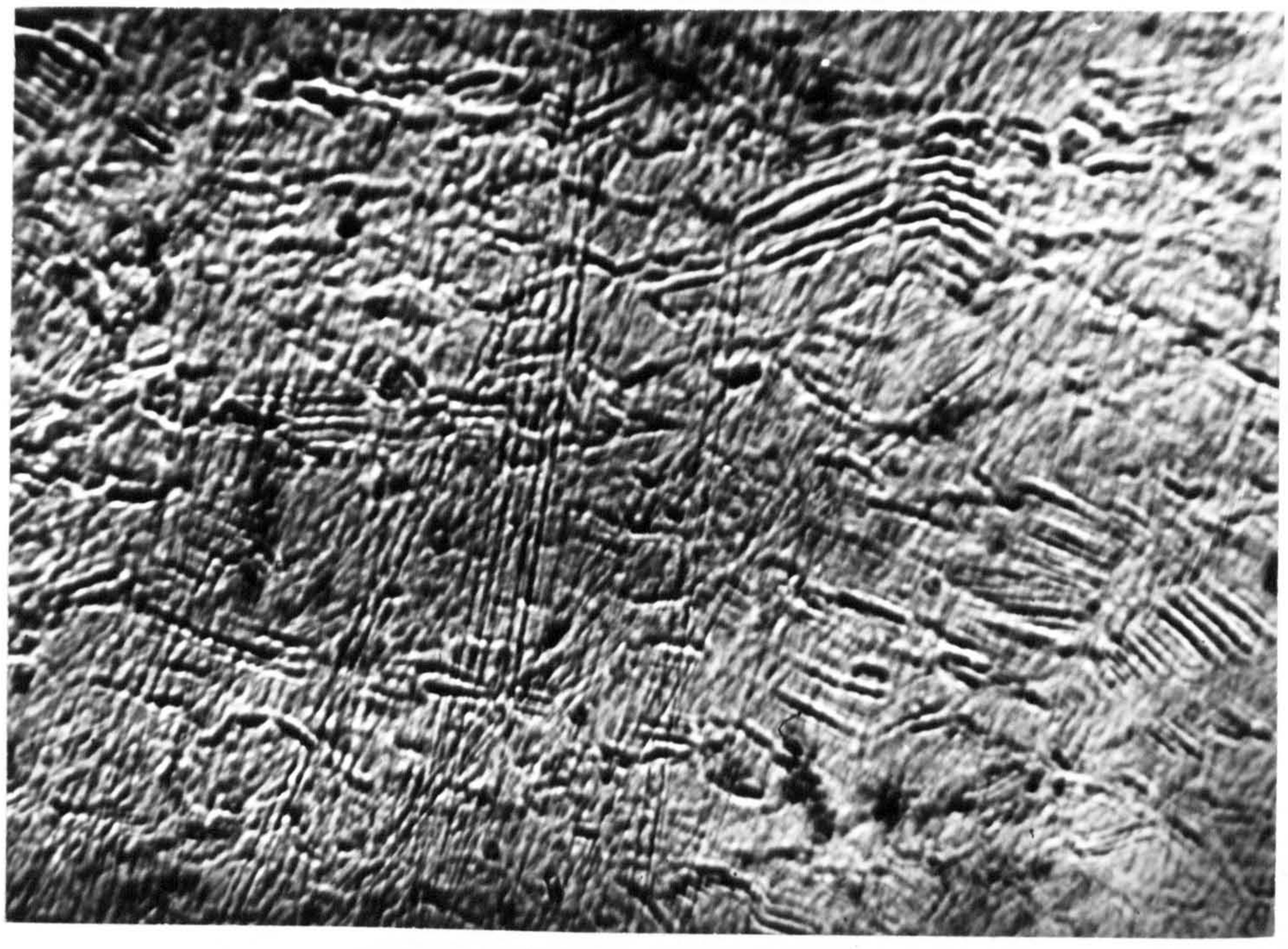

x 2000 (optical)

Figure 2.6.2

Etched Copper surface behind the mesh

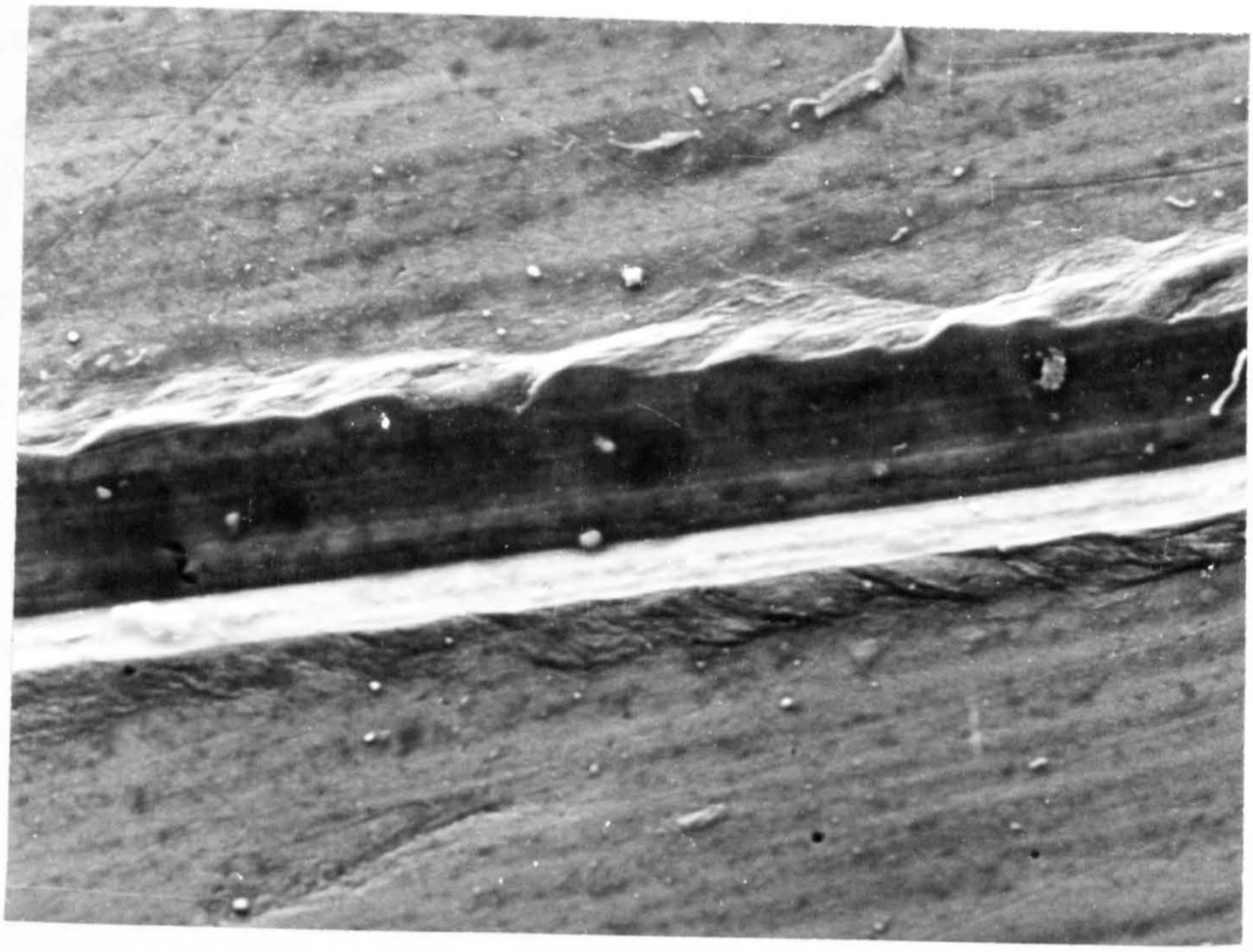

a) Behind the mesh

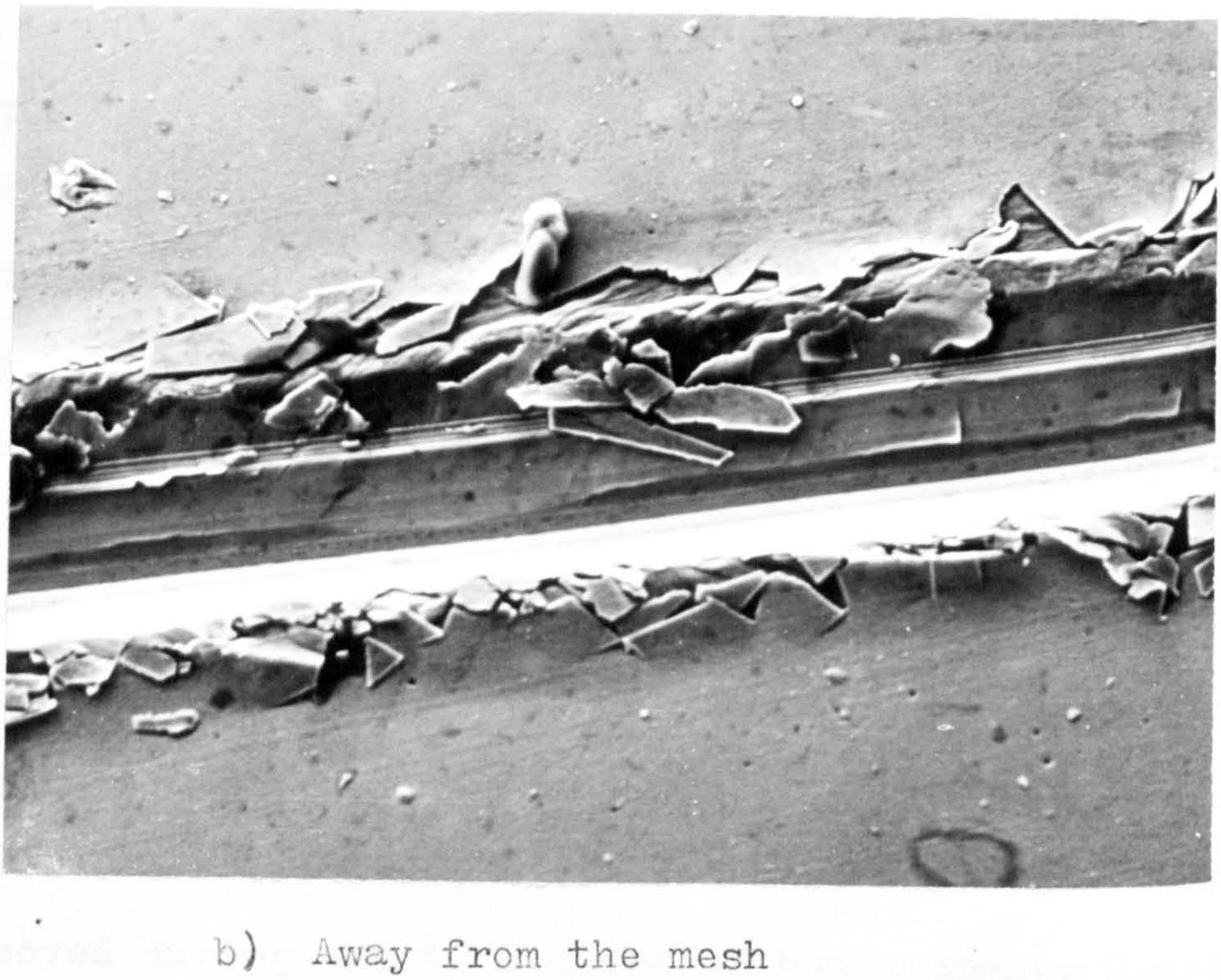

b) Away from the mesh

Figure 2.6.3

Silver on Copper - Scratch test (diamond)

Figure 2.6.4.a & b show the scratch track for silver films deposited on steel,and the adhesion of the film is also very good behind the mesh and poor away from it.

Figures 2.6.5. and 2.6.6. were obtained by performing the same test but using a hemispherically ended steel indentor and the results are comparable showing that the film deposited away from the mesh is not adhesive and brittle while the one deposited behind the mesh is adhesive and ductile.

As seen from these micrographs, the characteristics of the films deposited behind and away from the mesh are very different. The poor adhesion obtained on those parts not shadowed by the mesh, was to be expected since the films were produced under conditions equivalent to a vacuum or gas evaporation which is known to be a method giving nonadhesive films. Regarding the films deposited behind the mesh, their adhesion proved to be the same as for ion plated films. In the case of silver and copper, the enhanced diffusion could be the reason for the good adhesion since silver and copper are compatible and can alloy. But the oxides on the copper surface represent a barrier to diffusion, therefore they must have been removed during the 50 minutes of bombardment. Since the substrate was earthed, no ions could have penetrated through the mesh and the low current of electrons was unable to sputter clean the copper surface. It results that the copper was bombarded

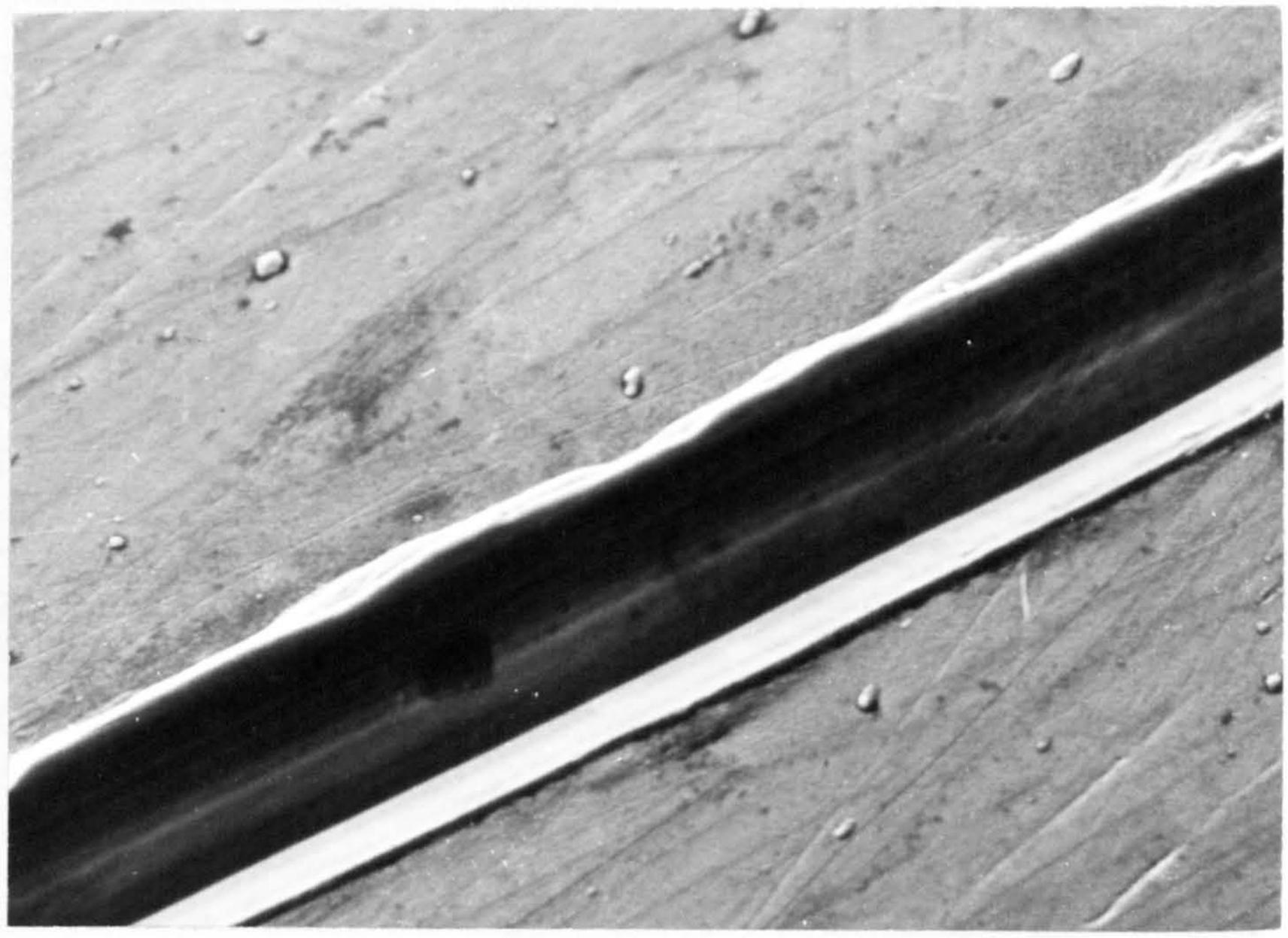

a) Behind the mesh

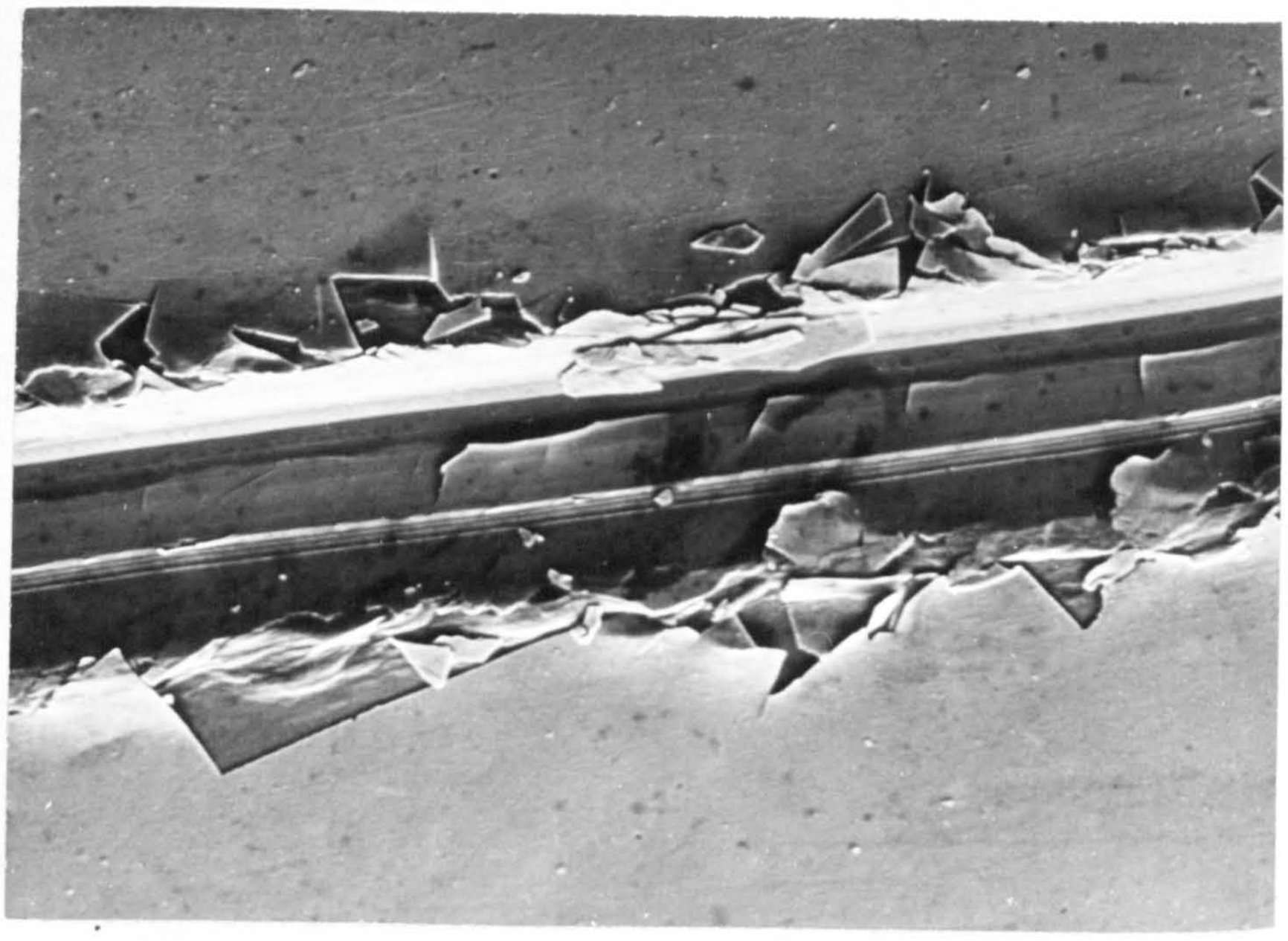

b) Away from the mesh

Figure 2.6.4

Silver on steel - Scratch test (diamond)

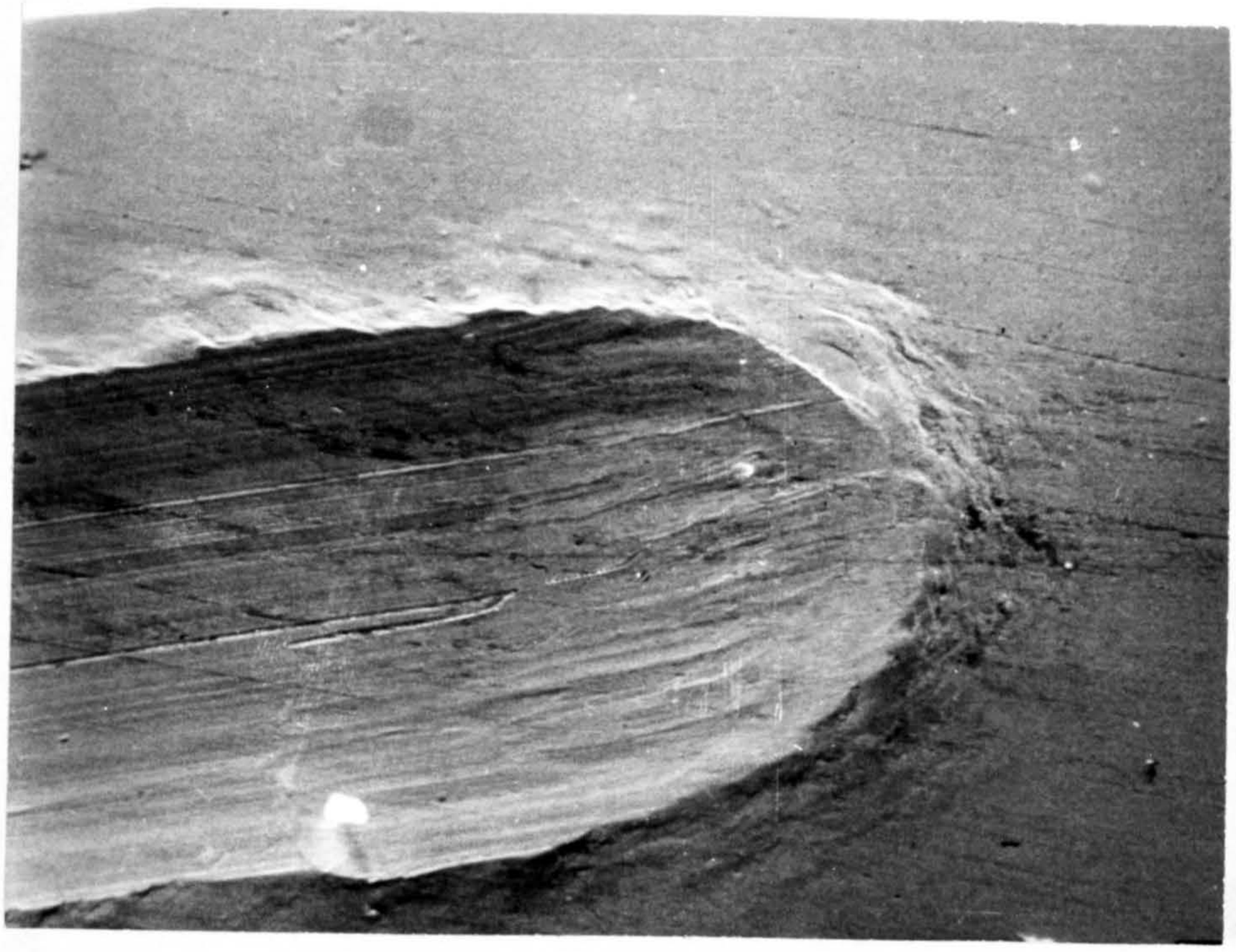

a) Behind the mesh

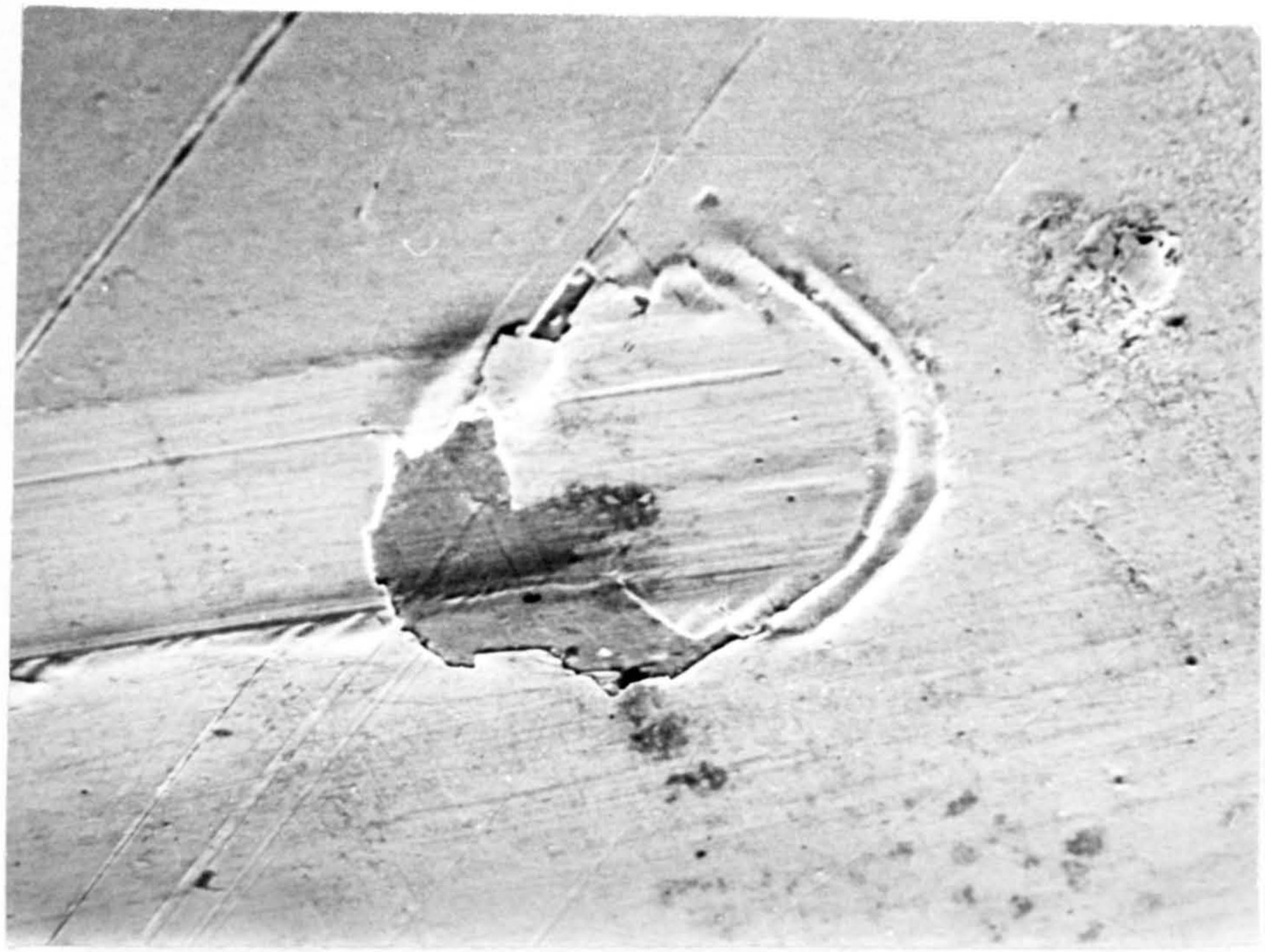

b) Away from the mesh

Figure 2.6.5

Silver on Copper - Scratch test (ball)

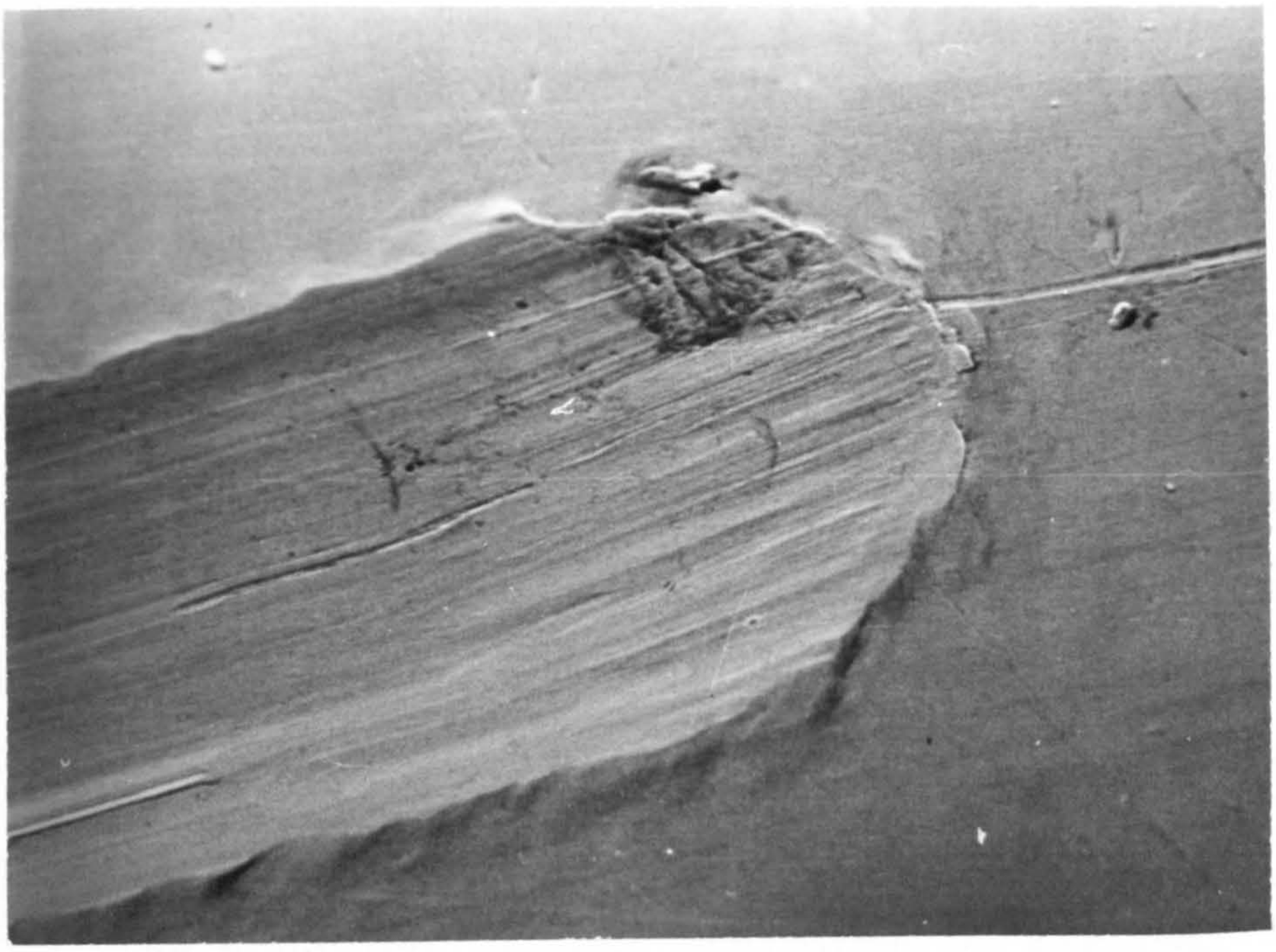

a) Behind the mesh

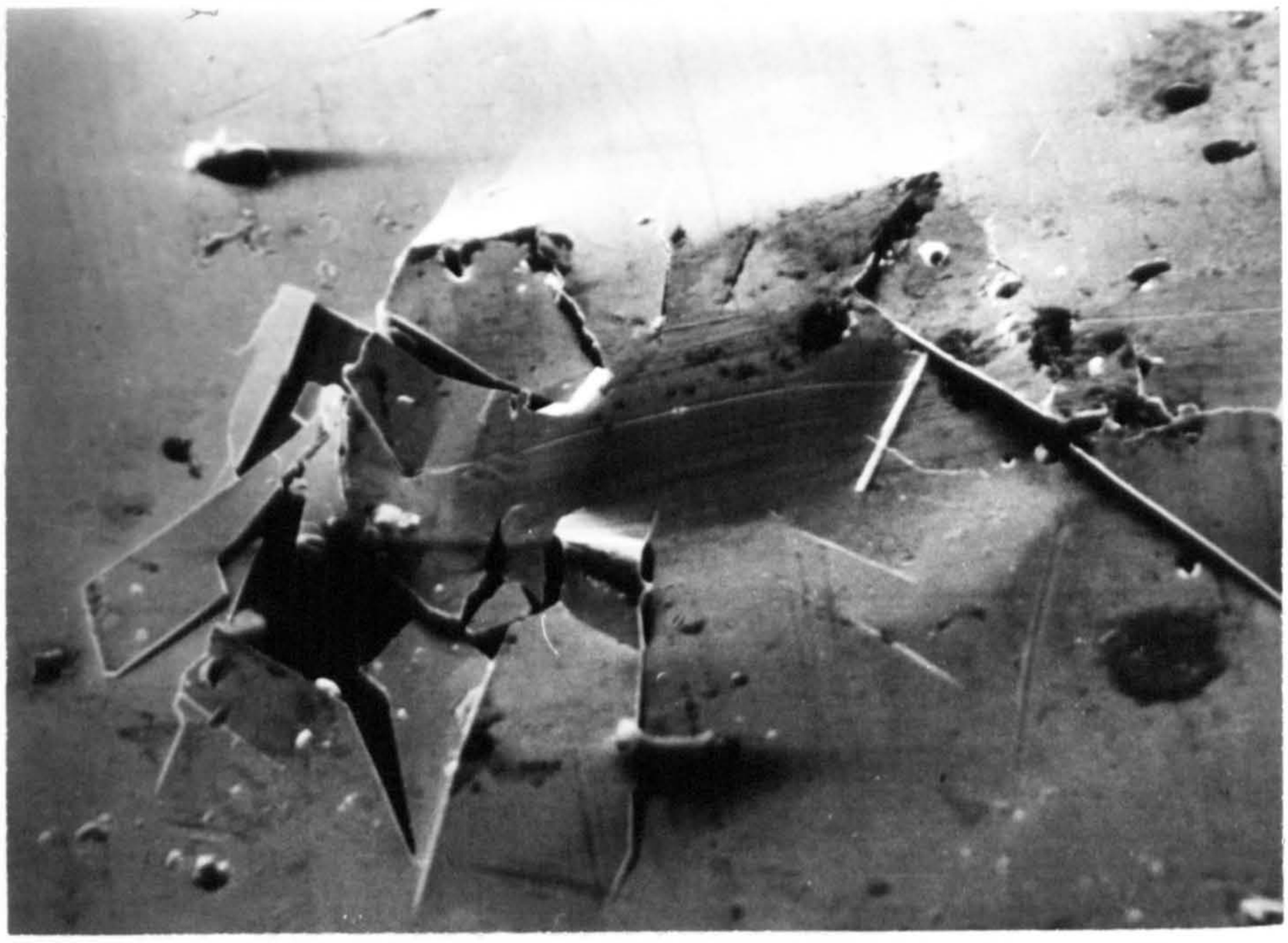

b) Away from the mesh

Figure 2.6.6

Silver on steel - Scratch test (ball)

by energetic neutrals and that the deposition was by energetic neutrals as well.

Regarding the silver deposited on steel behind the mesh, the adhesion was extremely good although the two materials are incompatible and therefore diffusion cannot occur. The explanation for the very good adhesion must be that the cleaning of the substrate was by energetic argon atoms and that the deposition was by energetic silver atoms.

There is a possibility of existing negative ions, but their number must be so small that they could not affect the adhesion, a fact explained by the low negative current drawn by the substrate. This current measured to the substrate was due to secondary electrons emitted by the mesh under bombardment with energetic particles.

Being proved that the energetic neutrals play an extremely important role in the adhesion for ion plated films, further work is required to determine the number of energetic neutrals as well as their energies.

It has been observed that when the evaporation is started, it is followed by a drop in the cathodic current indicating less ions going to the cathode (usually a 50% drop).

However, the ionization potential for argon is 15.7eV while most of the evaporated metals have ionization potentials of 4 - 10eV. Therefore it would be expected that the metal atoms to be easily ionized

in the plasma followed by a rise in the cathodic current.

The explanation for the drop in the ion current could lie in the fact that the evaporation rate is higher than the ionization capacity of the plasma, or it could be due to the fact that the metal vapours will group to form fine particles (clusters) and are more difficult to be ionized.

But, despite the low ionization efficiency,the good adhesion obtained must be due to the energetical neutrals

2.7. Energies of the Particles Involved in the Ion Plating Process

The following experiment was performed in order to determine the number of atoms reaching the cathode, their energy and also the energy carried to the substrate by the neutrals. The idea was to separate the ions from the neutrals, to determine their participation to the total power of the glow discharge and then, to simulate the power inputs by direct, equivalent,heat inputs. Thus, it is possible to determine the real power inflicted in the cathode by ions and neutrals and also to determine the energy lost in the process.

The arrangement which is schematically shown in Figure 2.7.1, was set in a vacuum chamber. The substrate is earthed and incorporates a heating resistor and a thermocouple T_1 which measures the bulk temperature. The substrate is earthed through an A-meter. By connecting a power supply to the contacts 'c' and 'd', the substrate can be indepen-dently heated and its bulk temperature measured with T_1. The substrate is made of copper and its dimensions are: 35 x 31 x 9cm.

A wire mesh with a diameter of o.3mm is fixed on a ceramic holder,and at a distance of 2 mm in front of the substrate.

The mesh is connected to the H.T. supply and

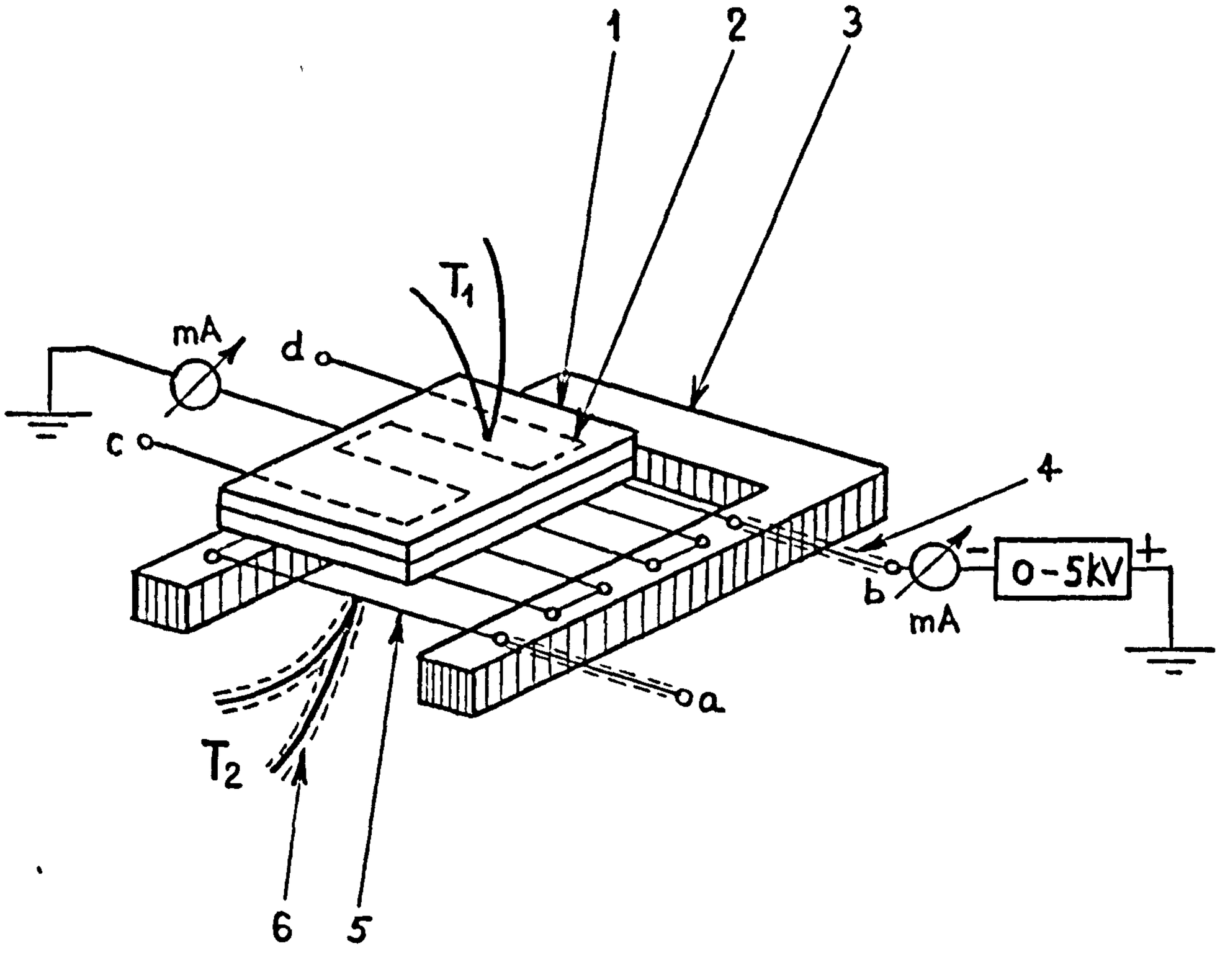

1. Earthed substrate
2. Heating resistor
3. Ceramic support
4. Shield
5. Wire mesh
6. Shield

T_1, T_2 - Thermocouple

Figure 2.7.1

Experimental arrangement

represents the cathode of the glow discharge. It can also be heated separately by connecting a power supply between the contacts 'a' and 'b'. In contact with the mesh, there is a thermocouple T_2 that measures its temperature. The thermocouple wire which is also connected to the H.T. was carefully screened so that the discharge is confined to the mesh only.

The geometrical transmission of the mesh 'A' is 92% which means that 92% of the neutrals will pass the mesh and strike the earthed substrate.

Assuming that the equipotential lines make a 90° angle as shown in Figure 2.7.2., it means that approximately 1/4 of the total number of secondary electrons emitted by the mesh will go to some other earthed parts of the system rather than to the substrate.

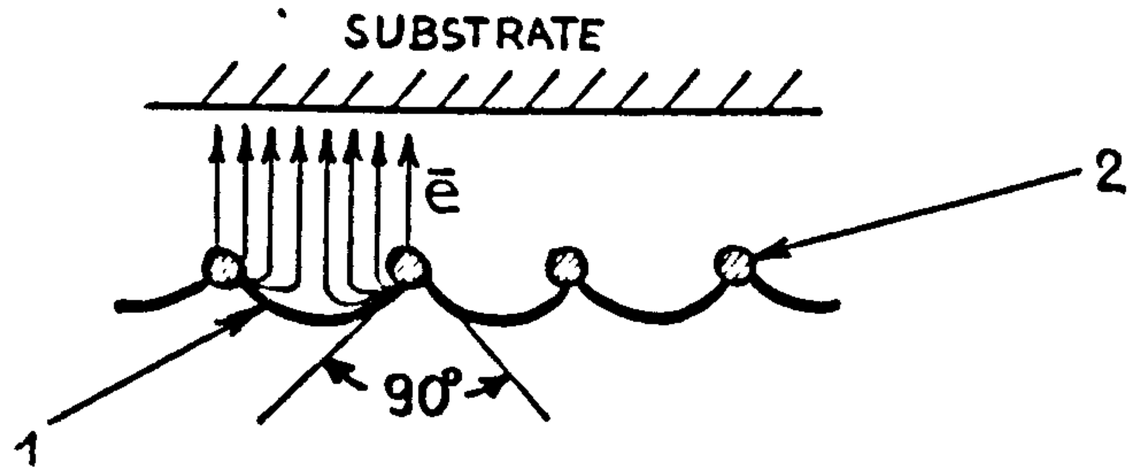

1. Equipotential lines
2. Wire mesh

Figure 2.7.2.

In the first stage of the experiment, after pumping the whole system to a pressure of 10^{-6}torr, argon is let in and a pressure of 10 mtorr is established in the chamber.

Then,the glow dischrge is struck between the remote earthed parts of the system and the cathode mesh. The dischrge is maintained to a certain power until the substrate and the mesh reach constant temperatures which are recorded. Then, the power is increased in steps (by increasing the bias voltage) followed by the same procedure as described above.

Figure 2.7.3. presents the temperatures of the mesh and substrate plotted versus discharge power.

Secondary electron current to the earthed substrate is measured and plotted versus discharge power in Figure 2.7.4.

The discharge power means the power calculated after making the correction for the electronic current (which must be substracted from the total cathodic current).

If Ie is the electronic current measured to the substrate and assuming that 1/4 of the electrons go to some other parts of the system, then the total electronic current leaving the cathode is 5/4 Ie.

The current to the mesh is given by the arriving positive ions and by the secondary electrons leaving the mesh. The discharge power will be:

$$W_G = (I_c - \frac{5}{4} I_e) \cdot V \quad \text{(watt)}$$

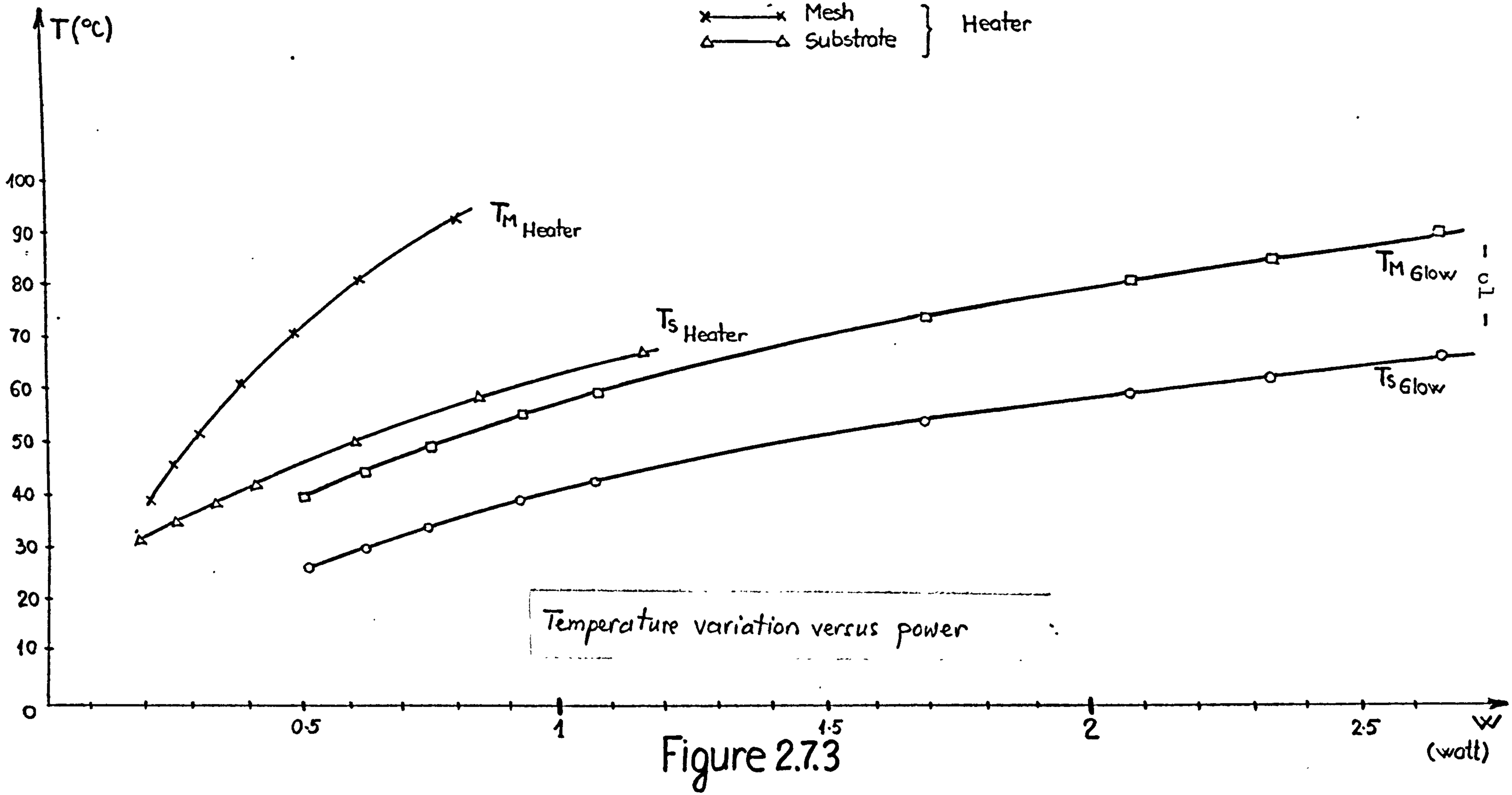

Temperature variation versus power

Figure 2.7.3

Electronic current versus power and kV

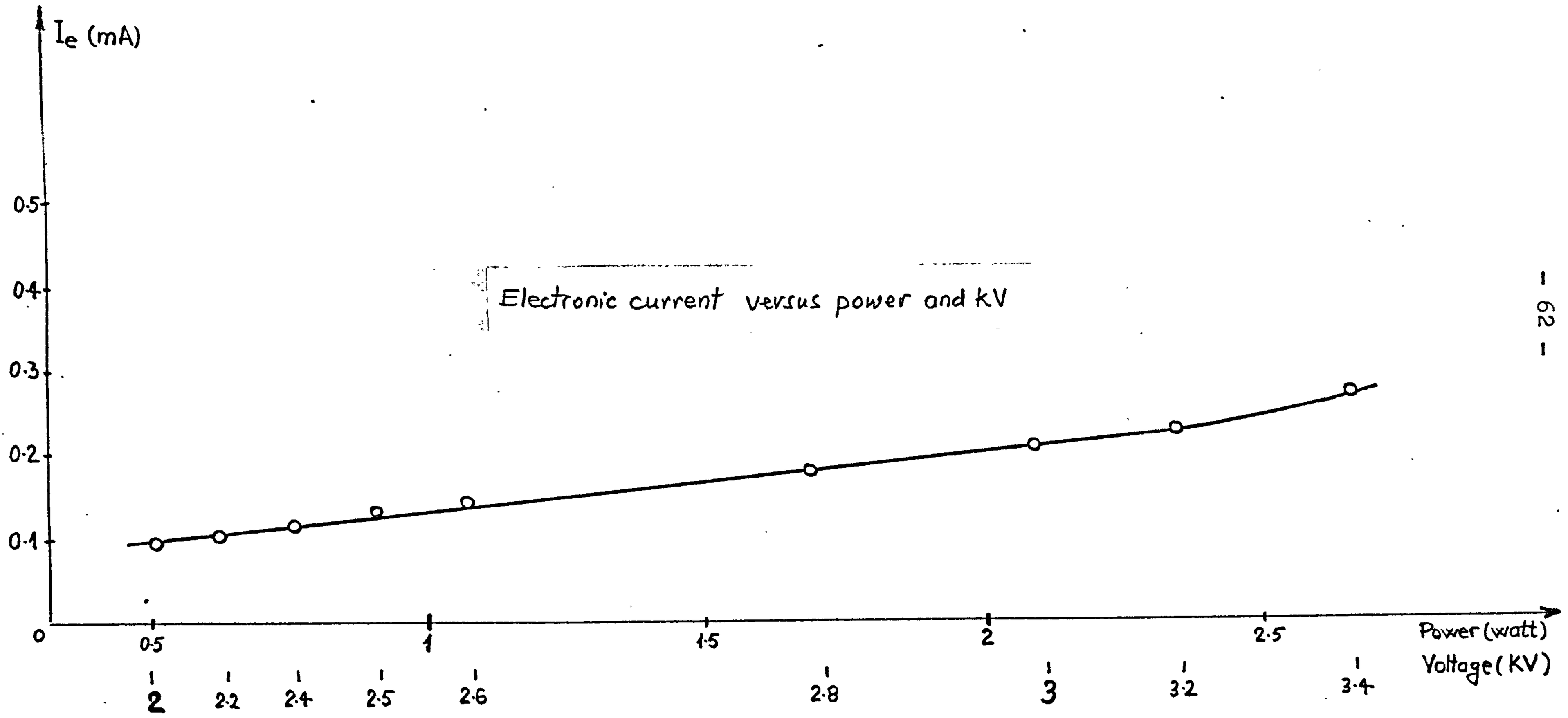

Figure 2.7.4

I_c is the total cathodic current (A)

V is the bias voltage (V)

The second stage of the experiment is to heat both the mesh and the substrate (by means of the resistive heating) and the power is adjusted to obtain temperature pairs correspondent to those obtained by glow discharge bombardment. These temperatures are plotted versus heating power in Figure 2.7.3.

The heating powers represent the real power of the neutral and ion bombardment, the difference representing the power lost in the process.

The mesh is subjected to the bombardment by 100% of the ions and 8% of the neutrals, while the substrate is bombarded by 92% of the neutrals and the secondary electrons.

Choosing a certain discharge power, two corresponding temperatures are determined on T_{SGlow} and T_{MGlow} curves, and corresponding to these temperatures on $T_{SHeater}$ and $T_{MHeater}$ curves (Figure 2.7.3.), it is possible to determine the power inflicted by direct heating which represents the real power of the ion and neutral bombardment. Adding these two values and substracting them from the correspondent value of discharge power, the result represents the power lost in the process.

Since the two heaters were kept on simultaneously for a sufficiently long period of time and the powers adjusted continuously to give the two

correspondent temperatures, the power loss is not due to heat lost through radiation and convection. The Power loss is plotted versus voltage in Figure 2.7.5.

Since the argon pressure was kept constant at lo mtorr it can be noticed that increasing the voltage over 2.5. kV, the power loss reaches a steady value of 30%. This loss in power is explained later in this chapter (2.10).

Using the results plotted in Figure 2.7.3., it is easy to calculate the energies of ions and neutrals as percentages of the total discharge power, after substracting the losses, and these are presented in Figure 2.7.6.

From figure 2.7.6., it can be concluded that for a 3 kV bias voltage,around 60% of the total energy (ions + neutrals reaching the cathode) is carried by neutrals and considering that the 30% loss in power is due to the neutrals being scattered to other parts of the system, it results that the ions will transfer ~ 75-80% of their energy to the neutrals which coincide with Teer's results[20]. With these figures available, energetic neutrals cannot be neglected any more and it is important to determine their number and energy spectrum, as well as their role in obtaining the adhesion of ion plated films.

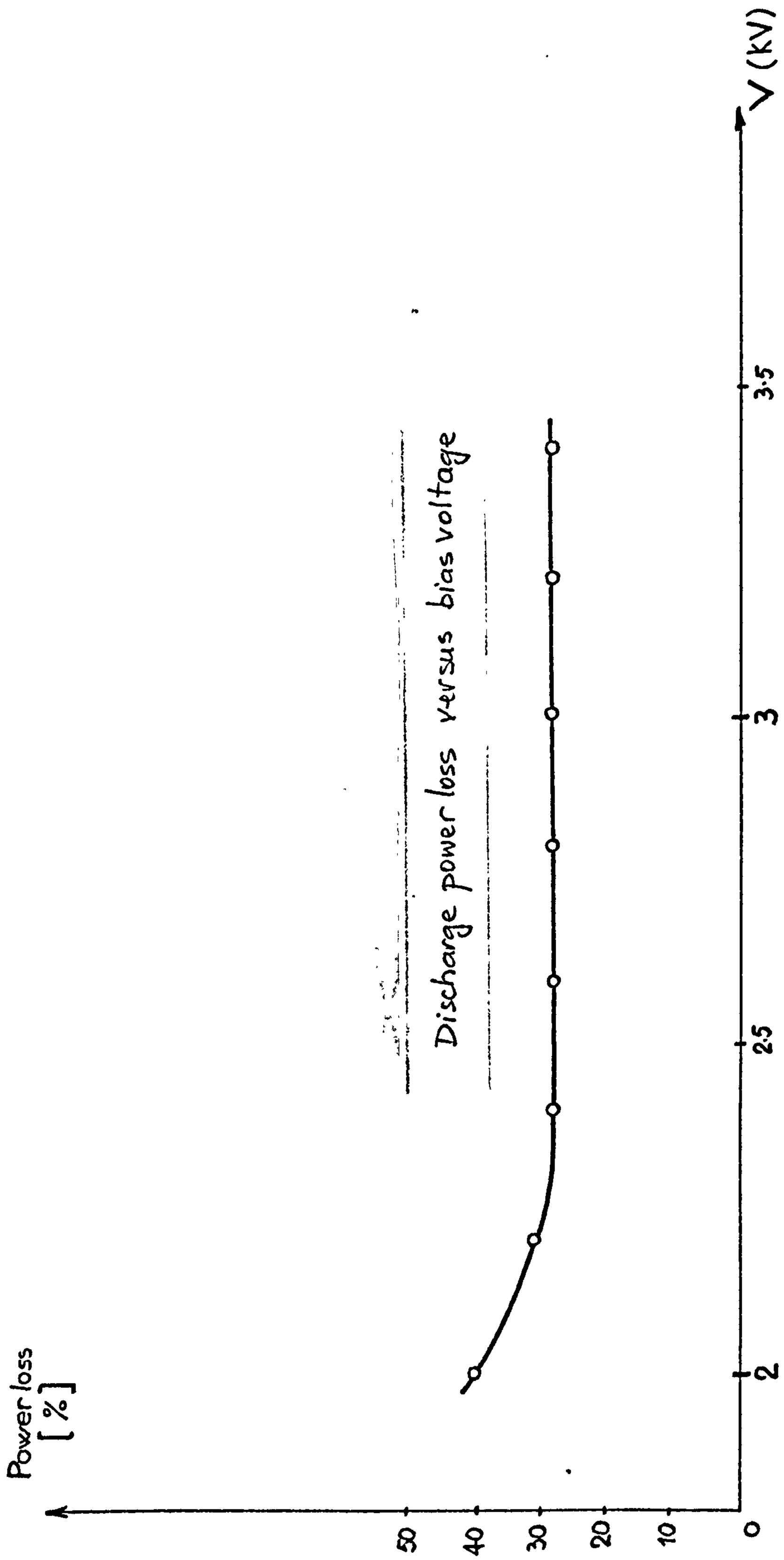
Power loss [%]
50
40
30
20
10
0
2
2.5
3
3.5
V (KV)
Discharge power loss versus bias voltage

Figure 2.7.5

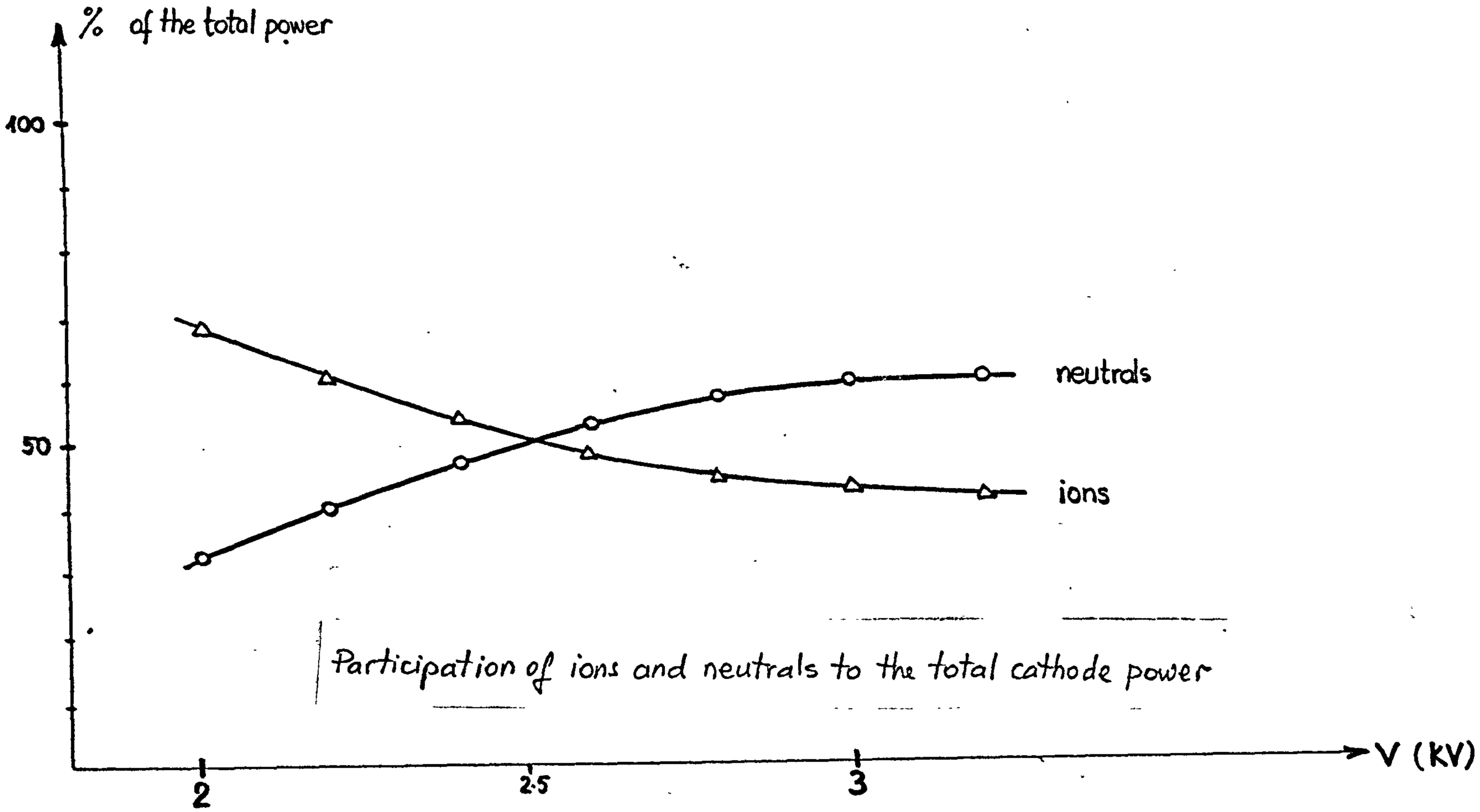

Participation of ions and neutrals to the total cathode power

Figure 2.7.6

2.8. Ionization Efficiency

Initially, ion plating has been defined as being the deposition of high energetic metal ions on a clean substrate. The metal ions followed the electric field lines which was the only explanation for the throwing power.

Different authors[24,25] estimated the ionization efficiency and controversial figures have been reported ranging from 1% up to 30%, and in the case of using an arc evaporation source even 50%.

Since film thickness on the back surface was found to be around 30% of the thickness on the front surface, it was considered that this was caused by the fact that 30% of the metal atoms being ionized will follow the field lines and will deposit onto the back surface. However, recent experiments using gas evaporation (evaporation in a gas atmosphere at pressures comparable to those used in ion plating) indicated that even in this case, when there is no electric field, due to the gas scattering effect, hidden surfaces are coated with a thickness of around 30% of that on the front surface[6].

Therefore, it appears that the throwing power of ion plating is more due to gas scattering and less due to the ions following the field lines.

The ionization efficiency can be calculated as being the percentage of ions in the total number of

particles striking a square centimetre of the cathode surface in a second.

Using the results previously obtained from the ion current to the mesh (after substracting the electronic current), it is possible to calculate the number of ions striking the mesh, knowing that $1A = 10^{19}$ ions per second.

The total area of the mesh subjected to the ion bombardment being 3.5 cm^2, the current density N_i $(\frac{ions}{sec.cm^2})$ can be calculated.

From the kinetic theory of gases, for a given gas pressure 'p', the number of collisions received by a square centimeter of surface is :

$$N_{np} = \frac{1}{4} n\bar{u} \qquad (2.8.1)$$

where 'n' is the number of molecules in a cubic centimeter and 'u' is the mean velocity of the molecules.

If the components of the velocity 'c' of a typical molecule (argon) along rectangular axes , perpendicular to and parallel to the surface are u,v,w, then:

$$c^2 = u^2 + v^2 + w^2 \qquad (2.8.2.)$$

Having no preferred directions in the gas, the mean values of u^2, v^2 and w^2 taken for all the gas molecules will be equal.

$$c^2 = 3u^2 \qquad (2.8.3.)$$

It results:

$$u^2 = \frac{c^2}{3} \qquad (2.8.4.)$$

which is the component perpendicular to the wall.

From the theory of gases :

$$mNoc^2 = 3RT \qquad (2.8.5.)$$

From (2.8.5.) it results :

$$c^2 = \frac{3RT}{mNo}$$

It follows :

$$u = \frac{RT}{mNo} \qquad (2.8.6.)$$

Introducing u in (2.8.1.) it results :

$$Nnp = \frac{1}{4} n \frac{RT}{mNo} \qquad (2.8.7.)$$

Where :

- No represents the number of molecules in a cubic centimetre of gas at atmospheric pressure

  $No = 2.68 \times 10^{19} \frac{mol}{cm^2}$

- R is the gas constant

  $R = 8.31 \times 10^{7} \frac{g.cm^2}{sec}$

- T is the absolute temperature of the gas

  $T = 296^{o}K$

Another method of calculating Nnp is the following: the force with which a molecule is striking a wall, integrated over a second is :

$$f = 2m\bar{u} \frac{gf}{s} \qquad (2.8.8.)$$

where : m is the molecular mass

u is as calculated from (2.8.6.)

In the given pressure conditions 'p' ($\frac{g}{cm^2}$), the force applied on a square centimetre of the wall is :

$$Fp = p \cdot g \left(\frac{gf}{cm^2} \right) \qquad (2.8.9)$$

The number of molecules necessary to strike 1 cm^2 of the wall in order to obtain an applied force equal to Fp is :

$$Nnp = \frac{Fp}{f} = \frac{pg}{2m\bar{u}} \qquad (2.8.10)$$

Nnp is plotted versus pressure in Figure 2.8.11. The ionization efficiency will then be :

$$Ief = \frac{Ni}{Nnp} \; x\_100 \; \% \qquad (2.8.12.)$$

Its values are plotted versus voltage in Figure 2.8.13. and versus pressure in Figure 2.8.14. As it can be noticed, for voltages under 2.5 kV, the ionization efficiency has extremely low values followed by an increase to a nearly steady value of 0.08 - 0.1% for voltages exceeding 4.5 kV. The usual ion plating voltages being 3 - 5 kV, the ionization efficiency is 0.03 - 0.1 %

The conclusion is that the ions are in a very small number compared to the total number of particles striking the cathode surface.

Analysing Figures 2.8.13. anf 2.8.14. it can be noticed that alteration of pressure gives little change in the value of ionization efficiency. Therefore, the only means to control ionization efficiency in a classical diode system, is by varying the bias voltage which however, cannot bring a substantial increase in efficiency.

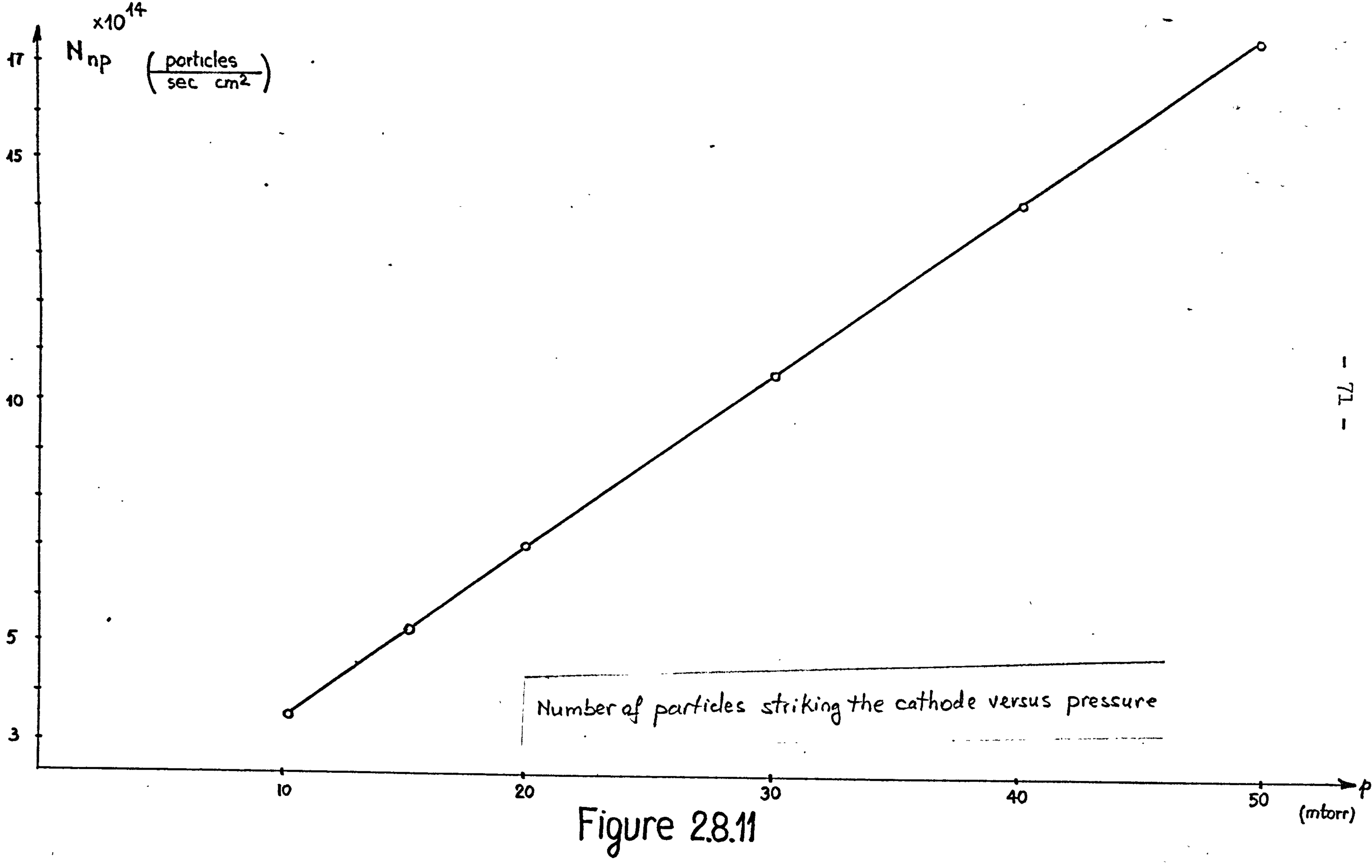

Number of particles striking the cathode versus pressure

Figure 2.8.11

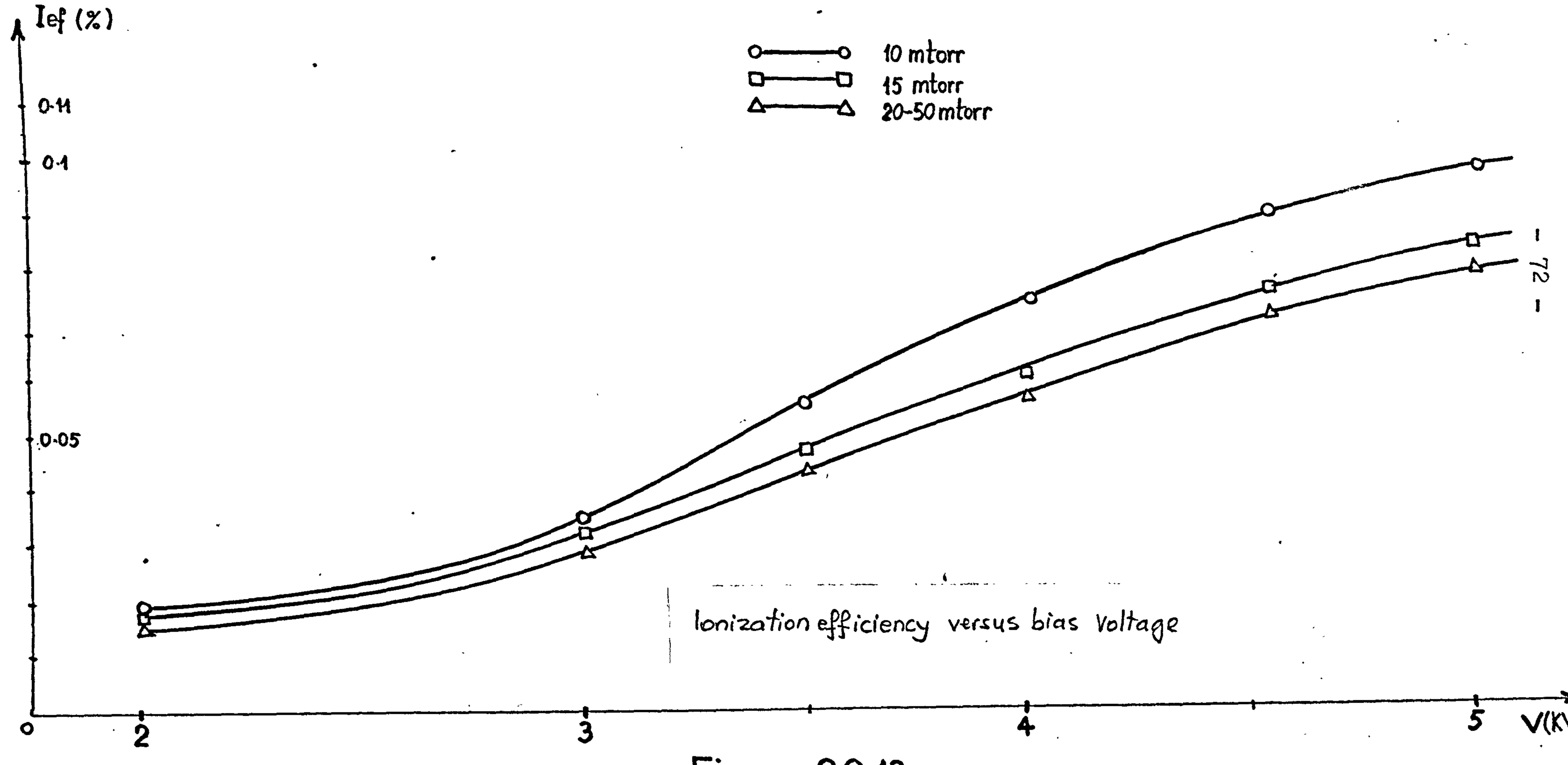

Ionization efficiency versus bias voltage

Figure 2.8.13

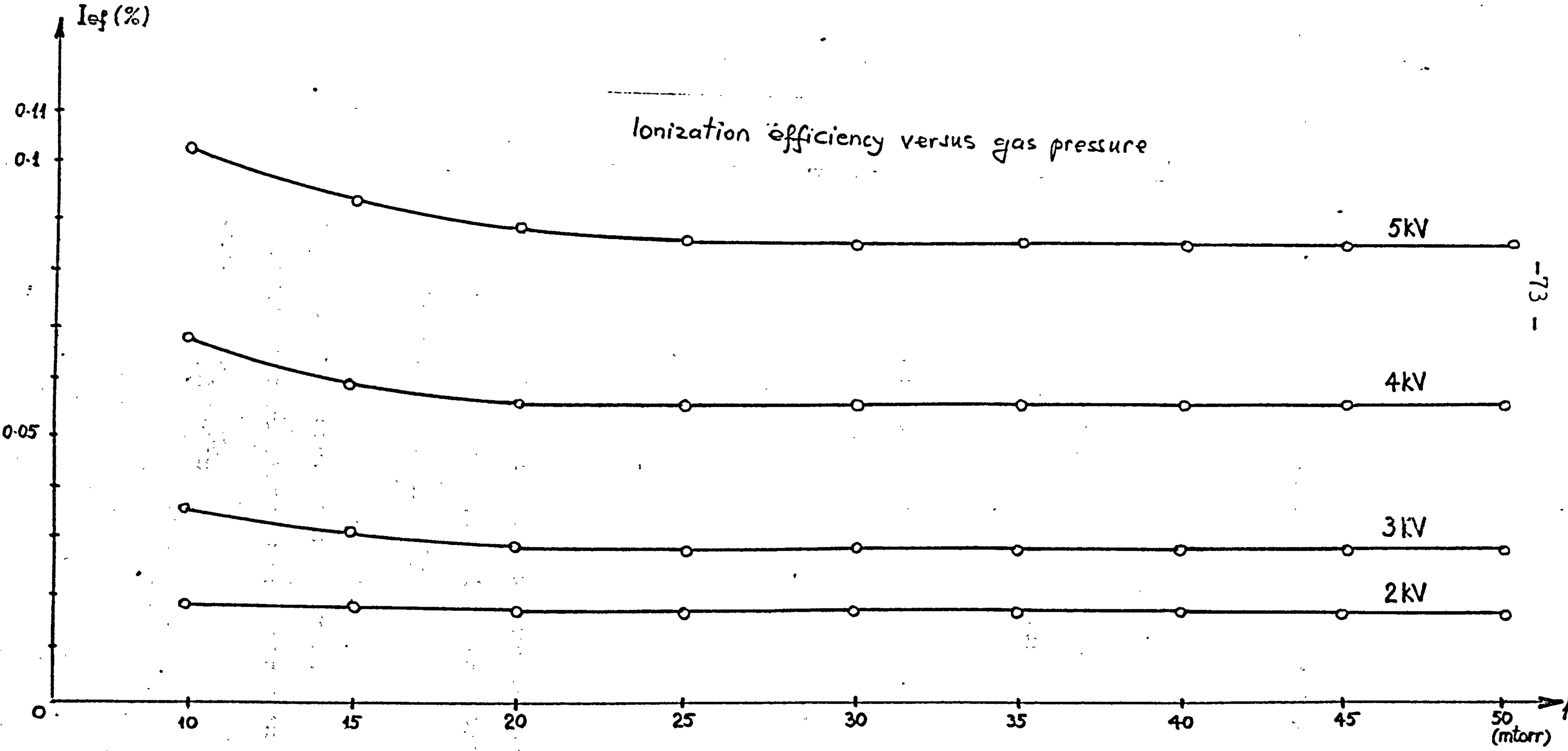
Ief (%)
0.11
0.1
0.05
0
Ionization efficiency versus gas pressure
5kV
4kV
3kV
2kV
10
15
20
25
30
35
40
45
50
(mtorr)

Figure 2.8.14

2.9. Neutrals Energy

Using the results presented in Section 2.7., it results that there are :

N_i = the number of ions striking the cathode surface with their mean energy $\bar{e}V_i$

N_n = the number of energetic neutrals striking the cathode-substrate surface with their mean energy $\bar{e}V_n$

Since the arrangement separates the neutrals from the ions and the mesh has a geometrical transparency A, it means that A % of the neutrals will pass through and strike the substrate behind the mesh. Therefore :

N_i = the number of ions striking the mesh and their total energy is $N_i \bar{e}V_i$

$\frac{100-A}{100} N_n$ = the number of energetic neutrals striking the mesh and their total energy is $\frac{100-A}{100} N_n \bar{e}V_n$

$\frac{A}{100} N_n$ = the number of energetic neutrals striking the substrate and their total energy is $\frac{A}{100} N_n \bar{e}V_n$

N_e = the number of secondary electrons striking the substrate and their total energy is $N_e \bar{e}V_e$

From Figure 2.7.3. , we can determine the heat inputs L_M to the mesh and L_S to the substrate simulated by the resistive heating which will be equal to the heat inputs due to ion, neutral and electron bombardment.

$$L_M = N_i \bar{e}V_i + \frac{100-A}{100} N_n \bar{e}V_n \qquad (2.9.1.)$$

$$L_S = \frac{A}{100} N_n \bar{e}V_n + N_e \bar{e}V_e \qquad (2.9.2.)$$

A = 92 %

N_i $(\frac{\text{ions}}{\text{sec.cm}^2})$ is obtained from the cathodic current minus the electronic current Ie.

The energetic neutrals being a result of ion-neutral collisions, their number N_n is a function of N_i. Assuming that every collision takes place after an ion has crossed a mean free path, it results:

$$N_n \sim kN_i \qquad (2.9.3.)$$

where k is a factor depending on the length of the cathode dark space 'L' and the mean free path 'ℓ' for a given pressure:

$$k = \frac{L}{\ell} \qquad (2.9.4.)$$

'L' has been previously plotted for different p-V conditions and 'ℓ' can be easily calculated using the following expression :

$$\ell = \left(\frac{N}{V} \pi \sigma^2 \sqrt{2} \right)^{-1}$$

or :

$$\ell = \frac{kT}{p \pi \sigma^2 \sqrt{2}} \qquad (2.9.5.)$$

where $\frac{N}{V}$ represents the number of molecules per unit volume

σ is the molecule diameter

k is the gas constant

T is the absolute temperature of the gas.

p is the gas pressure

The mean free path is defined as being the average length over which a gas molecule can travel without collision with another molecule and depends upon gas pressure and temperature.

The mean free path for argon and room temperature is plotted versus pressure in Figure 2.9.6. Using the values of the cathode dark space 'L' previously plotted (figures 2.4.5. and 2.4.6.), the values of $k = \frac{L}{\ell}$ were plotted for different voltages and argon pressures in Figure 2.9.7.

As it can be noticed, for a given bias voltage, there is no variation of the ratio $\frac{L}{\ell}$ in the pressure range 15 - 25 mtorr which means a constant yield of energetic neutrals.

For the particular conditions in which the experiment described in Section 2.7. was performed namely p = 10 mtorr, the mean free path is $\ell \simeq 0.47$cm

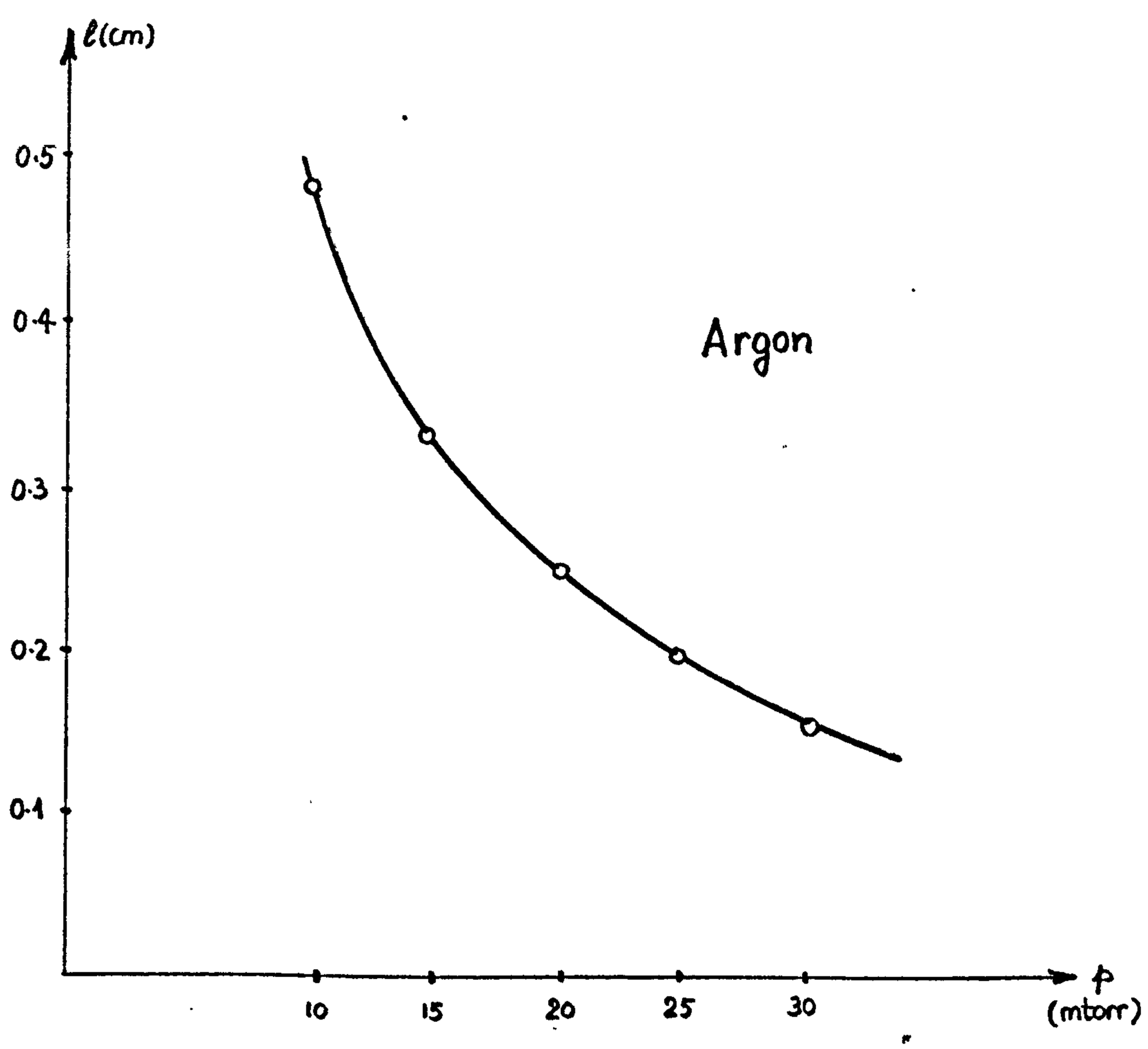

Figure 2.9.6

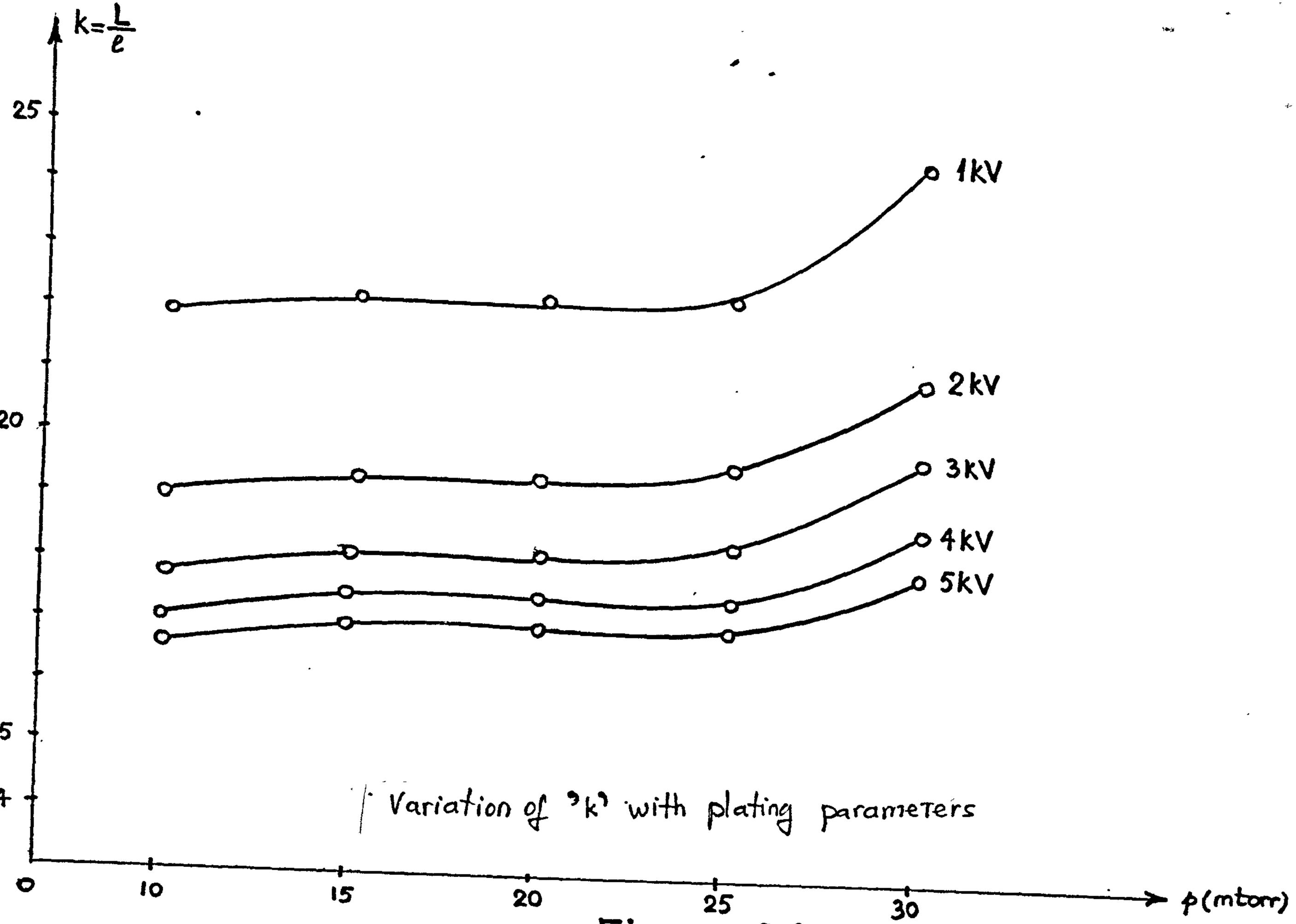

Variation of 'k' with plating parameters

Figure 2.9.7

The cathode dark space L can be divided into k equal intervals as shown in Figure 2.9.8.

Applying Davis and Vanderslice's theory[15], it results that an ion entering the cathode dark space must travel a length equal to the mean free path 'ℓ' before having the first collision with a neutral and this collision is a charge transfer collision. This means that the positive charge is transferred to the neutral which becomes an ion and is accelerated by the electric field across the next 'ℓ' space before having the next charge transfer collision with a neutral.

The previous ion, by losing its charge, becomes a neutral but it keeps the energy gained while accelerated across the first 'ℓ' space as an ion. Thus it becomes in fact, an energetic neutral and travels another ℓ space with this energy before colliding with a nonenergetic neutral in a billiard balls collision (share of energy and change of direction, so called 'scattering effect').

It means that, while crossing the cathode dark space (due to the electric field), an ion will generate a total number of energetic neutrals $n_{n\bar{e}}$

$$n_{n\bar{e}} = \sum_{n=1}^{k} (2^n - 1) = 2^{k+1} - (k+2) \quad \left(\frac{\text{energetic neutrals}}{\text{ion}}\right) \qquad (2.9.9.)$$

It can be observed that according to this theory, an

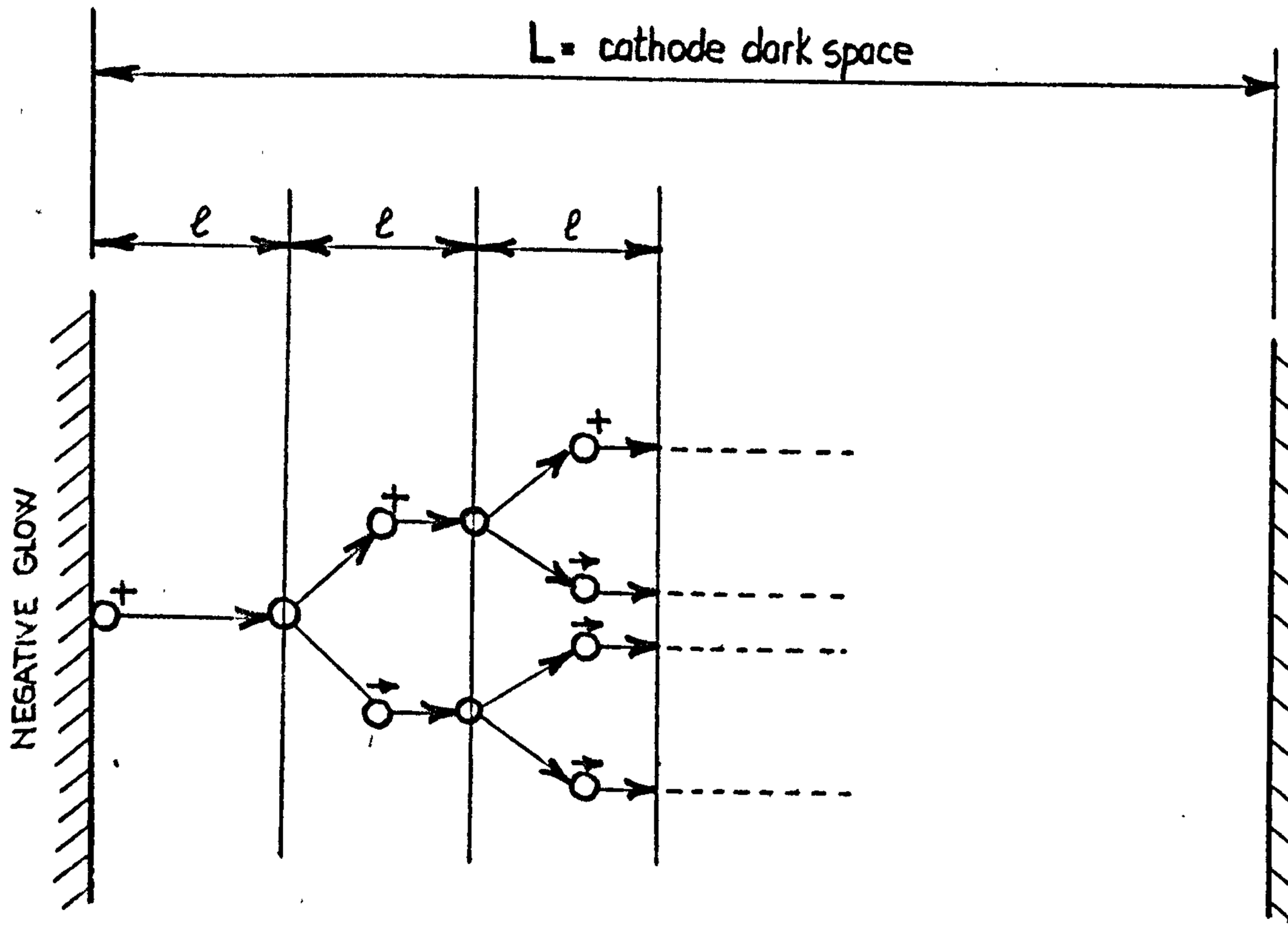
L = cathode dark space
ℓ
ℓ
ℓ
NEGATIVE GLOW
CATHODE
o+ positive ion
o→ energetic neutral
o non energetic neutral

Figure 2.9.8

ion cannot generate more ions but only energetic neutrals through transfer of the charge. Thus, the number of ions which enter the cathode dark space after undergoing subsequent charge transfer collisions, will reach the cathode in the same number. Therefore we can consider the number of ions N_i calculated from the ion current, as being the total number of ions extracted by the electric field from the negative glow and accelerated towards the cathode.

From (2.9.9.), it is possible to calculate the total number of energetic neutrals produced by ion-neutral collisions across the dark space.

An energetic neutral is defined as being a neutral which has undergone at least one collision with an ion or with another neutral having more than the thermal energy.

The total number of neutrals born in an ion-neutral collision is :

$$N_{n\bar{e}} = N_i x\, n_{n\bar{e}} = N_i\left[2^{k+1} - (k+2)\right] \simeq N_i 2^{k+1}$$

$$\left(\frac{\text{energetic neutrals}}{\text{sec. cm}^2}\right) \qquad (2.9.10.)$$

For the particular case of 3 kV bias voltage and p = 10 mtorr, ($K = \frac{L}{\ell} = 18$), $N_{n\bar{e}}$ thus calculated exceeds the total number N_{np} of particles striking the cathode in a second on a square centimetre. This means that energetic neutrals will have further collisions amongst themselves, thus contributing to

reducing the energetic differences and to enhancing the scattering effect.

A simplifying restriction that could be introduced is to determine the number of 'ℓ' spacings, starting from the cathode in which , collisions taking place, the number of energetic neutrals thus formed is equal to N_{np}.

For the 3 kV and p = 10 mtorr conditions, it was calculated that this number of mean free paths is 9. This means that the neutrals formed at a distance longer than 9ℓ from the cathode, lose their energy in further collisions and in these conditions could reach the cathode with energies comparable to the thermal energy. But, entering the last 9 'ℓ' spacings, they will receive energy in collisions with ions. Therefore, all collisions that took place before 9ℓ are neglected, and from (2.9.10) making k = 9, 8...2, 1, 0, it is possible to determine the number of neutrals N_n that could be produced at the end of each 'ℓ' space provided all the charge transfer collisions took place at that level.

From the heat input to the substrate (Figure 2.7.3.) and expression (2.9.2.), it is possible to determine the energy of neutrals produced at different levels (k = 9, 8...2, 1, 0)

$$\bar{e}V_n = \frac{100}{AN_n}\left(L_s - N_e\bar{e}V_e\right) \qquad (2.9.11)$$

These energies are calculated in Table 2.9.12.

k	9	8	7	6	5	4	3	2	1	0
$\bar{e}Vn$ (eV)	447	894	178	357	715	143	286	572	1144	2288

Table 2.9.12.

Note : k is also given the value 0 (zero) because a charge transfer collision could take place in the very vicinity of the cathode surface.
From Table 2.9.1.2. it results that the average neutral energy for a 3 kV bias is about 150 eV.

The probability of a neutral to reach the cathode with a certain energy decreases exponentially due to the probability of an ion to reach a 'k' level without previous collisions and due to the fact that a neutral at level 'k' will have further collisions with other neutrals.
Considering that this probability is an exponential decay function, it was plotted versus energy in Figure 2.9.13.

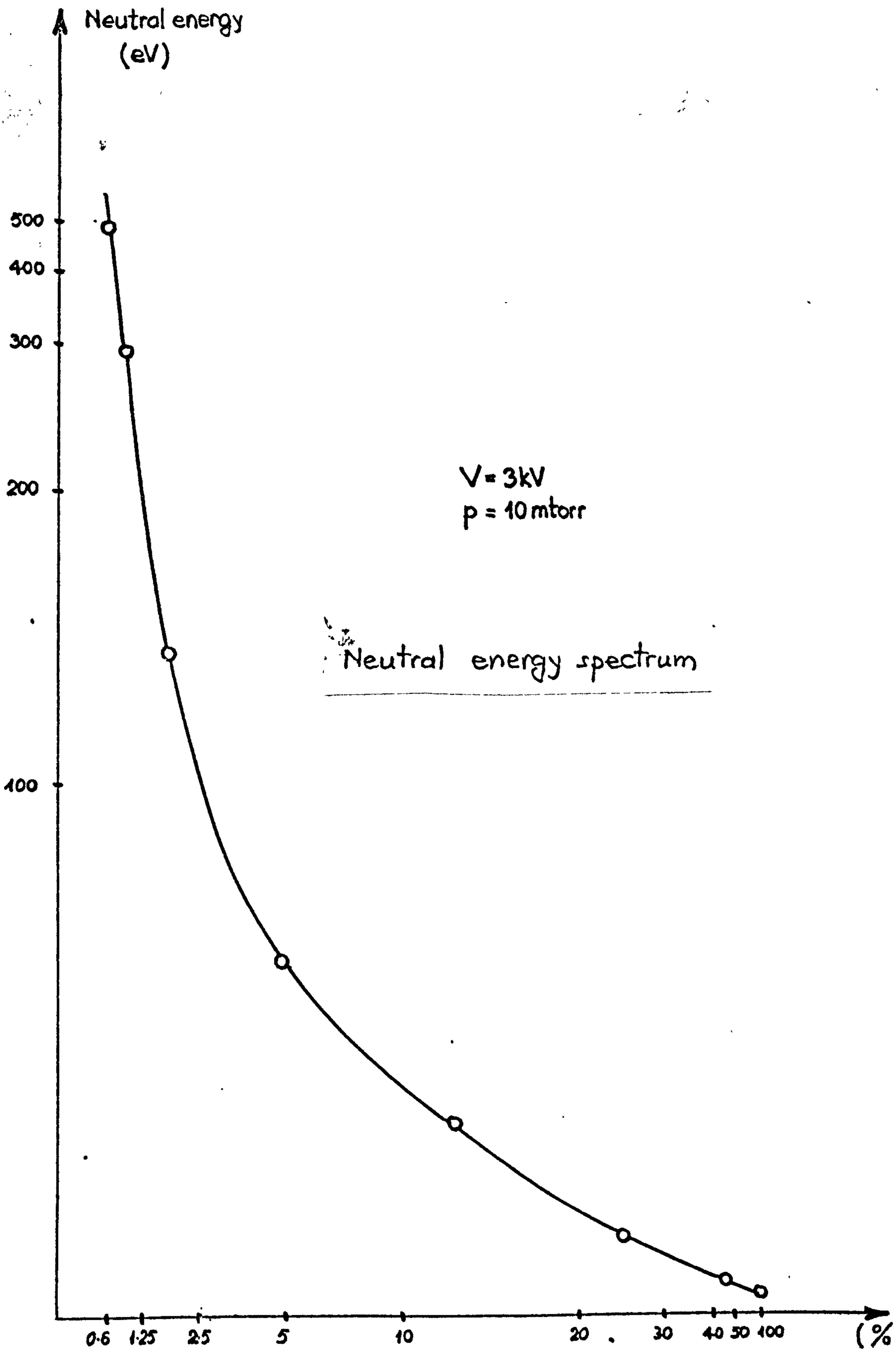
Neutral energy
(eV)
500
400
300
200
100
V = 3kV
p = 10 mtorr
Neutral energy spectrum
0·6
1·25
2·5
5
10
20
30
40
50
100
(%)

Figure 2.9.13

2.10. Neutrals Energy Spectrum

A theoretical approach to the neutrals energy can be done by making the assumption that an ion cannot travel without collision more than a mean free path 'ℓ' and therefore cannot have more energy than the one gained during the acceleration across an 'ℓ' space.

Let us consider[15] that the field strength varies linearly from the negative glow to the cathode surface, as shown in Figure 2.10.1. That means :

$$\frac{dV}{dx} = Kx$$

which integrated gives :

$$\left[V\right]_{o}^{-Vc} = \left[K\,\frac{x^2}{2}\right]_{o}^{L} \qquad (2.10.2.)$$

From boundary conditions :

$$K = -\,\frac{2Vc}{L^2} \qquad (2.10.3.)$$

The cathode dark space is then devided into $k = \frac{L}{\ell}$ equal intervals. Considering an 'ℓ' space having the rank 'm', an ion accelerated across the(m-1; m) interval will gain an energy equal to :

$$Ei_m = \bar{e}(V_m - V_{m-1}) \qquad (2.10.4)$$

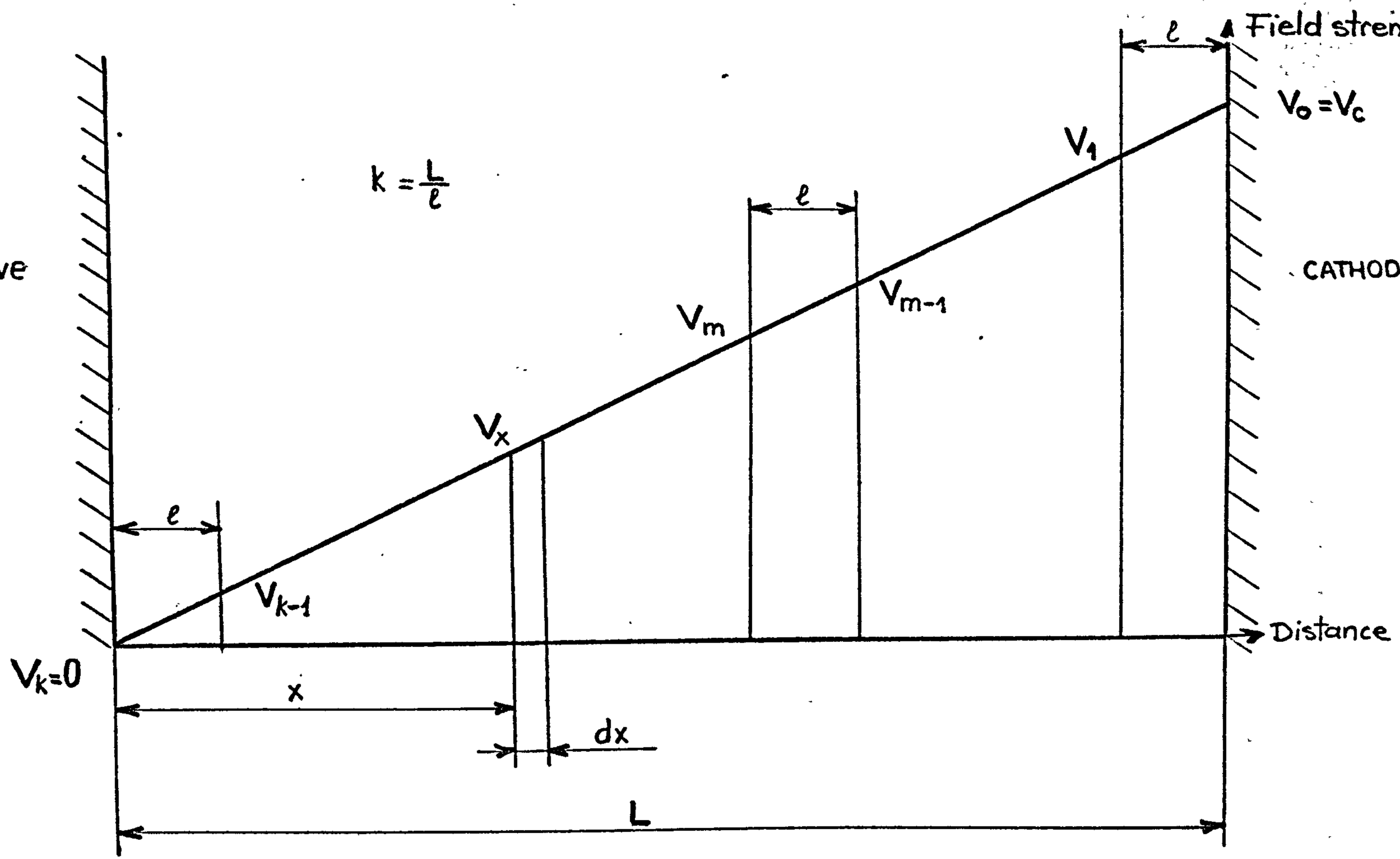

Figure 2.10.1

Field strength across the cathode dark space

From (2.10.2) and (2.10.3.), it is possible to calculate V_m and V_{m-1} :

$$\left[V\right]_o^{V_m} = -\frac{2Vc}{L^2}\left[\frac{x^2}{2}\right]_o^{L-m}$$

$$\left[V\right]_o^{V_{m-1}} = -\frac{2Vc}{L^2}\left[\frac{x^2}{2}\right]_o^{L-(m-1)} \qquad (2.10.5)$$

It results :

$$V_m = \frac{-Vc\ (L-m\ell)^2}{L^2}$$

$$V_{m-1} = \frac{-Vc\ \left[L-(m-1)\ell\right]^2}{L^2} \qquad (2.10.6)$$

Introducing these expressions into (2.10.4.) :

$$Ei_m = \frac{\bar{e}Vc}{L^2}\,\ell\left[2L - \ell(2m-1)\right] \qquad (2.10.7)$$

For this particular case :

$Vc = 3$ kV

$p = 10$ mtorr

$L = 9$ cm

$\ell \simeq 0.5$ cm

$k = 18$

E_m is plotted for m = k....0 in Figure 2.10.8.

The highest energy that an ion can achieve is of about 330 eV.

Although an ion can travel longer or shorter

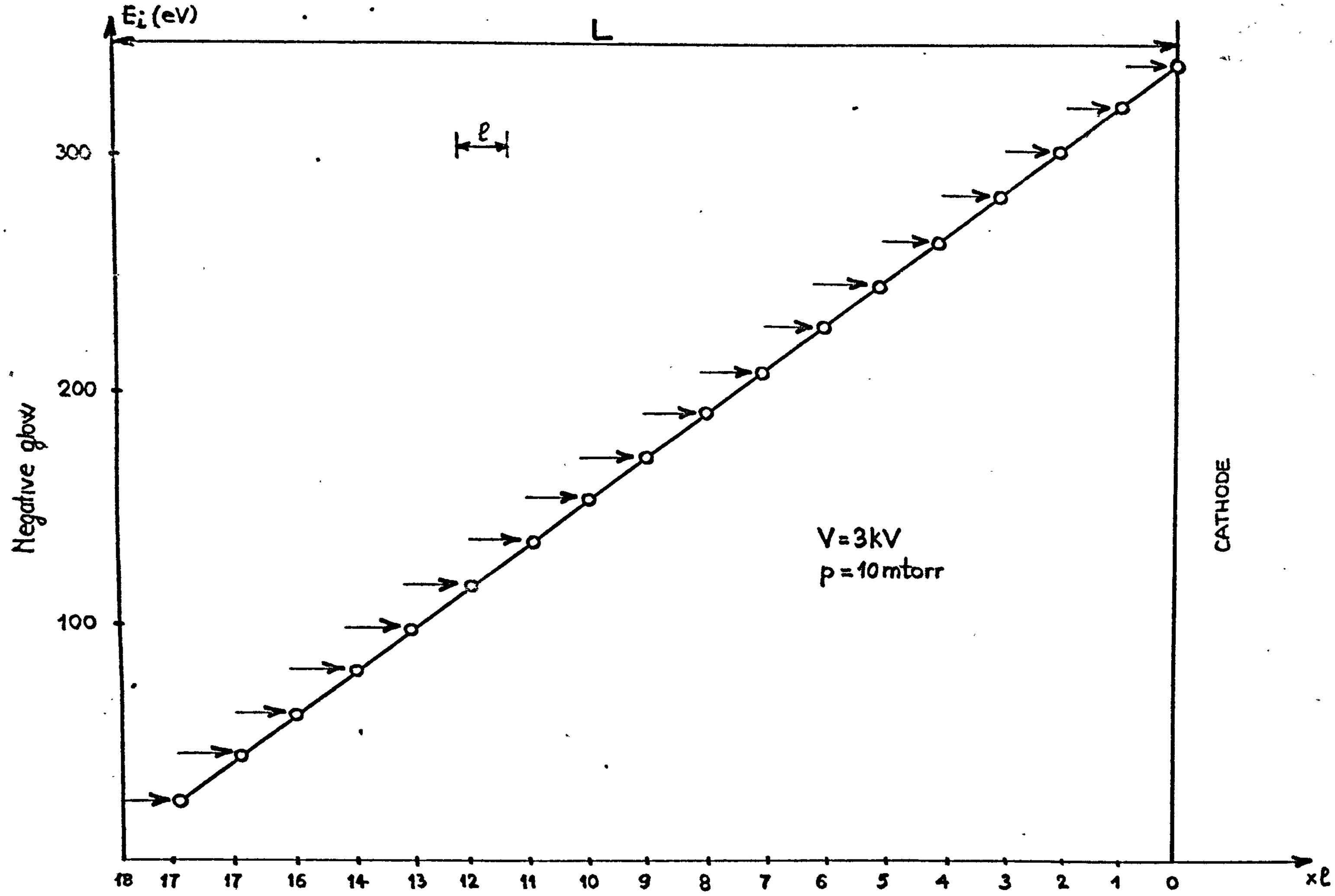

Energy gained by an ion while accelerated across subsequent 'ℓ' spaces.

Figure 2.10.8

than a mean free path, if we restrict its free movement to a mean free path, average figures for the energy distribution can be obtained.

Supposing that an ion-neutral collision takes place at the beginning of the last 'ℓ' space, as shown in Figure 2.10.9., the ion comes with an energy of 320 eV gained while accelerated across the previous mean free path.

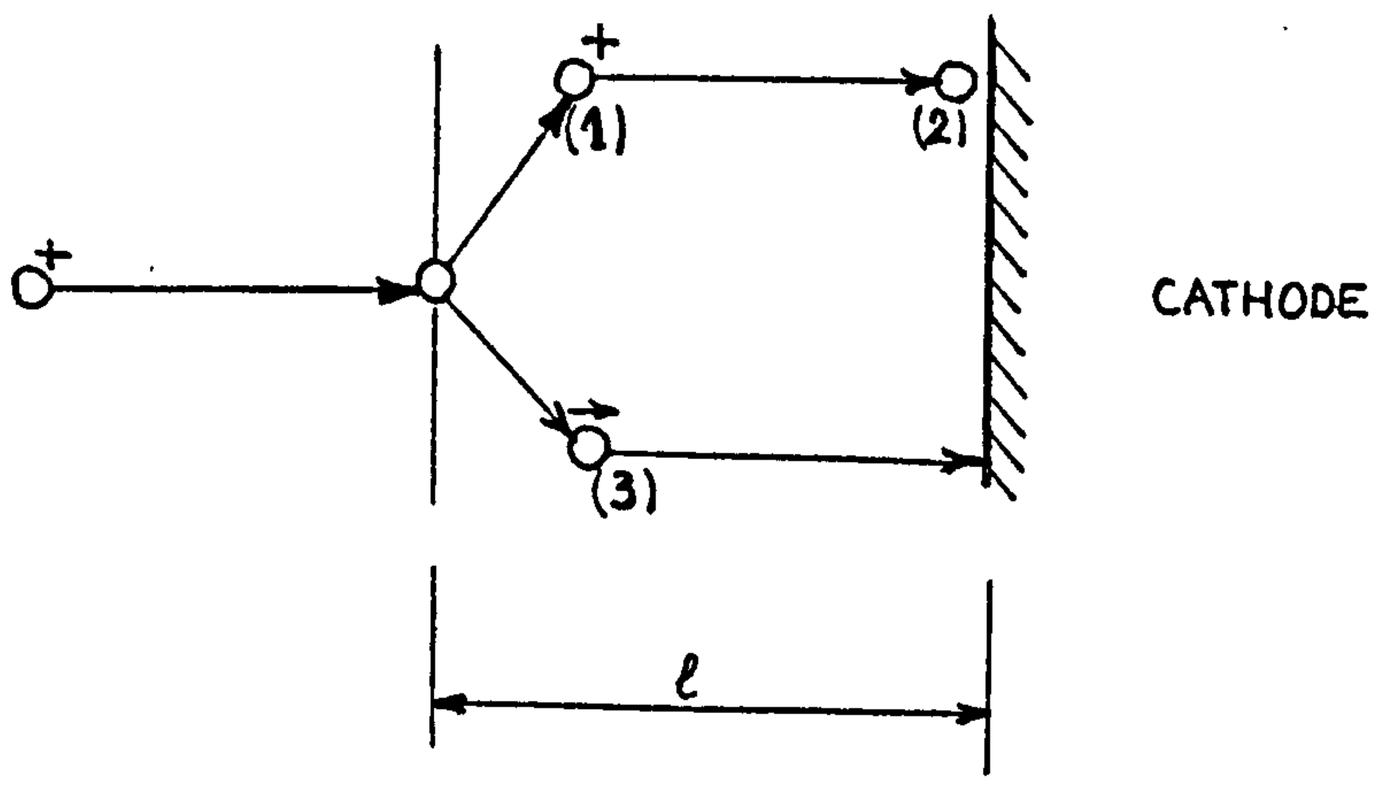

Figure 2.10.9.

It undergoes a charge transfer collision with a neutral and it, itself becomes an energetic neutral (3) while the previous neutral becomes an ion (1). (1) is accelerated across the last 'ℓ' space gaining an energy of 330 eV, but just before striking the cathode, it can have a last charge transfer with a neutral (2). The ion (1) then becomes an energetic neutral striking the cathode with an energy of 330eV.

The conclusion that can be drawn so far is that both ions and neutrals strike the cathode with their average maximum energy equal to approximately $\frac{eVc}{10}$ for a 3 kV bias.

Looking now at an energetic neutral produced at an 'm' level having the energy E_m and travelling towards the cathode, it will undergo collisions with other neutrals shearing energy in each collision as shown in Figure 2.10.10.

Thus , a neutral produced at the level 'm' will reach the cathode after subsequent collisions with an energy equal :

$$\frac{E_m}{2^{m-1}} \qquad (2.10.11.)$$

Since an energetic neutral is produced from an ion that loses its charge keeping the energy gained while accelerated across the previous 'ℓ' space, then :

$E_m = Ei_{m+1}$ (the energy of an ion accelerated across the (m+1) 'ℓ' space)

Thus, the energy with which a neutral produced at the 'm' level will arrive at the cathode is :

$$\frac{Ei_{m+1}}{2^{m-1}} \qquad (2.10.12)$$

Ei has benn plotted in Figure 2.10.8.

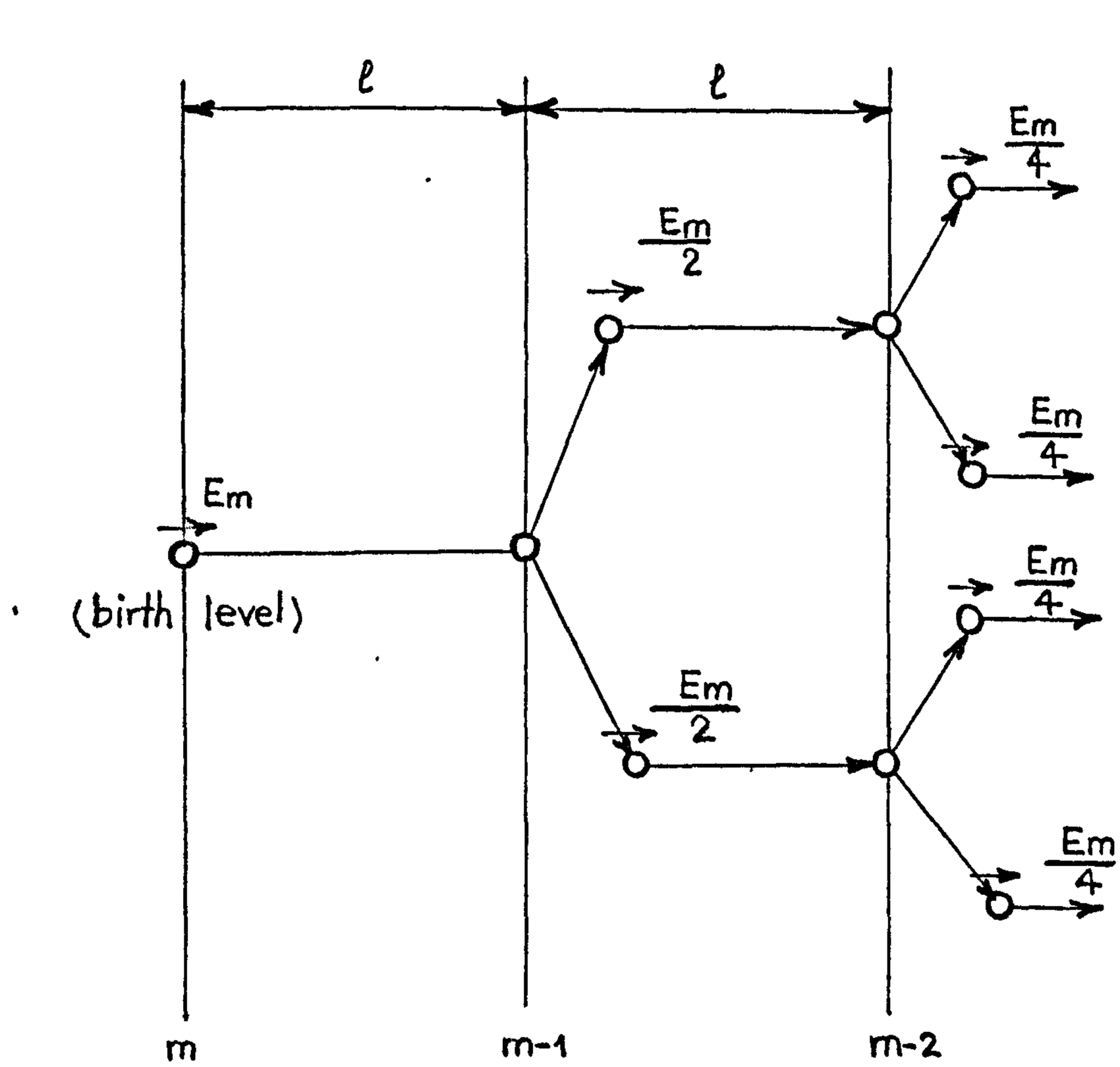

o non energetic neutral

→o energetic neutral

Figure 2.10.10

neutral-neutral collisions

Using (2.10.12.), it is possible to plot the energy with which a neutral produced at different levels of the dark space, could reach the cathode surface, as shown in Figure 2.10.13.

Assuming that for a neutral to be considered energetic, it must have an energy higher than the thermal energy ($\simeq$o.2 eV), it means that only those neutrals produced within the last 9 mean free paths are energetic and it can be considered that they carry most of the neutrals energy to the cathode, a result which is similar to that obtained from the heat imputs experiment.

Considering that an ion enters the last 9 mean free paths, the entire sequence of ion-neutral and neutral-neutral collisions are schematically shown in Figure 2.10.14. Below each level line, it is given the number of energetic neutrals which are produced through subsequent collisions as well as the energy they carry.

At the end of the 'k' interval, there are :

Number of energetic neutrals	Energy of each neutral
2^{k-2}	$\frac{E_1}{2^{k-2}}$
2^{k-3}	$\frac{E_2}{2^{k-3}}$

$$\begin{array}{c} 2^{k-4} \\ \vdots \\ 2^{k-k} \end{array} \qquad \begin{array}{c} E_3 \\ \hline 2^{k-4} \\ \vdots \\ E_{k-1} \\ \hline 2^{k-k} \end{array} \qquad (2,10.15.)$$

This represents the total number of neutrals and their energies produced by by one ion crosssing the cathode dark space.

For 3 kV and 10 mtorr, the number of neutrals $\left(\frac{\text{neutrals}}{\text{ion}}\right)$, their energies and percentages in the total number are given in Table 2.10.16.

Nn/ion	$\bar{e}$Vn (eV)	%
128	1.37	50
64	3	25
32	6	12.5
16	14.5	6.2
8	31	3.1
4	67	1.6
2	143	0.8
1	305	0.4

Table 2.10.16.

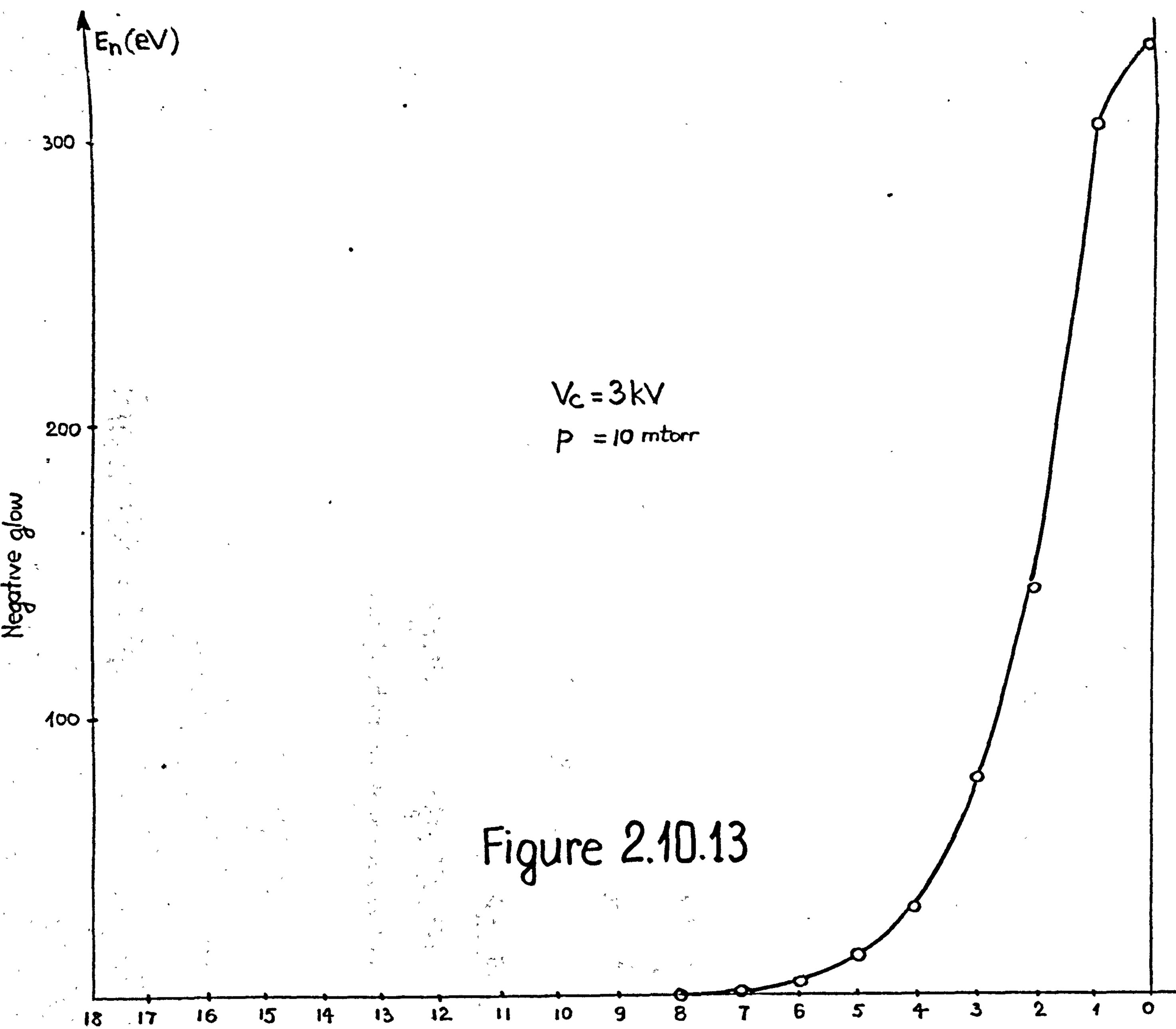

Figure 2.10.13

NOTE

The last point of the curve is positioned on the cathode surface since an ion-neutral collision (charge transfer) can take place in the very vicinity of the cathode surface and the energetic neutral thus formed will have the full energy of the accelerated ion.

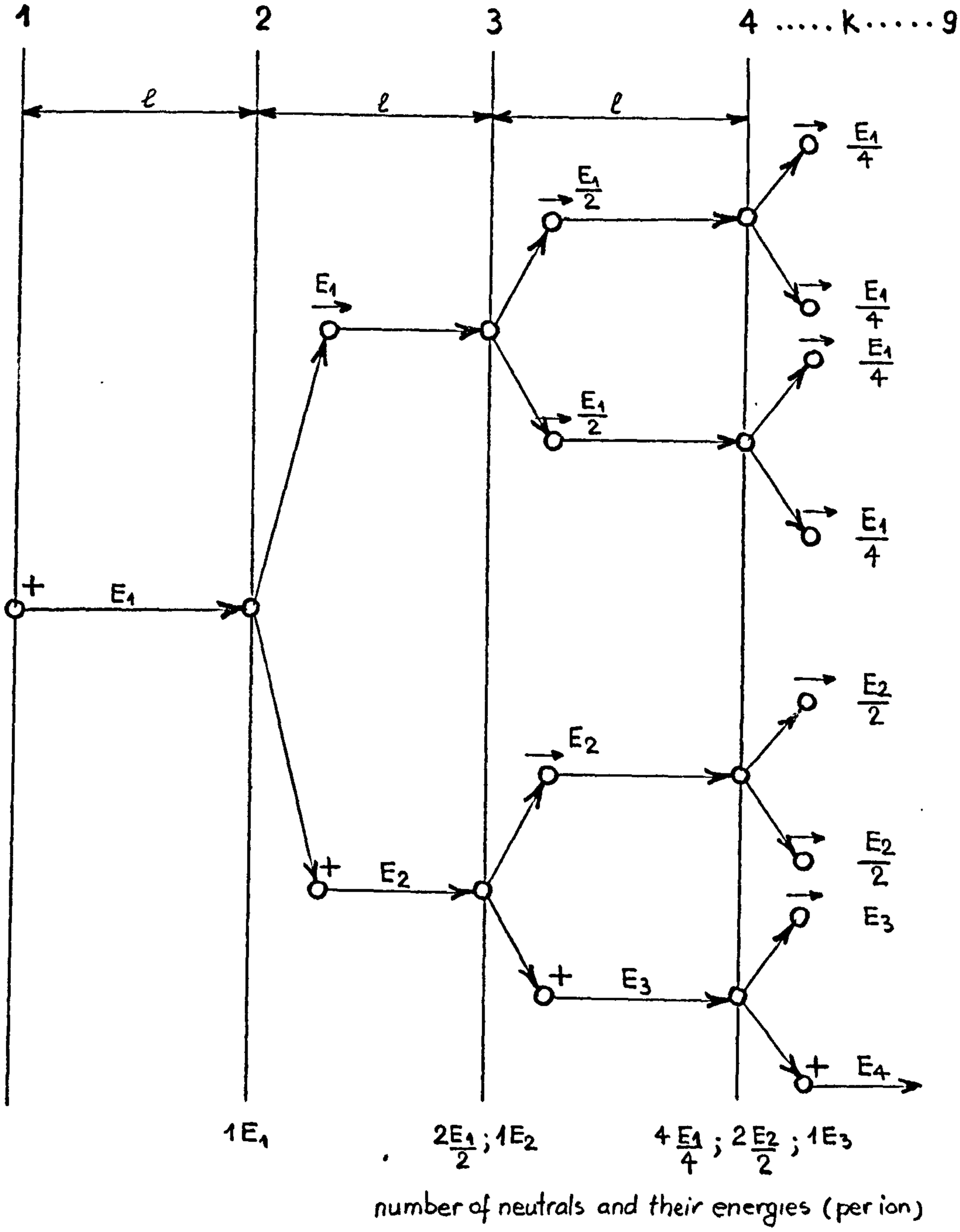

Figure 2.10.14

From Table 2.9.16., it can be concluded that 50 - 75 % of the neutrals will arrive the cathode with energies of several electron volts, but since the numbers are given for one ion, it results that multiplying this number by N_i ($\frac{ions}{sec.cm^2}$) it comes out that a number of neutrals equal to the total number of ions will strike the cathode with an energy of 300 eV for a 3 kV bias voltage.
The neutral energy spectrum is drawn in Figure 2.10.17.

*

* *

Following this calculation, the explanation for the power lost in the ion plating process (plotted in Figure 2.7.5.) could be as follows :
The current drawn by the cathode is due to the coming positive ions (after substracting the secondary electrons current).
The energetical neutrals, practically taking their whole energy from the ions, are scattered in collisions with other neutrals and could go to some other parts of the system.
At first sight, a percentage of the total energetic neutrals equal to $\frac{S_c}{S}$ x 100 % should be lost, where :

S_c = cathode frontal surface area

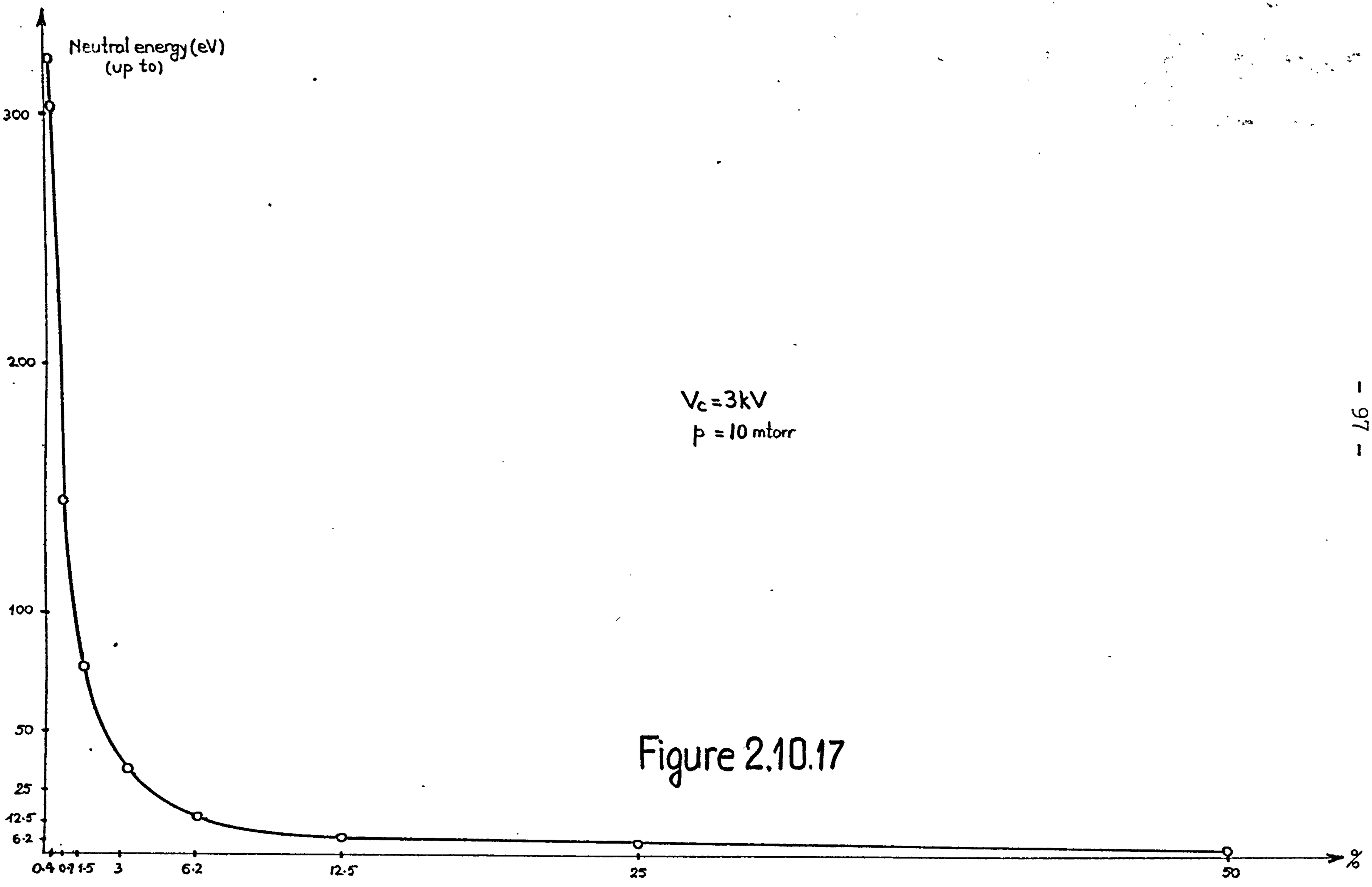

Figure 2.10.17

S = the area of a plane crossing the chamber at the same distance with the cathode surface.

Since all the ions will go to the cathode, the energy lost through the neutrals should be :

$$\left(1 - \frac{S_c}{S} \right) E_n$$

where E_n is the total energy transferred to the neutrals.

For the experiment previously described, approximately 98 % of the energy should be lost. But the experimental work showed only a 30 % loss.

This is due to the fact that collisions between the neutrals take place at discreet angles. Since an energetic neutral is produced from an ion (through a charge transfer collision) travelling along the field lines towards the cathode, it means that colliding with a nonenergetic neutral at a discreet angle will more or less direct it towards the cathode surface.

Therefore, the energetic bombardment of the cathode is an oriented ion and neutral bombardment. The less strong the electric field is, the more chances are that energetic neutrals will go to parts of the system other than the cathode.

The conclusion is that ion plating is a cathode oriented energetic deposition process,. and due to the low ionization efficiency, this orientation is

mainly due to neutral scattering which is not at random but at discreet angles with the electric field lines going to the cathode. The throwing power is a result of the neutrals scattering.

2.11. Ions Energy Spectrum

The experiments presented in this part are aimed at determining the number of ions and their energy distribution for the diode ion plating system. The effect of argon pressure and bias voltage upon the ion energy is also studied.

2.11.1. Experimental Arrangement

In order to determine the number of ions and the energy with which they strike the cathode of a glow dischrge , a similar arrangement to the one presented in Figure 2.7.1. was built but in this case, a high voltage can be applied on the substrate behind the wire mesh. At the same time, an earthed shield was also placed behind and around the substrate at 2 mm distance, leaving unshielded only that area of the substrste placed behind the wire mesh. The schmatic arrangement is shown in Figure 2.11.1.1. This set up was intended to act as an ion energy analyser due to the possibility of appying a fixed voltage to the mesh and a variable one to the substrate. Of course, this arrangement does not satisfy all the requirements for obtaining very accurate results for the following reasons :

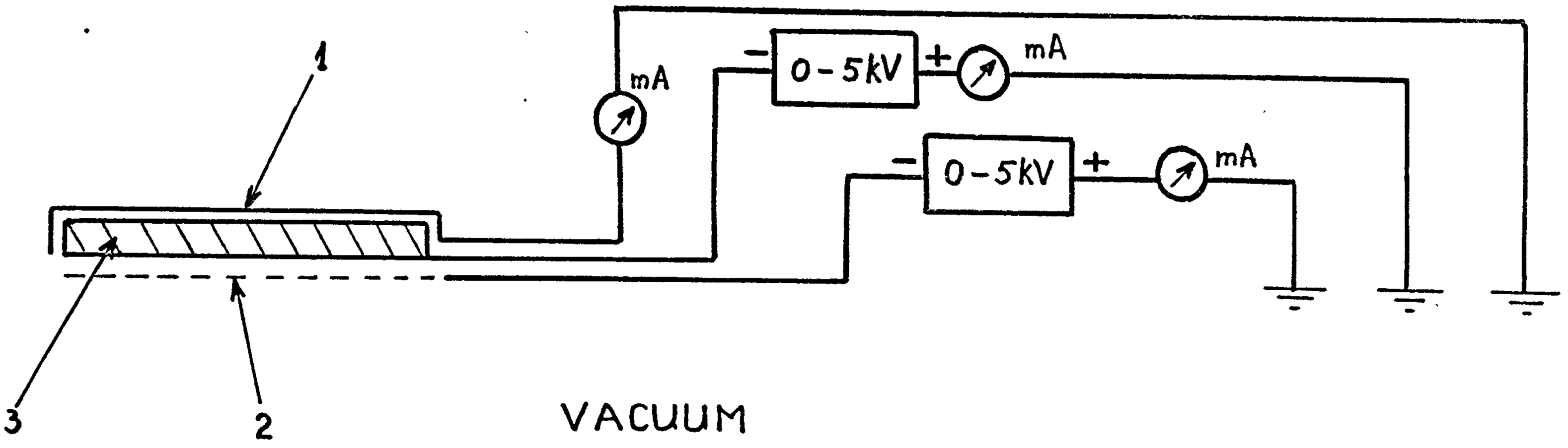

1. Earthed shield
2. Mesh (A = 92%)
3. Substrate

Experimental arrangement

Figure 2.11.1.1

- the accuracy of the instrumentation was not better than 0.01 mA
- The exact form of the field lines is not known and therefore it had to be approximated.
- The paths of the electrons had also to be approximated
- The potential lines giving the paths followed by the ions are assumed to run parallel to the substrate surface when in reality their configuration is much more complex.

All this leads to inaccurate results being obtained but, since little is known in this area of investigation, these results could prove worthwhile by giving information about the shape of ion energy spectrum.

Returning to the arrangement presented in Figure 2.11.1.1., the geometrical transparency of the mesh is A = 92 % and all the H.T. parts are carefully shielded so that the glow discharge is confined only to the mesh in front of the substrate. The whole arrangement is placed in a vacuum chamber which is then pumped down to 5×10^{-6} torr and following this, argon is let in to the required working pressure (p).

A negative votage (V_M) is applied on the mesh with the substrate at zero potential, and a glow dischrge is thus established. Then, a negative voltage (V_S) is applied to the substrate and is

slowly increased until $V_S = V_M$.
The current to both the mesh (I_M) and the substrate (I_S) is monitored and plotted versus V_S.

2.11.2. Theoretical Approach

One explanation of the phenomena taking place at the mesh - substrate system could be as follows:

a. With V_M applied to the mesh and $V_S = 0$, due to the opposing electric field, no ions can pass through the mesh to the substrate, while A % of the neutrals (energetic and nonenergetic) not being affected by the electric field, can pass and strike the cathode.
This neutral bombardment leads to secondary electrons being emitted by the substrate drawing a negative current I_e .
At the same time, the mesh is exposed to energetic particles bombardment (ions & energetic neutrals) and therefore, secondary electrons are emitted by the mesh surface.
The question that arises is how can these electrons be detected and measured. One possible method is to draw the approximate equipotential field lines between the mesh and the substrate, and this was done by simulating the arrangement on a conductive

graphite paper. This gives the approximate configuration as presented in Figure 2.11.2.1

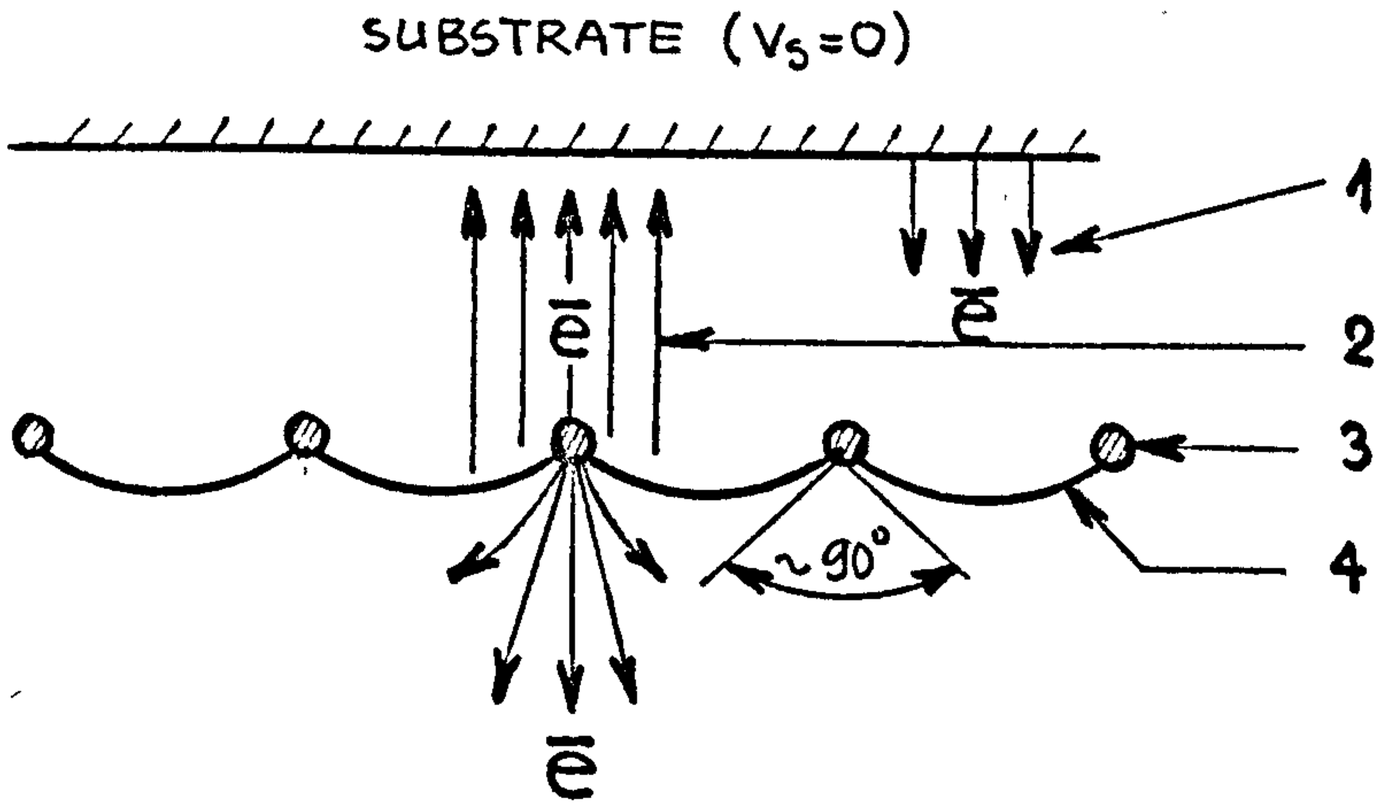

1. Electrons due to neutral bombardment of the substrate
2. Electrons emitted by the mesh under energetic bombardment
3. Wire mesh (V_M)
4. Equipotential field lines

Figure 2.11.2.1.

According to this, it is reasonable to assume that approximately 75 % of the secondary electrons emitted by the mesh are attracted by the substrate and contribute to the total substrate current. I_S .

b. With V_M applied on the mesh and a variable (increasing) V_S applied on the substrate, and assuming that the potential lines run parallel to the substrate surface, the only ions that pass through could be considered to be those having an energy equal or higher than the potential difference. That is :

$$E_i \geq \bar{e} (V_M - V_S) \qquad (2.11.2.2.)$$

As these ions start passing through the mesh secondary electrons are emitted by the ion bombarded substrate which add to those produced by the neutral bombardment, the overall value of the electric current increasing with the increase in the number of ions.

Another effect of the increase in V_S is that the configuration of the field lines changes again modifying the paths of both ions and electrons and the result is that the actual cathode surface is not represented by the geometrical surface any more, but it probably becomes equal to the total surface given by the equipotential lines. This will probably modify the electrical transparency of the mesh to a value different from the geometrical one (A %) .

However, by measuring the current drawn to the

substrate and subtracting the approximately calculated electronic current, it is possible to determine the current given by the positive ions for subsequent potential difference values ($V_M - V_S$).

c. With $V_M = V_S$ the maximum number of ions pass through the mesh.

The equipotential lines were drawn again and their approximate configuration is presented in Figure 2.11.2.3.

According to this, it is possible to assume that all secondary electrons emitted by the mesh go to some other parts of the system rather than to the substrate and it can be assumed that the only electronic current leaving the substrate is due to the ion and neutral bombardment

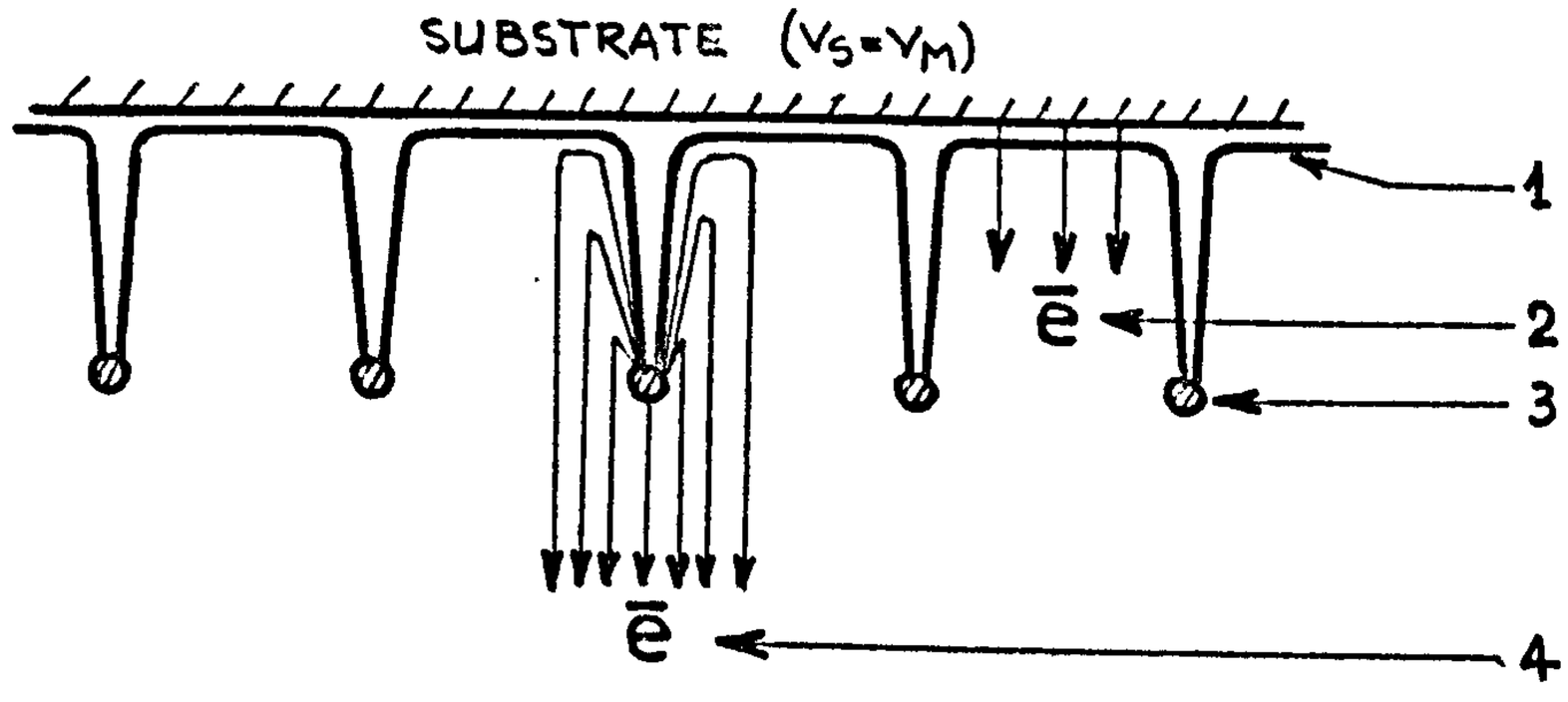

Figure 2.11.2.3

1. Equipotential lines
2. Electrons emitted by the substrate
3. Wire mesh (V_M)
4. Electrons emitted by the mesh

2.11.3. Experimental Procedure and Results

After pumping the system and setting the argon pressure (p) to the required value, V_M was applied to the mesh and a glow discharge was established between the earthed parts of the system and the H.T. wire mesh. Following this, a negative voltage is applied (V_S) to the substrate and increased in small steps until it equals the mesh voltage. All this time, the current drawn by the mesh (I_M) and by the substrate (I_S) are monitored and plotted versus V_S .

For V_M = 2 kV and p = 10 mtorr, I_M and I_S are plotted in Figure 2.11.3.1. and Figure 2.11.3.2. With V_S = 0, an electronic current I_e = -0.1 mA was detected to the substrate and assuming that no ions can pass through, this current is probably due to the secondary electrons emission by the substrate under neutral bombardment and due to the flow of secondary electrons (~75 %) emitted by the mesh.

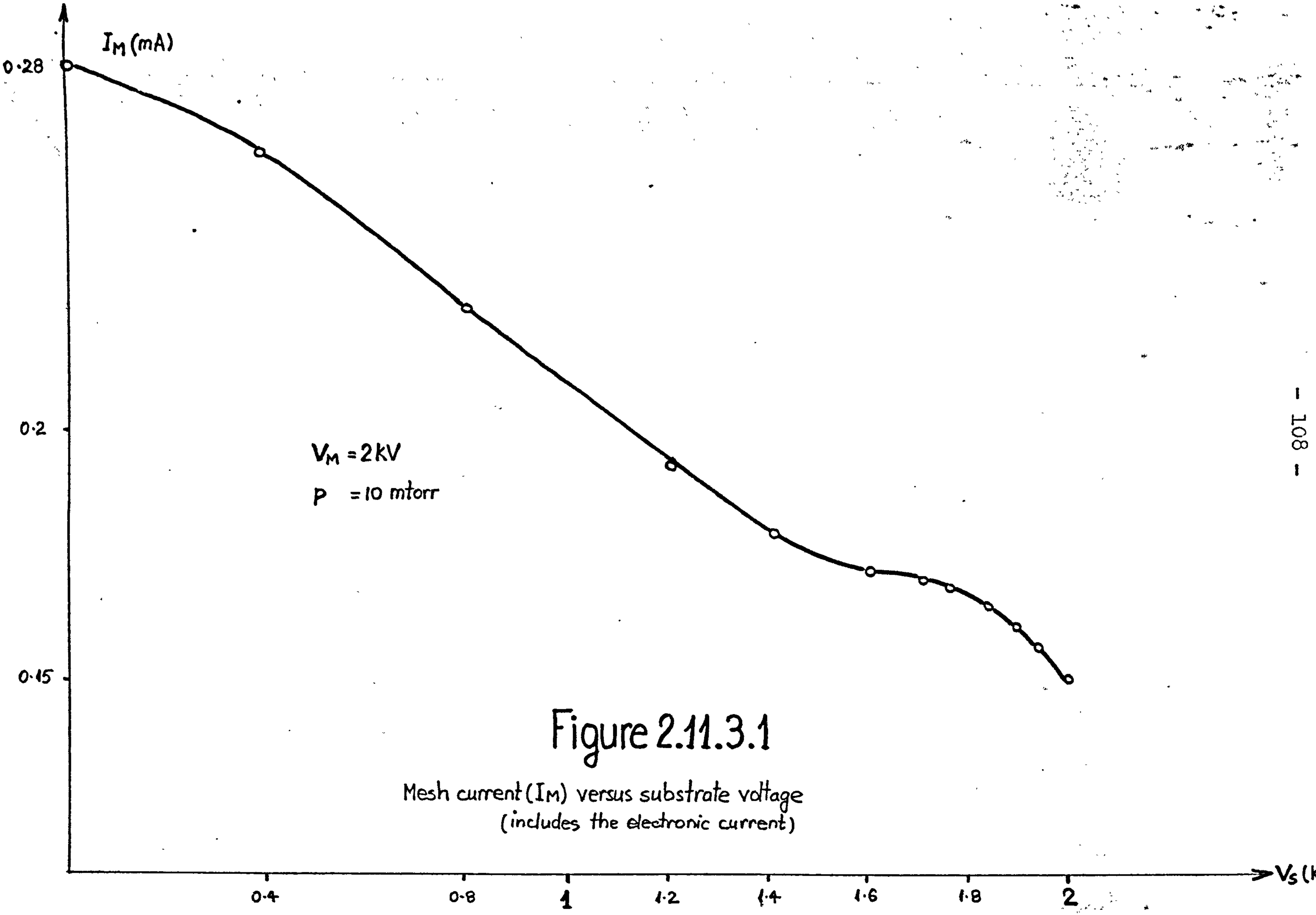

Figure 2.11.3.1

Mesh current (I_M) versus substrate voltage
(includes the electronic current)

I_S (mA)

0·2

all possible ions pass through

a. ion current (ions pass through)

b. seccondary electrons produced by the ion & neutral bombardment

Figure 2.11.3.2

Substrate current (I_S)
(includes the electronic current).

$V_M = 2kV$

$p = 10$ mtorr

0·1

Due to the modified electric field lines no measurable quantity of mesh electrons can go to the substrate.

All electronic current is due to the secondary emission by the substrate under ion and neutral bombardment.

A. electronic current
- electronic current emitted by the mesh (M→S) - decreasing with V_S
- electronic current emitted by the substrate (S→Earth) due to ion & neutral bombardment - increasing

B. ion current
- ions having $E \geq V_M - V_S$ pass through the mesh

-0·04

0·4 0·8 1 1·2 1·4 1·6 1·8 2 (kV)

V_S

Looking at the graph in Figure 2.11.3.2., it can be noticed that when V_S reaches a certain value, thre is a sharp increase in the total substrate current and it is reasonable to assume that this is entirely the effect of the ion current (going to the substrate) and the secondary electronic current (leaving the substrate) produced by the ion and neutral bombardment. This is due to the change in the field configuration preventing the mesh electrons from reaching the substrate.

Most probably, the entire electronic current measured at the substrate is due to the secondary electrons emitted under ion and neutral bombardment. (Figure 2.11.3.3 a)

The electronic current going from the mesh to the substrate was -0.1 for $V_S = 0$ and decreases to zero as $V_S \nearrow V_M$ (Figure 2.11.3.3 b).

It was assumed that all the electrons emitted by the substrate go to the earthed shield and their current was measured and plotted in Figure 2.11.3.3c.

The curve plotted in Figure 2.11.3.2. is given by the combination of these electronic currents superimposed over the ion current given by the ions having $E \geqslant V_M - V_S$ which are passing through the mesh in ever increasing numbers as $V_S \nearrow V_M$.

Let us draw a separate shape of the plot 2.11.3.2. as presented in Figure 2.11.3.3 d .

For the region where V_S approaches V_M, it is possible to assume that the curve incorporates two effects : one is the current given by the ions and the second is the current given by the secondary electrons produced by the ion and neutral bombardment and leaving the substrate. These two effects add together to give the total current. Since the plasma is neutral (equal number of ions and electrons), let us assume that the total number of ions reaching the substrate equals the total number of electrons leaving it. It means that the ion current is half of the total current (the dotted curve).

For the origin O' ($V_S = 0$), it is assumed that virtually, no ions pass through and the entire current is due to secondary electrons (from the mesh to the substrate and from the substrate to the earthed shield.).

Thus, we end up with a sequence of points for the region where V_S approaches V_M and a point in the origin,representing the values of the ion current. Since the ion extraction is a smooth and continuous process, by filling the gap between O and the dotted plot with a curve that follows the shape, it is possible to draw the approximate ion current going to the substrate (Figure 2.11.3 d).

Appying these assumptions to the graph presented in Figure 2.11.3.2. and choosing new

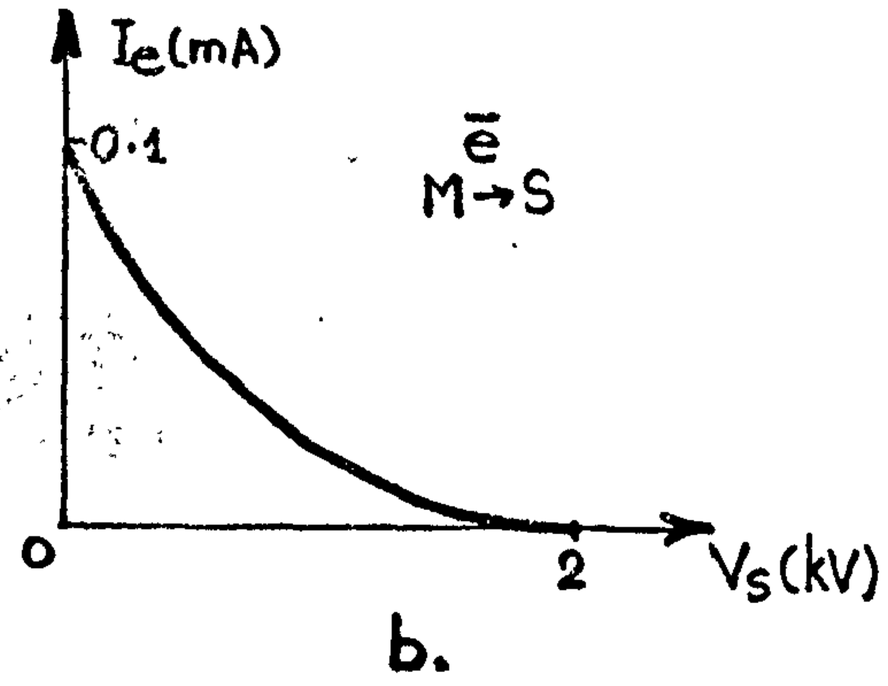

b.

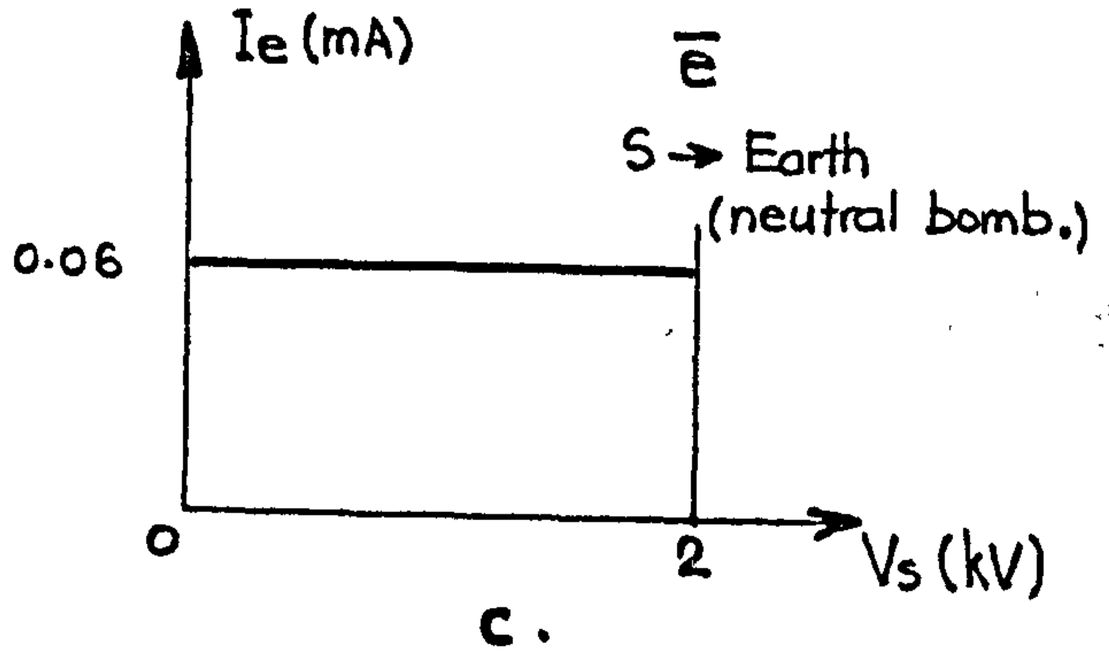

c.

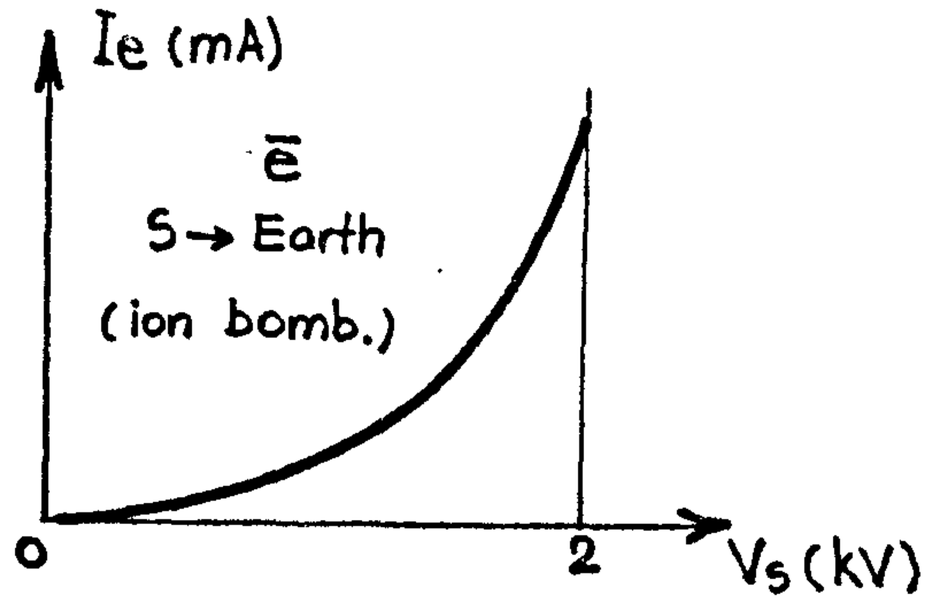

a.

d.

Figure 2.11.3.3

axes, the ion current plot appears in the shape shown in Figure 2.11.3.4. (dotted line)(△——△). The same curve is plotted versus $E = V_M - V_S$ in Figure 2.11.3.5. which represents the ion energy spectrum.

Applying Davis and Vanderlice's theory[15], the ion energy distribution is also plotted in Figure 2.11.3.5. and despite all the assumptions made during this experiment, there is a striking similarity between the two graphs, the difference being of maximum 5 %. This difference could be due to the assumptions made as regards the participation of the electrons to the total current and could also be due to the fact that the experimental results are for $k = \frac{L}{\ell} = 18$, while Davis and Vanderslice's curve is plotted for $k = \frac{L}{\ell} = 15$.

A theoretical approach to the ion energy spectrum could be done on a probabilistic basis. Since intermolecular collisions are statistical events and the actual free path 'λ' can be longer or shorter than the mean free path 'ℓ', the distribution is given by an exponential decay function[49] .

$$\frac{N}{N_o} = \exp\left(-\frac{\lambda}{\ell}\right) \qquad (2.11.3.6.)$$

where $\frac{N}{N_o}$ represents the fraction of particles

(ions or neutrals) which have not undergone any collisions as yet after travelling a free path 'λ'. According to (2.11.3.6.), only 38 % of the molecules travel over a mean free path length 'ℓ' without collisions and around 1 % of them can travel without collisions as long as 4.5ℓ .

The probability of a molecule to travel over a distance x without collisions is :

$$\varepsilon_x = e^{-\frac{x}{\ell}} \qquad (2.11.3.7.)$$

Therefore, the probability of an ion to reach the cathode with the energy $\bar{e}Vc$ is :

$$\varepsilon_L = e^{-\frac{L}{\ell}} = e^{-k} \qquad (2.11.3.8.)$$

for 3 kV and 10 mtorr (k = 18)

$$\varepsilon_L = 1.52 \times 10^{-8}$$

or

$$\varepsilon_L = 1.52 \times 10^{-6} \ \%$$

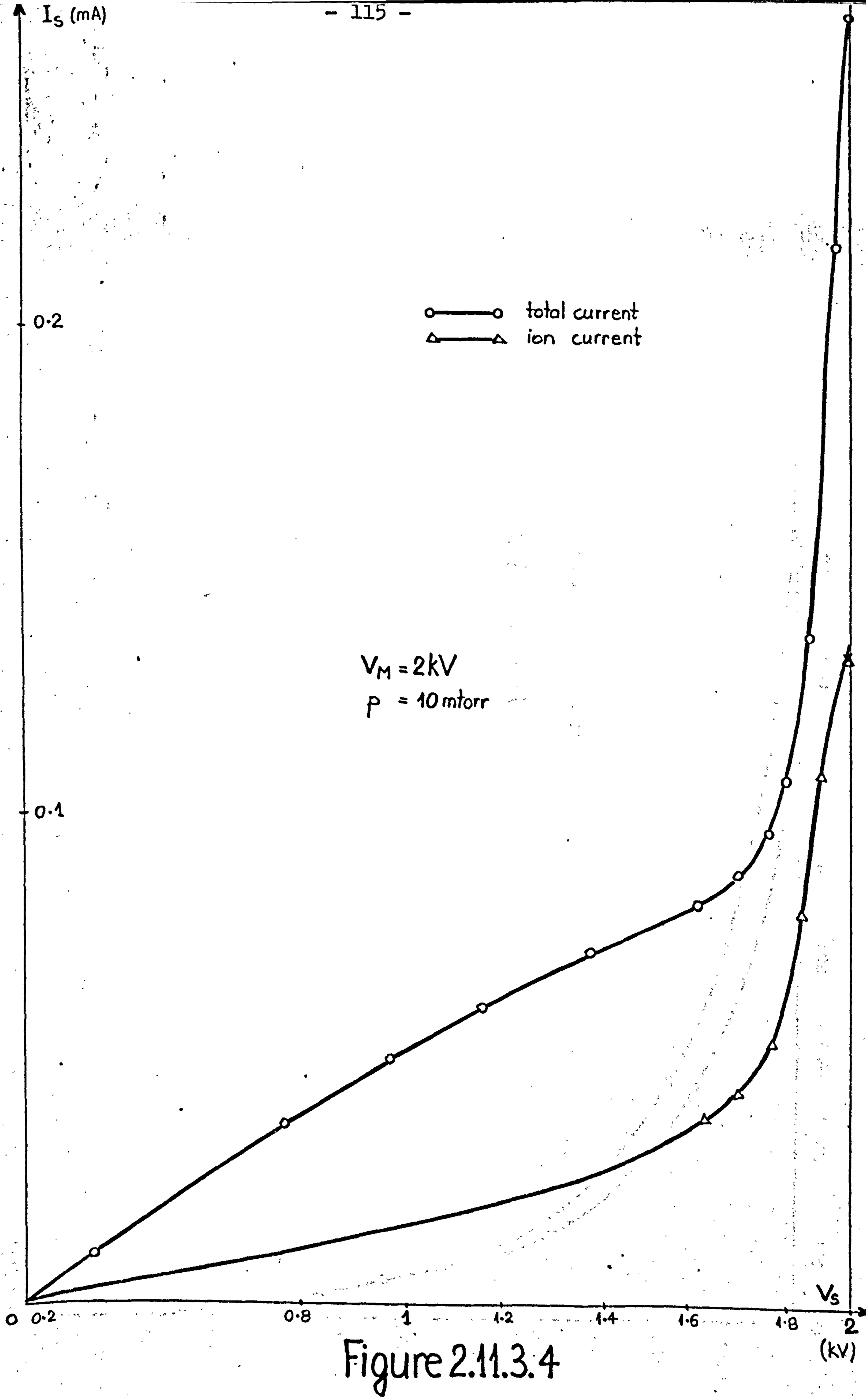

Figure 2.11.3.4

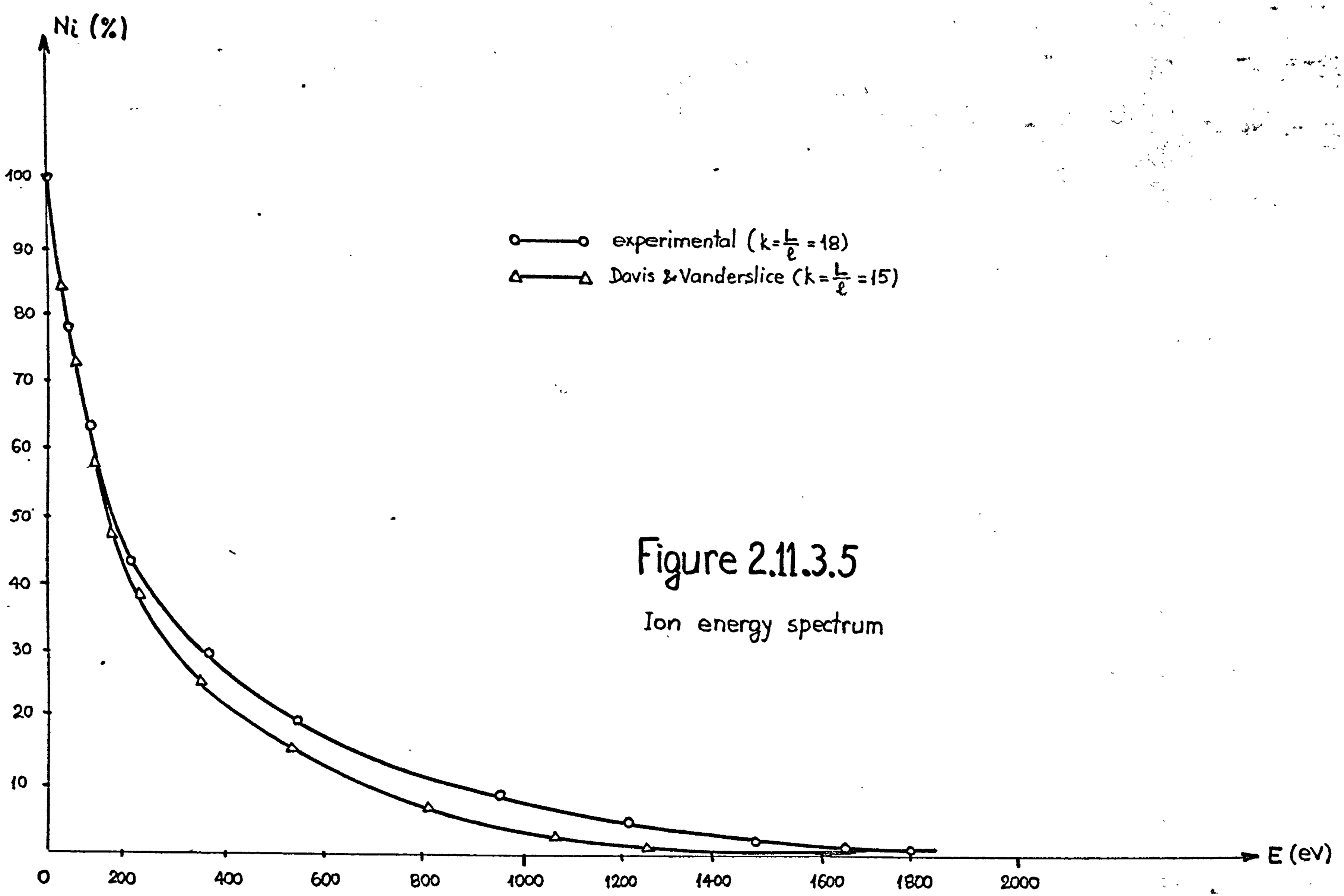

Figure 2.11.3.5

Ion energy spectrum

2.11.4. The effect of parameters upon the dark space / mean free path ratio

The ratio 'k' between the length of the cathode dark space 'L' and the mean free path 'ℓ' is an important factor in determining the collision mechanisms thus affecting the entire spectrum. 'k' is defined as :

$$k = \frac{L}{\ell}$$

a. An increase in the value of 'k' results in the energy being better shared, through an increased number of collisions.

Assuming that the electric field varies linearly across the cathode dark space, it means that an ion can be accelerated across one mean free path up to

$$E = \bar{e}\,\Delta V_{\ell} \qquad (2.11.4.1.)$$

where ΔV_{ℓ} is the potential difference between the two points along the dark space at a distance equal to the mean free path 'ℓ' Therefore, an increase in the value of 'k' is equivalent to a reduction of the mean free path relative to the cathode dark space

length, thus implying a decrease in ΔV_ℓ which leads to a reduction in the value of the ion maximum energy.

b. A decrease in the value of coefficient 'k' leads to an increase in ΔV_ℓ which means that the ions can be accelerated to higher energies. At the same time, this leads to a smaller rate of collisions and therefore the total energy is less shared among the energetic particles.

Since the value of 'k' is so determinant for the ion energy spectrum and consequently for the neutral energy spectrum, it is useful to see how it is influenced by the ion plating parameters. 'k' is plotted for different argon pressures and voltages in Figure 2.9.7. It can be seen that 'k' remains constant for pressures up to 25 mtorr and increases for higher pressures.

Therefore, when a better sharing of energy is required which implies an enhanced transfer of energy from ions to neutrals, working pressures higher than 25 mtorr are more favourable. This could prove useful when a mesh is used to plate insulators or ceramics and when the coating material deposits as energetic neutrals.

The value of 'k' decreases with the increase in voltage which means that ions can be accelerated to higher energies,but, this is accompanied by a

reduction of the collision rate and therefore, less energy is expected to be transferred to the neutrals.

2.11.5. The effect of parameters upon the ion current

A standard sq. in. steel substrate was subjected to a glow discharge bombardment and the bias voltage and argon gas pressure were varied independently.

The value of the cathodic current was measured and plotted versus parameters in Figure 2.11.5.1.

- As it can be seen, an increase in the voltage leads to an increase in the cathode current due to the fact that a higher potential can extract more ions from the plasma region. The cathode current drops to a steady value in time and one possible explanation is a twofold one :

  a. The ions and the energetic neutrals have higher energies for a higher bias voltage and therefore they are capable of removing through sputtering, other impurity layers not removed by the energetic bombardment at a lower voltage.

Cathodic current versus pressure and bias voltage

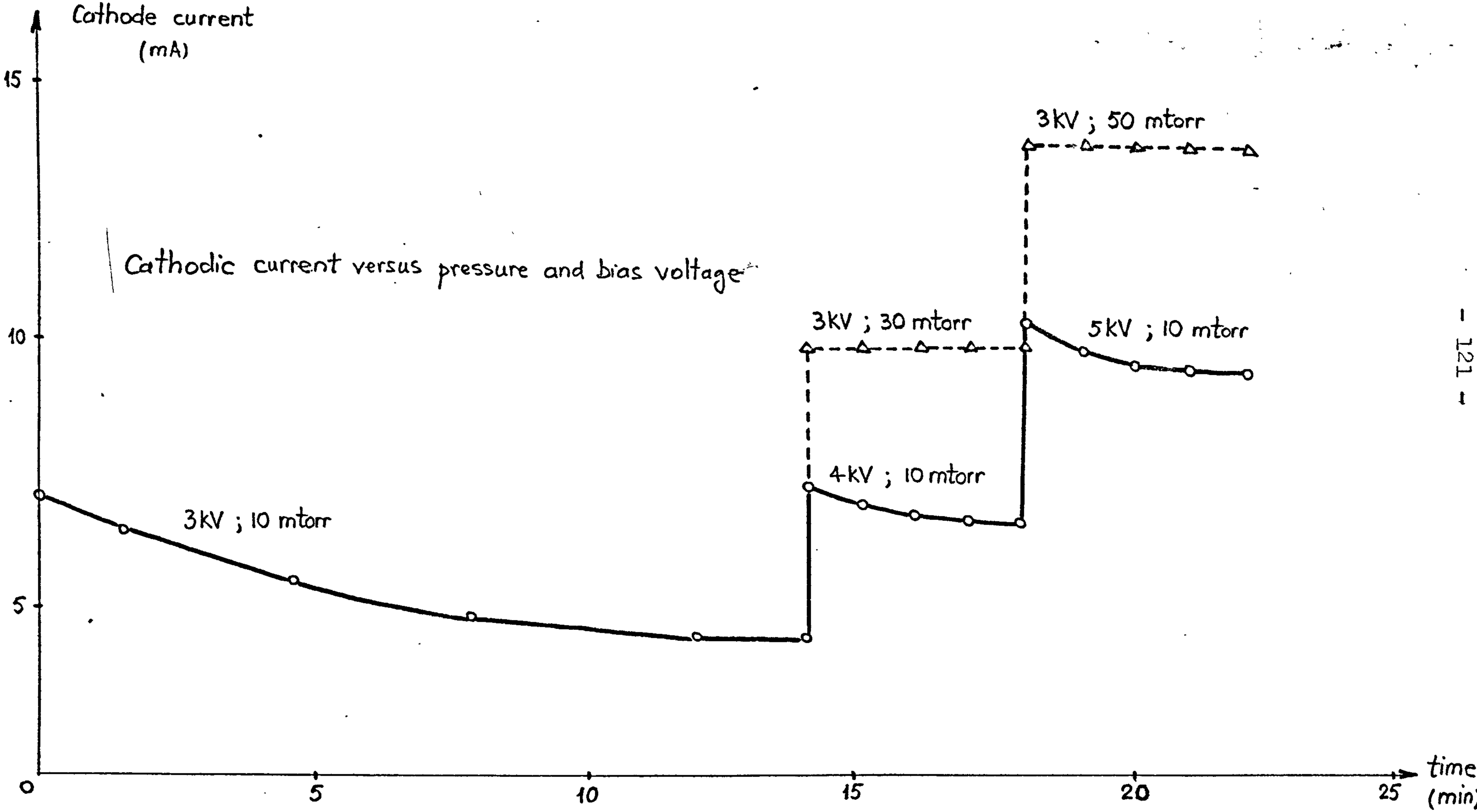

Figure 2.11.5.1

b. The micropeaks on the surface are further eroded leading to a drop in the secondary electron emission (sharp peaks concentrate the field lines giving higher secondary electrons emission).

- An increase in the argon pressure leads to an increase in the cathodic current which remains constant in time.

The increase is due to the fact that the plasma becomes stronger at higher pressures and therefore more ions can be extracted. The fact that this current remains constant is most probably due to the fact that the energy spectrum is not modified as regard the maximum ion and neutral energies. Although the total energy is higher, it is distributed to a larger number of particles.

2.11.6. Conclusions

Although the experiments presented in this section did not give accurate results, some valuable information was acquired concerning the ion energy distribution and the effect of process parameters (p;V) upon theenergy spectrum.

The ion energy spectrum experimentally determined, is almost identical to that calculated by Davis and Vanderslice and based on the assumption that the only collisions that take place in a glow discharge and are responsible for the energy spectrum, are the charge transfer and the elastic spheres collisions.

The difference between the two graphs is most probably due to the fact that the contribution of the electrons to the total substrate current had to be roughly approximated.

C H A P T E R 3

NUCLEATION AND INTERFACE.

ADHESION OF ION PLATED FILMS.

The experiments presented in this chapter are concerned with the early stages of nucleation of ion plated films, as well as with the interface formation and composition. The adhesion of ion plated films is analysed and discussed.

3.1. Nucleation and Growth

3.1.1. Theoretical Approach

Most of the time, the physical properties of a thin film are different from the bulk material and this is mainly due to the microstructure of the film which in its turn, is dependant upon the processes that take place during film formation in the early stages of nucleation and during the film growth.

Therefore, a study of nucleation of thin ion plated films could prove useful for understanding and possibly controlling the microstructure which at the moment, is one of the most pressing problems facing the ion plating technology.

Due to the fact that ion plated film atoms have much higher energies than the vacuum evaporated

atoms, the difference between the two films is expected to be noticed in the very early stages of nucleation and growth.

In the case of vacuum evaporation, the process of nucleation is a condensation process involving a phase transformation from the vapour (gas) phase to the solid phase. Condensation is initiated by the formation of small clusters (groups of atoms) called nuclei and the process is called nucleation.

Other depositing particles thermo - migrate on the surface and are incorporated in the initial nuclei which thus grow into small islands. Nucleation and growth are two simultaneous processes taking place during the evaporation. Finally, the small islands coalesce to form a continuous film[49] .

Parallel with these two processes and depending on substrate temperature, the diffusion of film atoms into the substrate lattice can take place in the case when the two materials (film & substrate) are metallurgically compatible[49] .

In the case of ion plating when most of the arriving film atoms have energies higher than the thermal energy, the production of nucleation centres is different from the case of vacuum evaporation . As presented in Section 2.12, the subjection of the substrate surface to the energetic bombardment creates lattice defects such as lattice steps,

point defects and vacancies, which act as nucleation centres[4,52] . Also, the penetration of film atoms into the substrate lattice in small depths (sticking) generates additional nucleation centres. Thus, for ion plating, it is expected to find a high density of nucleation centres, uniformly distributed on the substrate surface.

Due to the continuous energetic bombardment, the nonadhesive film atoms are sputtered from the surface and new nucleation centres are continuously produced.

Thermo - migration is probably reduced by the energetic bombardment since the migrating particles having a minimum adhesion to the substrate are the easiest to be sputtered.

Therefore, the process of film formation is expected to be one of a continuous generation of nuclei and growth around these nuclei which however, will remain small in size compared with the size of vacuum evaporated film islands[6].

The density and size of nuclei, for ion plating, depend upon parameters like : pressure, bias voltage and ratio :

$$\frac{\text{energetic particles}}{\text{total depositing particles}}$$

where the energetic particles are the film ions and neutrals with energies higher than the thermal

energy and capable of producing sputtering.
This ratio is highly dependant upon the ionization efficiency.

Nucleation and Growth have an essential effect upon the structure of the film. A film beginning to grow in a small number of large islands will have an island structure which will persist even after the film becomes continuous, facilitating the formation of large grains and a columnar structure. On the other hand, a film consisting of a very large number of small islands that grow more in number than in size, will become continuous at a small thickness and will have a much finer grain structure.

3.1.2. Experimental Results

In order to study nucleation and growth, carbon films of approximately 500 Å in thickness were vacuum deposited from an arc source onto microscope glass slides.[6]

On the carbon films, small quantities of copper were vacuum evaporated and ion plated and then, the carbon films containing the copper deposit were detached from the glass slide by immersion into a solution of alcohol in distilled water. The small flakes were then collected on transmission electron microscope grids.

The vacuum evaporation was performed at a background pressure of 5×10^{-6} torr.

In the case of ion plating, owing to the small thickness of the carbon film which can be easily removed by sputtering, the glow discharge was set on a few seconds before the evaporation started.

0.8 and 1.2 mg of copper were vacuum evaporated and then analysed in the TEM as shown in Figure 3.1.1. (a, b). As it can be noticed, the nuclei are not uniformly distributed on the surface and the growth is mainly due to the islands growing larger and coalescing, parallel with the formation of a few new nuclei.

The ion plated films were obtained by evaporating 0.8. and 1.2 mg copper at 3 and 4.5 kV bias voltage and argon pressures of 10 and 20 mtorr. A wire

mesh, attached to the H.T. was set in front of the glass slides at a distance of approximately 2 mm. The results are shown in Figure 3.1.2. (a,b,c,d). Figure 3.1.3. shows the nucleation of a similar ion plated copper film, at 3 kV and 10 mtorr argon pressure but, with an ion current three times higher which results in a threefold increase in the ionization efficiency.

As it can be seen from Figure 3.1.2. (a,b), the variation of the bias voltage (the other parameters kept constant) induces important changes in the nucleation process. With the increase in voltage, the nuclei become smaller in size and denser which is explained by the increase in the energy of ions and neutrals, as well as their number (due to the increase in the ion current that follows an increase in the bias voltage at constant pressure). This leads to a higher density of nucleation centres and also, the nuclei are not allowed to grow larger by the intense energetic bombardment.

In Figure 3.1.2. c, a larger quantity of copper was evaporated and the result is that more nuclei appear and the older ones are bombarded and become smaller in size due to sputtering.as compared to Figure 3.1.2.b .

The increase in argon pressure, from 10 mtorr to 20 mtorr, did not seem to produce any marked difference in the nucleation as shown in Figure 3.1.2c but the remanent pattern of island type growth is

completely removed for 20 mtorr.

Comparing the ion plated films with the vacuum evaporated ones, it can concluded that the tendency of growing in small islands is practically nonexistent for 4.5 kV, whereas for 3 kV small islands, though much smaller in size, still persist. As the deposition continues (Figure 3.1.2.c), the growth is mainly due to the formation of new nucleation centres filling the gaps rather than the other nuclei growing larger in size..

Figure 3.1.3. presents the nucleation of a copper film ion plated in similar conditions with those shown in Figure 3.1.2.a (0.8 mg Cu, 3 kV, 10 mtorr) but using a triode system. he ion current was independently increased to a three times higher value, resulting in a three times increase in the ionization efficiency. It results in the creation of very dense nucleation centres. The growth is in much smaller nuclei uniform distributed on the surface.

The effect of increasing the current density but not chanching the pressure is a threefold increase of the ratio :

$$\frac{\text{sputtering rate}}{\text{d position rate}}$$

This also leads to slightly thinner films, for the same quantity evaporated.

The conclusion is that variation of ion plating parameters, e.g. voltage and ion current density, can induce important changes in the thin films right from the beginning of the nucleation process and possibly, can affect the microstructure of thicker films. These early stages of nucleation are also the first steps towards the formation of the interface which is important for the adhesion of the film to the substrate. A large number of nuclei, uniformly distributed, will lead to a continuous interface throughout the substrate surface and therefore a better overall adhesion.

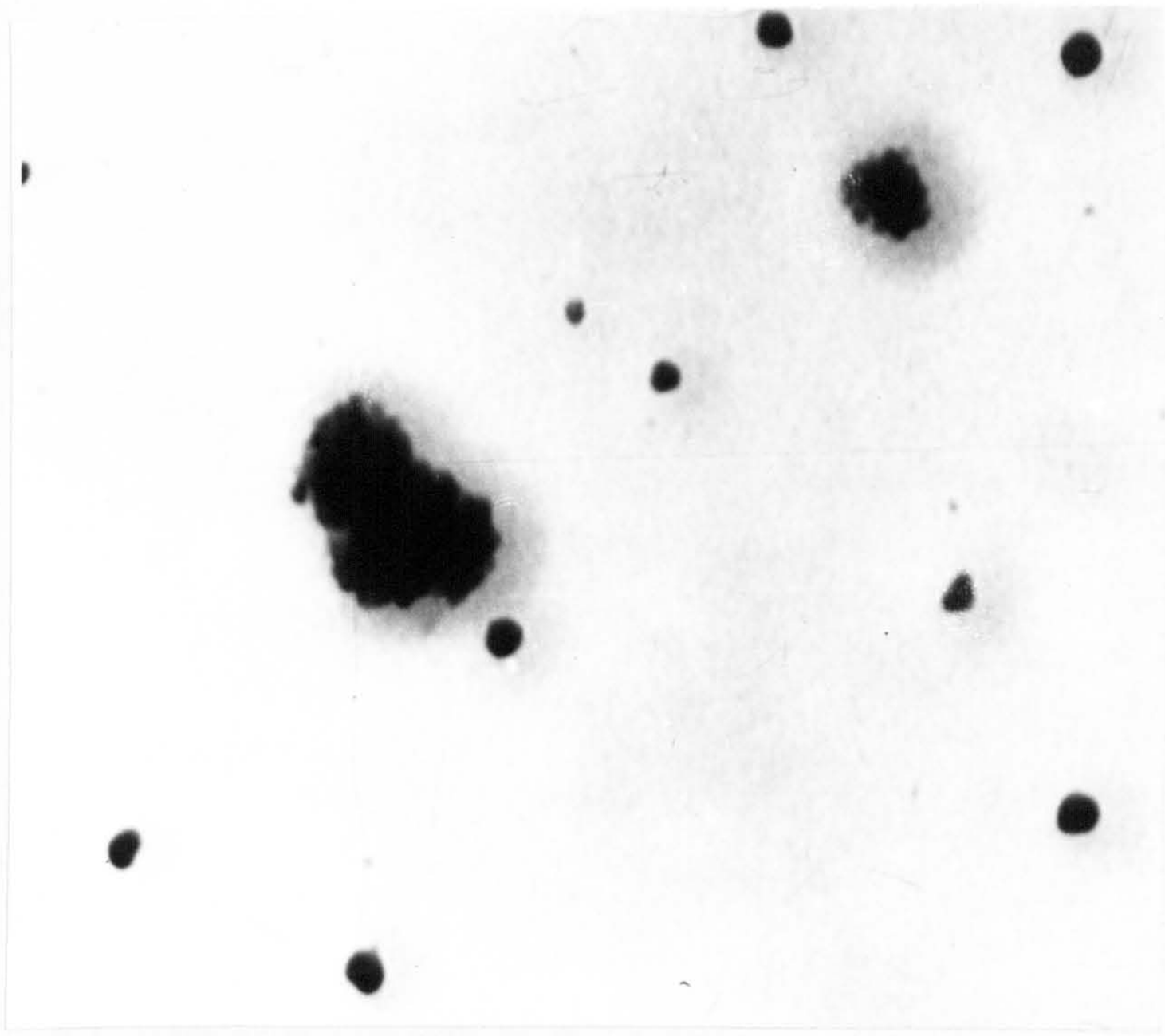

a. 0·8 mg Cu - vacuum evaporated ×150,000

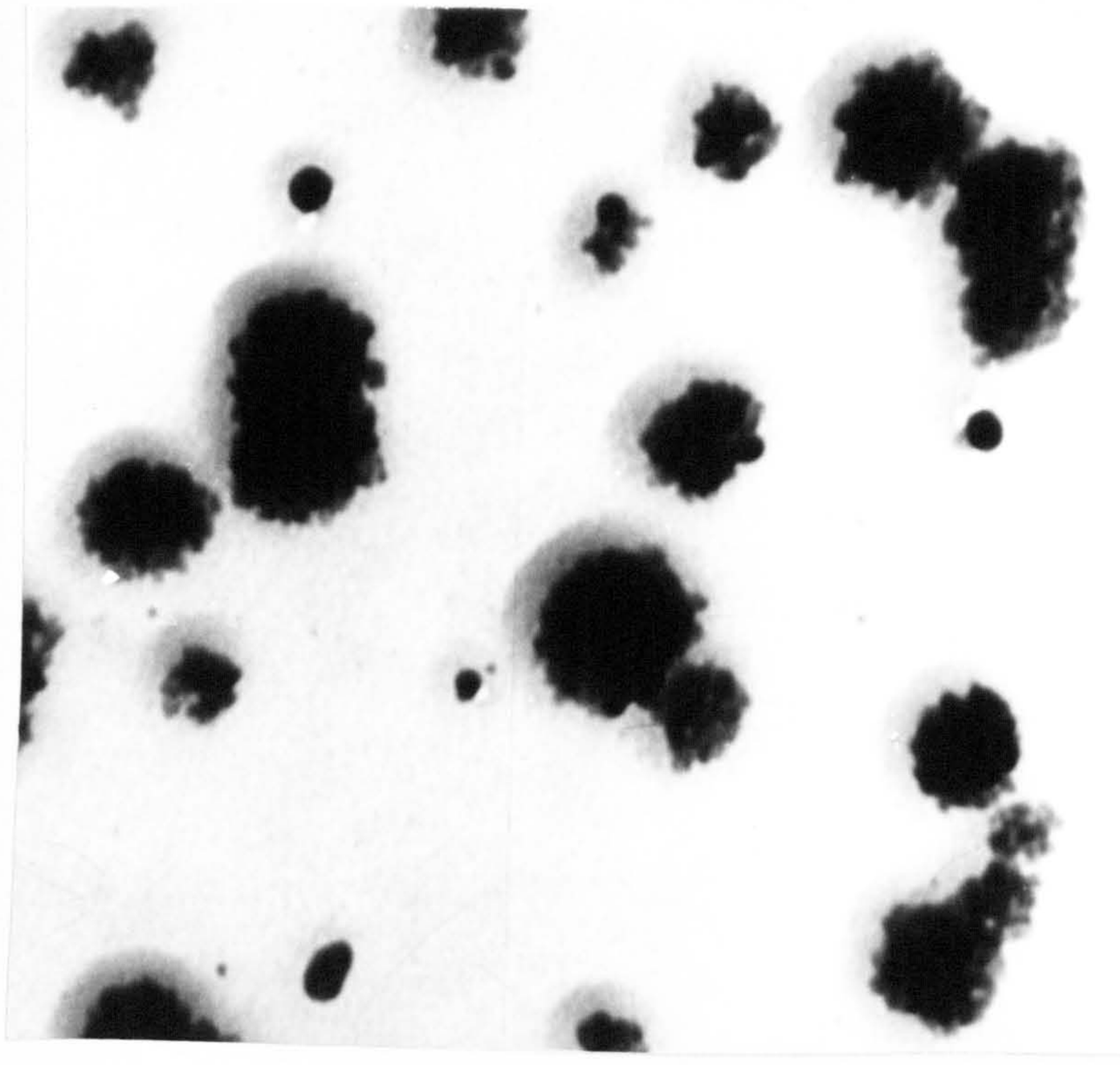

b. 1-2 mg Cu - vacuum evaporated × 150,000

Figure 3.1.1

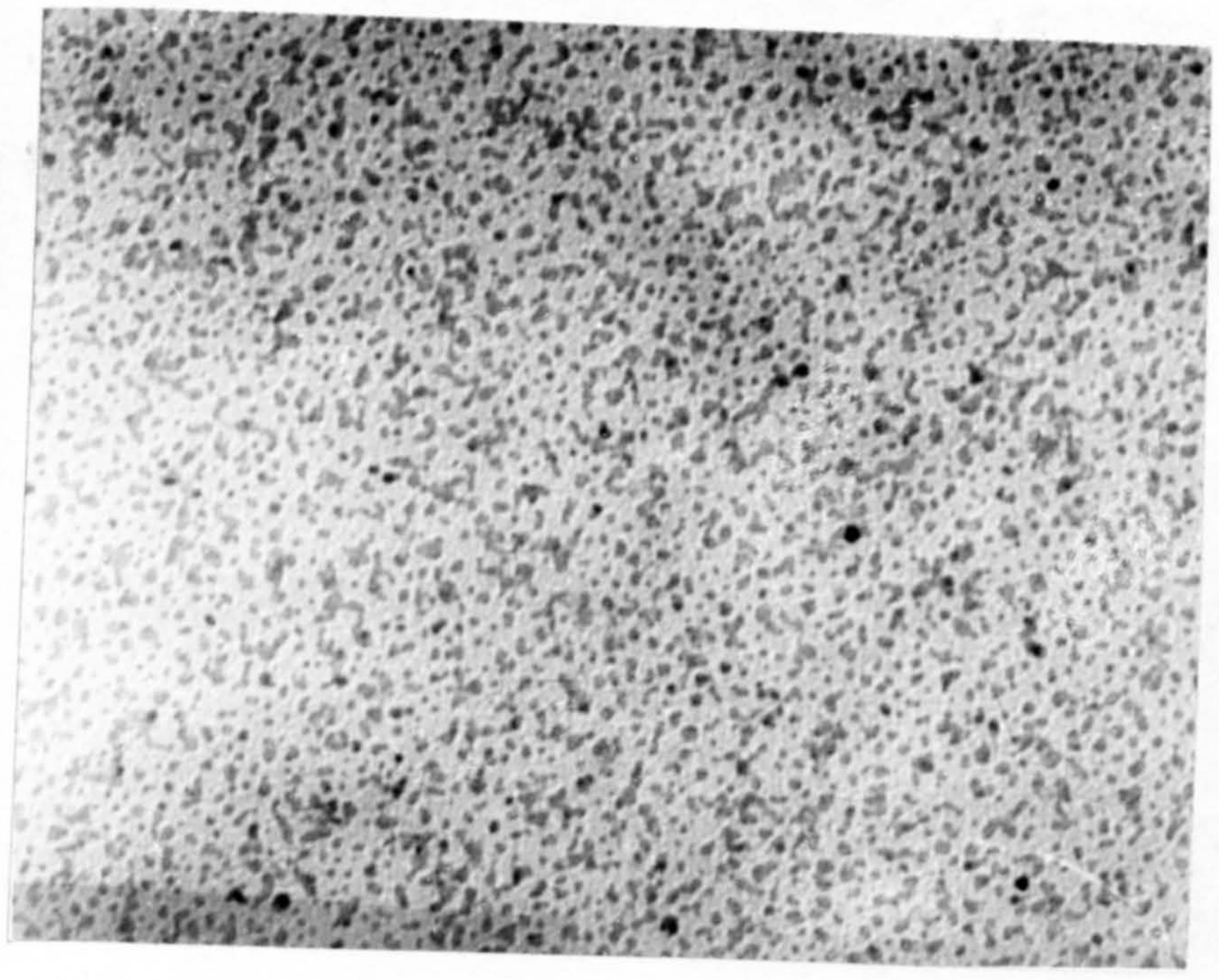

a. 0·8 mg.Cu, ion plated at 3kV & 10 mtorr × 150,000

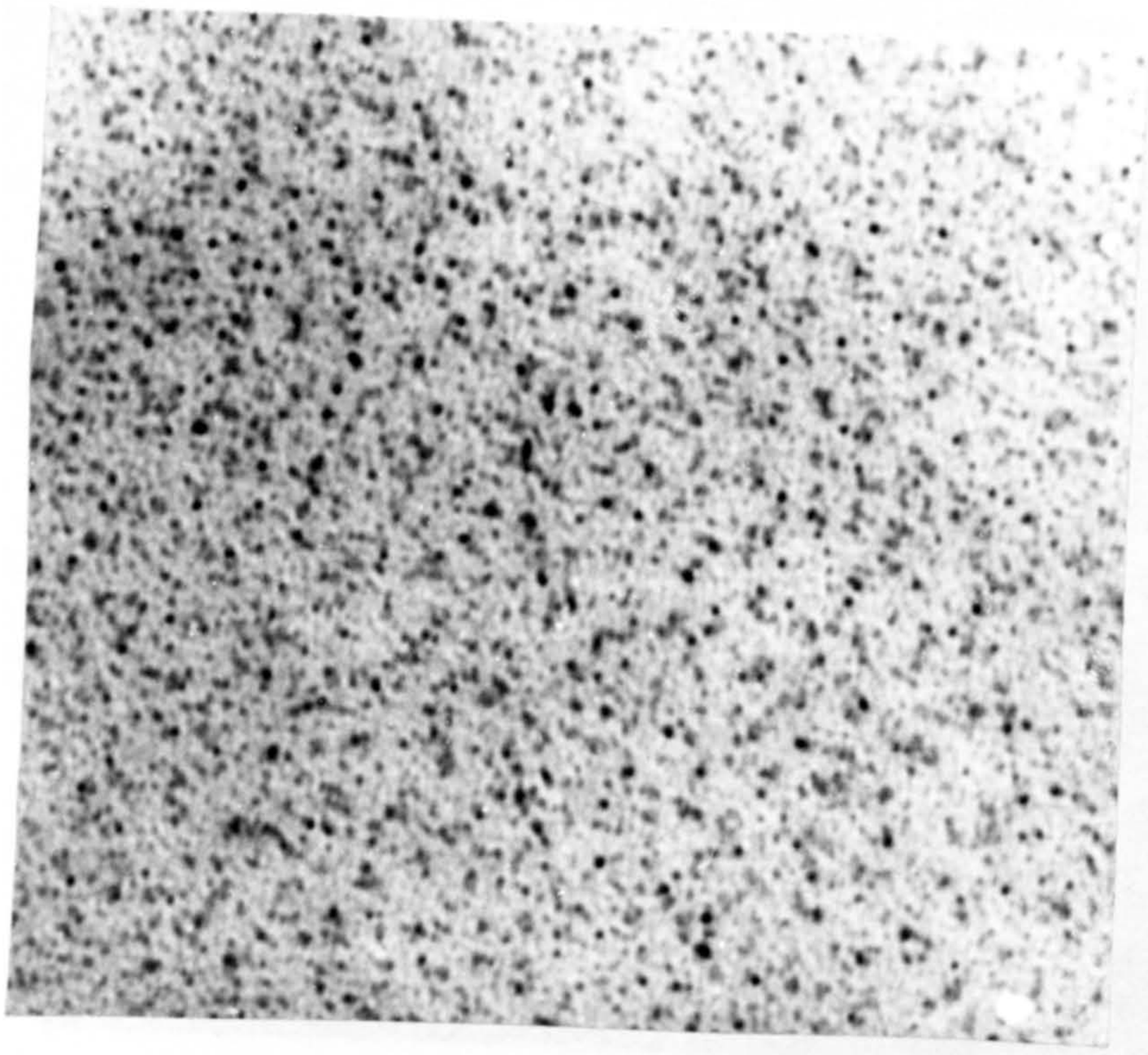

b. 0·8 mg Cu, ion plated at 4·5 kV & 10 mtorr. ×150,000

Figure 3.1.2

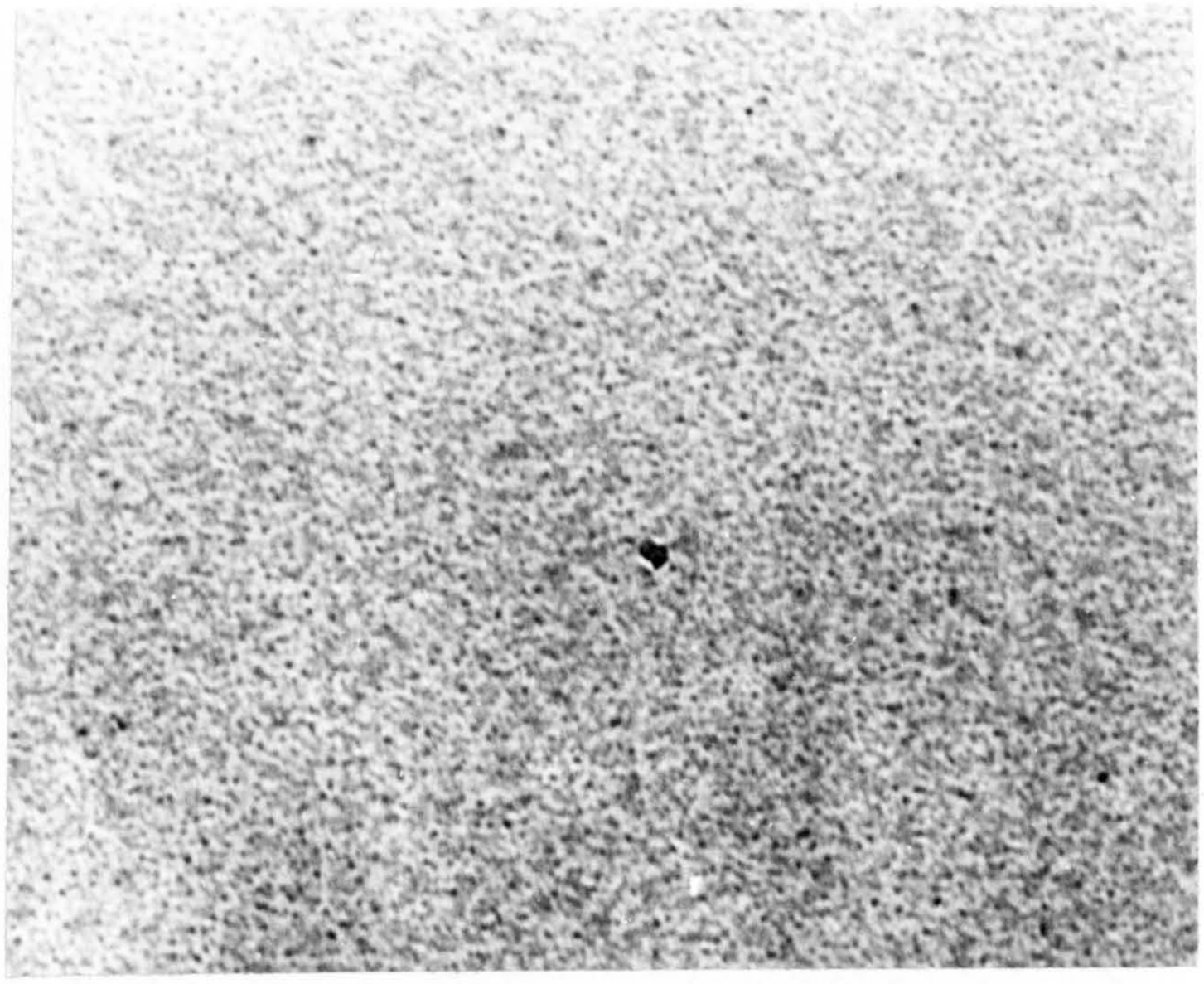

x 150,000

c. 1·2 mg. Cu, ion plated at 4·5 kV & 10 mtorr

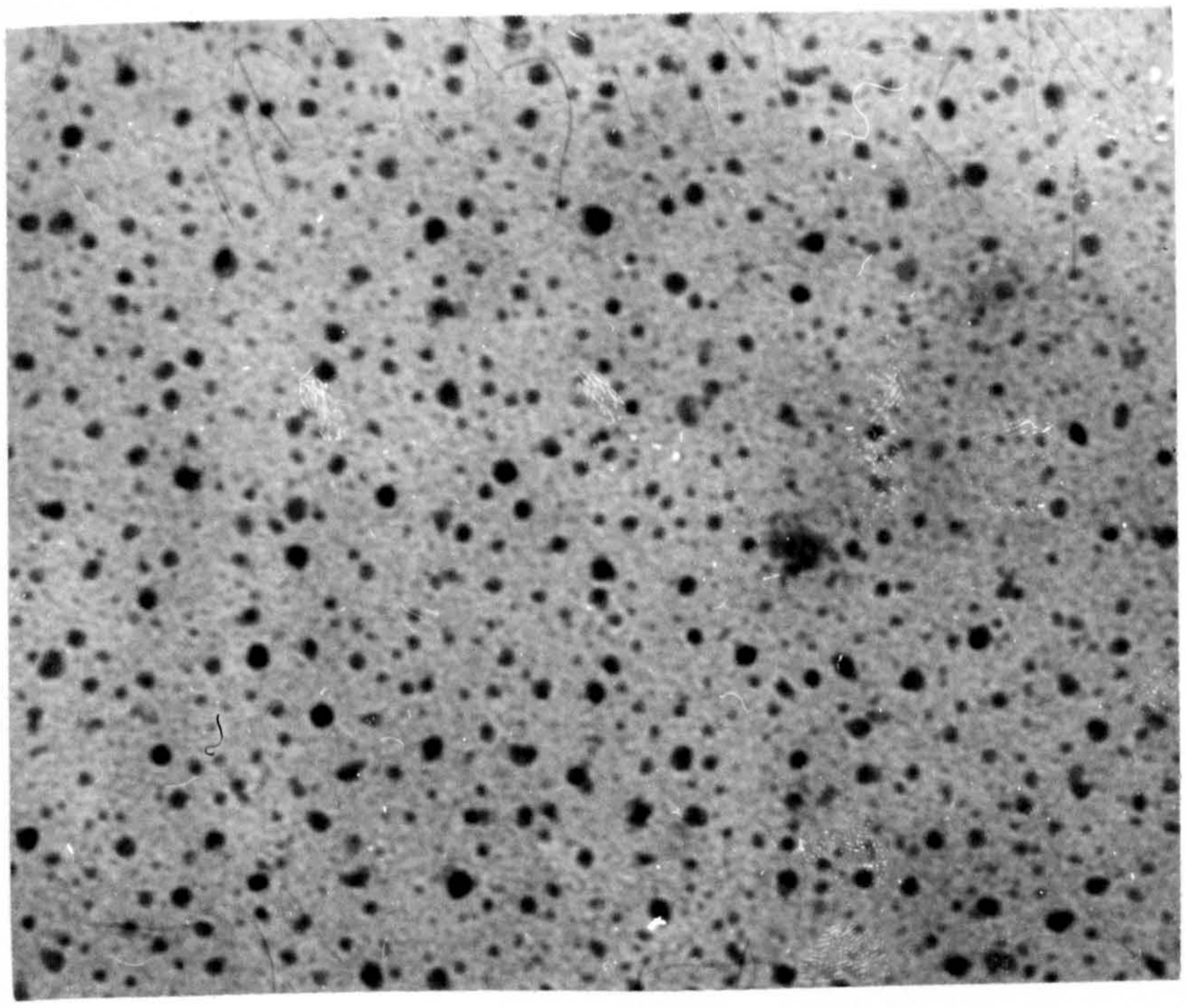

x 150,000

d. 0·8 mg. Cu, ion plated at 3kV & 20 mtorr

Figure 3.1.2

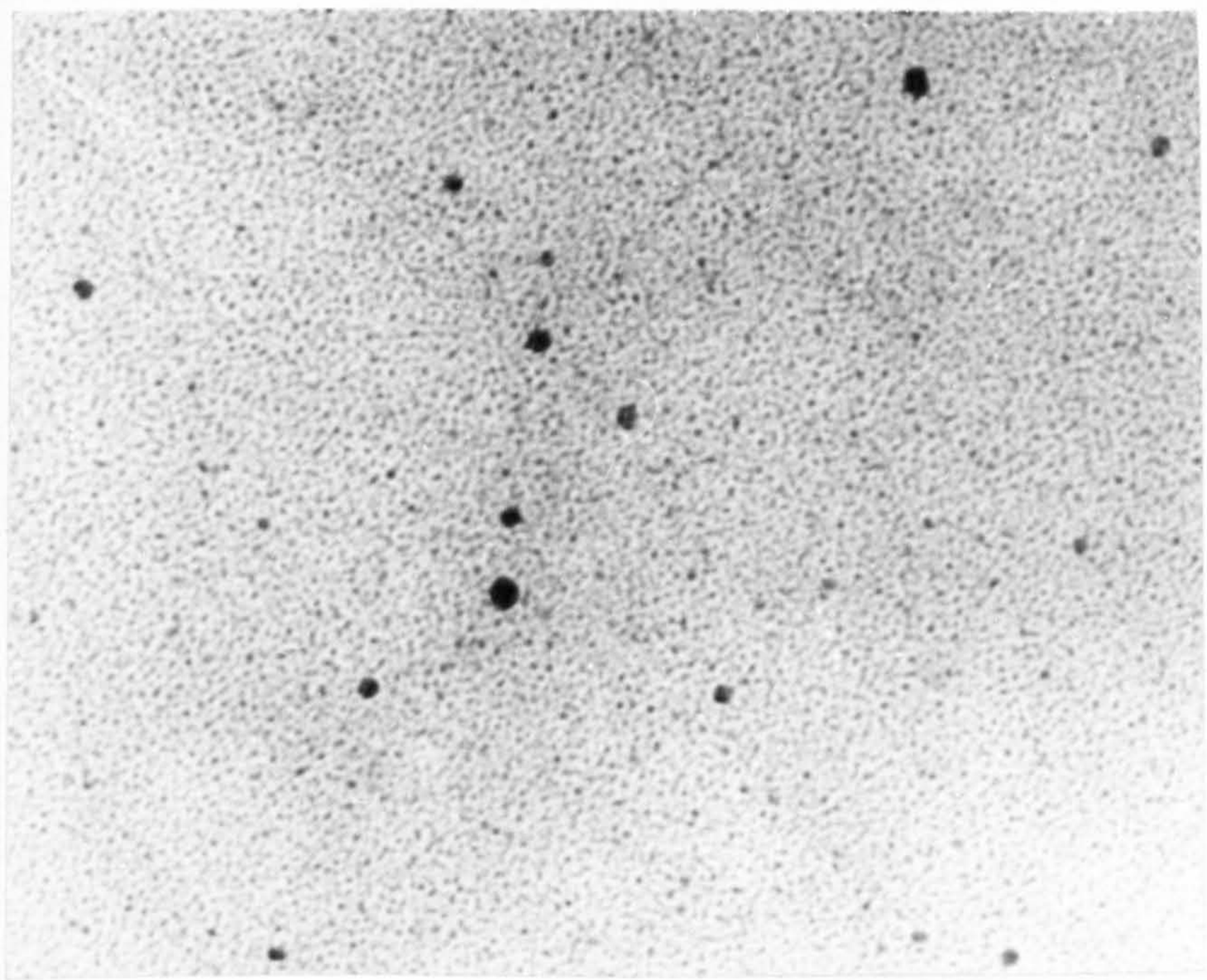

× 150,000

0·8 mg. Cu, ion plated at 3kV, 10mtorr & $3I_i$

I_i is the ion current drawn to the cathode in similar p-V conditions but without a positive probe in a normal diode system.

Figure 3.1.3

3kV – positive probe-activated

3.2. Interface

3.2.1. Experimental

The problems encountered so far concerning the interface of ion plated films are connected with analysing its composition and measuring its depth. Several authors[21,24,53] reported the existance of a graded interface between the ion plated films and the substrate.

The basic reasons for the formation of such graded interfaces in the case of ion plating, are :

a. Thermal diffusion, when the two materials (film and substrate) are compatible (e.g. Cu on Steel[21]), giving an interface whose depth depends upon temperature and the amount of time for which this temperature is kept, as well as upon the nature of film and substrate materials.

b. Atomistic mixture[4] due to sputtering, back sputtering, ionization and back scattering of the substrate material which will mix with film atoms and deposit together, producing a mixed interface.

c. The induction of a large number of defects in the substrate lattice leads to an enhanced diffusion process possibly even for non-

compatible materials[26] (in smaller depths). Ion implantation was another process considered to take part in the formation of the interface[21] but due to the fact that the bulk energetic particles (ions and neutrals) have energies lower than the acceleration energy, the implantation, though it occurs (for the ions and neutrals having the highest energies), happens in very small depths[22] and therefore it cannot be responsible for the deep graded interface.

The existance of a graded interface, as well as the determination of its composition and depth is possible using the modern technique of Scanning Auger Electron Spectroscopy[27]. The analysis was performed using a Varian 10 keV Scanning Auger Electron Spectrometer*. Beam diameter was $< 10 \mu m$ and primary electron beam energies of 3 keV and currents of 3A were used in a background pressure of 1×10^{-9} torr.

In order to calculate approximate values for the relative concentrations of the elements, the peak to peak heights of selected Auger peaks were measured[28]. The composition profiles were obtained by removing succesive atomic layers by means of ion beam sputtering. The composition profiles were plotted against sputtering time and approxi-

---

*The work on the SAES was performed by Dr.J.M. Walls at the University of Loughborough - U.K.

mate values for the depth were obtained using published sputtering yields[29,30]. The substrates were made of high purity electrolitic Nickel polished down to magnezia grade.

The surfaces were flat, 1 sq.cm in area. On these substrates, copper and silver were vacuum evaporated at 10^{-5} torr chamber pressure and ion plated at 3 kV bias voltage and 15 mtorr argon pressure . Prior to ion plating and vacuum evaporation, the substrates were sputter cleaned for 30 minutes at 3 kV and 15 mtorr argon. The reason for sputter cleaning the substrates before vacuum evaporation was to compensate the effect of temperature rise which could influence the diffusion process and therefore the interface depth. The bulk temperature reached was approximately 120°C.

Film substrate pairs Cu/Ni and Ag/Ni were chosen to give a set of metallurgically compatible and incompatible materials. Copper alloys with nickel while silver does not.

3.2.2. Results

a. Sputter cleaned Nickel

A sputter cleaned nickel substrate was analysed and a few layers on the surface were found to contain carbon, oxygen and sulphur due to atmospheric contamination.

These impuritie were quickly removed by ion sputtering as shown in the concentration depth profile presented in Figure 3.2.2.1. Argon was introduced in the nickel surface both due to the sputter cleaning and the ion profiling process employed by the method. But the maximum concentrations of this element were found to be approximately 1 atomic percent.

b. Silver on Nickel

Silver and nickel are two incompatible materials and thermal diffusion is expected to be nonexistent in the case of vacuum evaporation. The concentration of silver, vacuum evaporated on nickel, is plotted as a function of sputtering time in Figure 3.2.2.2.

A few layers on the surface were contaminated with carbon, sulphur and oxygen impurities due to their subjection to atmospheric environment. The level

of contaminating species (S,O) in the interface were found to be less than 1 atomic percent. The width of the interface was found to be approximately 50 nm. Although a sharp interface was expected to be found, the broadening of its depth could be caused both by some diffusion due to the inducement of lattice defects during sputter cleaning, but most likely it is caused by the preferential sputtering and knock - on effects associated with the sputter profiling technique.

The composition profile of ion plated silver on nickel is shown in Figure 3.2.2.3. The same contaminants were found on the topmost of the surface which were quickly removed by sputtering. The width of the interface was approximately 250 nm which is very much broadened in comparison with the vacuum evaporated one. Since the same pre - deposition conditions were achieved, this broadening of the interface depth can only be due to the atomistic mixture and redeposition processes taking place during ion plating, Being incompatible materials, little diffusion will occur to influence the depth of the interface. Even if the 50 nm found for the vacuum evaporation are due to diffusion, then the 200 nm of interface must be the effect of processes other than diffusion.

As far as the purity of the interface is concerned, only argon and oxygen peaks.were present

and their total concentration was approximately 0.8 %. Levels of argon concentration throughout the film did not exceed 1 atomic percent.

c. Copper on Nickel

Copper and nickel are compatible and in this case, thermodiffusion can occur.
The topmost of the surfaces of both vacuum evaporated and ion plated films contained the same impurity elements as the silver films, and the levels of contamination in the film and interface were also similar and below 1 atomic percent.
In contrast to the silver - nickel pair, the width of the interfaces were broadly similar for both vacuum evaporated and ion plated films and were approximately 280 nm wide, as shown in Figures 3.2.2.4. and 3.2.2.5.
The explanation for these results is that due to the sputter cleaning treatment of the surface prior to vacuum evaporation, the substrate temperature was raised to a level similar to the one obtained for ion plating. Since a small quantity of material was evaporated and the evaporation lasted only a few seconds, there was not sufficient time for the surface to cool down and therefore, similar temperatures were obtained during vacuum evaporation and ion pla

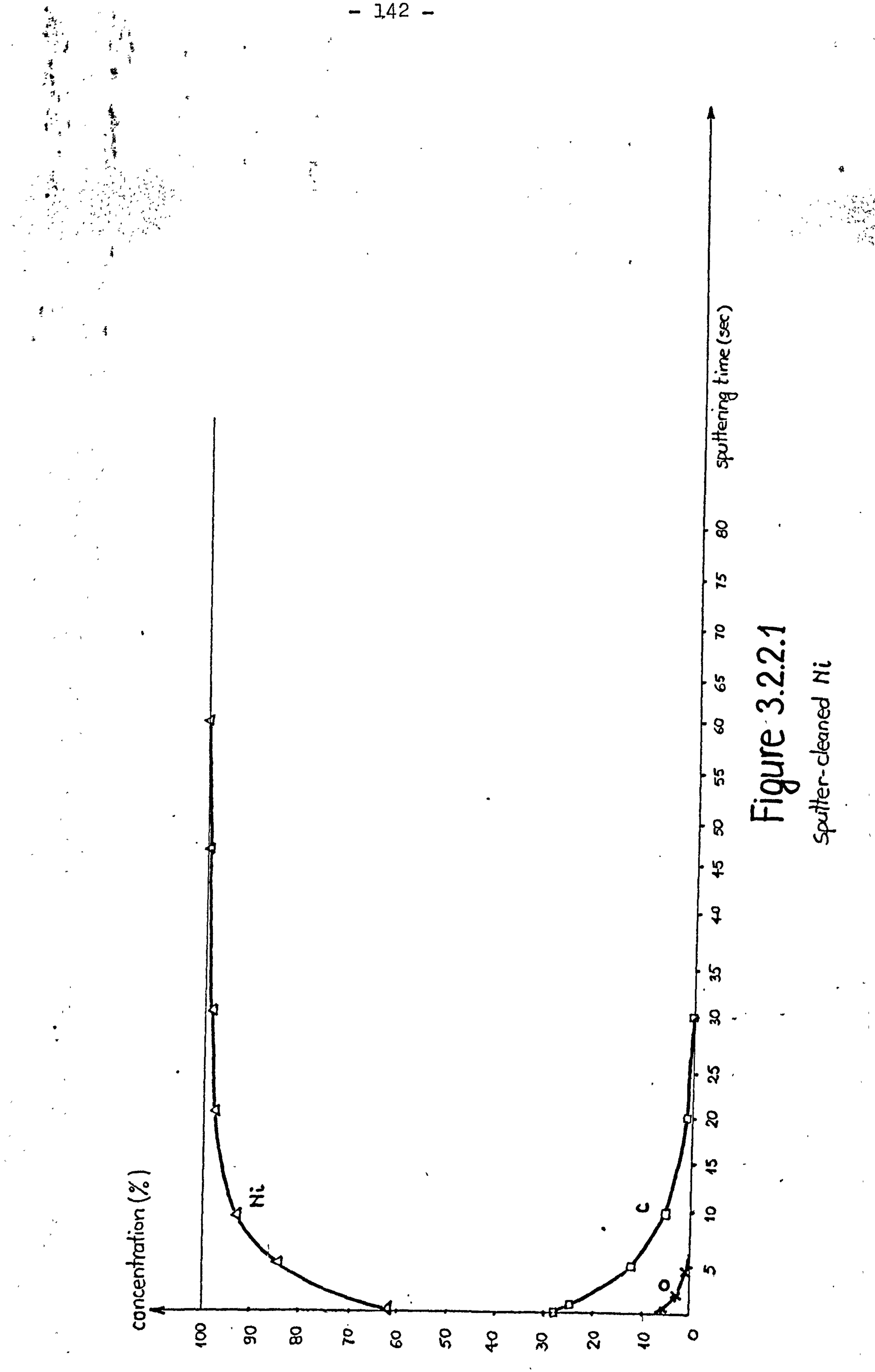

Figure 3.2.1
Sputter-cleaned Ni

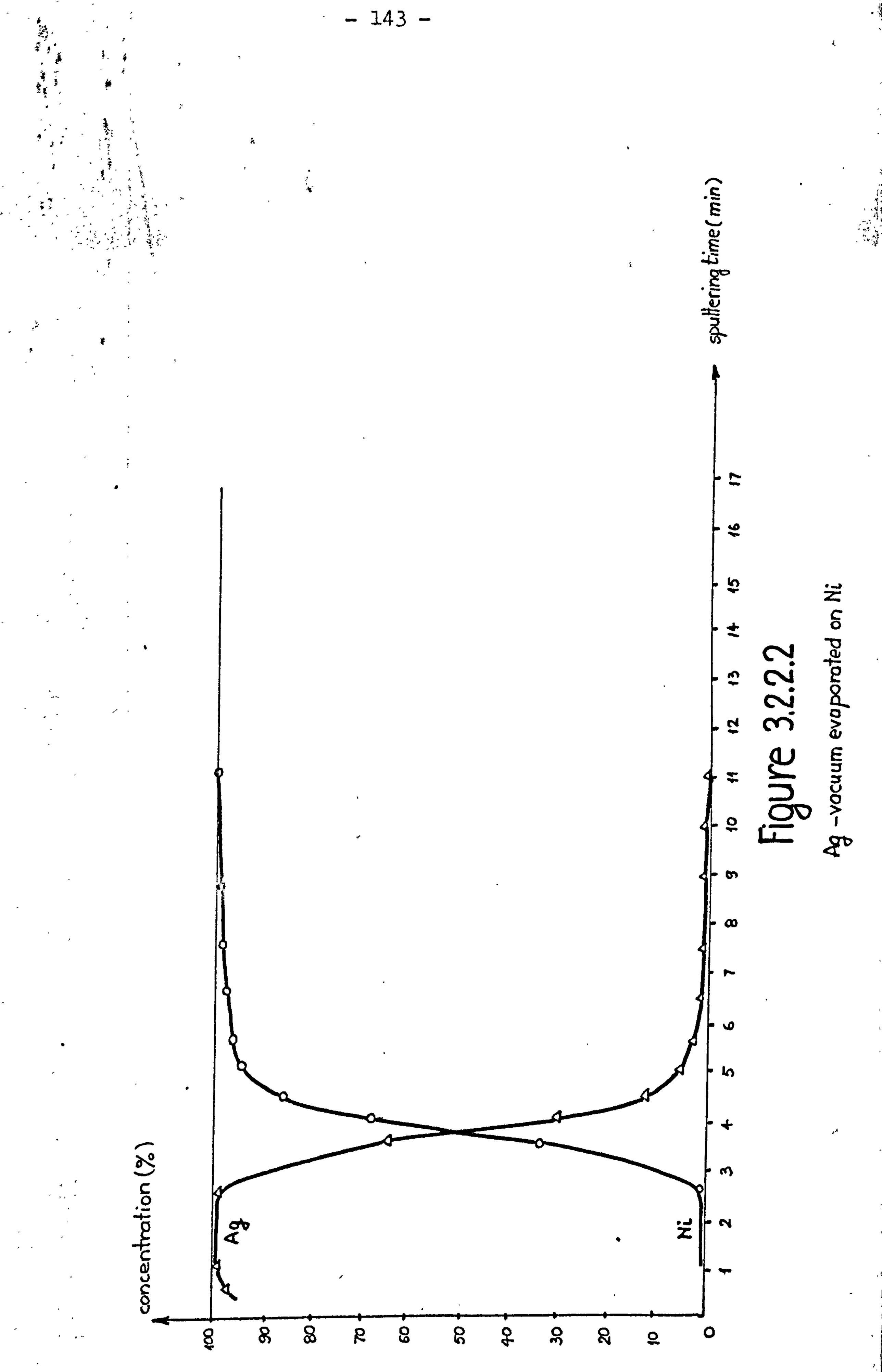

Figure 3.2.2.2

Ag - vacuum evaporated on Ni

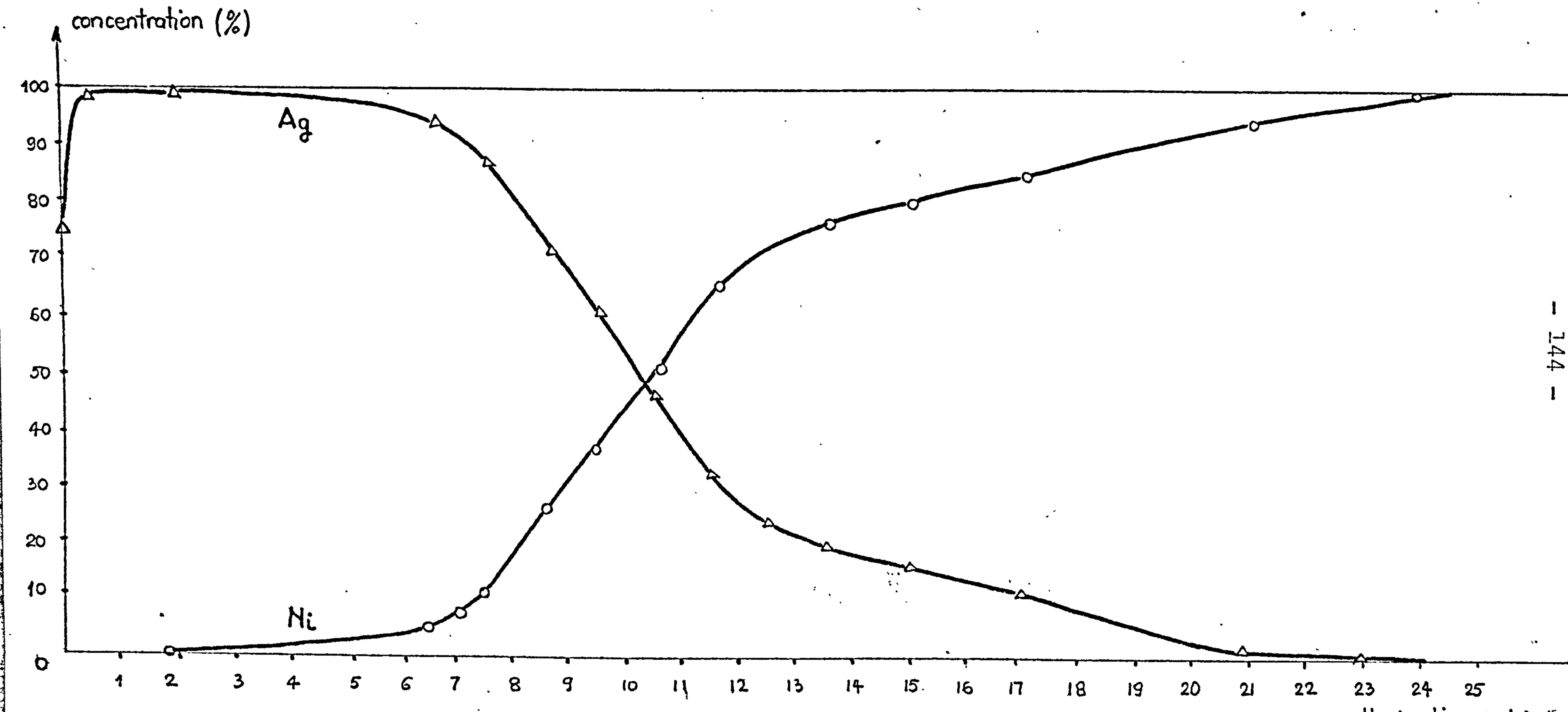

Figure 3.2.2.3

Ag - ion plated on Ni

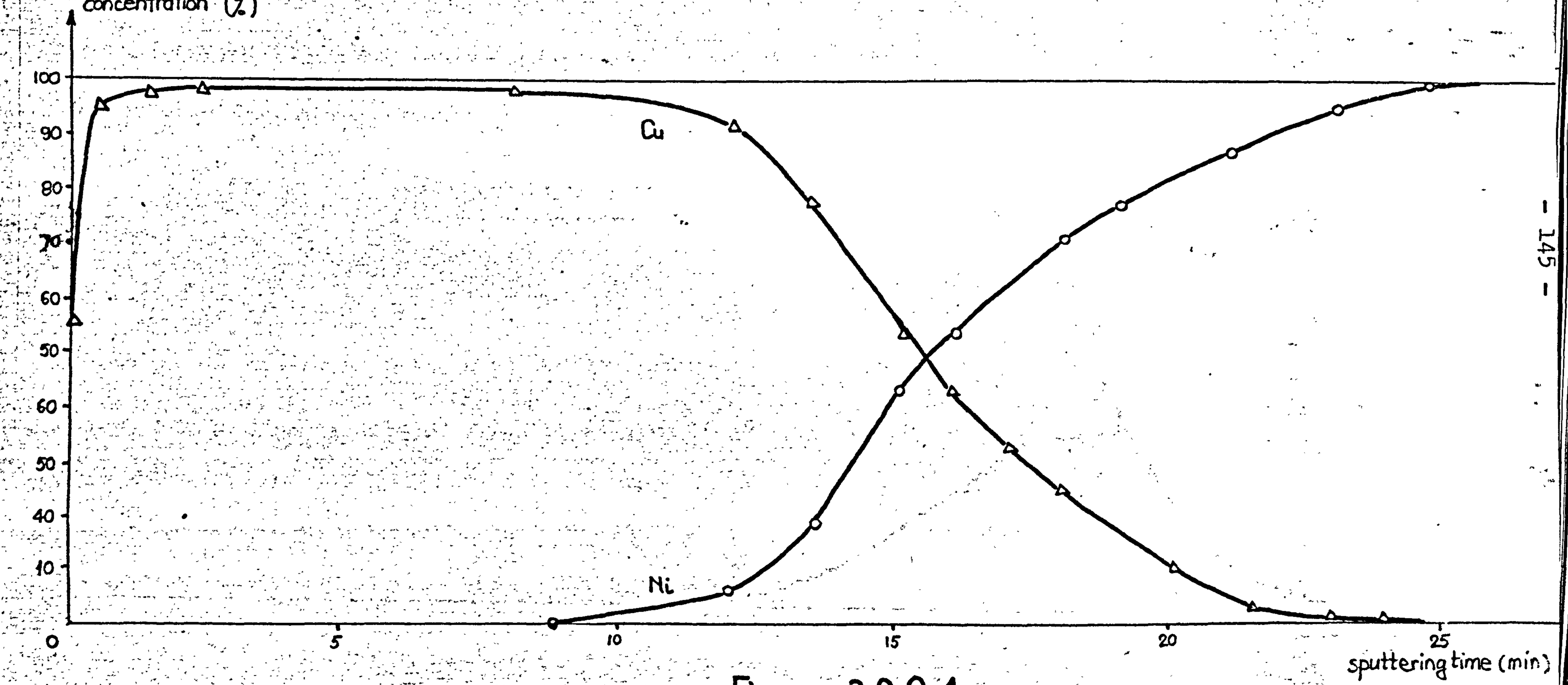

Figure 3.2.2.4

Cu - vacuum evaporated on Ni

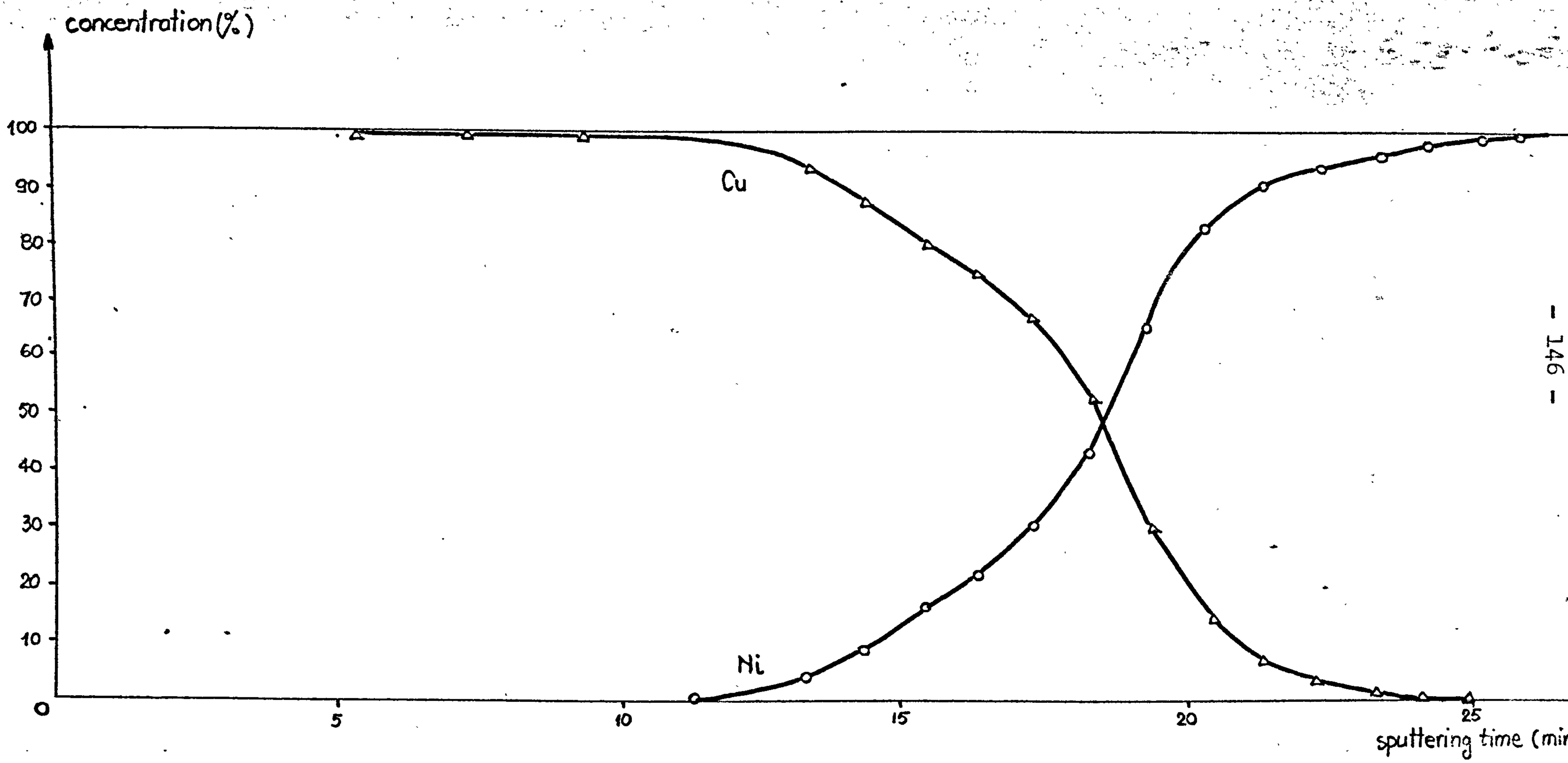

Figure 3.2.2.5

Cu – ion plated on Ni

The fact that similar interface depths are obtained in both cases leads to the conclusion that in the case of compatible materials, thermal diffusion is the main process responsible for the interface depth of the ion plated films.

3.2.3. Conclusions

The results presented above seem to prove the conclusions drawn in Section 2.1.2.
Since the good adhesion of ion plated film is a result of a deep graded interface, the main factors responsible for this graded interface are :

a. For compatible materials - enhanced physical diffusion due to high local temperatures and inducement of high lattice defects by the energetic particles bombardment.

b. For noncompatible materials - atomistic mixing and redeposition of film and substrate materials.

3.3. Adhesion of Ion Plated Films and Factor Determining it

D.M.Mattox was the first to describe the ion plating technique[2] and he presented some factors which determined the extremely good adhesion of ion plated films[8] compared with films deposited by other vacuum techniques. It was stated that in order to obtain a good adhesion, it is required to have a very clean substrate surface, free of contaminating layers (mainly oxides) which lead to a weak and brittle interface between film and substrate.

Another determinant factor for a good adhesion was considered to be the deep, graded interface obtained by the penetration of film atoms into the substrate lattice. This penetration can be caused by diffusion, due to high temperatures (in the case of compatible materials) and also due to the production of dense surface defects such as vacancies which have the effect of enhancing the diffusion process.

Another explanation given by Mattox and other authors[21] was the ion implantation of film atoms into the substrate lattice (mainly for noncompatible materials) combined with the physical mixing of film and substrate material (due to the sputtering) and redeposition onto the substrate.

Considering now the results previously obtained in this work regarding the energies of the ions and neutrals, the real reasons for the good a adhesion in ion plating could be: in the case of alloying materials, due to the rise in the surface temperature, the enhanced diffusion could be the most probable explanation.

More difficult is to explain the good adhesion obtained for non - alloying materials or for the deposition of metal films on ceramics, plastic or organic substrates.

Ion implantation in depths of several microns as it has been reported[21] cannot be a viable explanation since Carter and Colligon[22] demonstrated that for energies of 5 keV, the depth of implantation is about 50 Å.

But as previously demonstrated, the bulk ions have energies ranging 0 - 550 ēV for 3 kV bias voltage although there could be some ions in an extremely small number, having the full acceleration energy. With ionization efficiencies having values of around 0.1 % and even lower values during the deposition, such an extremely small number of ions cannot be responsible for the good adhesion of the total number of deposited particles.

But, as demonstrated in this work, the bulk of the arriving neutrals have energies ranging 0 - 550 ēV for 3 kV bias voltage,and a number of neutrals equal to the total number of ions reach the cathode

with energies of 550 ēV as compared to a very small number of ions (approximately 0.1 %) that arrive with this maximum energy.

Therefore, it can be concluded that ion plating is the deposition of a small number of energetic ions and a large number of energetic neutrals with overall mean energy of about 150 eV for 3 kV bias. Owing to these relatively low energies (compared to those previously reported), ion implantation is out of question, although it might occur in very small depths (sticking), and this can be due to neutrals and ions with the highest energies.

In the case of cpmpatible materials, the diffusion plays an important role due to the local heating produced by the energetic bombardment with ions and neutrals.

In the case of non - compatible materials, some diffusion might occur, due to the inducement of high deffects (vacancies) in the substrate lattice by the energetic bombardment.

This continuous bombardment during deposition and mainly in the early stages of nucleation and growth, leads to the removal (by sputtering) of nonadhesive film particles and to the formation of dense nucleation centres, very adhesive to the substrate, which represent in fact the strongholds for the overall film adhesion. The film grows around these nucleation centres parallell with the formation of new centres for nucleation due to

the continuous energetic bombardment.

Also, during the interface formation, substrate material is removed by sputtering, and some of these atoms are ionized and return to the substrate as ions or collide with energetic neutrals and are scattered back to the substrate (as energetic neutrals). This phenomenon leads to the deposition of a mixed film - substrate materials layer, graded in composition. However, when using SIMS, Ahmed[26] detected interpenetration of lead and copper over a depth of 40 Å which means that although the materials are incompatible, some diffusion could take place in a highly defective lattice. Some other explanation for this result could be that as a result of the surface bombardment during the SIMS analysis, some lead atoms are knocked into the copper lattice, which again means that for high energies and in a deffective lattice, some diffusion could take place even with non - compatible materials.

As a conclusion, the reasons for the good adhesion of ion plated films are :

- Removal of oxides and other impurity layers during the sputter cleaning
- Removal, by energetic bombardment, of any nonadhesive particles during the interface formation and throughout the deposition period
- Penetration of film atoms (ions and neutrals)

into the substrate, to depths of a few Angstroms.

- Enhanced physical diffusion due to the high local temperature induced by the energetic bombardment (for compatible materials)
- Enhanced diffusion due to the inducement of high lattice defects during bombardment (for compatible and noncompatible materials)
- Mixing and redeposition of film and substrate materials due to sputtering, ionization and scattering
- Formation of dense, relatively uniform distributed nucleation centres, very adherent to the substrate.

C H A P T E R 4

THIN FILMS CHARACTERISTICS

The internal characteristics of a thin film appear to be determinant for the physical and chemical behaviour of the deposit affecting strength, friction coefficient, wear resistance, corrosion resistance, ductility, adhesion, cohesion, etc. A dense film microstructure is preferred for different applications. A film with high internal stresses will crack or buckle and a porous structure offers less protection to corrosion.

The main characteristics of a thin film are :

- surface morphology
- microstructure
- lattice parameters
- crystallite size
- internal strain
- film thickness and uniformity

This chapter presents a theoretical approach to the methods of determining thin film characteristics.

4.1. Surface Morphology and Film Microstructure

These two characteristics are interdependant and the microstructure is generally reflected in the morphology of the surface which can be easily analysed by means of a Scanning Electron Microscope. Average grain size can be measured on the micrographs.

In the case of ion plated films, one very important aspect is to compare the film deposited on a frontal surface with one deposited on an out of sight surface, which reflects the capability of the coating method to produce uniform films on complex substrates.

Regarding the film microstructure, Movchan and Demchishin[31] presented a figure of merrit shown in Figure 4.1.1. This model refers to solid films formed by condensation directly from vapour stage. The structure is dependant upon temperature and kinetic energy of the arriving film particles (ions and neutrals) and Thornton[32] demonstrated that gas pressure has a great influence upon the microstructure of sputtered copper films.

Out of the three presented structures, the worst one is the tapered crystallites which is a highly defective structure.

I Tapered crystallites

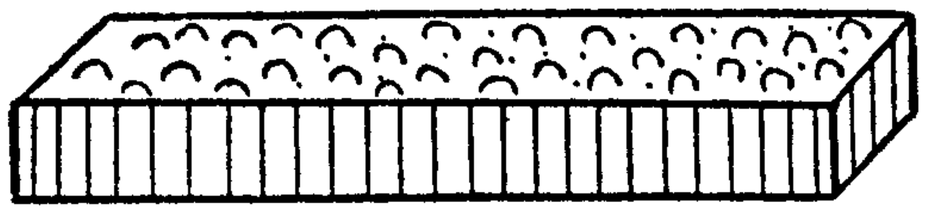

II Columnar structure

III Equiaxed grains

Movchan and Demchishin model of thin film structures.

Figure 4.1.1

Film adhesion could be affected, since the contact between the film and the substrate is on the peaks of the conical growth as shown in Figure 4.1.1'.

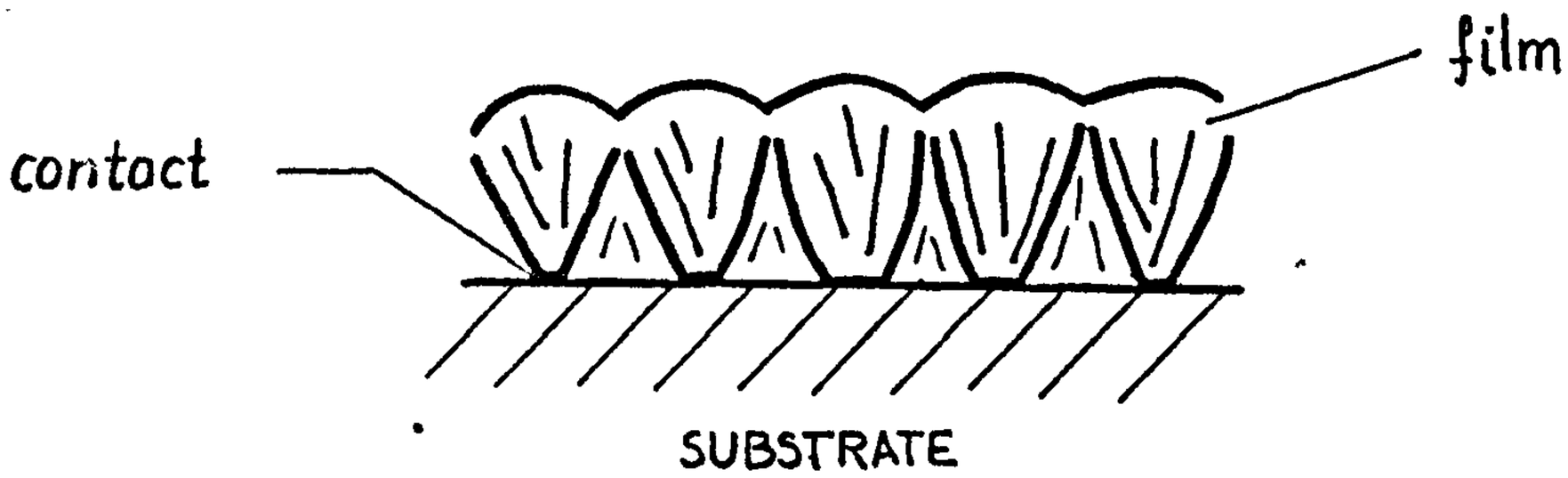

Figure 4.1.1'.

Generally, the ion plated films present a columnar structure when their thickness exceeds 1μ.

Electron beam evaporated deposits showed the property of having the axis of the columns directed towards the evaporation source[33]. Crystallite size measurements indicated that the columns are made of a large number of small crystallites which have a preferred orientation.

The explanation for the columnar growth could be the one previously presented[7] which assumes that the formation of peaks and valleys (due to the microroughness of the surface or due to the nucleation process), leads to the valleys being heavily shadowed while the peaks grow faster since they are

directly exposed to the stream of film atoms.

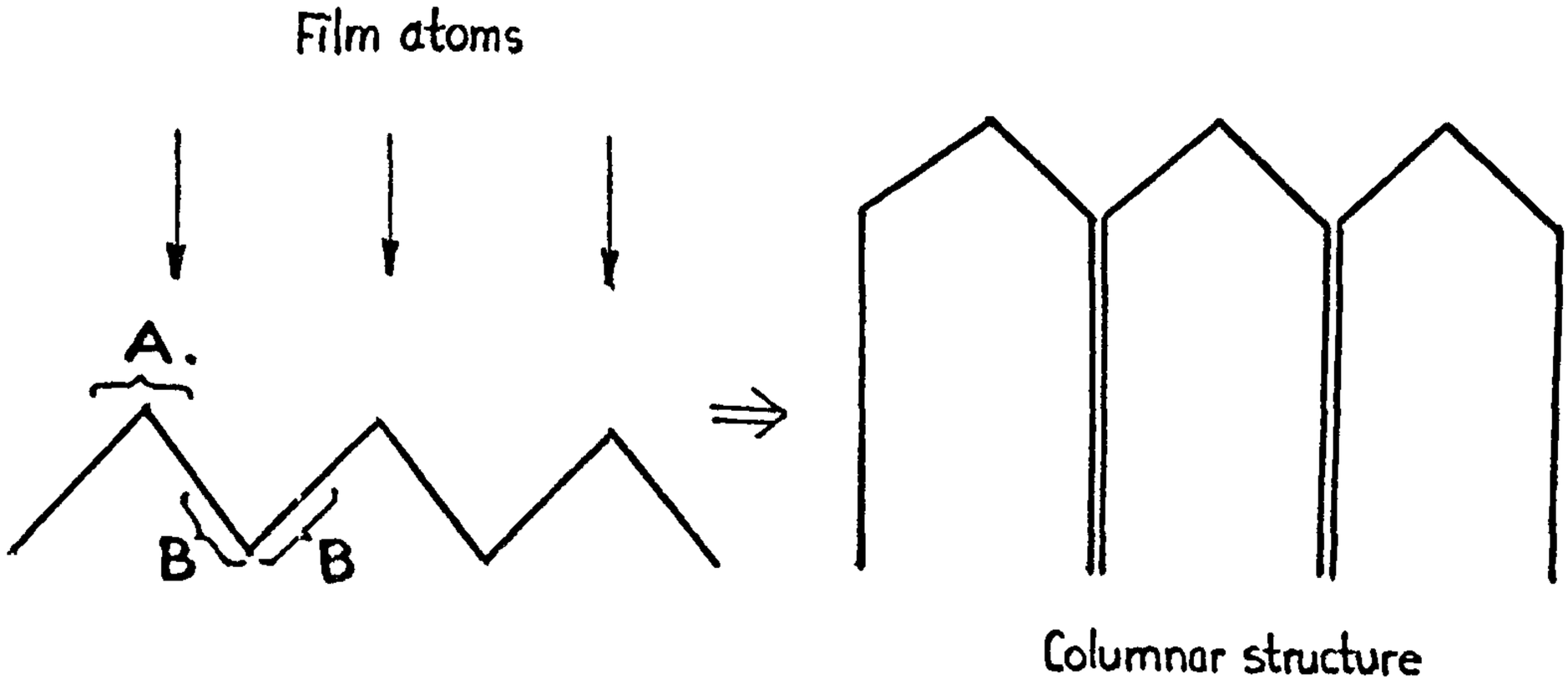

A. Exposed area

B. Shadowed area

Figure 4.1.2.

In the case of vacuum evaporation and sputter deposition, this effect is unremovable.
For ion plating, the variation of parameters could remove the columnar structure. Since the substrate is exposed to energetic particles bombardment, this could eróde the peaks which are more exposed and in the same time, forward sputtering and back scattering could fill the valleys. But for this effect to be obtained, high sputtering rates (to erode the peaks) and higher pressures (for a massive back scattering) could be required.

Another method of removing the columnar structure

is to aneal the film after deposition resulting in stress relief, recrystallization and grain growth. Table 4.1.3. presents the recrystallization temperatures of some more common metals[34] .

Table 4.1.3.

Metal	Approximative recrystallization temperatures(°C)	Melting point
Nickel	600	1455
Iron	450	1533
Copper	200	1083
Aluminium	150	660
Magnezium	150	651
Zinc	Room temp.	419
Lead	Room temp.	327
Tin	Room temp.	232

This method could be applied for low melting point films but it is not acceptable for high melting point materials, since a high temperature could produce unwanted changes in the substrate internal structure. At the same time, since anealing requires a long time, it is a very uneconomical method and sometimes as in the case of Titanium Carbide[35], even after heating it, the columnar structure was still present.

Two methods are most suitable for observing thin

film microstructure :

a. Cross sectioning followed by a metallurgical mounting which is then finely polished and chemically etched. The section is then analysed using an optical microscope and an oil immersion lens. A typical cross section of this type is presented in Figure 4.1.4.

b. Fracture cross section which is obtained by breaking the film together with the substrate which is then analysed in a Scanning Electron Microscope.

In this work, the second method was used to analyse the ion plated films microstructure.

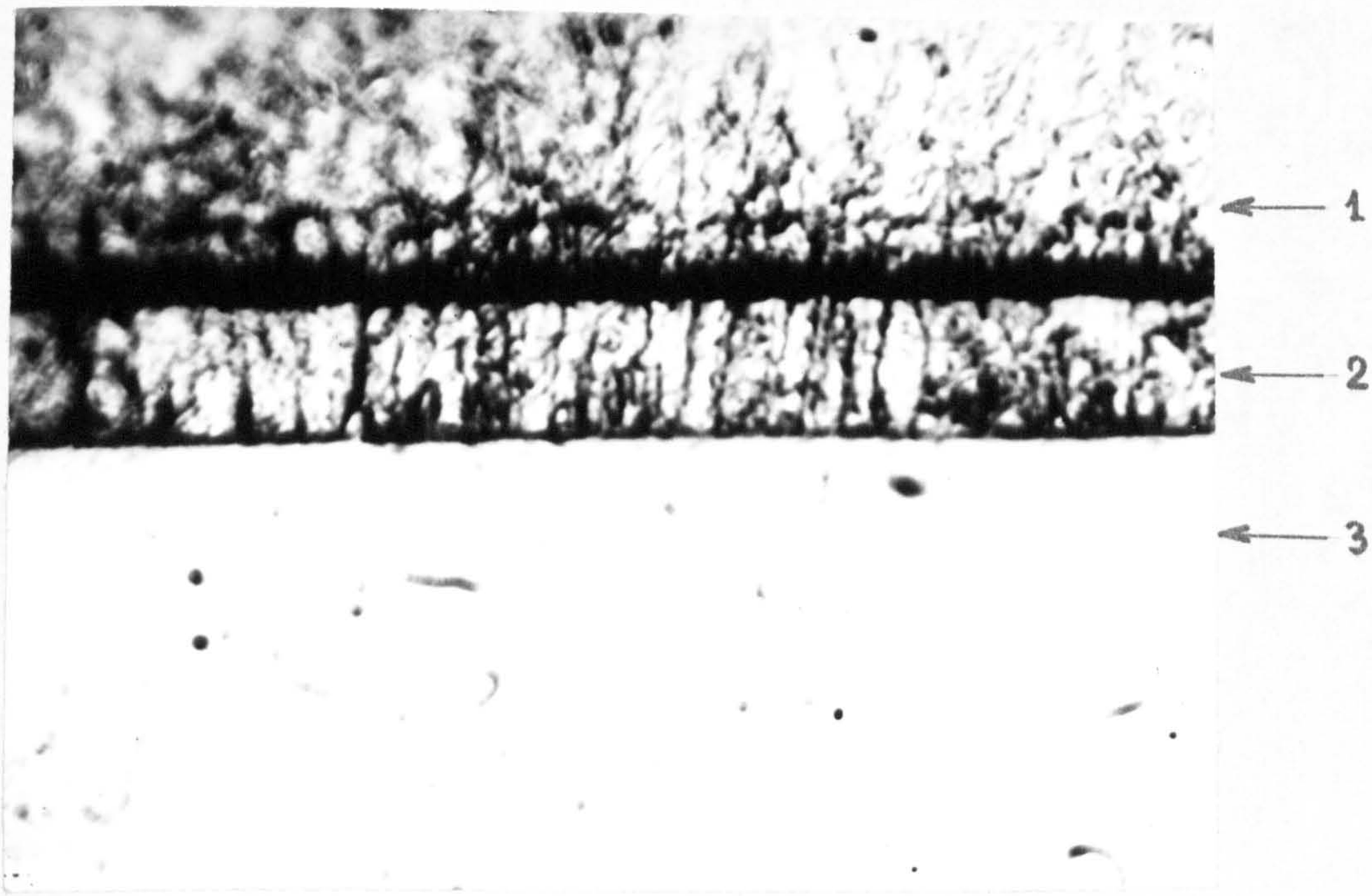

1. Electro-plated nickel (for protection and edge retention)

2. Chemically etched copper film

3. Nickel substrate

Figure 4.1.4

10 μ thick copper film, ion plated on nickel at 3 kV and 20 mtorr argon pressure.

4.2. Lattice Parameters

Metals are crystalline substances and when they solidify, their atoms take fixed positions in a regular pattern called 'space Lattice'. The points of such a lattice are occupied by positive ions surrounded by free electrons moving rapidly through the metal so that a uniform density is maintained. Most common metals crystallize in one of the three main types of metalic space lattice : face centred cubic, body centred cubic and hexagonal close packed as shown in Figure 4.2.1.. They represent the smallest crystalline units. The atoms are shown as solid spheres.

Microscopic examination of a pure metal surface reveals a polygonal grain structure as shown in Figure 4.2.2.

Each of the grains is built up of a multitude of small crystalline cells. In each grain, the axes of the cells point all in the same direction but this direction could vary from one grain to another as shown in Figure 4.2.3. This property is called crystalline orientation of the atoms.

Sometimes, when certain conditions are achieved, all the crystallites have their axis pointing in the same direction and the phenomenon is called preferred orientation

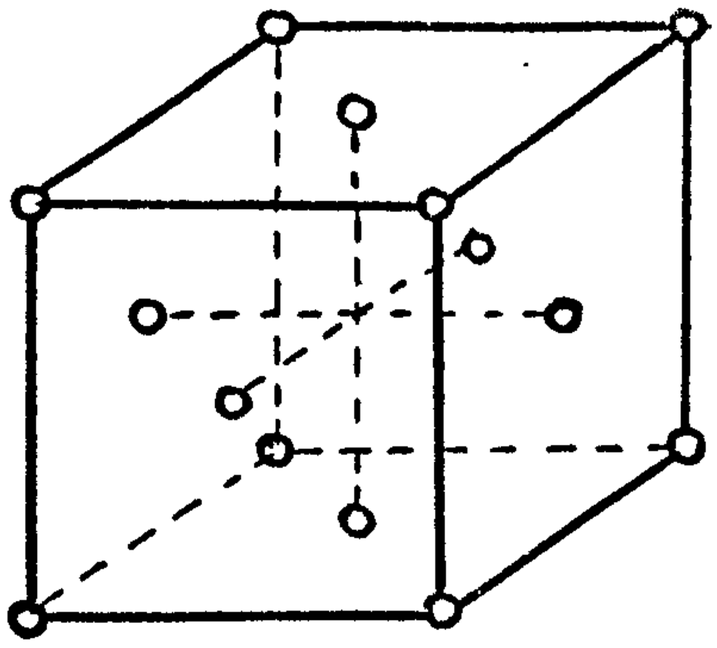

a. Face centred cubic lattice.
Ex: Cu,Al,Ni,Ag.

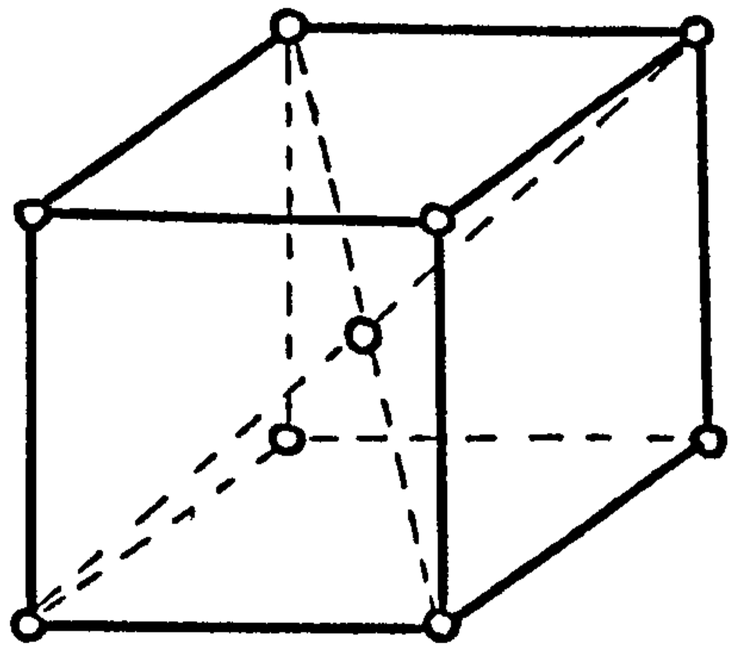

b. Body centred cubic lattice.
Ex: W,Cr,Mo.

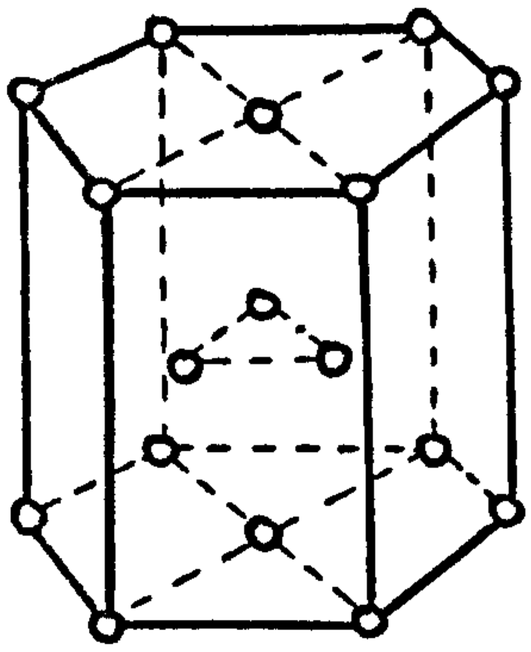

c. Hexagonal close packed lattice
Ex : Zn,Mg,Ti,Cd.

Figure 4.2.1

The three types of space lattices

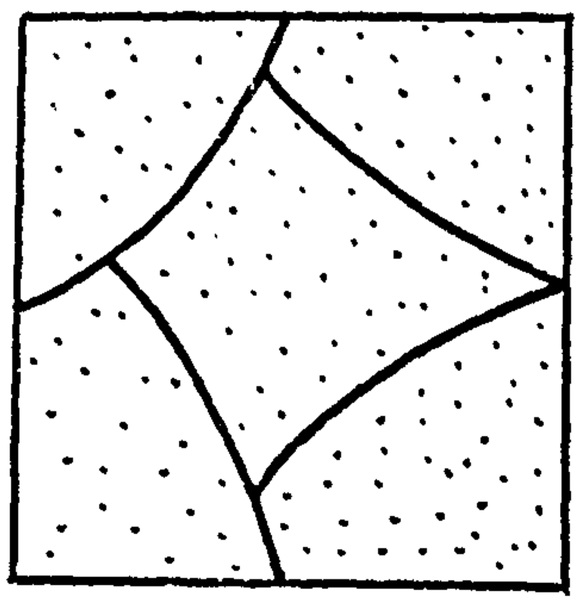

Figure 4.2.2.

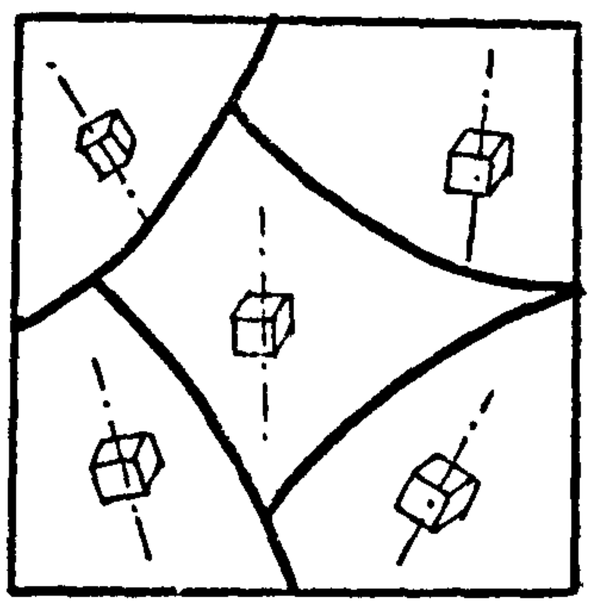

Figure 4.2.3.

If the orientation of the atoms in each grain is different, the atoms at the grain boundary are not arranged in a regular space lattice so that the lattices of the two neighbouring grains to fit each other. Since the grain boundary structure is different from the structure of the grains, it means that their properties will be different.

The same thing happens with the interface between the film and the substrate when two completely different space lattices must fit together in order to obtain a good adhesion, a thing that is even more difficult in the case of noncompatible materials when diffusion of one lattice into the other is not possible.

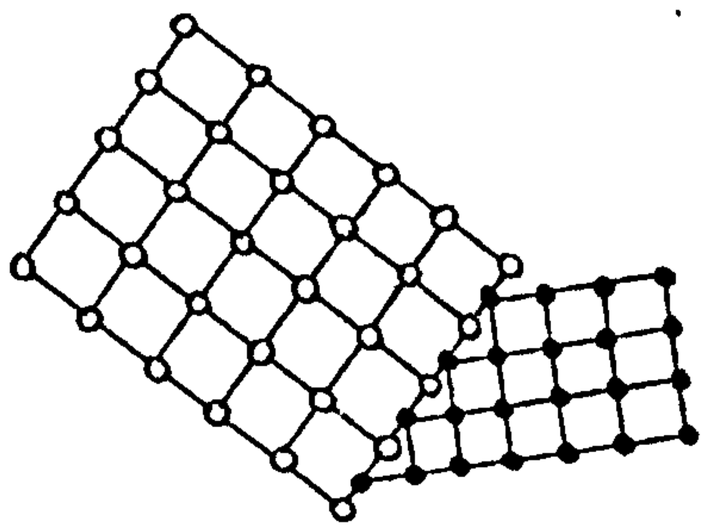

Figure 4.2.4. - Misfit at grain boundary

It has been proved[34] that for relatively low working temperatures, the grain boundaries are stronger than the grains, therefore a finer grain (more grain boundary) could be desired for resistant films, while for high working temperatures, the grain boundaries are weaker than the grains and therefore a large grain structure (less grain boundary) could be useful as shown in Figure 4.2.5.

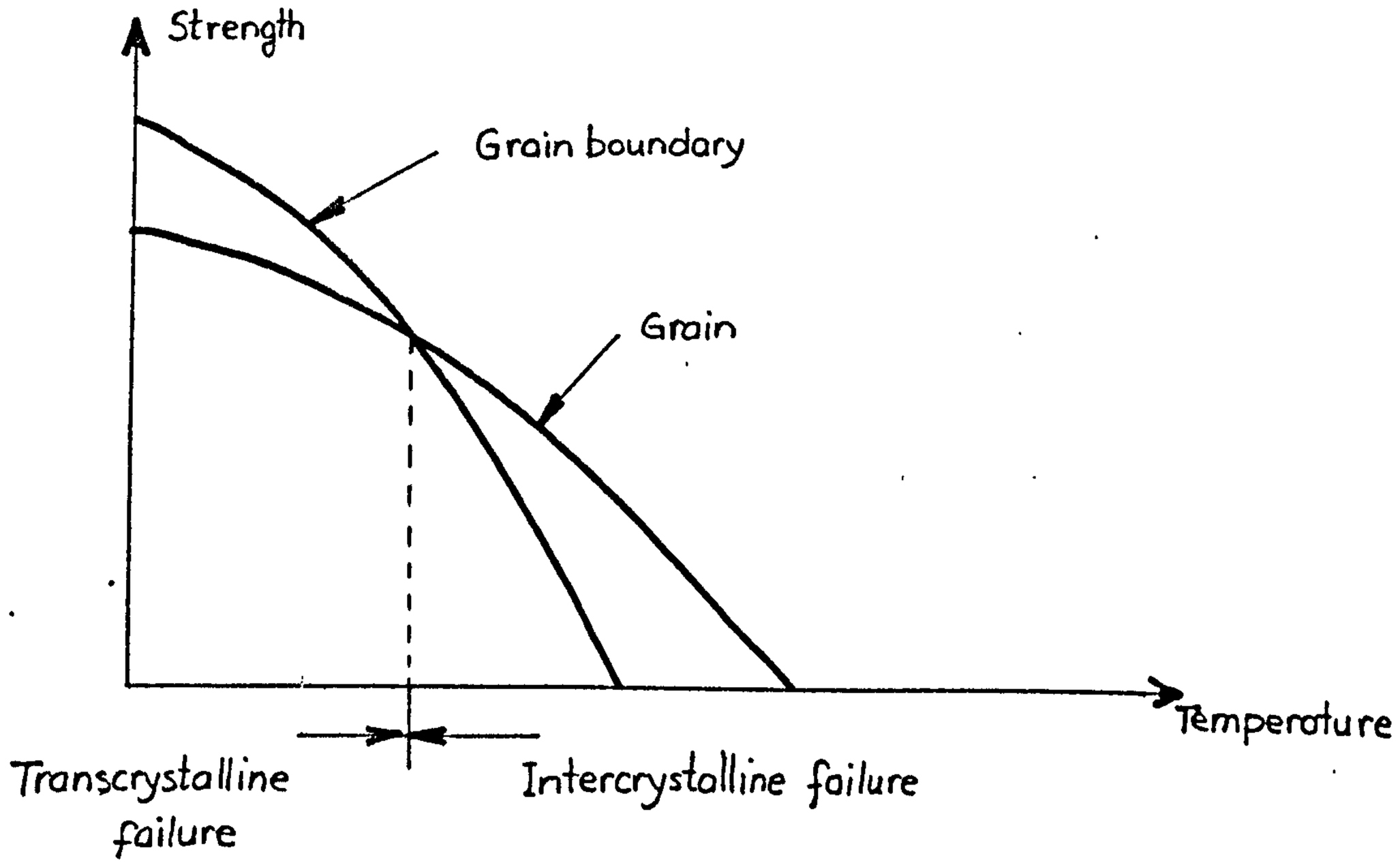

Figure 4.2.5.

If representing a crystal in three dimensions and choosing three unit lengths (parametric units) on the three axes e.g. a_1, a_2, a_3, the three points corresponding to these unit lengths determine a plane called the parametric plane.

The intercept of any plane with the three axes expressed as fractions of the parametric units are :

$$\frac{a_1}{h'} , \frac{a_2}{k'} , \frac{a_3}{\ell'} .$$

After removing the common factors the Miller indices (h,k,ℓ) are obtained and they can define any plane cutting the crystal as shown in Figure 4.2.6.

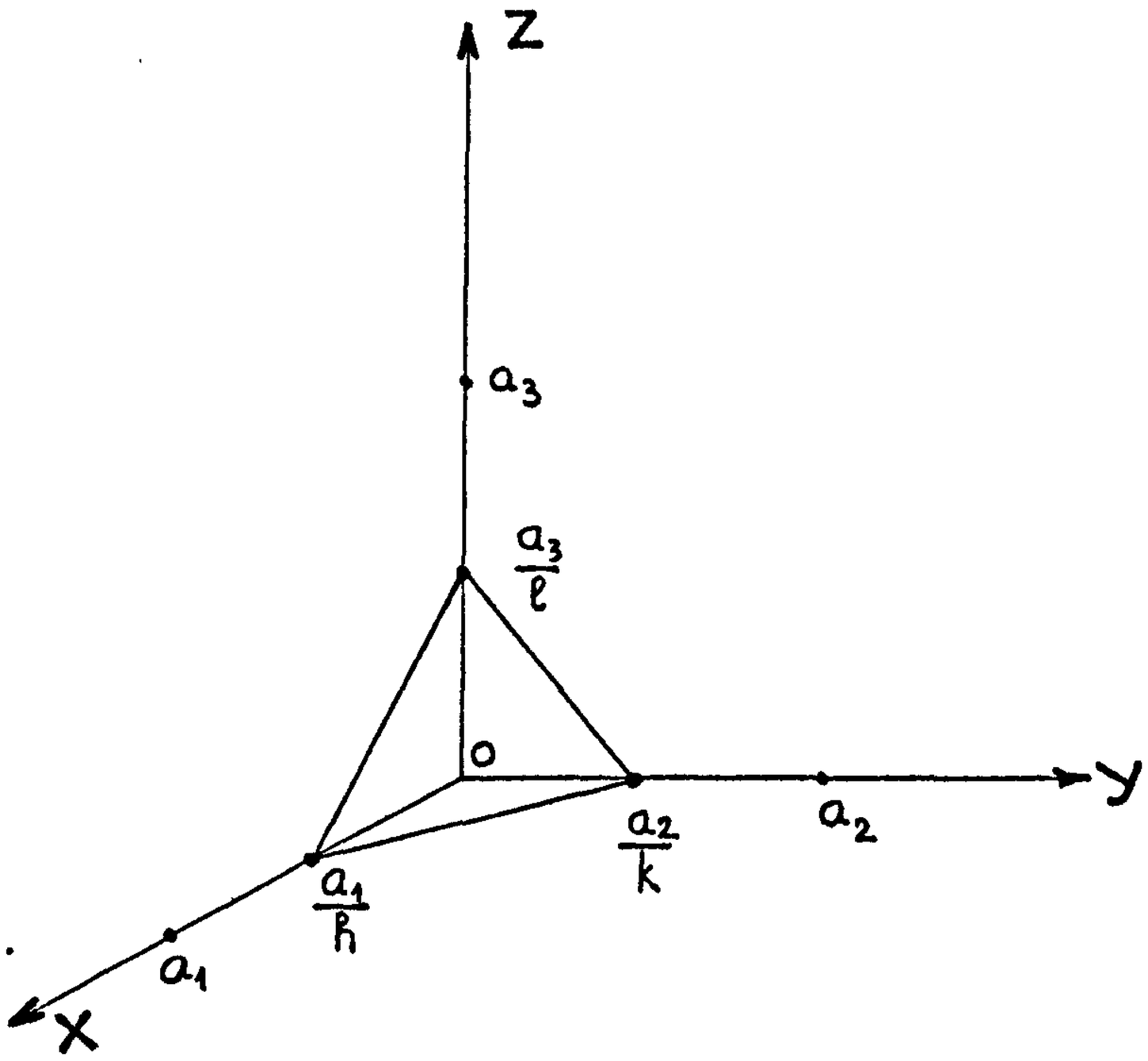

Figure 4.2.6.

h, k, ℓ , are integers without common divisor and the parametric plane is (h, k, ℓ). These indices enclosed in parantheses represent a whole 'family' of parallel planes in the crystal.

Because of sýmetry elements, some planes are sometimes repeated and the collection of similar planes is called a 'form' and is represented by $\{k, h, \ell\}$

A crystal can have elements of symetry with respect to which some parts of the crystal are symetrically repeated. These symetry elements are: axes, planes and centres of symetry.

All the crystals are incorporated in a unique space lattice. By joining the points of a space lattice, a series of parallel - sided 'unic cells' are obtained each of it containing a complete unit of the crystal pattern. The whole structure is obtained by packing these cells side by side.

To completely define a space lattice, one must give the distances between neighbouring lattice points alongthe three dimensions and the angles between the directions. These dimensions determine the unic cell and are usually designated as $[a_o, b_o, c_o]$.

*

* *

The phenomenon of X - ray diffraction[36,37,38] by crystals is the result of a process of scattering of the X - rays by the space lattice without a change in the wavelength (coherent scattering). A diffracted beam is produced by this phenomenon when certain geometrical conditions are satisfied which are expressed by Bragg's Law and are represented in Figure 4.2.7.

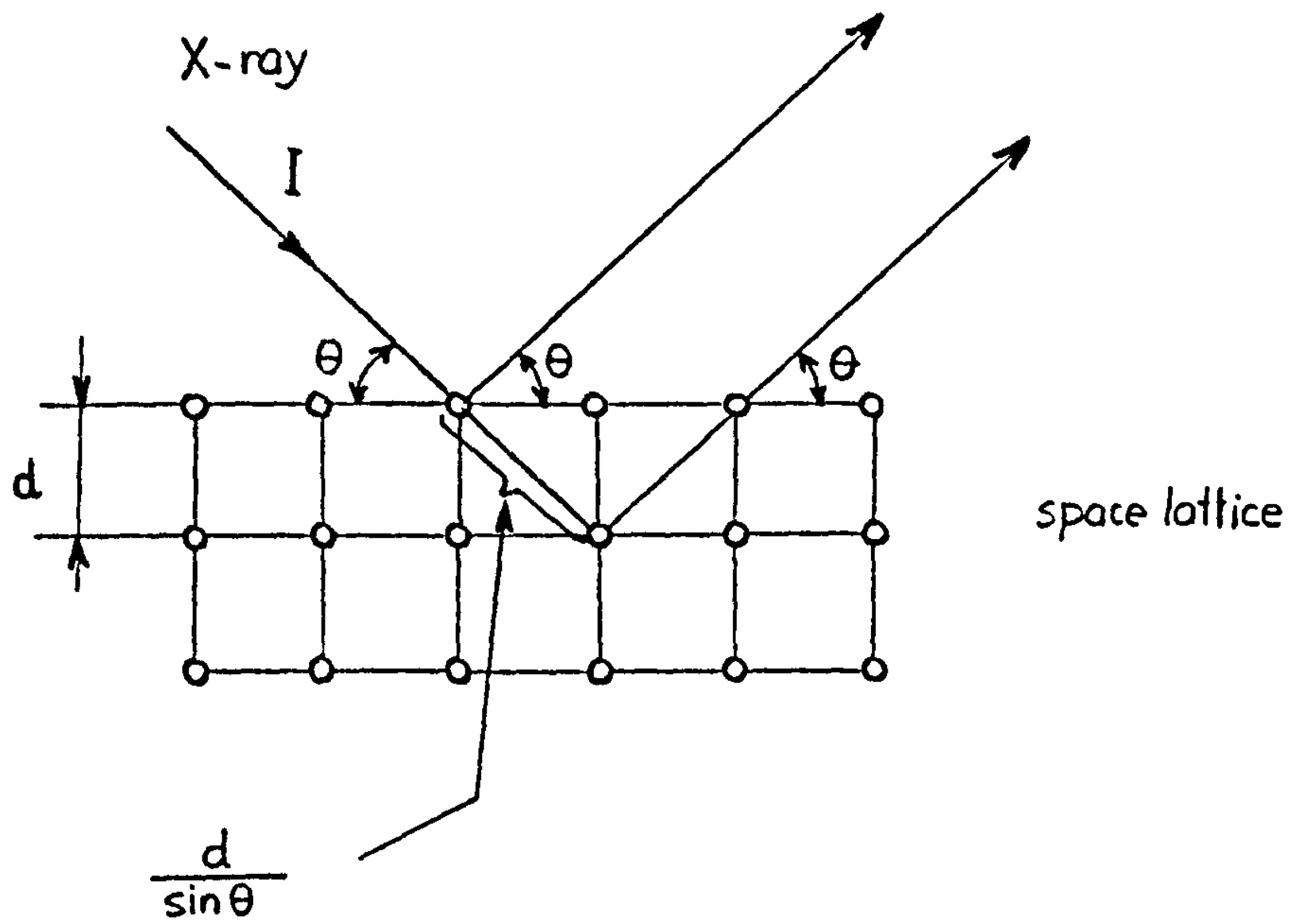

Figure 4.2.7.

Diffraction of the X - Rays

Bragg's Law is :

$$n\lambda = 2d \sin\theta \qquad (4.2.8.)$$

where :

n is an integer giving the order of the reflection

λ is the wavelength of the x - Rays

d is the interplanar spacing between succesive atomic planes in the crystal

θ is the angle between the atomic plane and both the incident and the reflected beams,

Choosing different incidence angles and analysing the positions of the diffraction effects, leads to knowledge about the size, shape and orientation of the unit cell and also leads to the identification of the substance.

The determination of the dimensions of the unit cell and the interplanar spacing for different crystallographic planes is referred to as 'indexing', and means the calculation of the dimensions of d, a_o, b_o, c_o.

The easiest to index are the cubic lattices where :

$a_o = b_o = c_o$.

4.3. Crystallite Size and Internal Strain

Crystallite size or the main dimensions L ($\mathring{A}$) of a crystallite composing a powder, can be determined from the pure x - ray diffraction broadening 'β' by the equation :

$$L_{(h,k,\ell)} = \frac{k\lambda}{\beta \cos} \quad (\mathring{A}) \qquad (4.3.1.)$$

k is a constant approximately equal to unity and its values are tabulated[36].

(h,k,ℓ) indicate the crystallographic plane in which the measurements are made.

Generally, a chart obtained by using a conventional x - rays diffractometer is handy for the determination of the breadth of a diffraction line measured at half of the intensity of the diffraction line and frequently noted as $B_{\frac{1}{2}}$.

The broadening of the x - rays is :

$$\beta = B_{\frac{1}{2}} - b_{\frac{1}{2}} \qquad (4.3.2.)$$

where :

$B_{\frac{1}{2}}$ is the half breadth as experimentally calculated

$b_{\frac{1}{2}}$ is the half breadth of a line produced

under similar geometrical conditions by a material with a cristallite size well in excess of 1000 Å and is usually called the instrumental broadening.

The broadening of the x - rays diffraction pattern is produced by a combined effect of crystallite size and lattice strains and a method often used to separate the two effects is the method of Integral Breadths[39,40,41] .

Internal stress in a thin film is very important for the film quality because, if a tensile stress exists, the film tends to contract and there is the possibility of cracking. If a compressive stress occurs, the film tends to expand and there is the possibility of buckling.

Internal stress in a thin film can be caused firstly by different thermal coefficients of the film and the substrate during cooling and secondly, by intrinsic causes[42].

The most usual methods of measuring the stresses in a thin film are :

- the cantilever method which measures the internal stress during film growth
- the interferometric method
- line broadening of the x - rays diffraction pattern

The first method showed that for small thichnesses (tens of Angstroms), the ion plated films are stress

free since in this stage, the film is still discontinuous[6] . as the thickness increases and the film becomes continuous, there is a sharp increase in the value of the value of the internal stress which remains approximatelly constant or even decreases slightly for thicker films.

In this work, the third method is employed, line broadening of the x - rays diffraction pattern being caused by the lattice distorsion (strain) which indicates the amount of lattice internal stress. The advantages of the method lie in the fact that it is a nondestructive method and there is no need to make measurements of the material in the unstressed conditions. Corelating the stress measurements with the crystallite dimensions, the kind of internal stress (tensile or compressive) can be determined as the crystallite is either elongated or compressed in the respective crystallographic plane.

X - rays diffraction procedures can only determine the elastic stresses.

The elastic stress - strain relationship is :

The strain 'e' is defined as :

$$e = \frac{\Delta \ell}{\ell} \qquad (4.3.3.)$$

where $\Delta \ell$ is the change in the length of a stressed body whose initial length was ℓ .

The strain is produced by a stress σ acting in a single direction and :

$$e = \frac{\sigma}{E} \qquad (4.3.4.)$$

which is Hooke's Law. 'E' is Young's modulus.

When starting to measure the line broadening of an x - ray reflection, first of all the pure line profile must be determined, and in this work the Rachinger correction[43] was used for this purpose. A low scanning speed and a fast chart speed were chosen in order to obtain the pure line with maximum accuracy. It is assumed that the $k\alpha_1$ and $k\alpha_2$ line profiles are identical in shape and that the α_2 reflection intensity is one half of the α_1 intensity but shifted from it towards larger angles by :

$$2\theta = 2 \tan\theta \left(\frac{\Delta\lambda}{\lambda}\right) \qquad (4.3.5.)$$

where $\Delta\lambda$ is the difference in the wavelength of α_2 and α_1 reflections, that is :

$$\Delta\lambda = \lambda(\alpha_2) - \lambda(\alpha_1) \quad (\text{Å})$$

It is also assumed that both α_1 and α_2 profiles are Gaussian profiles. After applying this correction and the pure line profile is determined, it is possible to separate the influence of crystallite size and lattice distorsion on the broadening of the x - ray diffraction line and for this purpose, the integral breadths method can be used.

The integral breadth is defined as the integrated intensity of the line profile above the background devided by the peak height.

$$B_{\frac{1}{2}} = \frac{1}{I_p} \int I(2\theta)\, d(2\theta) \qquad (4.3.6.)$$

The integral has the geometrical significance of being the width of a rectangle having the same area with the area enclosed by the profile and the length equal to the height of the line profile. The integral profile breadth can be written in 's' units ($\mathring{A}^{-1}$) or '2θ' units (radians). As shown by Wilson[44], the integral line profile breadth generated by the distorsion (strain) alone is :

$$(\delta \varepsilon)_i^D = 4e \frac{\sin\theta}{\lambda} = 2es = \frac{2e}{d_{hk\ell}}$$

on the 's' scale (4.3.7.)

or :

$$(\delta 2\theta)_i^D = 4e \tan\theta$$

on the '2θ' scale

in a direction perpendicular to the (h,k,ℓ) plane.

i designates integral breadth

D designates distorsion effect

$$s = \frac{2 \sin}{\lambda} \quad (\mathring{A}^{-1}) \qquad (4.3.8.)$$

The integral profile breadth generated by the crystallite size can be obtained from Scherrer equation :

$$L = \frac{k\lambda}{\beta \cos\theta} \qquad (4.3.9.)$$

where :

L is the main dimension of the crystallite

k is a constant usually equal to unity

$\beta = B - b$

B is the integral breadth

β is the geometrical (instrumental breadth) generated by a reference powder with crystallite size well in excess of 1000 Å

From Scherrer equation, the integral profile breadth generated by the crystallite size is :

$$(\delta s)_i^S = \frac{K}{L} \qquad \text{on the 's' scale}$$

$$(4.3.10.)$$

$$(\delta 2\theta)_i^S = \frac{k\lambda}{L \cos\theta} \qquad \text{on the '2θ' scale}$$

i designates integral breadth

S designates size effect

The combination of the two effect gives the overall broadening effect $(\delta S)_o$ or $[\delta(2\theta)]_o$ and it is based on the assumption that the two effects are either both Cauchy or both Gaussian as regards the

shapes of the two profiles.

Therefore it can be written :

$$(\delta s)_o = (\delta s)^S + (\delta s)^D$$

(Cauchy - Cauchy)

$$\left[(\delta s)_o\right]^2 = \left[(\delta s)^S\right]^2 + \left[(\delta s)^D\right]^2$$

(Gaussian - Gaussian)

(4.3.11.)

Making the substitutions :

$$(\delta s)_o = \frac{1}{L} + 2\ es$$

$$\left[(\delta s)_o\right]^2 = \left(\frac{I}{L}\right)^2 + (2\ es)^2$$

(4.3.12.)

Experimental results have shown that the strain broadening can be approximated well by a Gaussian function while the effect of the size can be approximated by a Cauchy function. An approximate equation was found by Halder and Wagner[45] .

$$\frac{B_C}{B} = 1 - \left(\frac{B_G}{B}\right)^2$$

(4.3.13.)

or :

$$\frac{B^S}{B} = 1 - \left(\frac{B^D}{B}\right)^2$$

where C designates the Cauchy profile, G designates the Gaussian profile and S and D have the usual meaning.

The maximum error given by this method does not exceed 10 %.

Introducing (4.3.7.) and (4.3.10.) into Halder's equation :

$$\frac{k}{(\delta s)_{oL}} = 1 - \left[\frac{2es}{(\delta s)_o}\right]^2 \quad \text{in 's' units } (\mathring{A}^{-1})$$

(4.3.14.)

or :

$$\frac{k\lambda}{\delta(2\theta)L\cos\theta_o} = 1 - \frac{16\ e^2}{[\delta(2\theta)]^2 \cot^2\theta_o}$$

in '2θ' units (radians)

These two equations take into consideration both Cauchy and Gaussian functions. θ_o is the position of the peak maximum.

The equations can be written for the $k\alpha_1$ pure line profile, as determined using the Rachinger correction. Substitution of doublets of $(\delta s)_o$ and 's' values or triplets of $\delta 2\theta$, $\cos.\theta_o$, $\cot^2\theta_o$ values from two, or more reflections leads to numerical values for L and e .

If a '2θ' scale is used, the equation can be written as :

$$\frac{[\delta(2\theta)]^2}{\tan^2\theta_o} = \frac{k\lambda}{L}\left[\frac{\delta(2\theta)}{\tan\theta_o \sin\theta_o}\right] + 16\ e^2$$

(4.3.15.)

and if we notify :

$$\frac{[\delta(2\theta)]^2}{\tan^2\theta_o} = Y$$

and :

$$\frac{\delta(2\theta)}{\tan.\theta_o \sin.\theta_o} = X$$

the equation becomes :

$$Y = \frac{k\lambda}{L} X + 16\ e^2 \qquad (4.3.16.)$$

which is the equation of a line.

Thus, it is possible to draw a linear plot of $\frac{[\delta(2\theta)]^2}{\tan^2\theta_o}$

against $\frac{\delta(2\theta)}{\tan\theta_o \sin\theta_o}$ and from the slope α it results:

$\tan\alpha = \frac{k\lambda}{L}$ which enables to calculate $L = \frac{k\lambda}{\tan\alpha}$.

From the ordinate intercept $n = 16\ e^2$, it is possible to calculate the strain $e = \frac{\sqrt{n}}{4}$.

Converting the equation into the 's' scale, it is possible to make a linear plot of $[(\delta s)_o]^2$ against s^2. The conversion equations are :

$$\underset{(\mathring{A}^{-1})}{\delta s} = \underset{(rad)}{\delta(2\theta)} \frac{\cos\theta_o}{\lambda} \qquad (4.3.17.)$$

For a cubic lattice : $\frac{\sin\theta_o}{\lambda} = \frac{(h^2 + k^2)^{\frac{1}{2}}}{2\ a}$

where a is the perfect lattice main dimension

θ_o is the incidence angle corresponding to the peak

$\delta(2\theta)$ can be taken as $\beta\frac{1}{2}$ in radians.

The strain alters the lattice size in different ways (in different crystallites) and in different directions (in the same crystallite)[46] :

$$\frac{\lambda}{d} = d^* = 2\sin\theta \qquad (4.3.18.)$$

Taking Logs and differentiating, the strain 'e' is :

$$e = \frac{\Delta d}{d} = \frac{\Delta d^*}{d^*} = \cot\ \theta\,\Delta\theta \qquad (4.3.19.)$$

where $d^*_{hk\ell}$ is the distance from the origin to the powder sphere.

$\Delta d^* = ed$

$\Delta\theta = e\tan\theta$

Thus : $\beta^S = 2\,\Delta\theta = 2e\tan\theta \qquad (4.3.20.)$

where β^S is the broadening due to the lattice strain.

The line broadening due to the crystallite size is:

$$\beta^C = \frac{\lambda}{L\cos\theta} \qquad (4.3.21.)$$

The combined effect of both stress and crystallite

size is :

$$\beta = \beta^S + \beta^C = 2\,e\tan\theta + \frac{\lambda}{L\cos\theta} \qquad (4.3.22.)$$

where $\beta = B - b$:

or :

$$\beta\cos\theta = 2e\sin\theta + \frac{\lambda}{L} \qquad (4.3.23.)$$

which is the simplified form of equation (4.3.15.) If $\beta\cos\theta$ is plotted against $\sin\theta$ for a number of minimum two reflections, a line is obtained with a slope $2e$ and an intercept $\frac{\lambda}{L}$.

This method assumes that strain and small size occur in the same crystallite when in fact it is more likely that they occur in different crystallites. But the accuracy with which β is measured from an x - ray diffraction chart does not justify the use of a more precise method.

Algebrically, 'e' and 'L' can be calculated using the following formulas :

$$e = \frac{1}{2}\sqrt{\frac{(B_1-b)^2\cos^2\theta_1-(B_2-b)^2\cos^2\theta_2}{\sin^2\theta_1 - \sin^2\theta_2}} \qquad (4.3.24.)$$

where B_1 and B_2 are the integral breadths of the reflections in (h_1, k_1, ℓ_1) and (h_2, k_2, ℓ_2) planes given by θ_1 and θ_2 incidence angles for the $k\alpha_1$ reflection.

b is the instrumental broadening.

The strain thus calculated is along a direction given by the intersection of (h_1, k_1, ℓ_1) and (h_2, k_2, ℓ_2) planes .

Crystallite size in a direction perpendicular to the plane (h, k, ℓ) and for $k\alpha_1$ radiation is :

$$L_{(h,k,\ell)} = \frac{\lambda k\alpha_1}{(B - b)\cos\theta_{k\alpha_1}} \qquad (4.3.25.)$$

The error introduced by this method is due to the fact that it assumes that the entire line broadening is produced by strain alone and by size alone, but approximate values can be quickly calculated.

The stress can be calculated using :

$$\sigma = eE \qquad (4.3.26.)$$

E is Young's modulus and it is tabulated.

4.4. Film Thickness

The determination of ion plated films thickness is important in order to observe film uniformity and also to determine the effect of deposition parameters upon the throwing power of the coating method.

For both thin and thick films, the x - ray diffraction method can be used[47,48] based on the absorbtion attenuation of the diffracted radiation due to the double transmission through the film. Therefore, the intensity will differ when a monocromatic x-ray is diffracted by the coated and the uncoated substrate material .

There is also the possibility to measure film thickness during the evaporation and several methods are available[49].

For thicker films (> 1μ) a handy and less exact method is the direct measurement of the thickness on a cross section polished and etched, by using a Scanning Electron Microscope.

This method is used in this work in order to determine the influence of ion plating parameters upon the thickness on the front and back surfaces of flat specimens, usually referred to as the 'throwing power'.

C H A P T E R 5

THE EFFECT OF PROCESS PARAMETERS UPON ION PLATED FILMS

5.1. Theoretical Approach

The effect of process variables has not been studied very extensively although it has been proved that variation of these parameters can induce changes in the structure of ion plated films[50].

The main parameters are :

- Gazeous discharge pressure (p)
- Substrate bias (V)
- Substrate temperature (T)
- Source to substrate distance (D)
- Substrate geometry
- Deposition rate (D_R)
- Current density (I_i)

Wan, Chambers and Carmichael[50] found that the gas pressure can influence film morphology independently of most of the other variables in the pressure range of 1 - 50 mtorr.

At 1 mtorr and below it, the coating structure and growth characteristics are more dependant on other

variables.

The collision rates of atomistic particles and the scattering effect are much dependant upon gas pressure thus affecting the ionization process, the energy spectrum and the throwing power.

The substrate bias is determinant for the energy of the arriving ions and neutrals with two effects: one on the sputtering yield and the other on the nucleation as proved early in this work.

The local heating is also affected by the arriving energy thus influencing the diffusion process that leads to the formation of a graded interface.

The substrate temperature can also influence the crystallite size and grain structure[51] .

Substrate geometry can affect the thickness uniformity because hidden parts and sharp edges have smaller thickness than other exposed parts of the substrate due to the hollow cathode and field concentration effects associated with these two geometries.

Deposition rate, which is a direct function of the evaporation rate, can interact with other parameters to affect the ionization efficiency and the ratio between the sputtering rate and the deposition rate.

Source - substrate distance can affect the current density as proved early in this work.

Ion current density is a direct measure for the ionization efficiency and affects the nucleation

and growth. It is also determinant for the sputtering rate which is essential for removing the nonadhesive particles (during deposition) and for eroding the peaks which lead to a columnar structure.

In this work, the source to substrate distance is kept constant at its optimum of 12 - 13 cm and a constant deposition rate of 1μ/min is achieved (limited by the resistive heating evaporation method employed).

The varied parameters are : p, V and I_i and at the same time, the bulk temperature T is measured during deposition.

As proved in the previous chapters, I_i determines the ionization efficiency 'I_{ef}' which is a parameter that can be generalized for any kind and shape of substrate.

The ionization efficiency is defined as the ratio between the number of ions (argon and film) and the total number of ions and neutrals striking a square centimetre of substrate surface in a second and is a direct function of ion current density.

$$I_{ef} = \frac{N_i}{N_i + N_n} \times 100\ \% \qquad (5.1.1.)$$

since $N_i \ll N_n$

$$I_{ef} \simeq \frac{N_i}{N_n} \times 100\ \% \qquad (5.1.1.a.)$$

But since it has been demonstrated that the energetic neutrals have energies similar to the ions and therefore play an important role in obtaining the characteristics of an ion plated film, the ionization efficiency having values of 0.01 - 0.1 % is not sufficient to describe the energetic status of the process. Therefore, another term is introduced to include those neutrals ($N_{n\bar{e}}$) which strike the cathode with energies comparable to the accelerated ions, called the 'activation efficiency' A_{ef} and defined by :

$$A_{ef} = \frac{N_i + N_{n\bar{e}}}{N_i + N_n} \times 100\ \% \qquad (5.1.2.)$$

where : N_i = number of ions

$N_{n\bar{e}}$ = number of activated or energetic neutrals

N_n = total number of neutrals

$$N_n = N_{n\bar{e}} + N_{no}$$

where : N_{no} = number of neutrals arriving with thermal energy

From the graphs previously plotted, it is possible to calculate for instance :

$$A_{ef}\ \begin{matrix} 30\ eV \\ 3\ kV \\ 10\ mtorr \end{matrix} = 3.6\ \%$$

which is the activation efficiency for energies higher than 30 eV giving the percentage of particles capable of producing sputtering .

The main importance of this parameter is that it reflects the energy spectrum of ion plating as a whole, since a small increase in the number of ions can induce a sensible increase in the number of energetic neutrals.

As the microstructure of ion plated films is one of the most important factors influencing the film properties, it is essential to analyse the way in which the parameters variation could lead to an improved structure.

By creating a sufficient density of nucleation centres during the first stage of deposition, it is possible to obtain a uniform and dense film even for a small thickness. But as the film grows, it is important to achieve an optimum ratio between the deposition rate and the sputtering rate.

$$\psi = \frac{D_R}{S_{pR}} \qquad (5.1.3.)$$

where : D_R is the deposition rate

S_{pR} is the sputtering rate

a. If the sputtering rate exceeds the deposition rate ($\psi < 1$), no film growth can occur.

b. If the deposition rate exceeds by far the sputtering

rate ($\psi >> 1$), nonadhesive particles and peak growths cannot be removed in time, and a columnar structure is obtained parallel with a worse adhesion to the substrate.

Therefore, a good balancing of D_R and S_{pR} could be the answer to the problem of removing the columnar structure. To reduce D_R is very uneconomical since the deposition rates are already low for ion plating and therefore, the only efficient way to adjust ψ appears to be by means of controlling S_{pR} which is a direct function of I_{ef} .

Most of the research so far tended to control the ion current density mainly by modifying the gas pressure but, as previously proved in this work, the ionization efficiency remains constant with pressure variation in an ion plating diode system.

Analysing S_{pR} and D_R , they are :

$$S_{pR} \sim K_1 \, (N_i + N_{n\bar{e}}) \qquad (5.1.4.)$$

$$D_R \sim K_2 \, (N_i + N_n) = K_2 \, (N_i + N_{n\bar{e}} + N_{no})$$

then :

$$\psi \sim \frac{K_2}{K_1} \; \frac{N_i + N_{n\bar{e}} + N_{no}}{N_i + N_{n\bar{e}}} = K \; \frac{N_i + N_n}{N_i + N_{n\bar{e}}} \qquad (5.1.5.)$$

where : $K = \frac{K_2}{K_1}$

but : $$A_{ef} = \frac{N_i + N_{n\bar{e}}}{N_i + N_n} \approx \frac{N_i + N_{n\bar{e}}}{N_n} \quad (\text{since } N_i \ll N_n)$$

Then (5.1.5.) becomes :

$$\psi \sim \frac{K}{A_{ef}} \qquad (5.1.6.)$$

but : $N_i + N_{n\bar{e}} = f(N_i)$ for p and V constant

and $N_n = f(E_R)$ where E_R is the evaporation rate

$$N_i = K_3 \frac{I_i}{S}$$

where : K_3 is a time constant

I_i is the ion current

S is the total area of the cathode surface exposed to the ion bombardment and is a constant

or : $N_i = KI_i$ where $K = \frac{K_3}{S}$

It results that $\psi = f(I_i, E_R)$ for p and V constant.

Therefore, it is possible to control ψ either by modifying E_R which is not economical or by controlling I_i for p and V constant which is not possible in a diode ion plating system.

One method of independently controlling I_i is by introducing an auxilliary anode in this case called

'positive probe', which having a positive voltage applied on it can accelerate electrons to sufficient energies to produce the ionization of neutral atoms. The voltage applied being +V, an electron could achieve a maximum energy of $V\bar{e}$ which must be :

$$V\bar{e} \geqslant \text{Ionization energy}$$

Theoretically, several volts sould be sufficient but due to the small mean free path, collisions take place before the electron gains this energy. Under normal ion plating conditions, voltages of at least 30 V were required to produce significant increases in the ion current.

Probe efficiency proved better for low gas pressures and the partial argon pressure could be dropped below the vapour pressure of the evaporant, creating the possibility to work with a plasma maintained by the film vapours in which case the film atoms ionization efficiency is maximum. When higher ionization efficiencies are required combined with low gas pressures (weak plasma), an auxilliary electron source could be introduced in the form of one or several saturated hot filaments.

In this work, the positive probe was in the shape of a semicircle placed within the dark space at equal distances from the cathode and the negative

glow. Voltages of 0 - 250 V were available on the probe.

5.2. Experimental

In order to study the influence of p, V and I_i, copper films of 10μ thickness were ion plated on flat, polished, nickel substrates having the dimensions 25 x 25 x 3 mm giving a total area of 15.5 cm^2 .

The sputter cleaning was performed at a bias voltage of 3 kV and an argon pressure of 15 mtorr for 45 minutes, drawing a current of 14 mA. The source to substrate distance was 12 cm and a constant(1μ/min) deposition rate was achieved. A thermocouple was connected to the back of the substrate to measure the bulk temperature.

The variation of the parameters is shown in Table 5.2.1.

Table 5.2.1.

Spec No.	V (kV)	p (mtorr)	Idep (mA)	T (°C)	+V (V)
1	2	20	7	95	
2	2	30	14	100	
3	2	40	19	110	
4	3	10	4	90	
5	3	20	16	130	
6	3	30	31	150	
7	3	40	45	165	
8	3	50	55	175	
9	4	10	8	100	
10	4	20	21	145	
11	4	30	38	170	
12	4	40	50	185	
13	5	10	10	115	
14	5	20	25	170	
15	5	30	42	200	
16	3	10	$8(2I_i)$	150	60
17	3	10	$12(3I_i)$	240	100
18	3	20	$32(2I_i)$	280	200

NOTE : I_i represents the ion current drawn in the p-V conditions but without the positive probe; $2I_i$ and $3I_i$ are obtained for the same p-V conditions by applying a positive voltage on the probe.

After ion plating, the film surface morphology was analysed in the Scanning Electron Microscope.
Copper being a cubic crystal, a single dimension L(Å) was required to calculate the crystallite size, by separating the two effects of crystallite size and distorsion on the line broadening of the X ray diffraction pattern. For this purpose, copper radiation was used in a standard x - ray diffractometer. For removing the instrumental broadening, a large grain silicon powder was used.
The scratch test was performed using a diamond indentor and a load of 200 g on a modified microhardness tester. All the ion plated films showed no sign of bad adhesion when using this test and a typical scratch is shown in Figure 5.2.2.
However, this test proves the superior adhesion obtained by ion plating but gives no quantitative indication about the strength of the bond.
Fracture cross sections were employed to reveal the films internal structures and these were observed in the Scanning Electron Microscope.
In order to measure and compare film thickness on the front and the back surfaces, the substrates were sectioned, mounted in bakelite, polished, chemically etched and then observed in the Scanning Electron Microscope.
The substrate bulk temperature during deposition is plotted versus parameters in Figure 5.2.3 and 5.2.4.
The deposition ion current is plotted versus parameters in Figure 5.2.5.

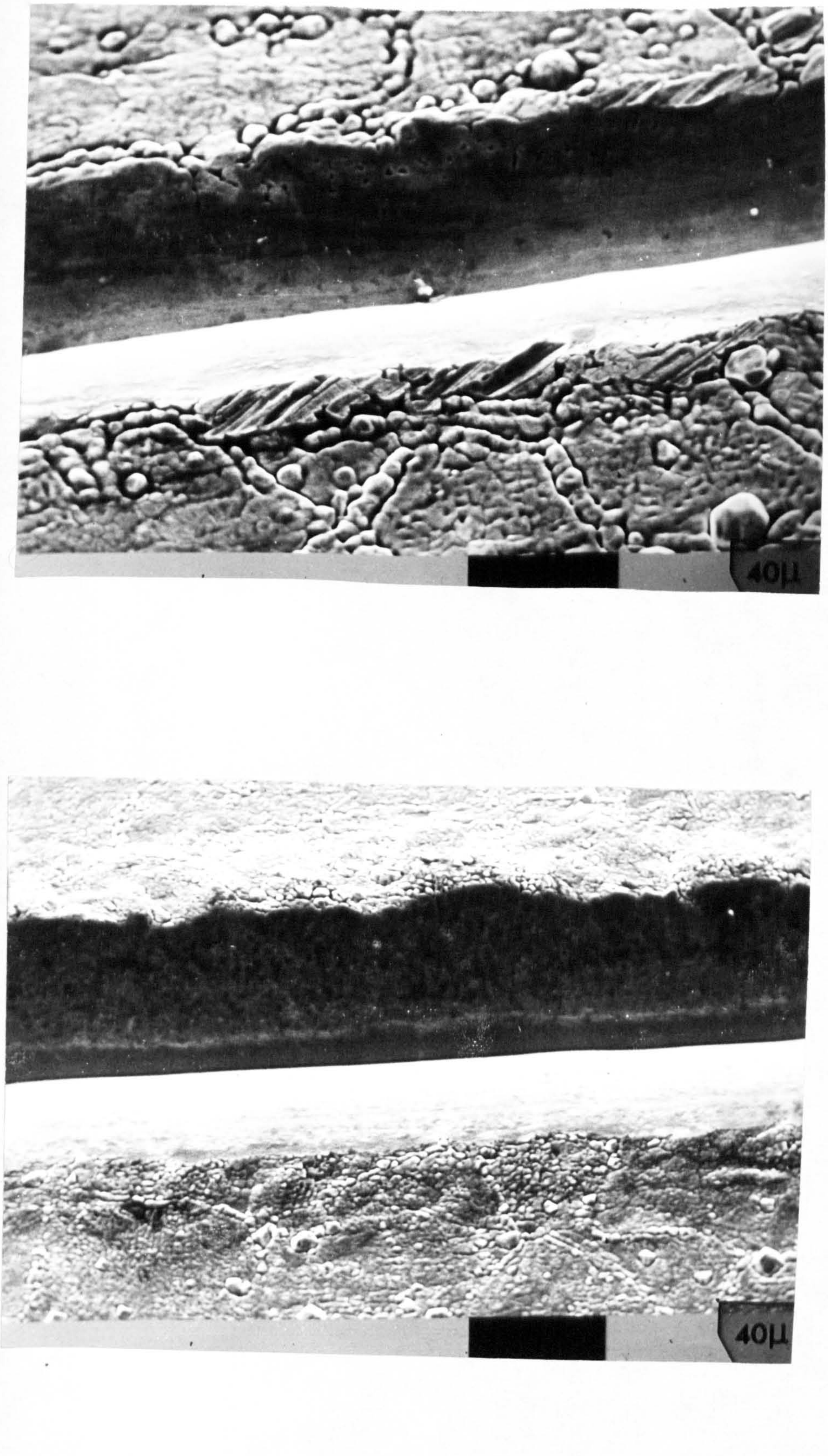

Figure 5.2.2

Tipical scratch tests

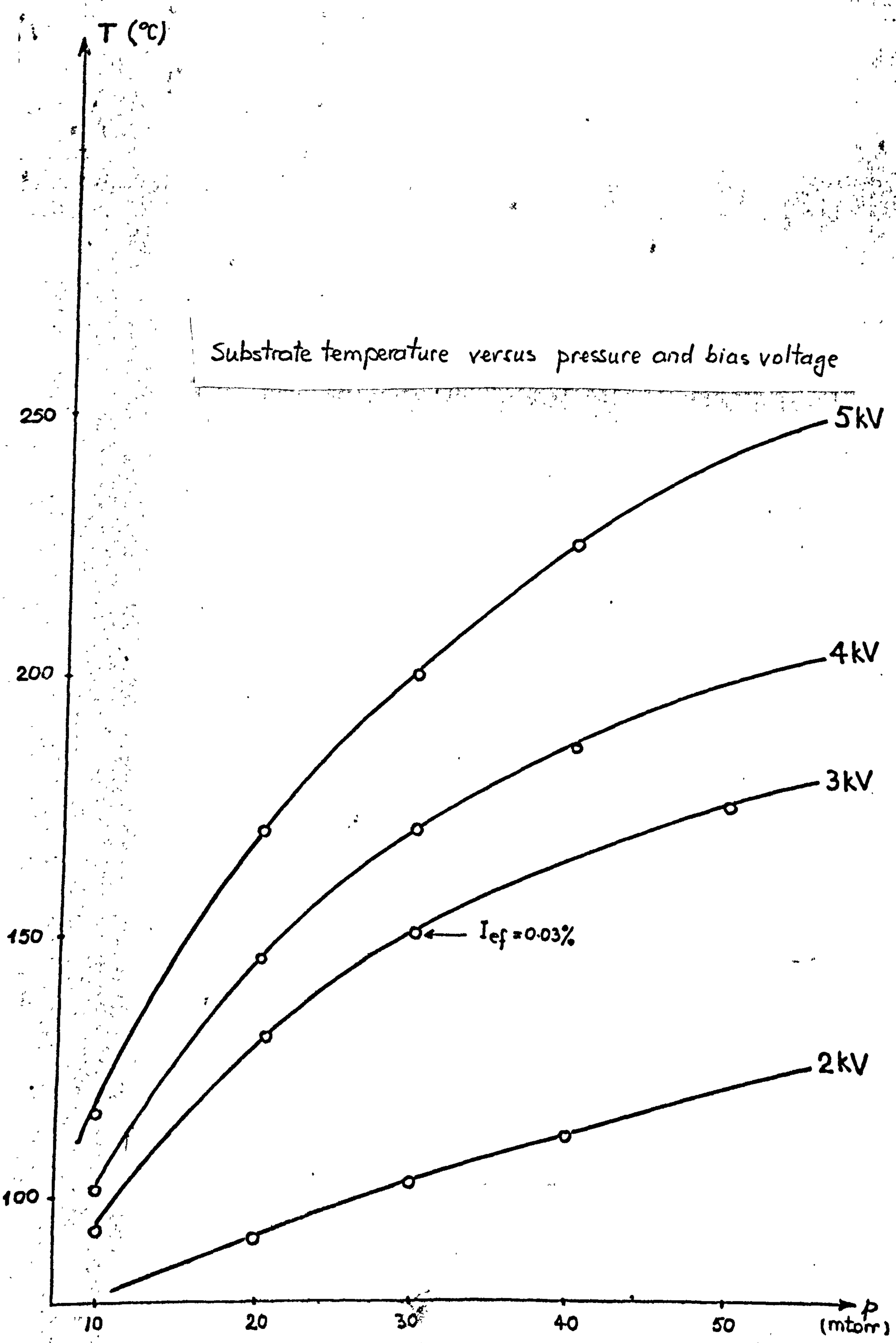
T (°C)
Substrate temperature versus pressure and bias voltage
250
200
150
100
5kV
4kV
3kV
2kV
I_{ef} = 0.03%
10
20
30
40
50
p
(mtorr)

Figure 5.2.3

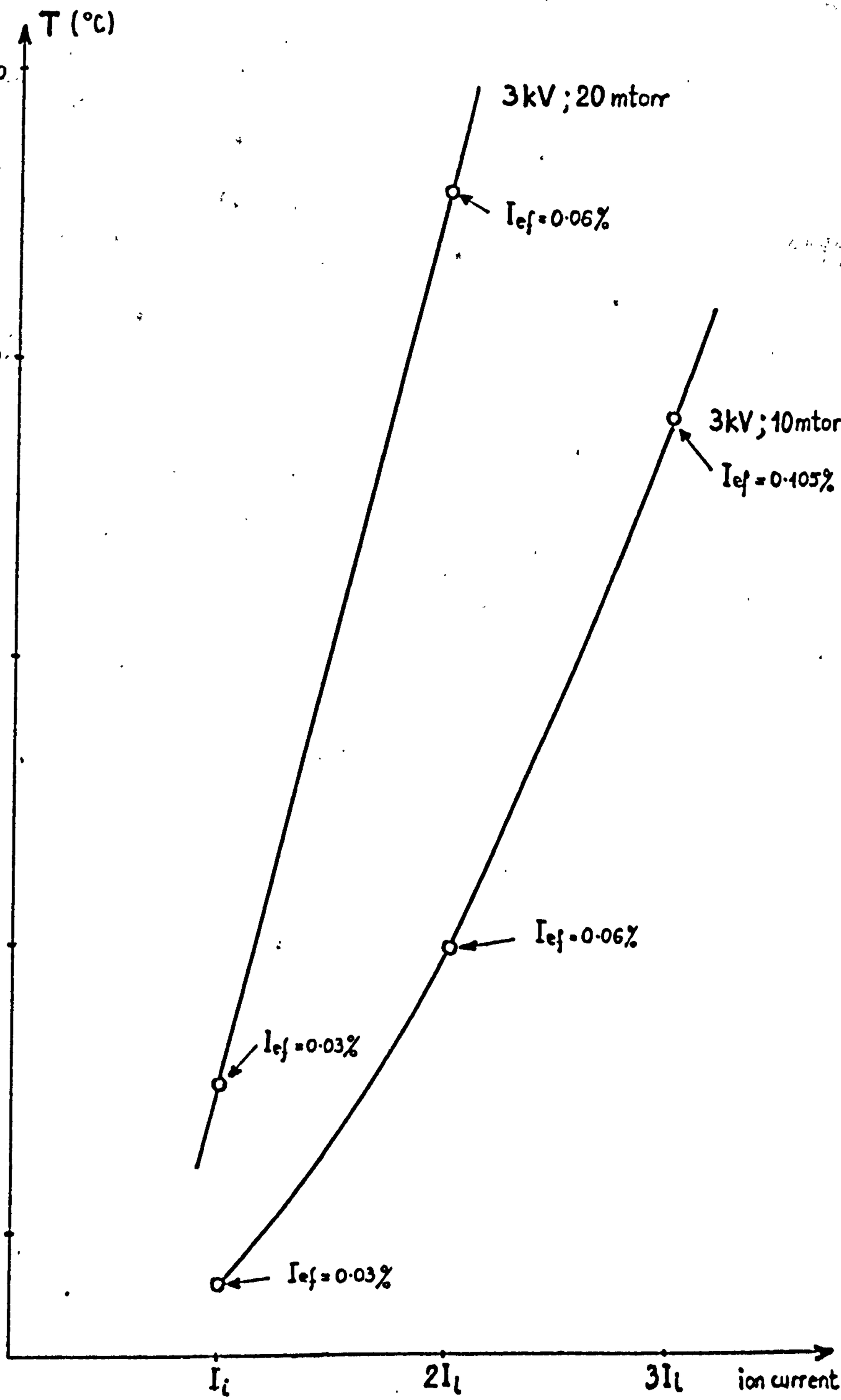

Figure 5.2.4

Positive probe-activated

Substrate temperature versus ion current

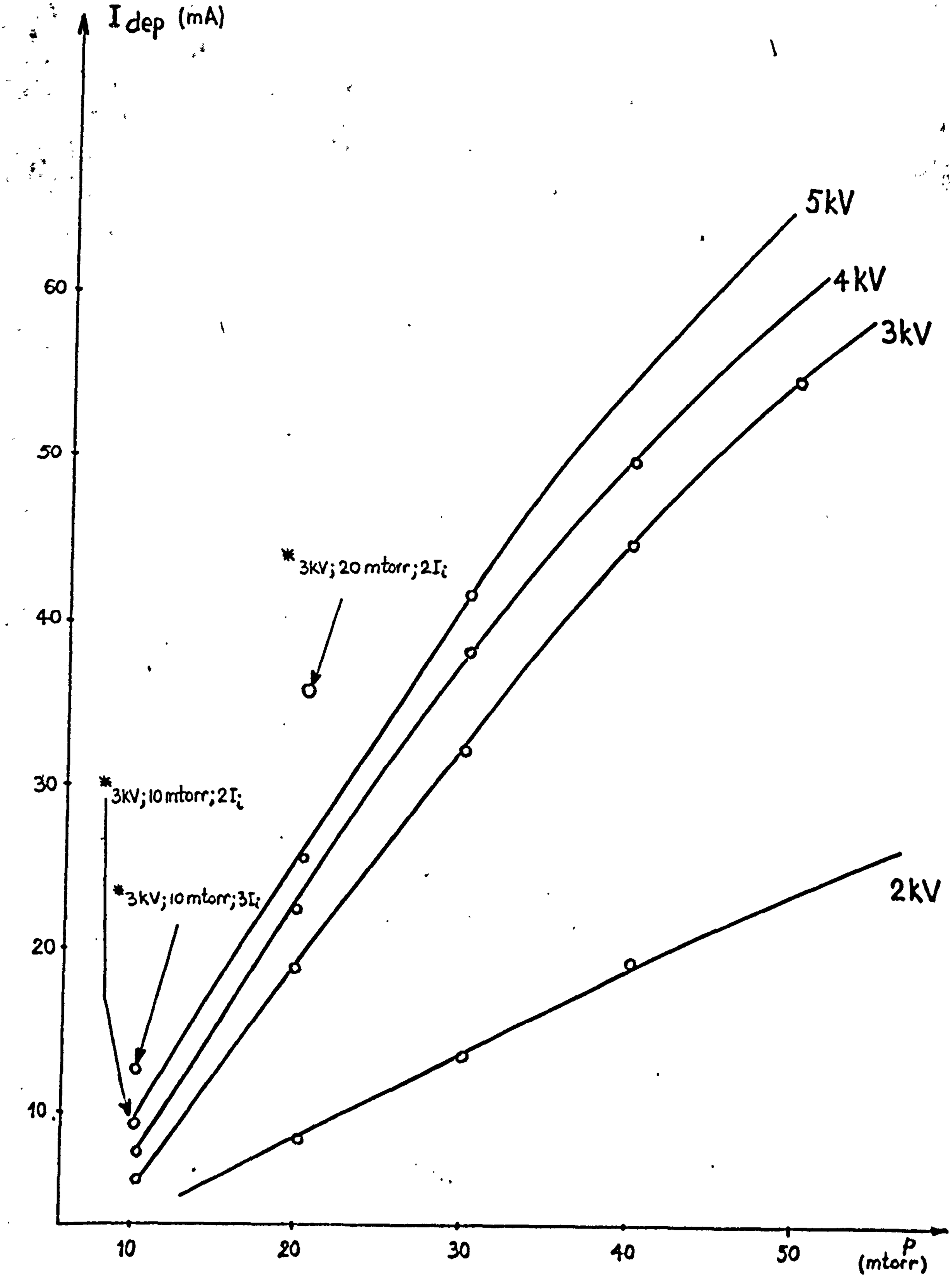

Figure 5.2.5

Deposition ion current

* positive probe - activated.

5.3. Results

5.3.1. Microstructure

The microstructure of the films was analysed on fracture cross sections by means of the SEM. The effect of argon pressure for 2,3,4 and 5 kV bias voltage is shown in Figures 5.3.1.1, 5.3.1.2, 5.3.1.3 and 5.3.1.4.

- For 2 kV, the pressure variation brings little improvement and the structure consists of tapered crystallites.

Of the three structures presented in Figure 5.3.1.1. corresponding to 2 kV bias voltage and 20,30 and 40 mtorr argon, the worst one is a) which consists of tapered crystallites embeded into a porous structure. As the pressure is raised to 30 mtorr the structure consists of large tapered crystallites alternating with some others smaller in size (Figure 5.3.1. 1 b) .

An argon pressure of 40 mtorr leads to a structure composed of tapered crystallites relatively uniform in size and separated by large voids.

- For 3 kV and 10 mtorr, the structure is more or less similar to that obtained for 2 kV and 20 mtorr (Figure 5.3.1. 2 a). For 3 kV and 20 mtorr, the doomed structure is nearly removed and a definite pattern of columnar growth is observed (Figure

5.3.1. 2 b) .

For 3 kV and 30 mtorr (Figure 5.3.1. 2 c), the structure is columnar and as it can be noticed, the columns are smaller in size than the tapered crystallites. The increase in pressure to 40 mtorr (Figure 5.3.1. 2 d) produces the same columnar structure but the columns are denser and smaller in size.

For 3 kV and 50 mtorr, the columnar structure is maintained similar to the previous one but it features signs of bonding taking place among the columns.

Figure 5.3.1. 2 f presents a fracture cross section of the copper film produced at 3 kV and 40 mtorr and as it can be noticed, the film was pulled away from the substrate during the tensile fracture. This could be either due to a bad adhesion created by a weak or not sufficiently deep interface, or more likely the fracture is between the interface and the film. However, during the scratch test, no signs of bad adhesion were observed and since the interface is expected to be harder than the film, it means that the fracture is more likely to occur within the copper film.

The improvement in the structure produced at 3 kV can be observed by analysing the surface topography as shown in Figure 5.3.1. 2 g,h & i. The increase in pressure is followed by a reduction in the grain

size and an improvement in the uniformity of the size of the grains.

As it can be noticed from Figure 5.3.1. 2 d, the film presents signs of lack of cohesion which indicates the existance of internal stress and a weak bonding among the columns.

- The film produced at 4 kV and 10 mtorr has a columnar structure (Figure 5.3.1. 3 a),and the increase of the argon pressure to 20 mtorr leads to the formation of a close packed columnar structure (Figure 5.3.1. 3 b). As the pressure is raised to 30 mtorr, the columns start to bond, a bonding which is apparently completed for 4 kV and 40 mtorr of argon (Figure 5.3.1. 3 d) .

The voids (cups and cones) that are observed in this microstructure are most probably produced as a result of a ductile fracture given by a denser film structure, since the surface topography (Figure 5.3.1. 3 e) also appears to indicate a denser, non-columnar structure.

- The films produced at 5 kV bias voltage (Figure 5.3.1. 4) have a better structure even for a low argon pressure of 20 mtorr although remanent nodular growth is still present (Figure 5.3.1. 4 a) .

Apparently, the structure is composed of parts similar to the structure obtained for 4 kV and 40 mtorr which could be due to a ductile fracture alternating with patches of some denser structure. The structure improves quickly as the argon pressure is raised to 30 and 40 mtorr. A recrystallization

process is possible to occur leading to a denser structure specially for 40 mtorr argon pressure (Figure 5.3.1. 4 c) ,
when the microstructure is composed of small patches resembling a ductile fracture (cups and cones) surrounded by a denser structure whose fracture features are similar to those given by a brittle material.

Looking at the surface (Figure 5.3.1. 4 d,e & f) a recrystallization process is observed specially for 5 kV / 40 mtorr conditions. The aspect of the surface is typical for the equiaxed grain structure with patches of less dense structure also noticed on the fracture. The approximative recrystallization temperature for copper being 200°C (table 4.1.3.) and analysing the temperature graph presented in Figure 5.2.3., it results that in the case of 5 kV and 40 mtorr the conditions for such a recrystallization to take place are met although the 10 minutes time during which the deposition takes place is not sufficient for a complete recrystallization. It is possible that recrystallization takes place as the film grows layer by layer and does not allow the growth of large crystallites , fact confirmed by the x - ray back reflection method (using a 400 μ in diameter beam) which indicated fine crystallites alternating with some larger ones.

- The activation of the positive probe leads to a definite improvement in the microstructure.

At 3 kV and 10 mtorr and with +60 V applied on the positive probe to double the initial cathodic current, the resulting structure is a combination of patches approximately giving a ductile fracture and some denser fractures (Figure 5.3.1. 5 a), although the temperature was well bellow 200°C, (Figure 5.2.4.) which removes the recrystallization possibility. The surface aspect (Figure 5.3.1. 5c) also reveals the denser structure obtained under these conditions. One effect of the positive probe is that the ionization efficiency is increased from 0.03 % to 0.06 % followed by an increase in the temperature which reaches the level obtained for 3 kV and 30 mtorr. But the structure for these conditions is a typical columnar one (Figure 5.3.1. 2 c) which leads to the conclusion that the improved structure obtained with the positive probe is not due to the rise in temperature but, is an effect of the increase in the ionization efficiency and therefore an increase in the value of the coefficient ψ (higher sputtering rate).

For the same conditions of 3 kV and 10 mtorr, but with +100 V applied on the positive probe to give a threefold increase in the cathodic current, a very dense film structure is obtained giving a fracture that appears to be due to a brittle material as shown in Figure 5.3.1. 5 b.

The corresponding surface micrograph (Figure 5.3.1. 5 d) shows a very fine structure probably due to the

intense energetic bombardment, with no signs of large grains being formed although a temperature of approximately 240°C was achieved. The line broadening of the x - ray diffraction pattern indicated crystallites in excess of 1000 Å and the x - ray back reflection method (using a 400 μ in diameter beam) indicates that the structure is in fact a combination of relatively small crystals and a few larger crystals (Figure 5.3.1.7).

A polished and slightly etched cross section was also analysed in the Scanning Electron Microscope as shown in Figure 5.3.1.8. Owing to the chemical etching as it can be seen, the grain structure is revealed as being composed of fairly small grains with the presence of some relatively larger ones. This leads to the conclusion that the dense structure is not entirely due to a recrystallization and grain growth process, but is mainly due to an even film growth through the errosion (due to a balanced coefficient ψ) of all the peaks and the valleys. The ionization efficiency for this case was 0.105 %.

The microhardness measurement indicated that the copper film is less hard than pure copper for the tapered crystallites and the columnar structures, while the very dense structure obtained using the positive probe has a hardness approximately equal to that of the pure copper.

The x - ray back reflection and the chemically etched cross section showed very small grains and

this indicates that the fracture presented in Figure 5.3.1.5 b is not a brittle one. Such a brittle fracture could be obtained at very low temperatures and since all the fracture cross sections in this work were performed at room temperature, the explanation for the section in Figure 5.3.1.5b could be as follows :

A very dense film consisting of small grains is produced and therefore the fracture that takes place along the grain boundaries and following the grains shape takes a straight line thus giving the appearance of a brittle fracture.

Since these experiments were carried out towards the end of the period affected to this work, there was not enough time for further investigations in the nature of these very dense films but however, some more research will be done and reported later on.

The production of films at 3 kV and 20 mtorr and with +200 V on the positive probe to increase twice the value of the initial cathodic current (ionization efficiency 0.06 %) , leadsto a film structure shown in Figure 5.3.1.6. which is similar to the structure obtained for 3 kV and 10 mtorr argon pressure and a twofold increase in the cathodic current (Figure 5.3.1.5a), although the temperature reaches 280^{o}C which is a much higher value.

This confirms the fact that although temperature has a role in obtaining the structure, the ionization

efficiency is the parameter which balanced against the deposition rate, can lead to radical improvement in the microstructure of ion plated films.

*

* *

Aluminium films approximately 5 μ thick were ion plated on flat steel substrates at 3 kV and 10 mtorr argon and then , in the same V-p conditions but with the positive probe activated to give a three-times increase in the cathodic current. The deposition rate was approximately 0.5 μ/min and the microstructures obtained through the fracture section are presented in Figure 5.3.1.9 a and b.

The structure obtained without the positive probe is columnar,as also revealed by the surface morphology (Figure 5.3.1.10 a).

The film lacks in cohesion and breaks easily under tensile stress as shown in Figure 5.3.1.11 a .

In contrast with these, the aluminium film ion plated with the positive probe ($3I_i$) presents a dense structure as shown in Figure 5.3.1.9 b, with obvious signs of recrystallization in cubic crystals easily noticed on the surface (Figure 5.3.1.10b).

The film is cohesive and adhesive to the substrate (Figure 5.3.1.11b).

*

* *

The general conclusion that can be drawn is that the main parameter that could lead to improved structures is the ionization efficiency which is a function of ion current density, followed by temperature which for low melting materials in particular, could lead to some recrystallization taking place.

The introduction of a triode system to allow the variation of I_i independently and in a controlled manner, proved successful in producing controlled structures beginning with tapered crystallites and ending with some unusually dense structures.

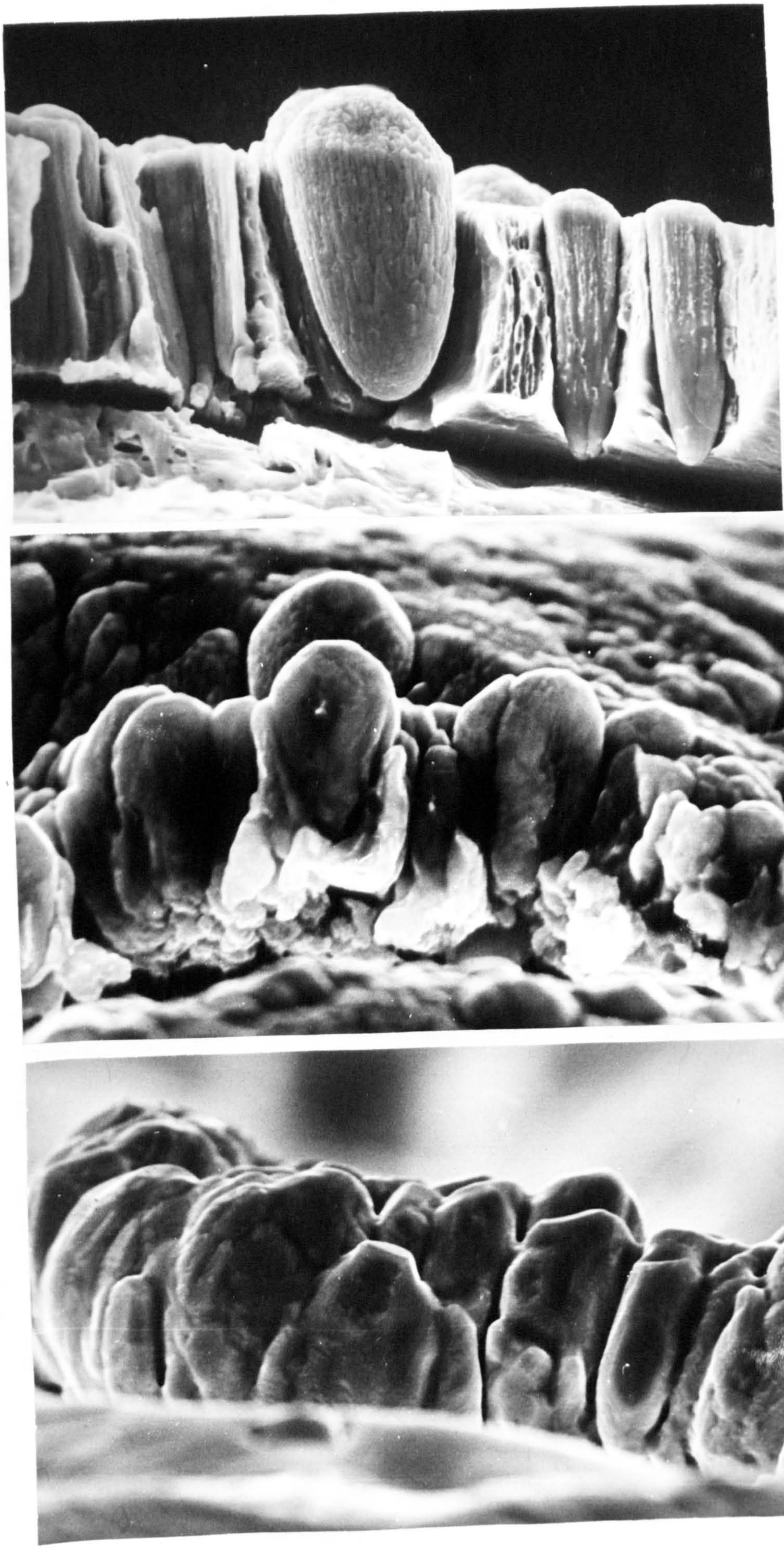

a.
2 kV
20 mtorr

b.
2kV
30 mtorr

c.
2kV
40 mtorr

Figure 5.3.1.1
2kV

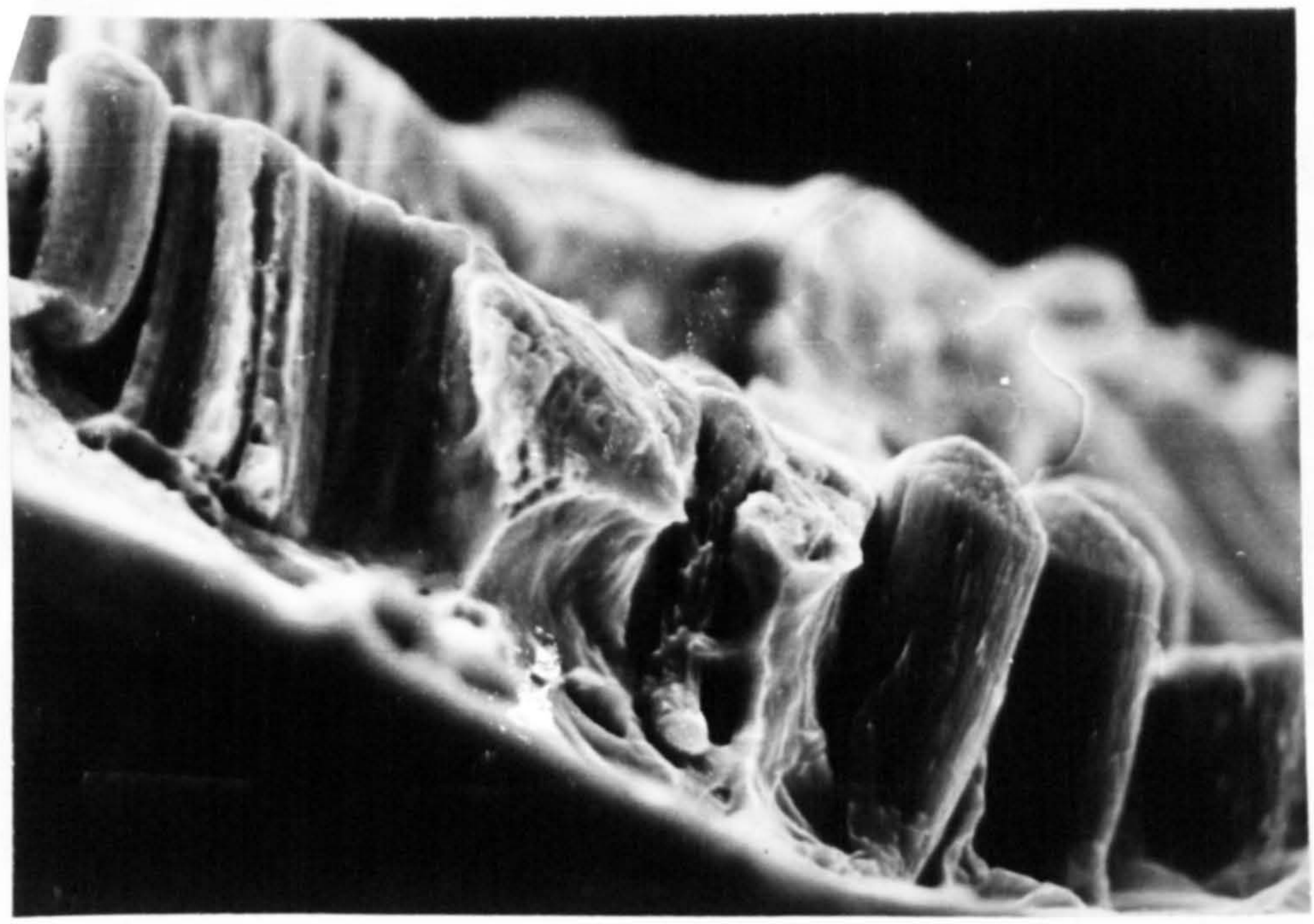

a. 3kV ; 10 mtorr

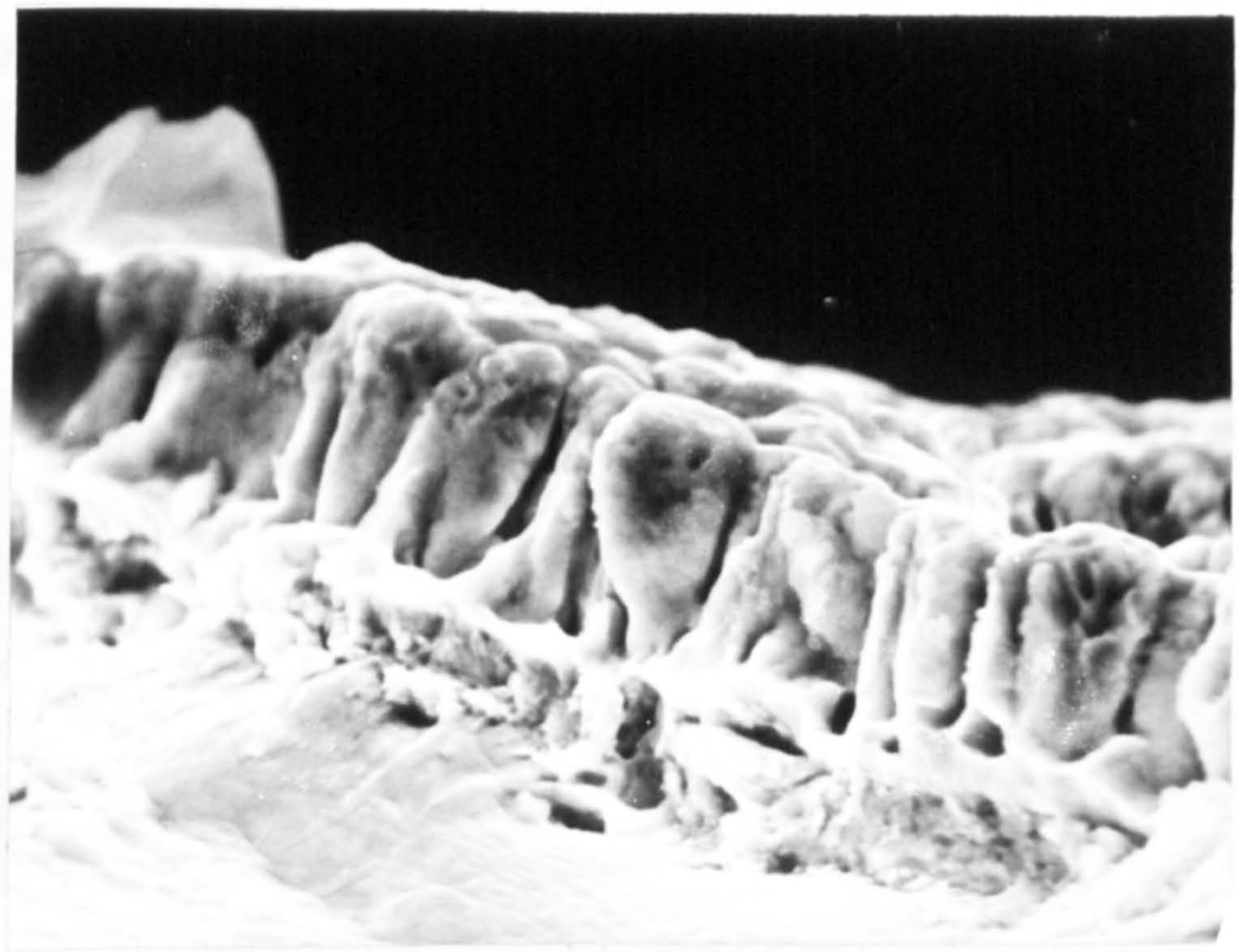

b. 3kV ; 20 mtorr

Figure 5.3.1.2

3 kV

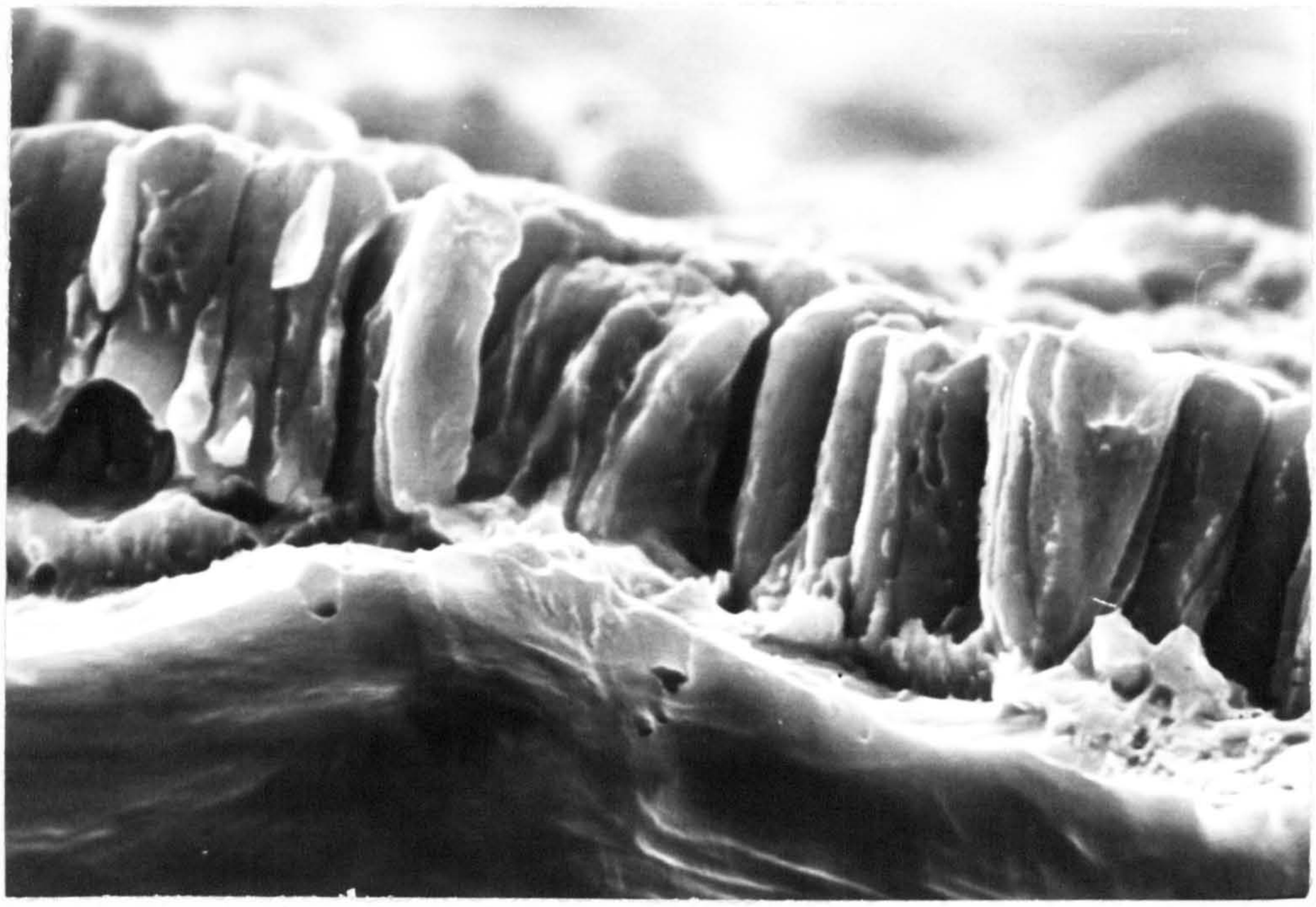

c. 3KV ; 30mtorr

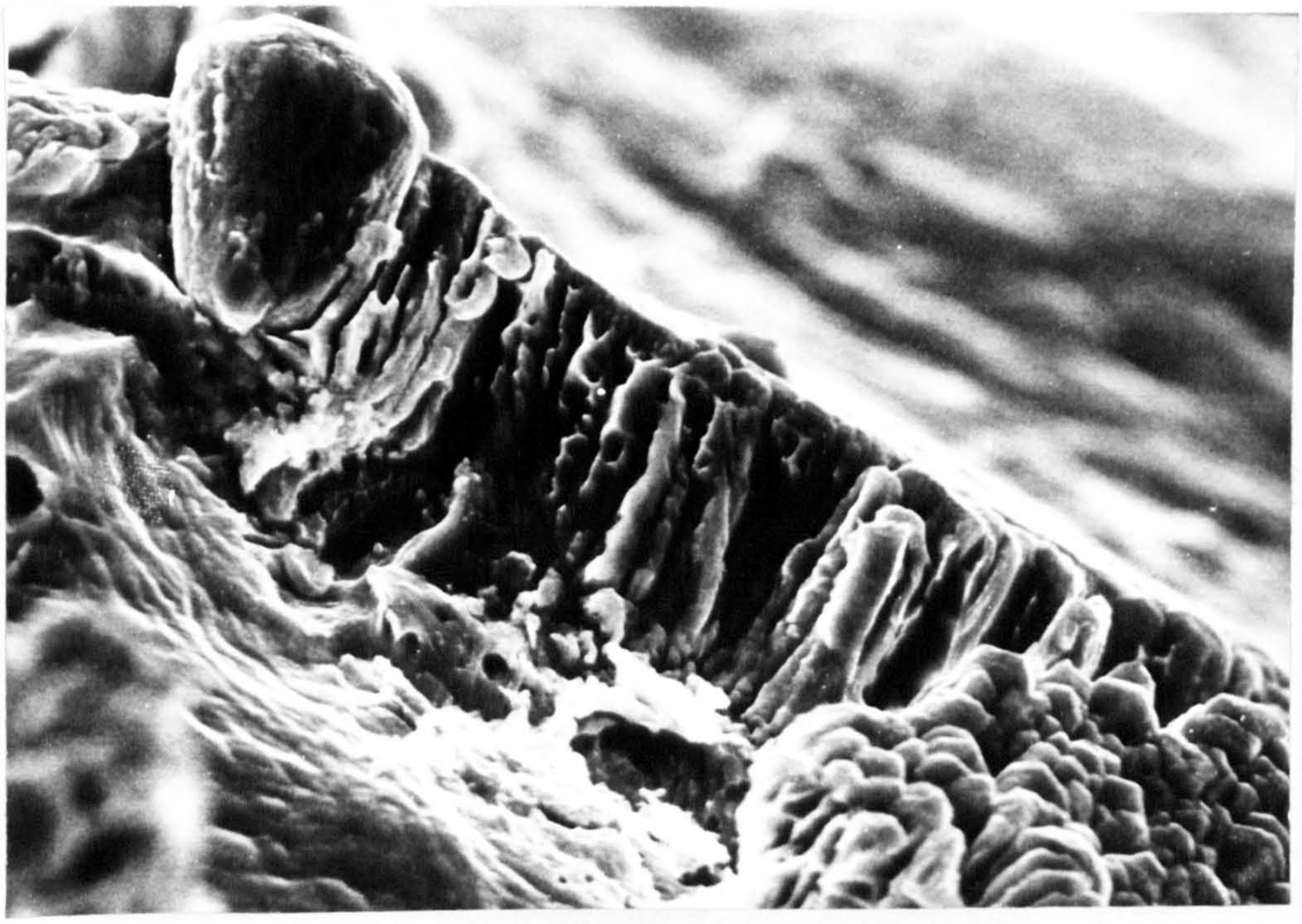

d. 3kV ; 40mtorr

Figure 5.3.1.2

3kV

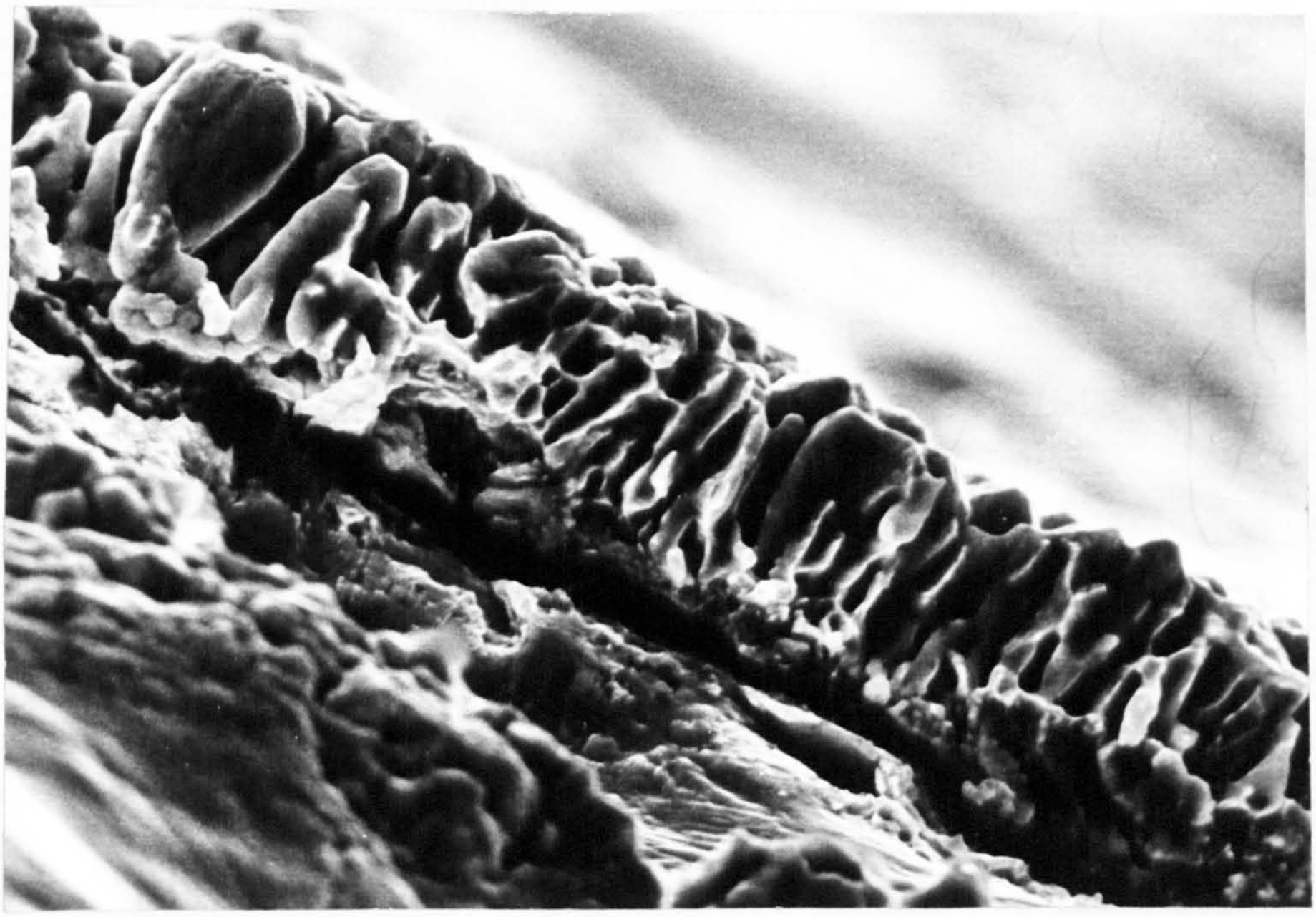

e. 3kV ; 50 mtorr

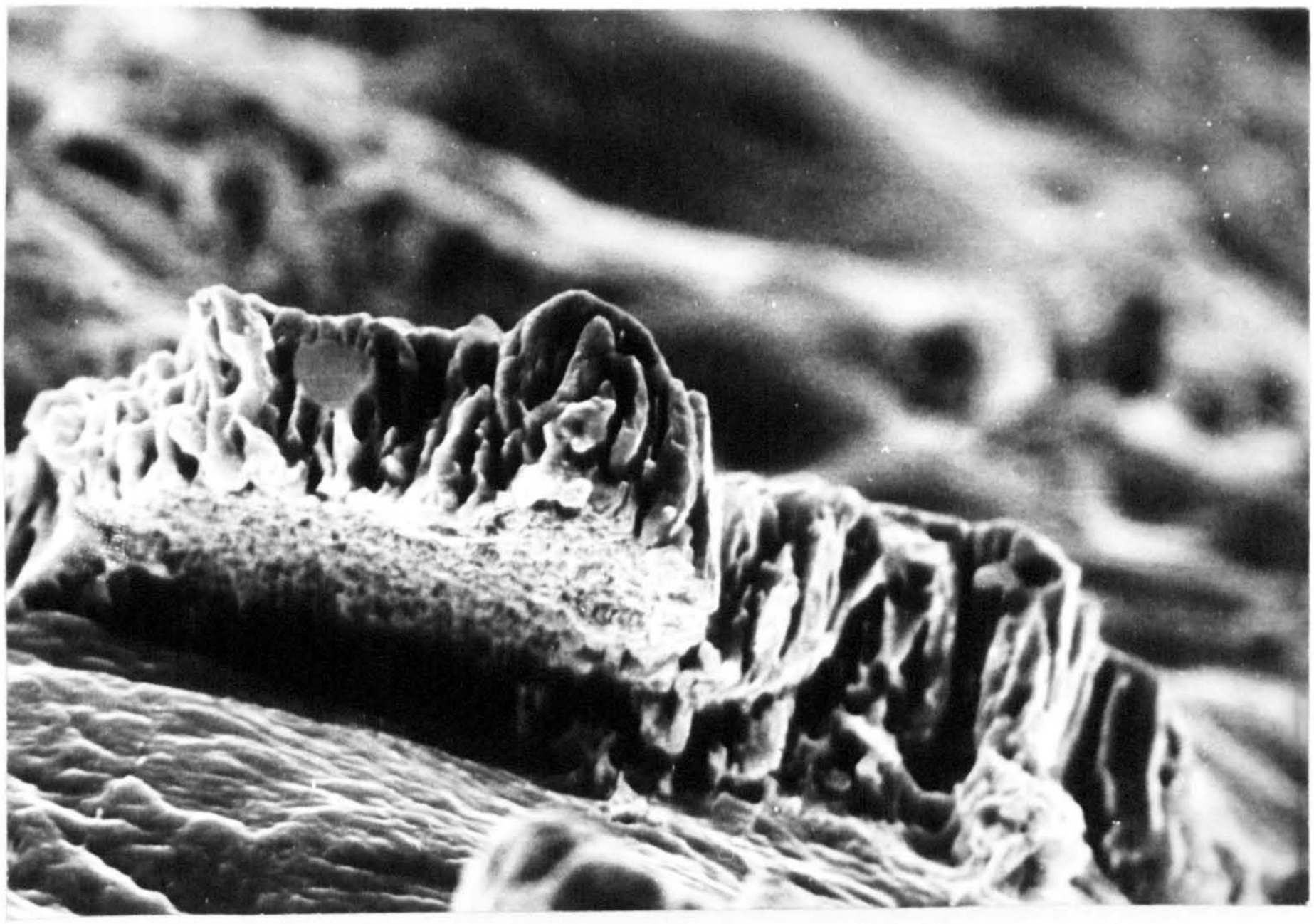

f. 3kV ; 40 mtorr - the film pulls away

Figure 5.3.1.2

3kV

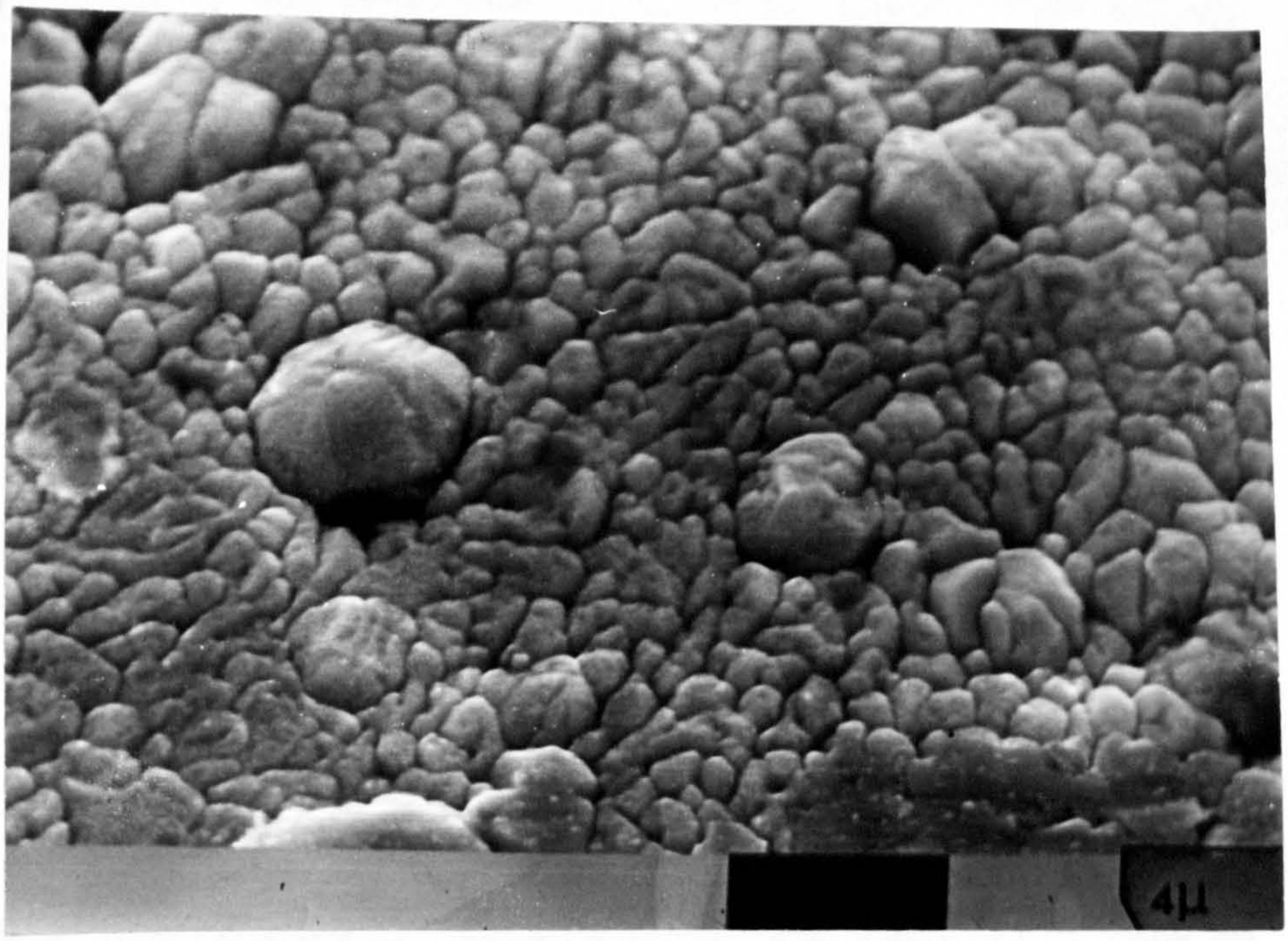

g. 3KV ; 10 mtorr

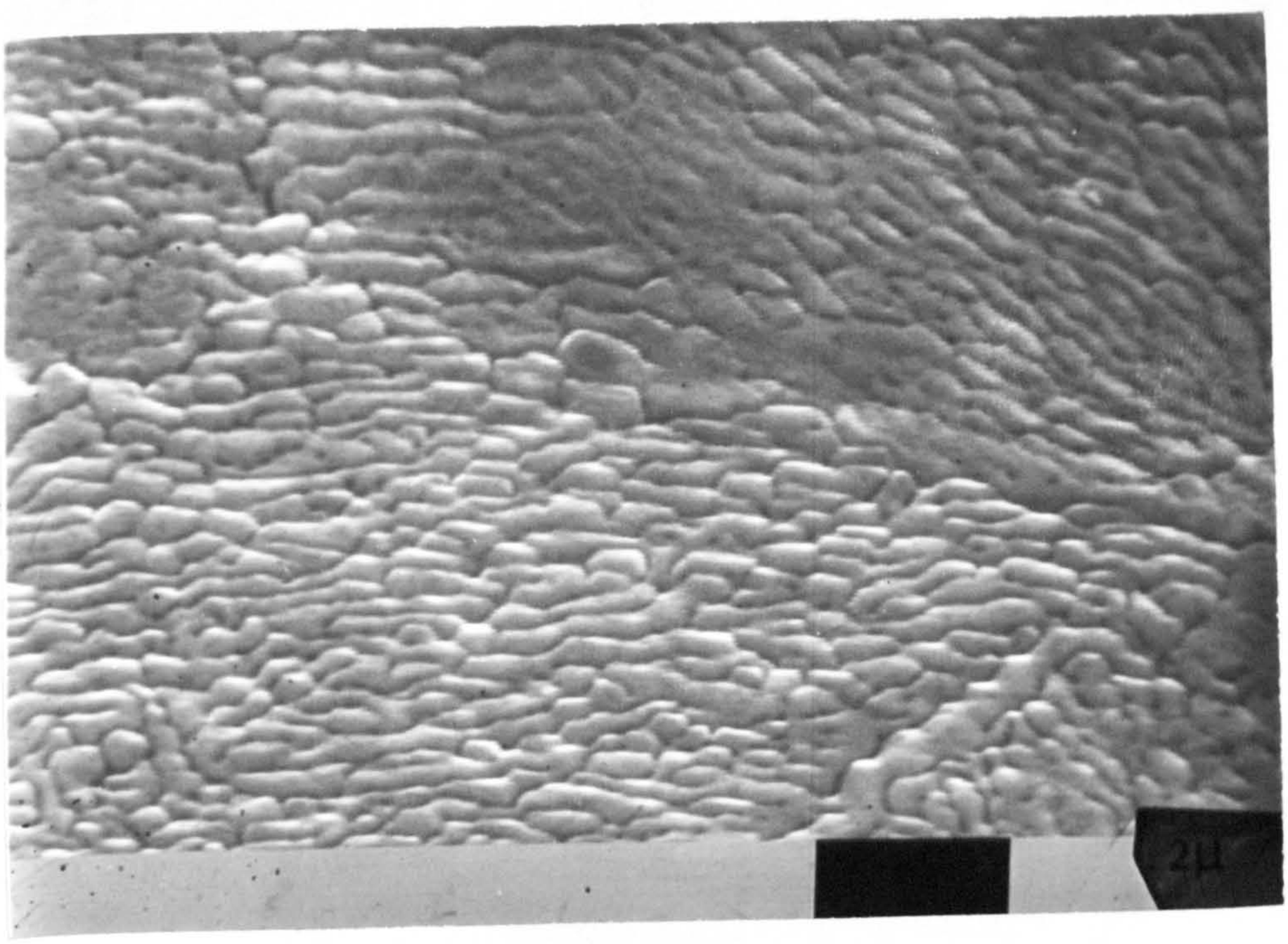

h. 3kV ; 40 mtorr

Figure 5.3.1.2

3kV

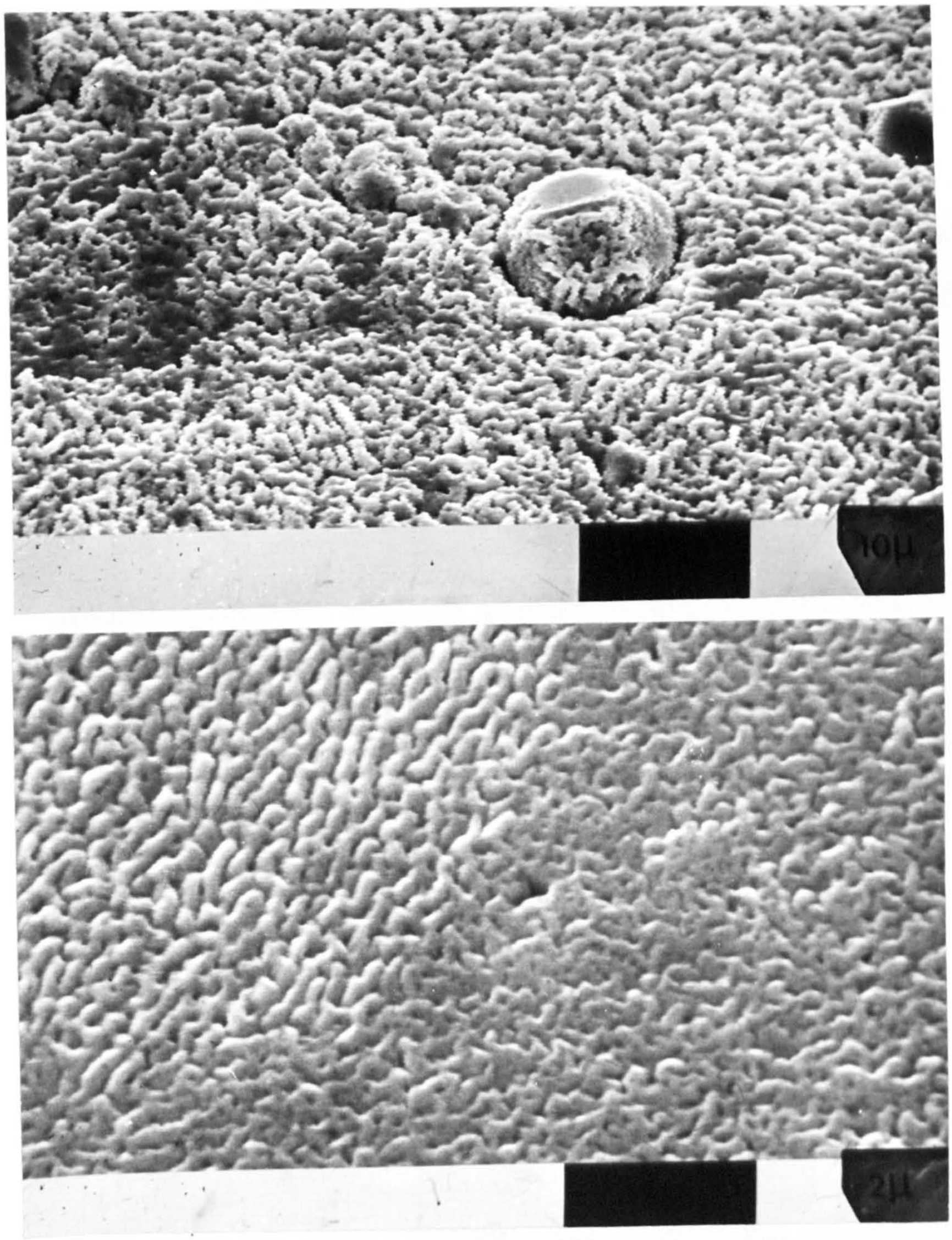

i. 3kV ; 50 mtorr

Figure 5.3.1.2

3kV

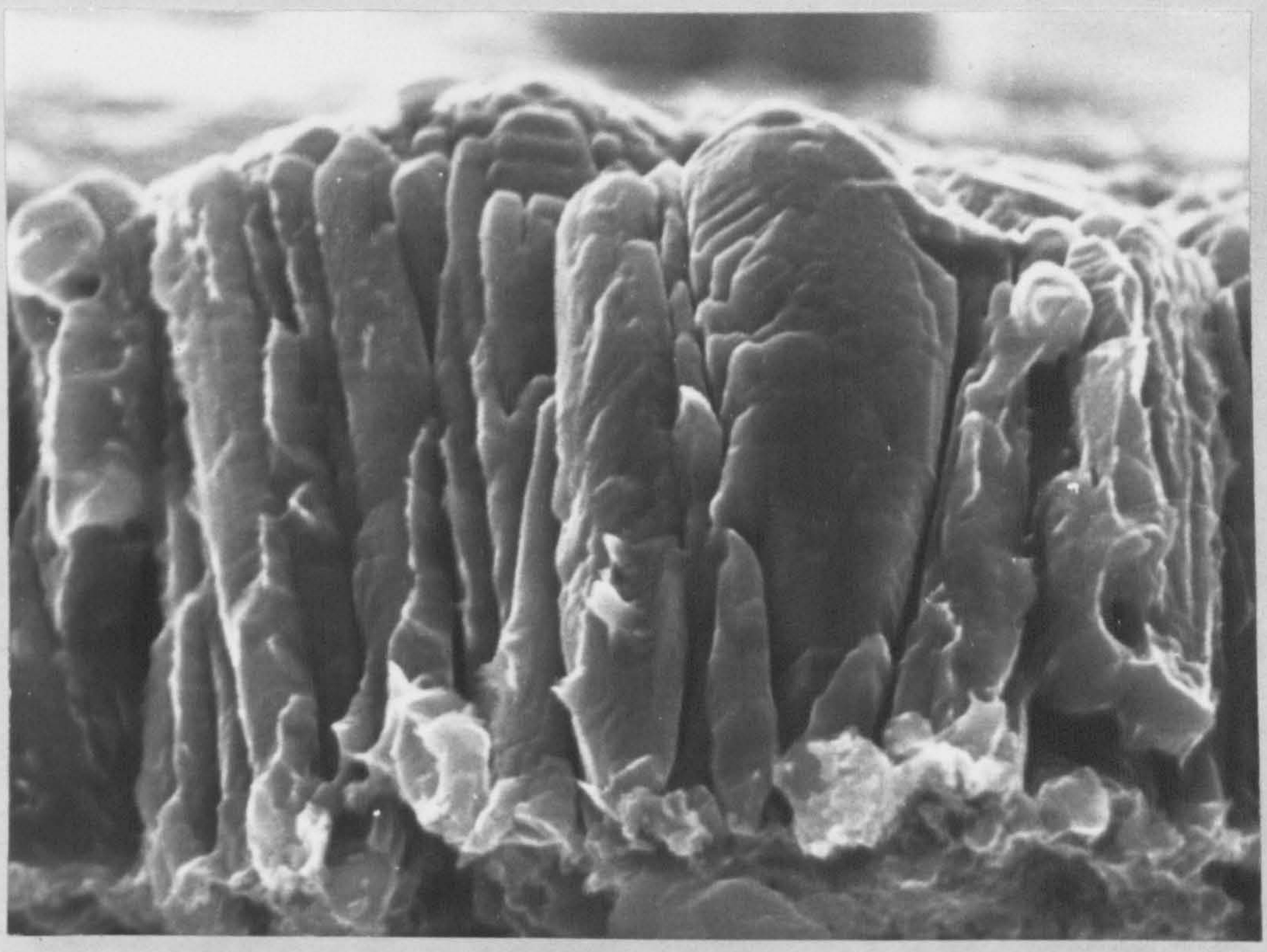

a. 4kV ; 10 mtorr

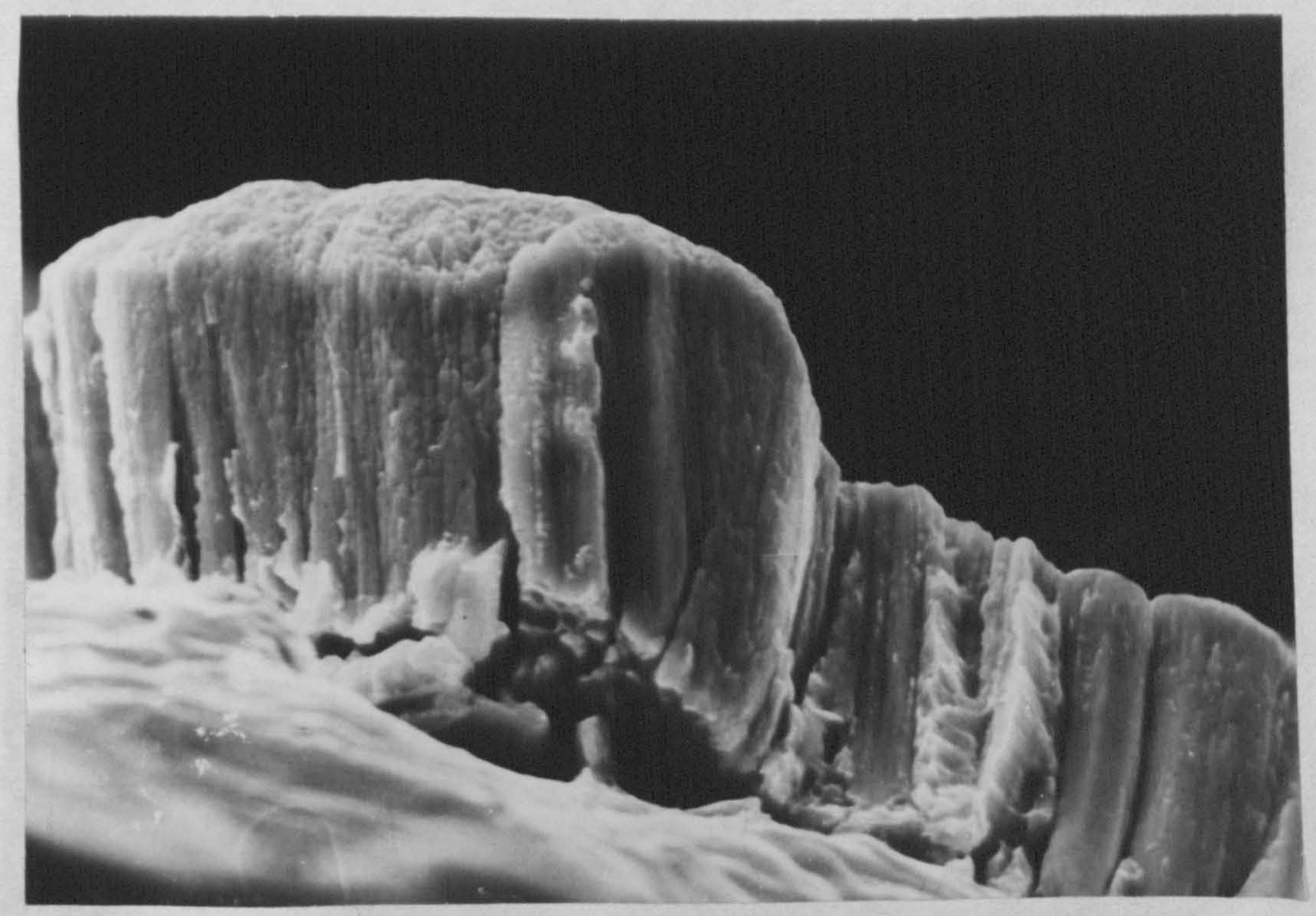

b. 4kV ; 20 mtorr

Figure 5.3.1.3

4kV

c. 4kV ; 30 mtorr

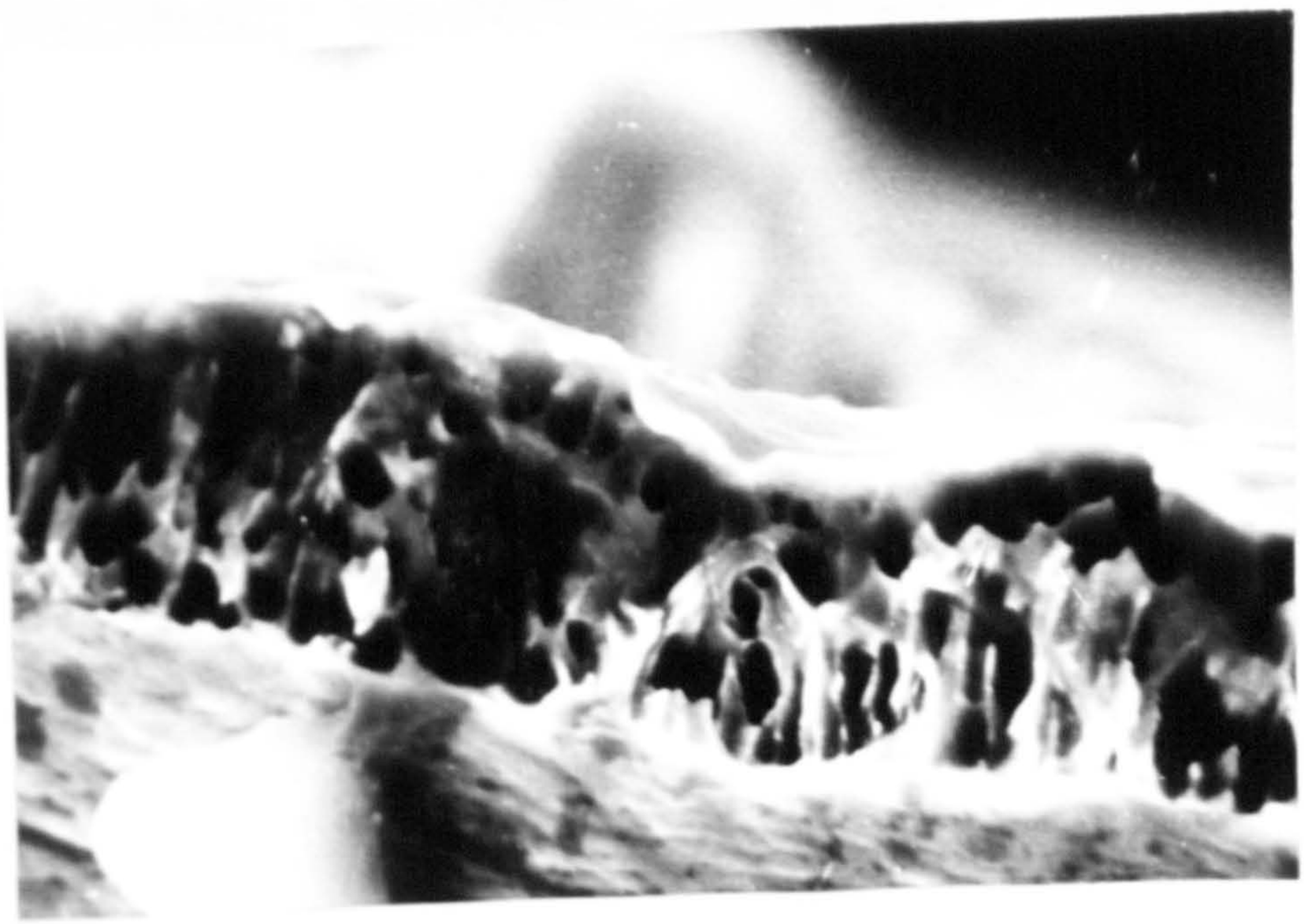

d. 4kV ; 40 mtorr

Figure 5.3.1.3

4kV

c. 4kV ; 30 mtorr

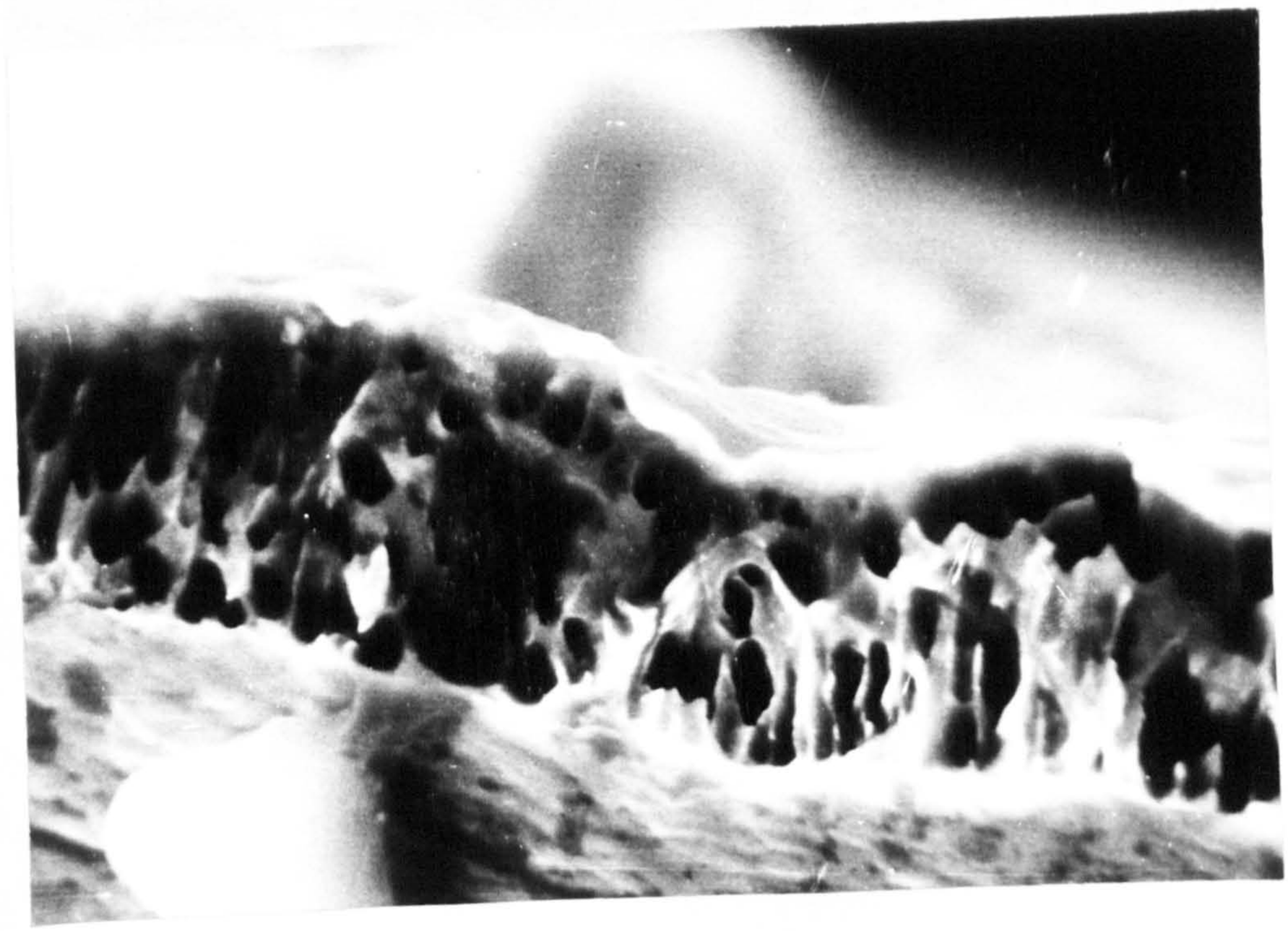

d. 4kV ; 40 mtorr

Figure 5.3.1.3

4kV

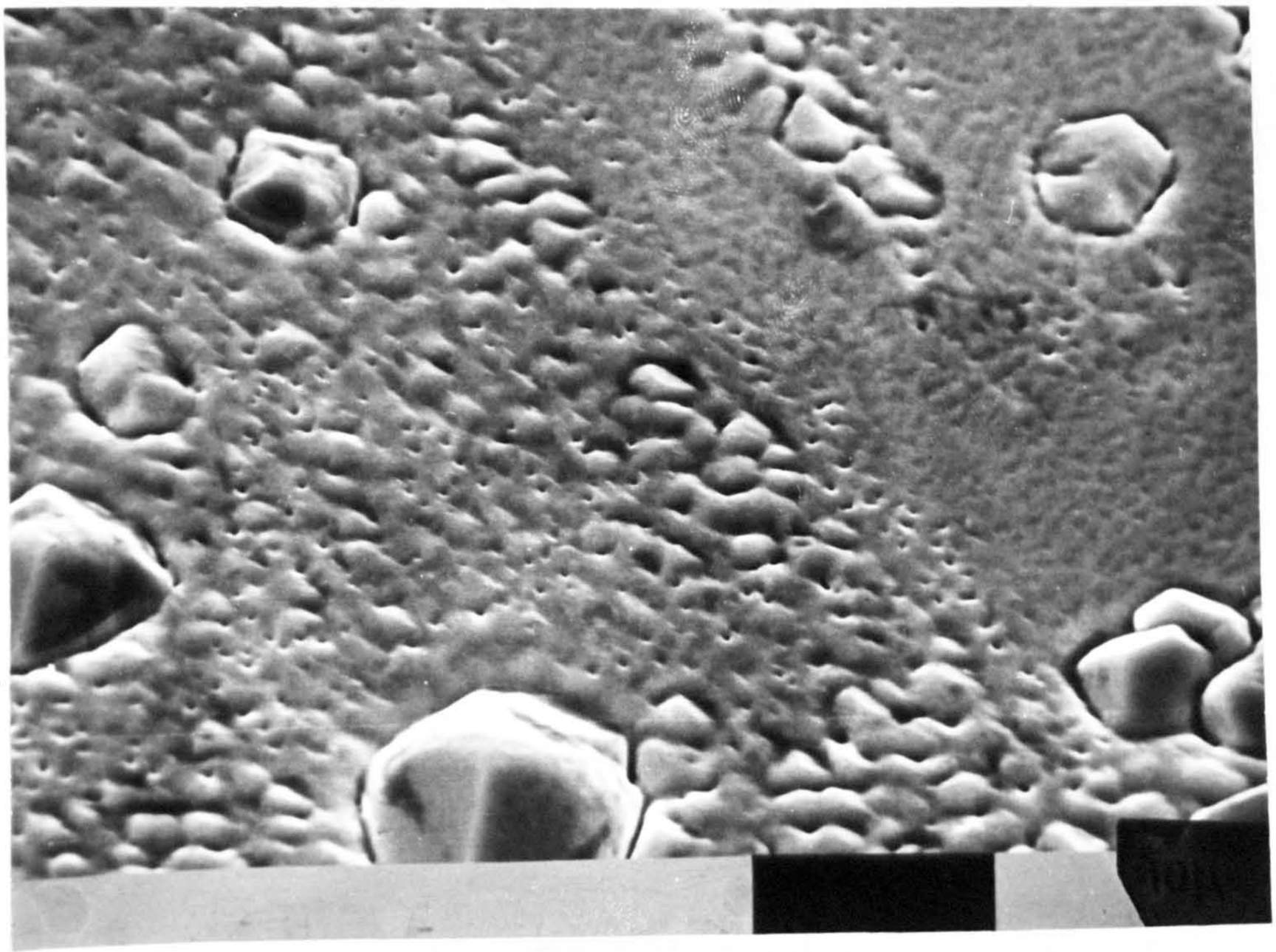

e. 4kV ; 40 mtorr

Figure 5.3.1.3

4kV

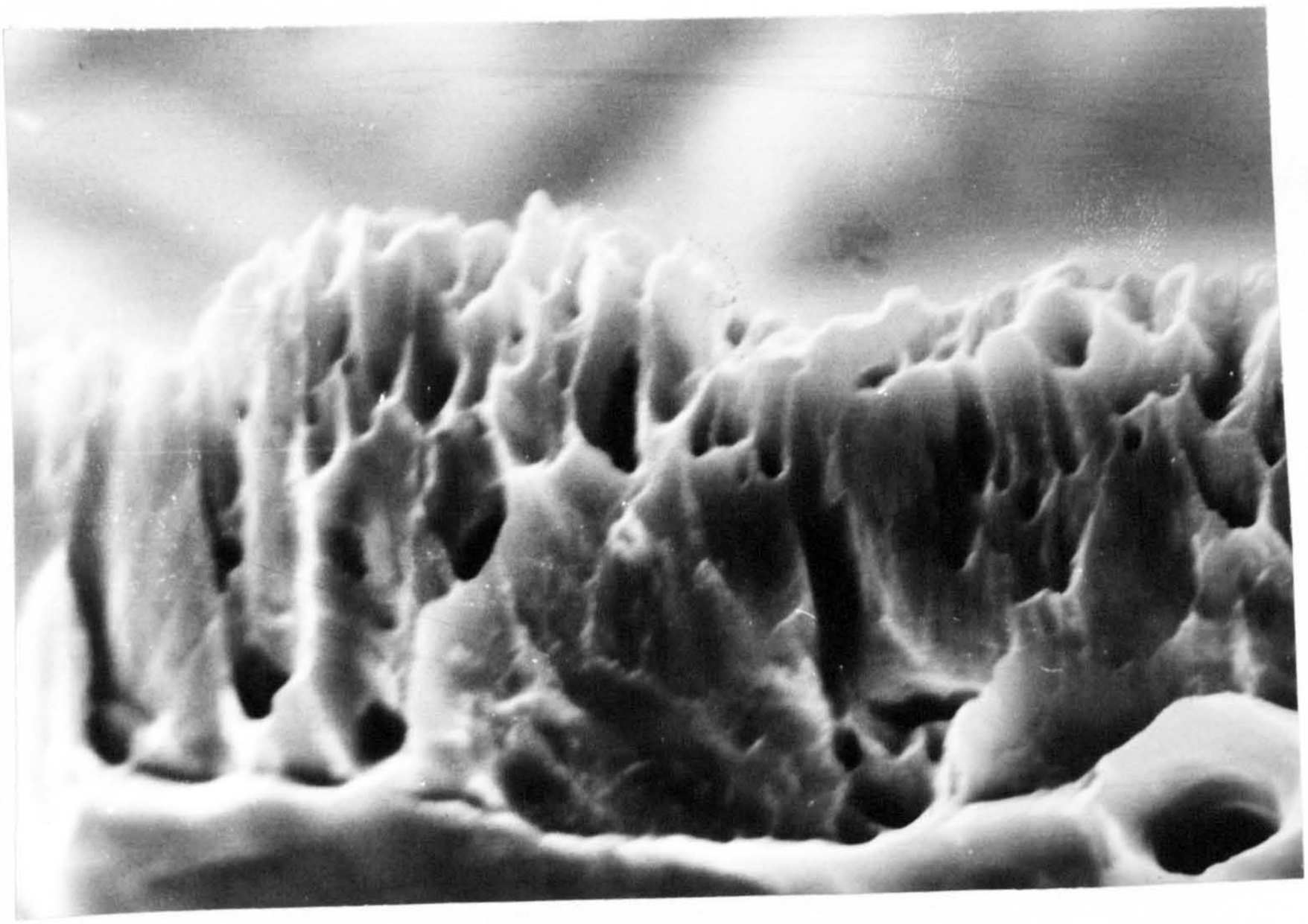

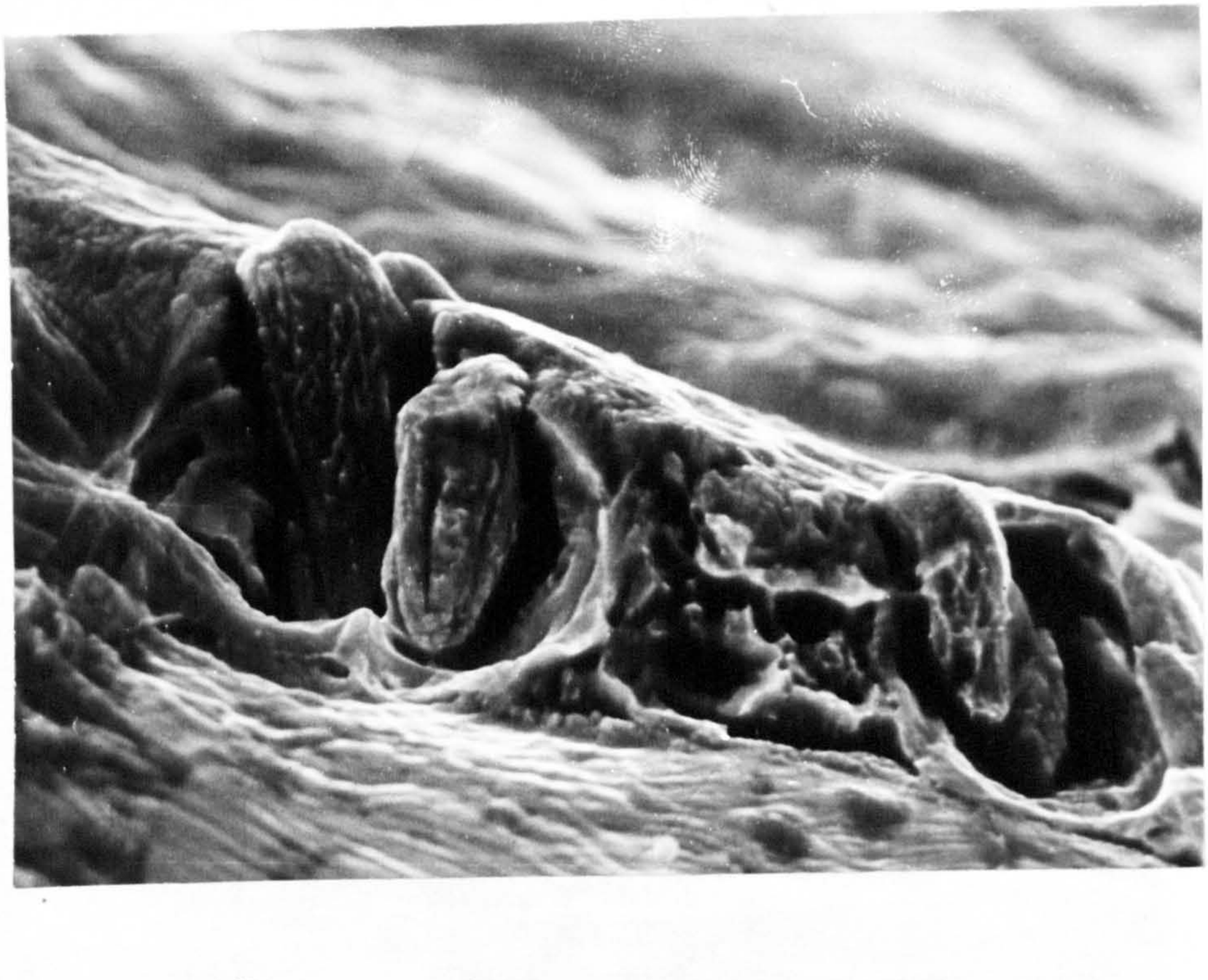

a. 5kV ; 20 mtorr

Remanent nodular growth.

Figure 5.3.1.4

5kV

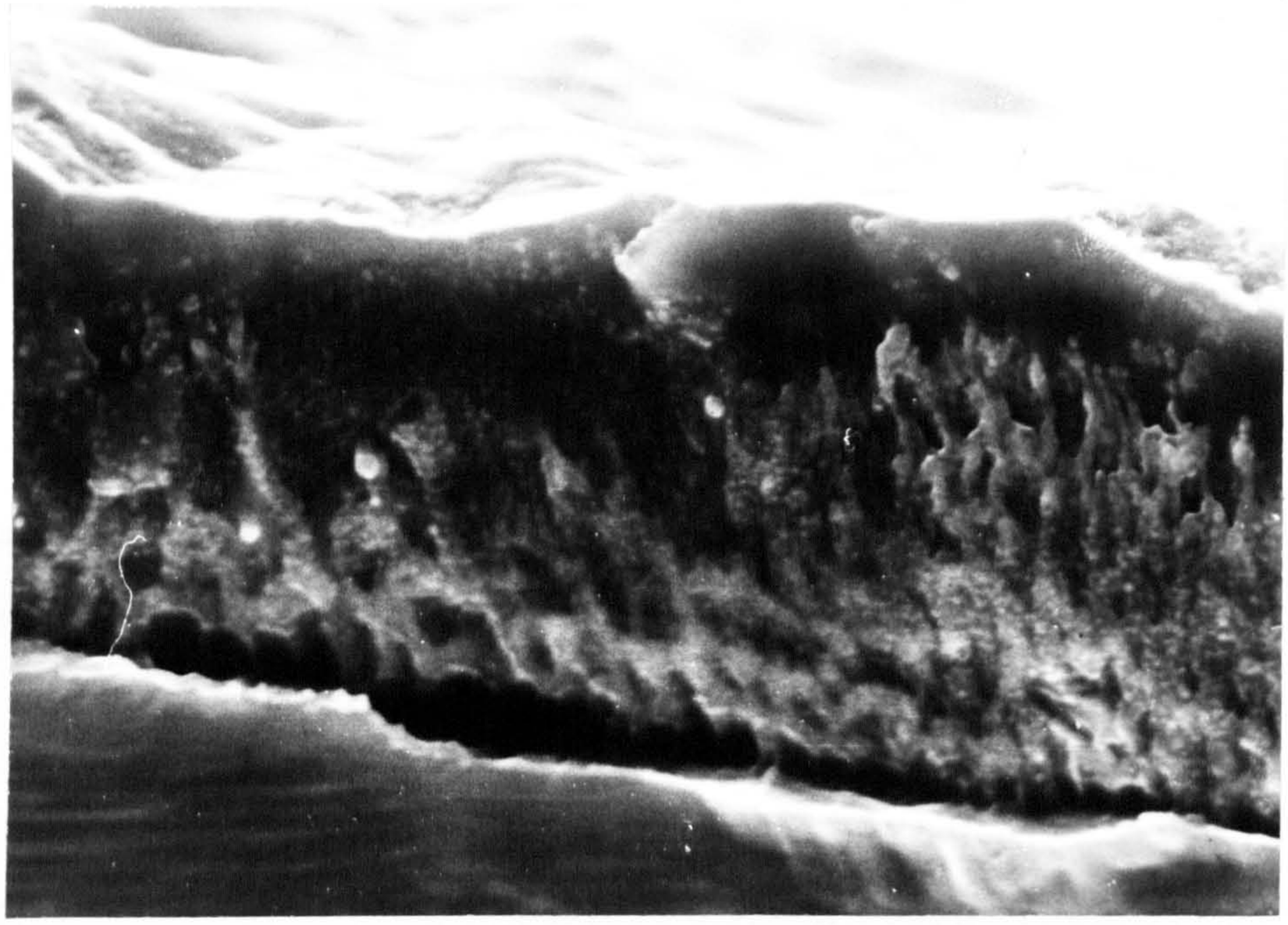

b. 5kV ; 30 mtorr

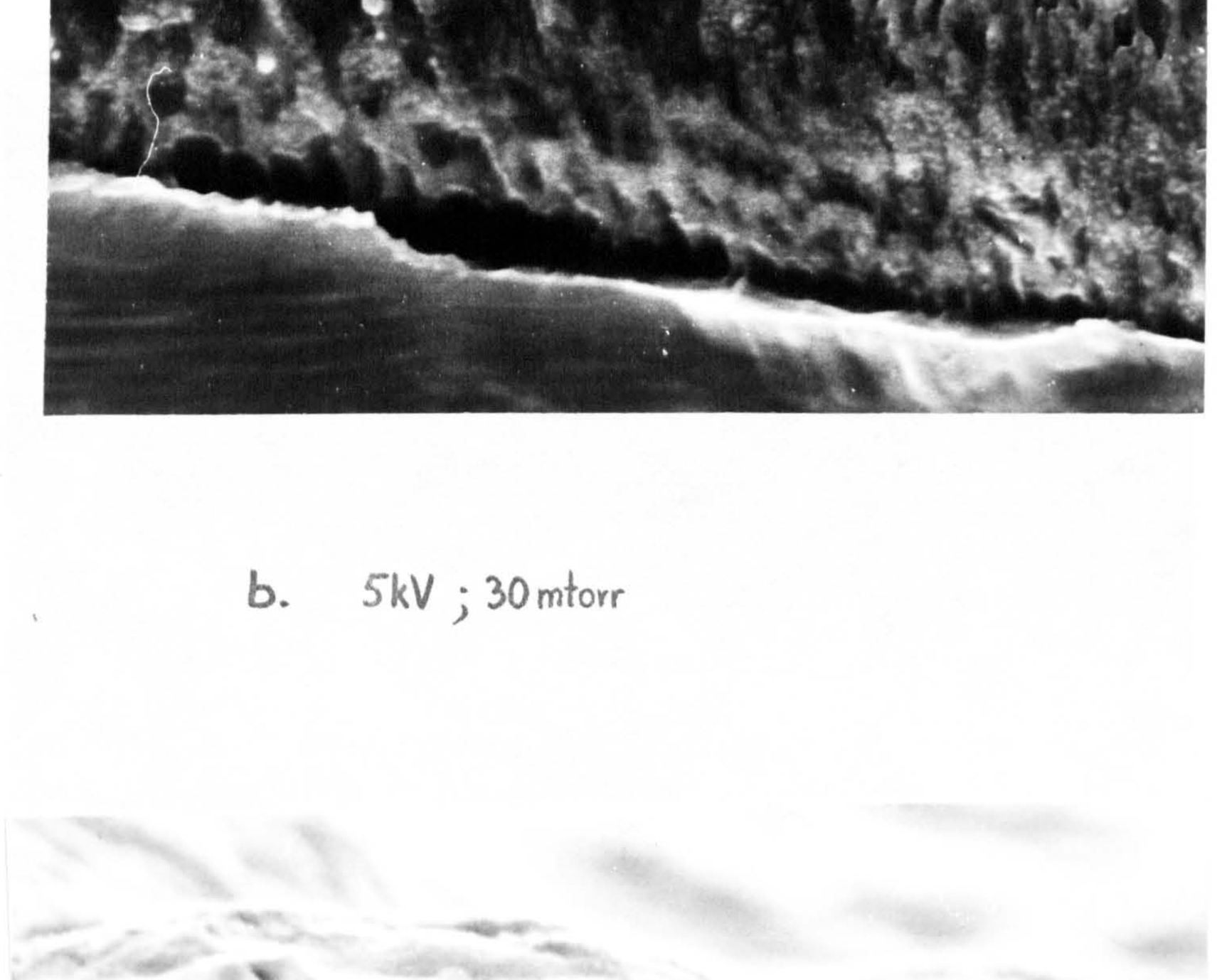

c. 5kV ; 40 mtorr

Figure 5.3.1.4

5kV

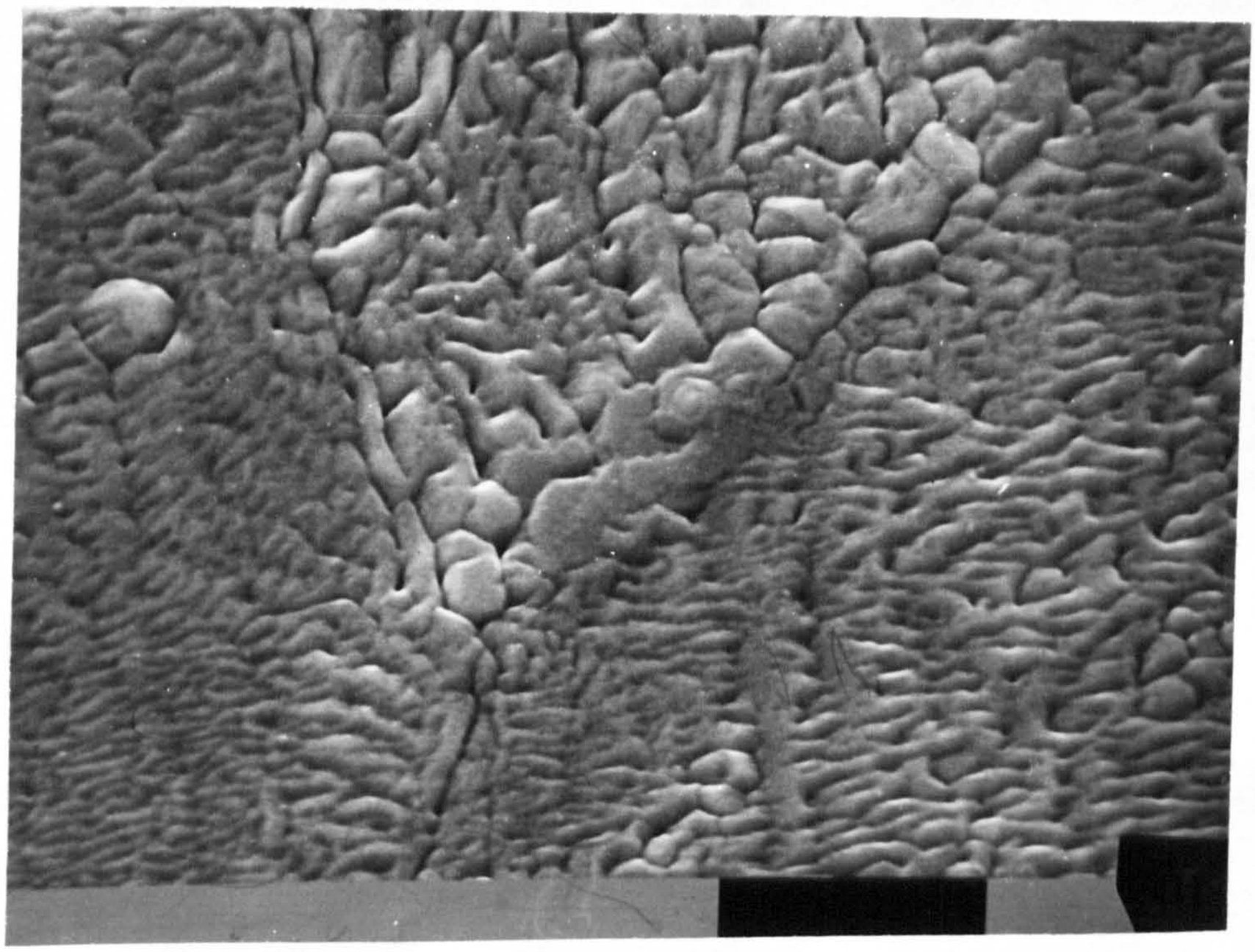

d. 5kV ; 20 mtorr

Figure 5.3.1.4

5kV

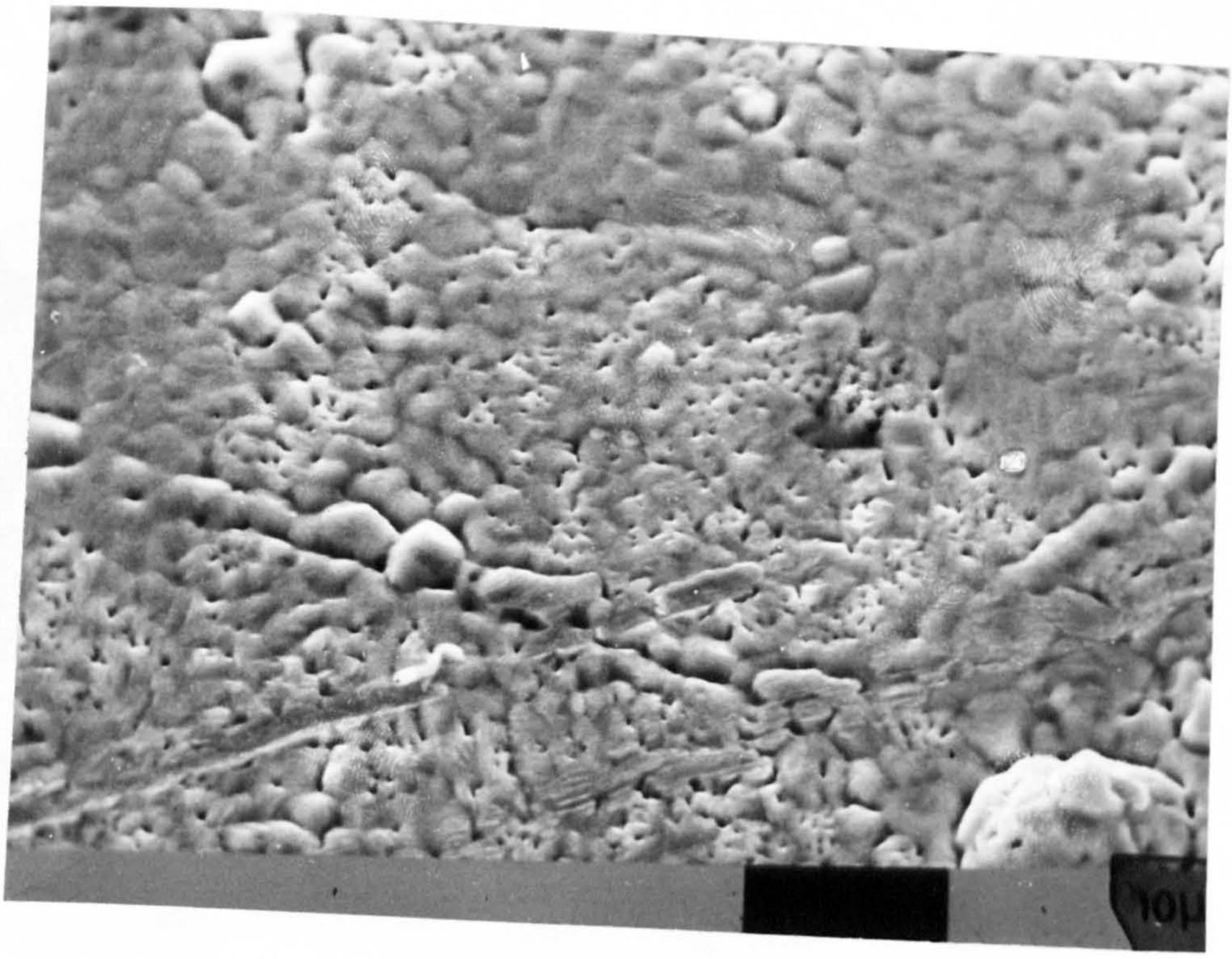

e. 5kV ; 30 mtorr

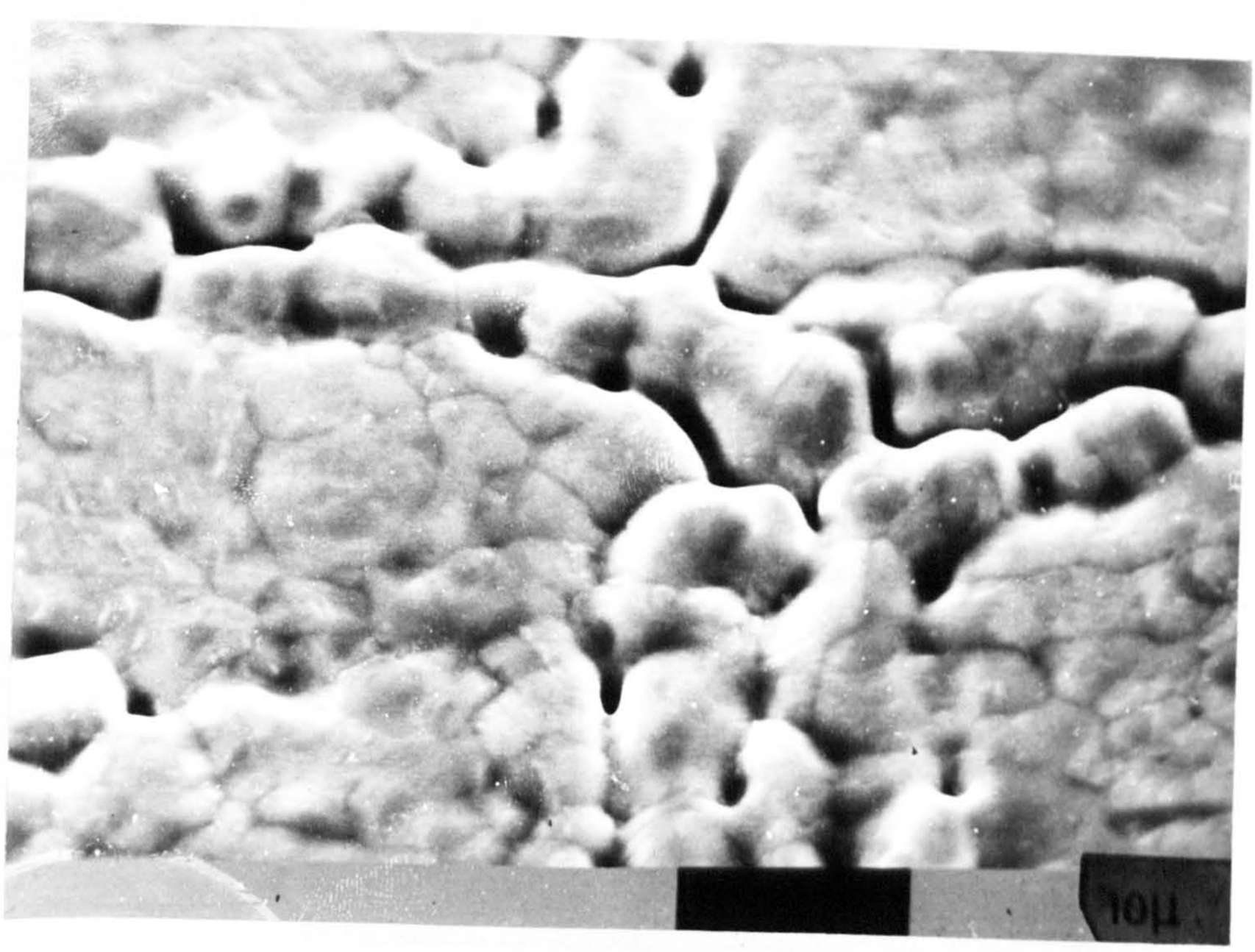

f. 5kV ; 40 mtorr

Figure 5.3.1.4

5kV

PAGE NUMBERING AS ORIGINAL

a. 3KV ; 10 mtorr - $2I_i$ (+60V)

b. 3kV ; 10 mtorr - $3I_i$ (+100V)

Figure 5.3.1.5

3kV & positive probe

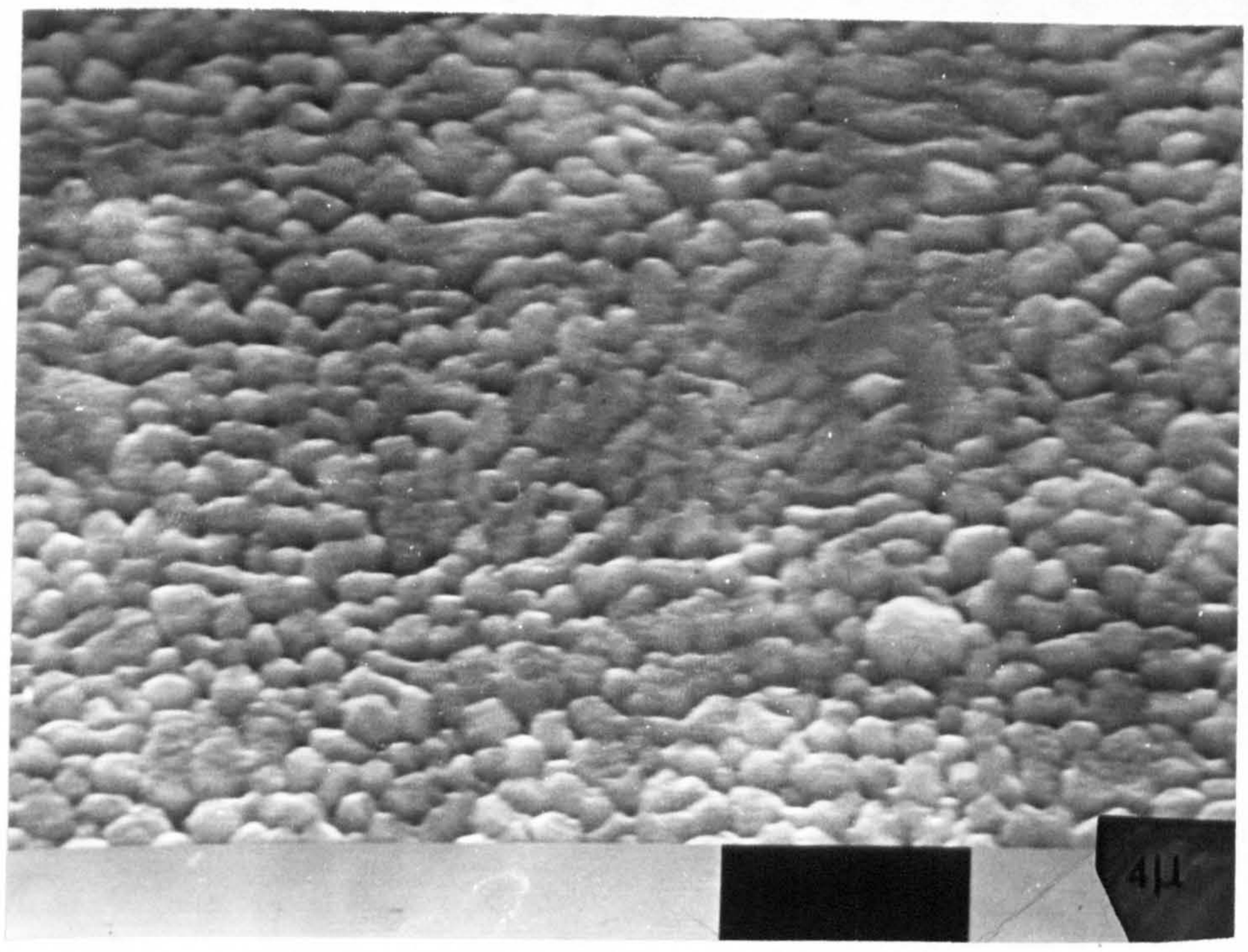

c. 3KV ; 10 mtorr - $2I_i$ (+60V)

Figure 5.3.1.5

3KV & positive probe

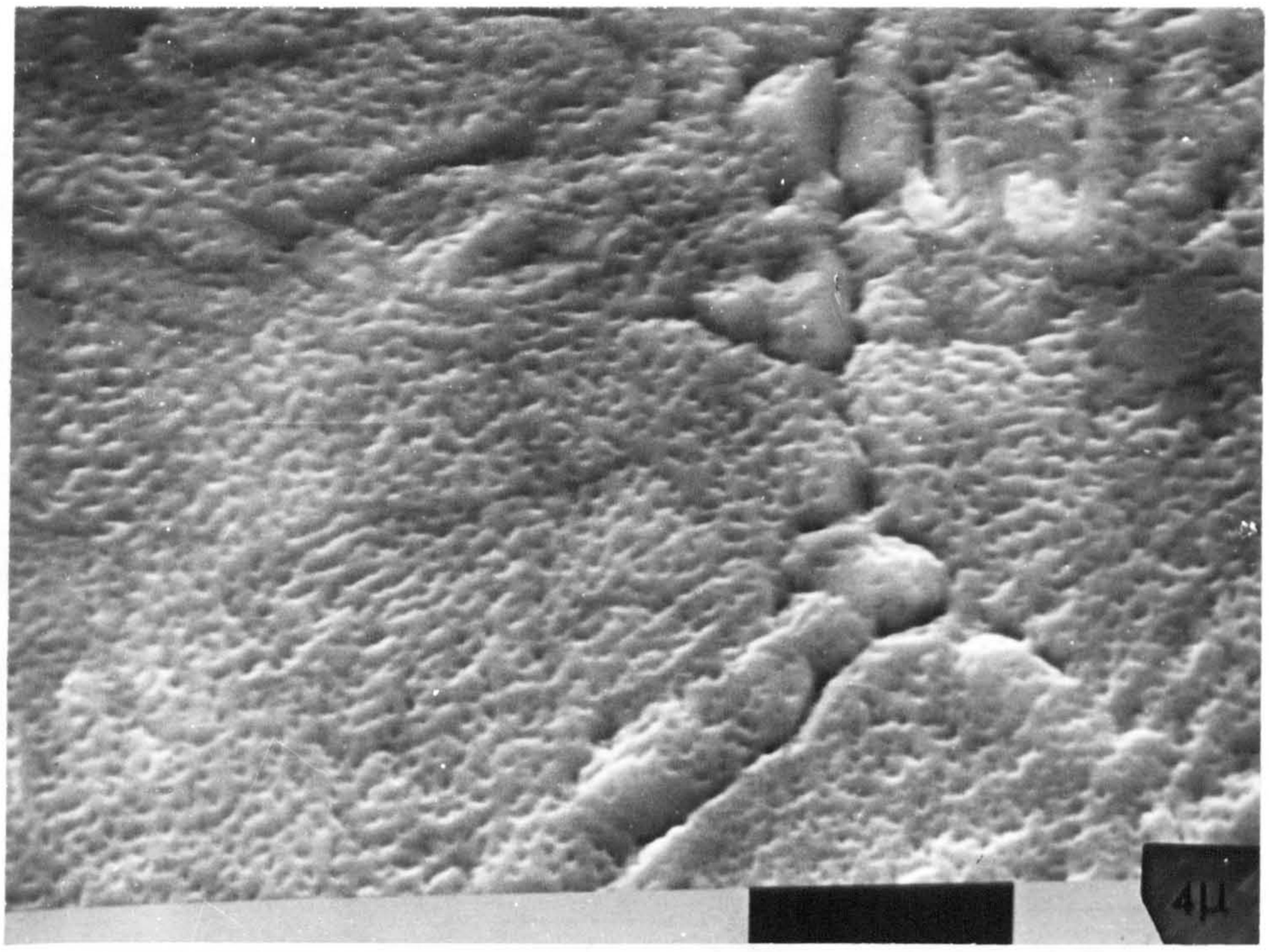

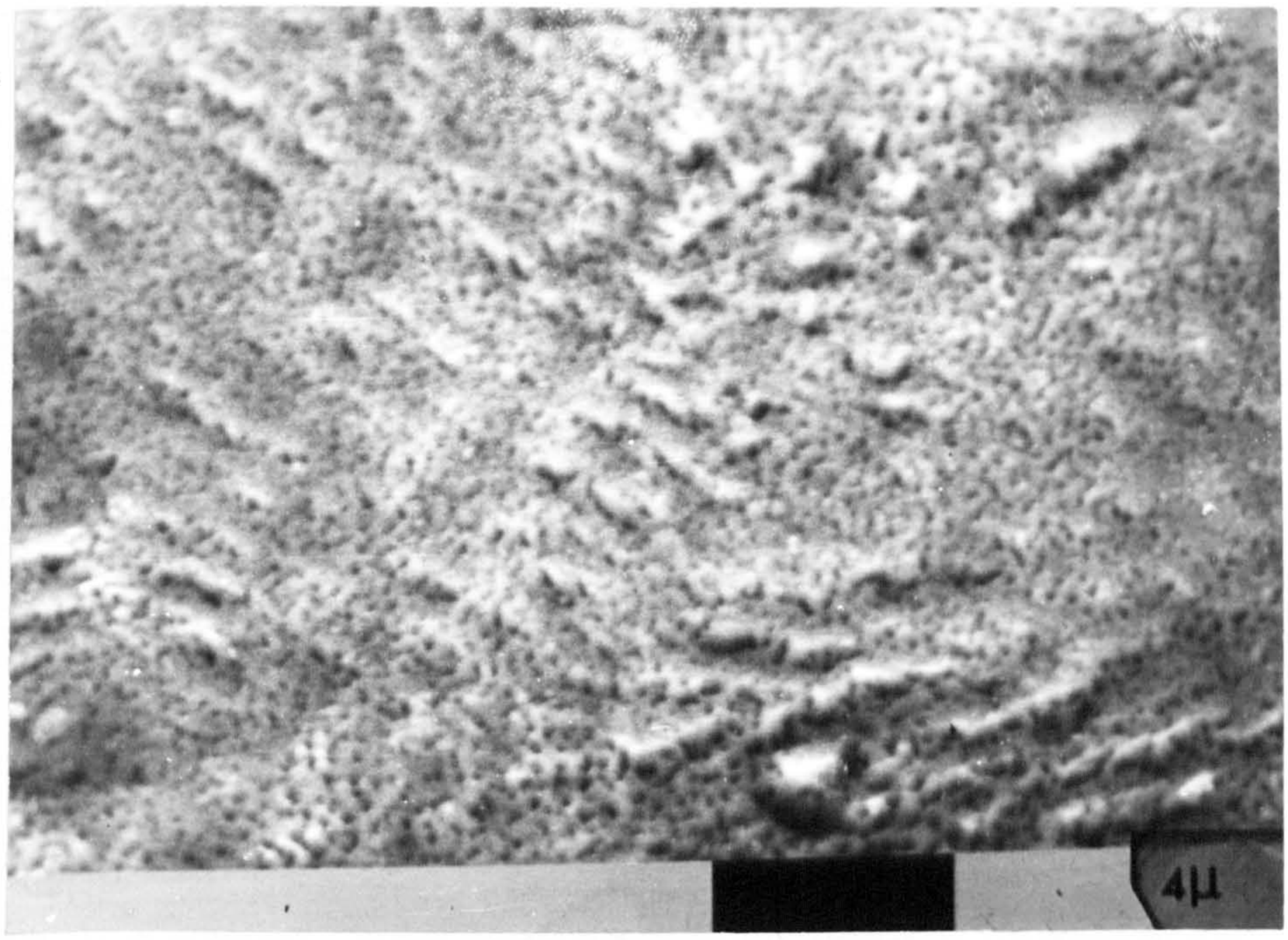

d. 3kV ; 10 mtorr - $3I_i$ (+100V)

Figure 5.3.1.5

3kV & positive probe

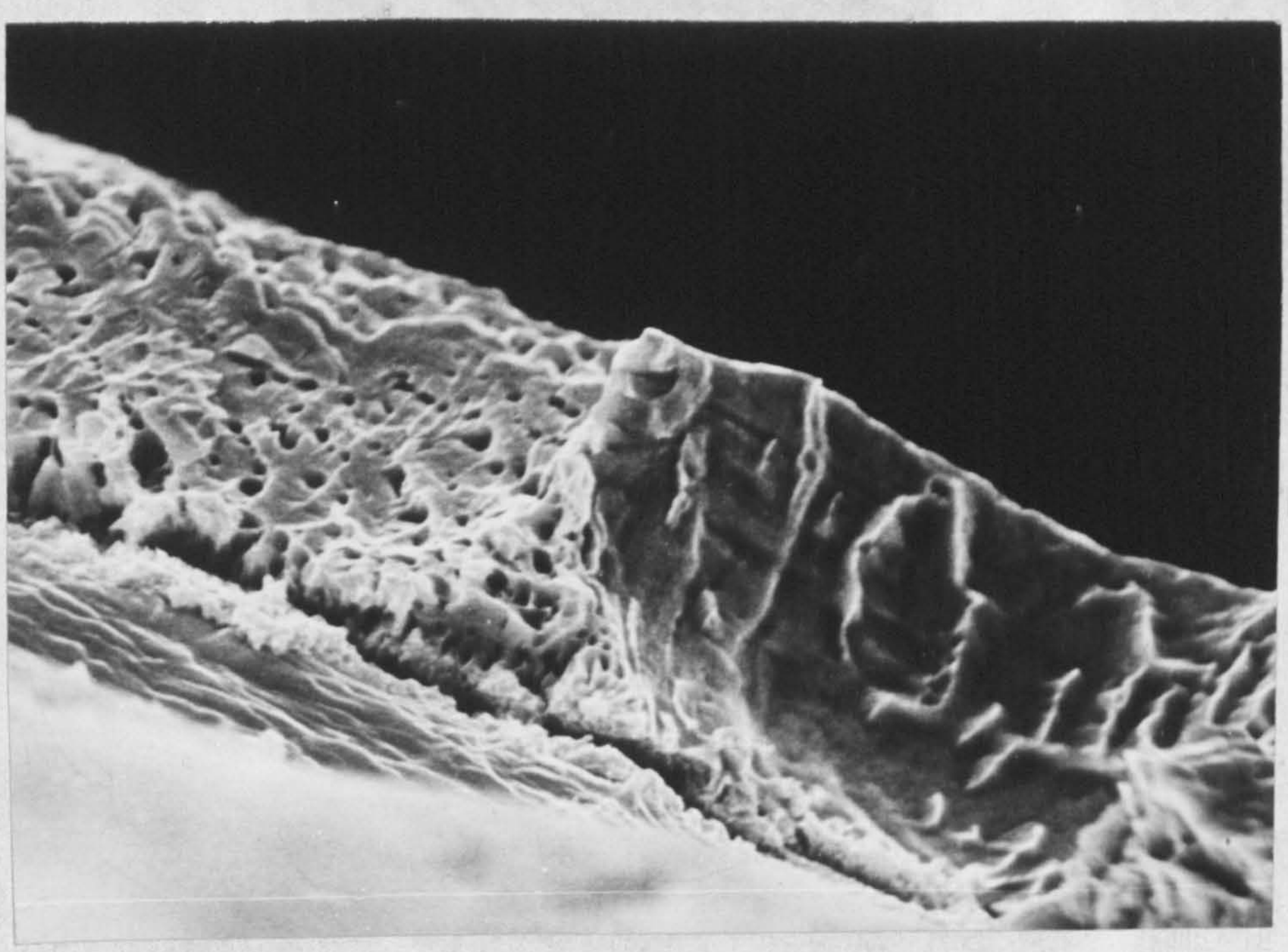

a. Microstructure

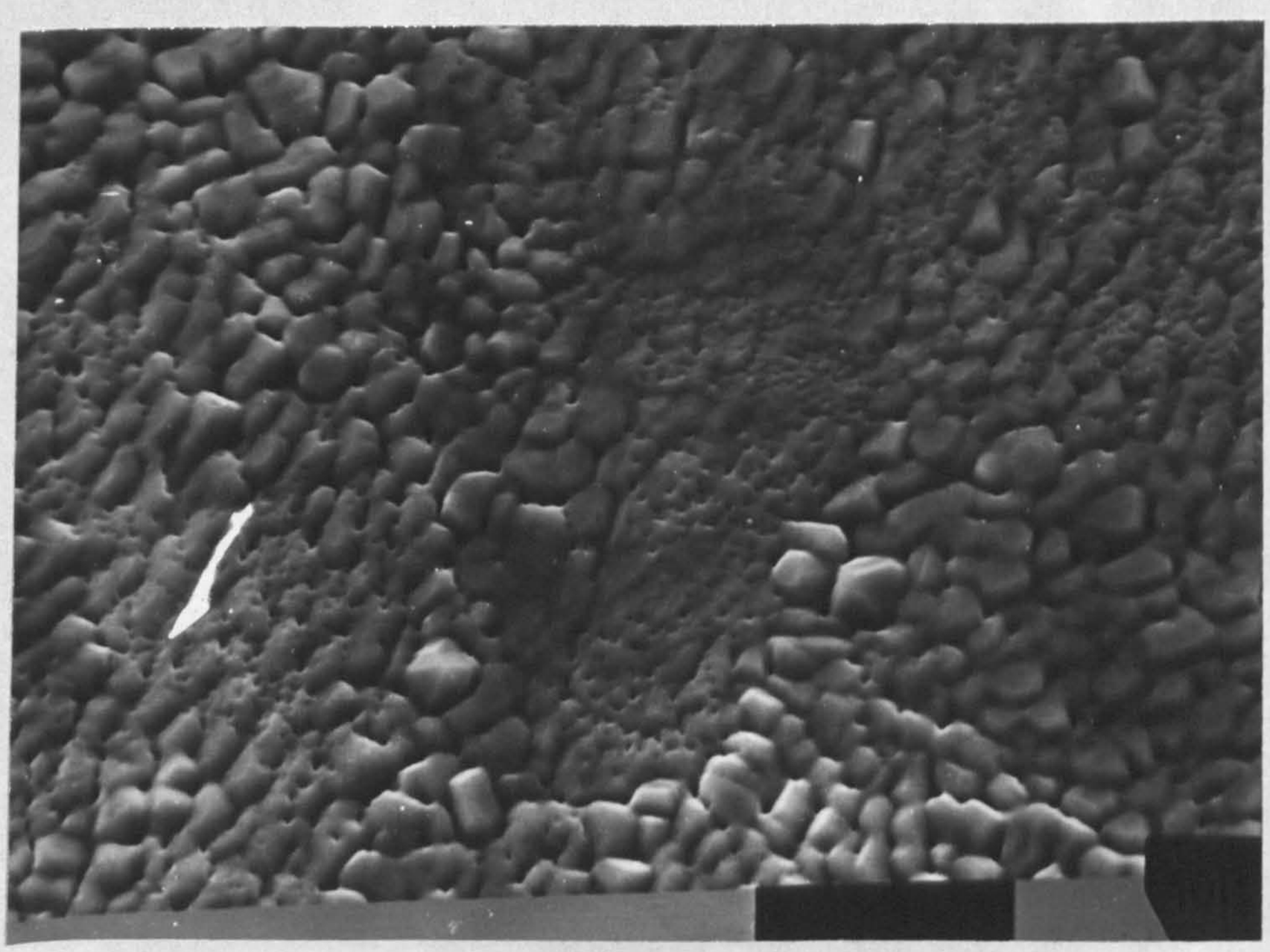

b. Surface

3KV ; 20 mtorr $-2I_i$ (+200V)

Figure 5.3.1.6

3kV & positive probe

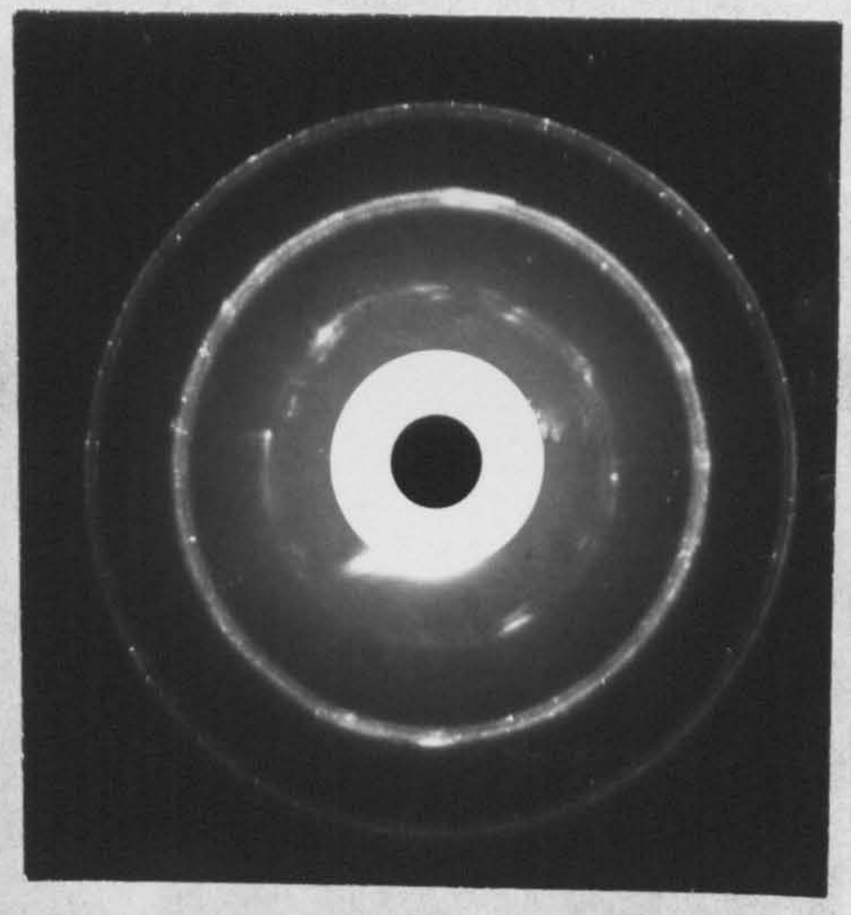

3kV ; 10 mtorr $-3I_i$ (+100V)

Figure 5.3.1.7

X-ray back reflection (400 μ beam)

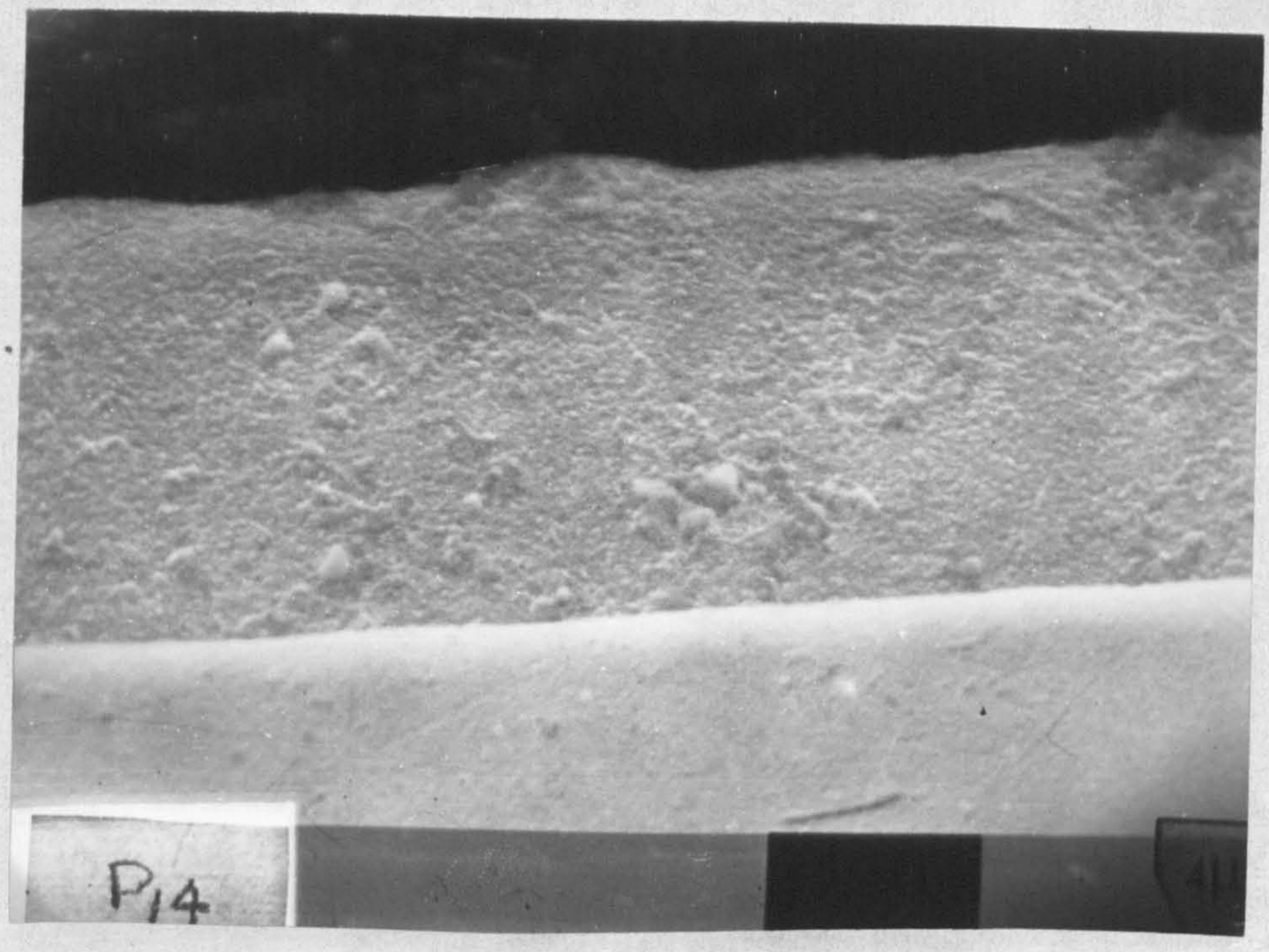

3kV ; 10 mtorr $-3I_i$ (+100V)

Figure 5.3.1.8

3KV & positive probe

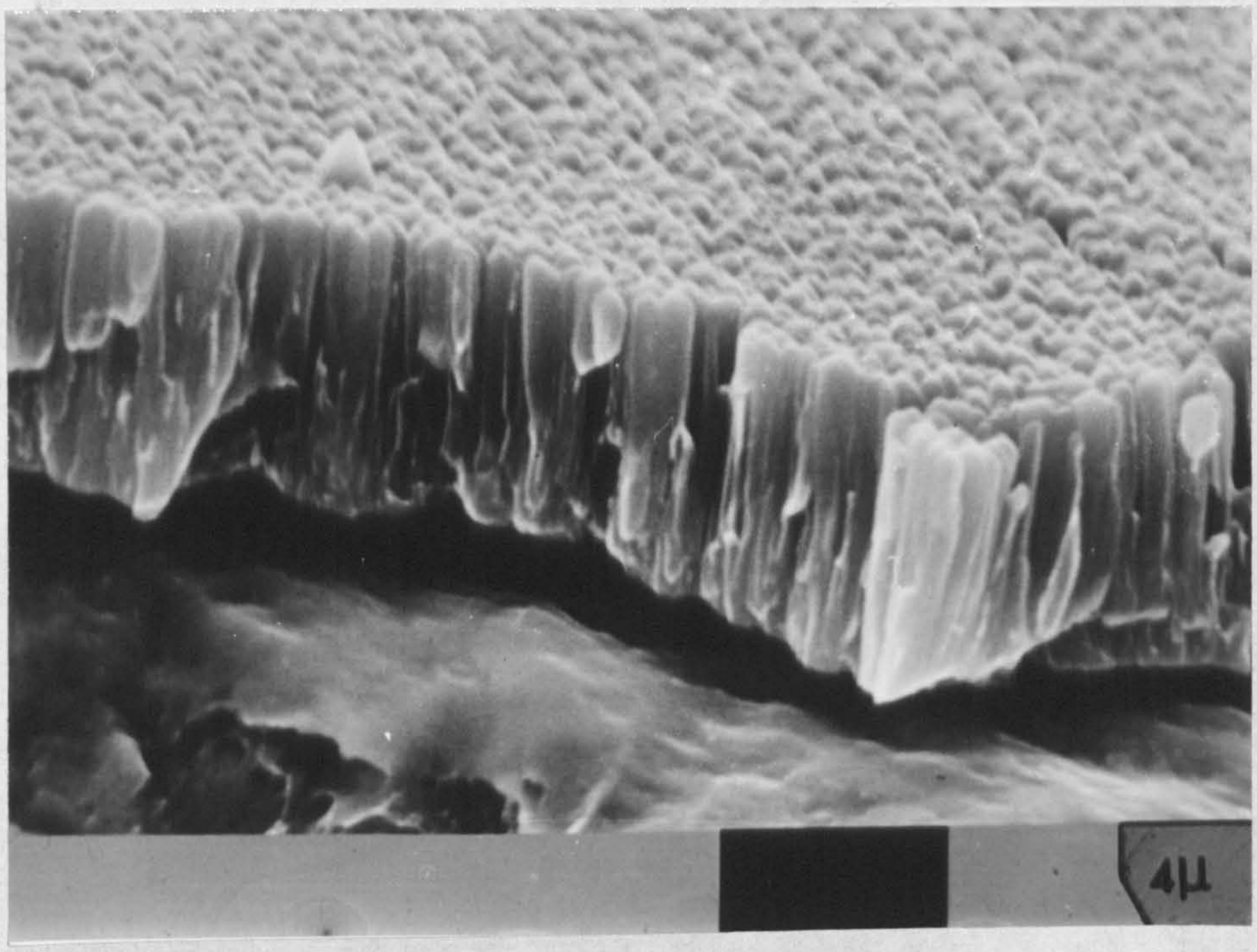

a. 3kV ; 10 mtorr

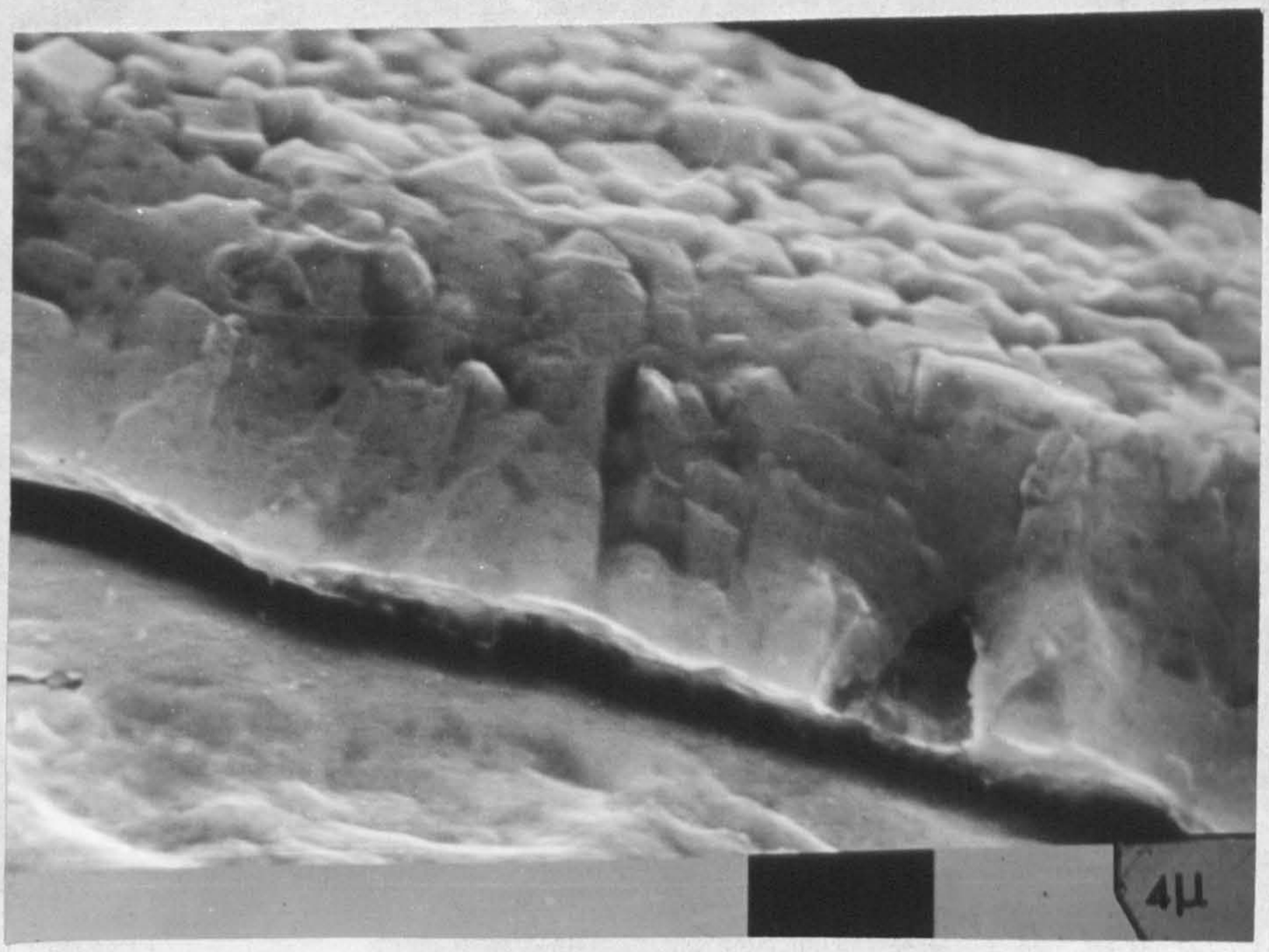

b. 3kV ; 10 mtorr - $3I_i$ ($D_R = 0.5\ \mu/min$)

Figure 5.3.1.9

Aluminium

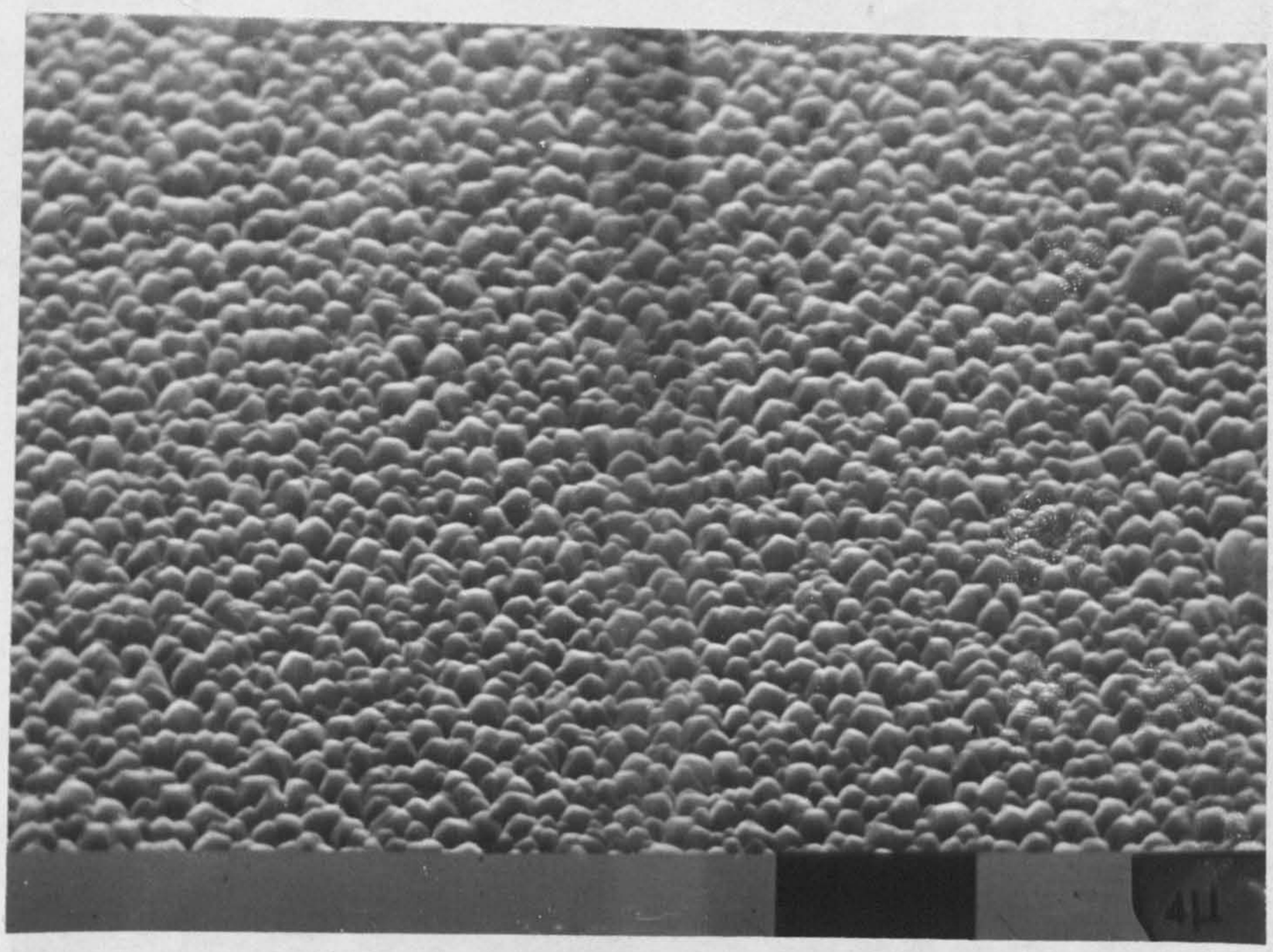

a. 3KV ; 10 mtorr

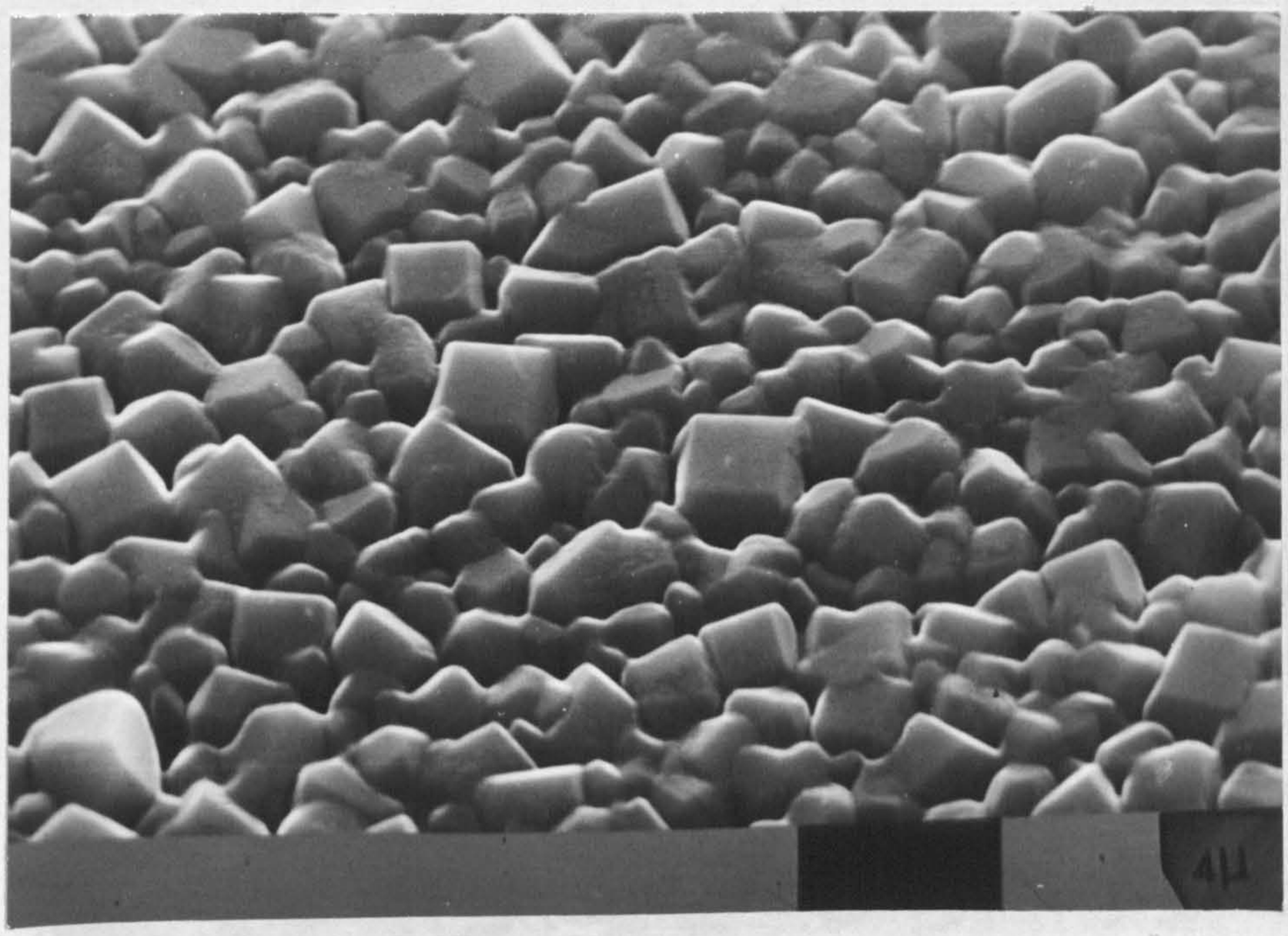

b. 3kV ; 10 mtorr $-3I_i$

Figure 5.3.1.10

Aluminium

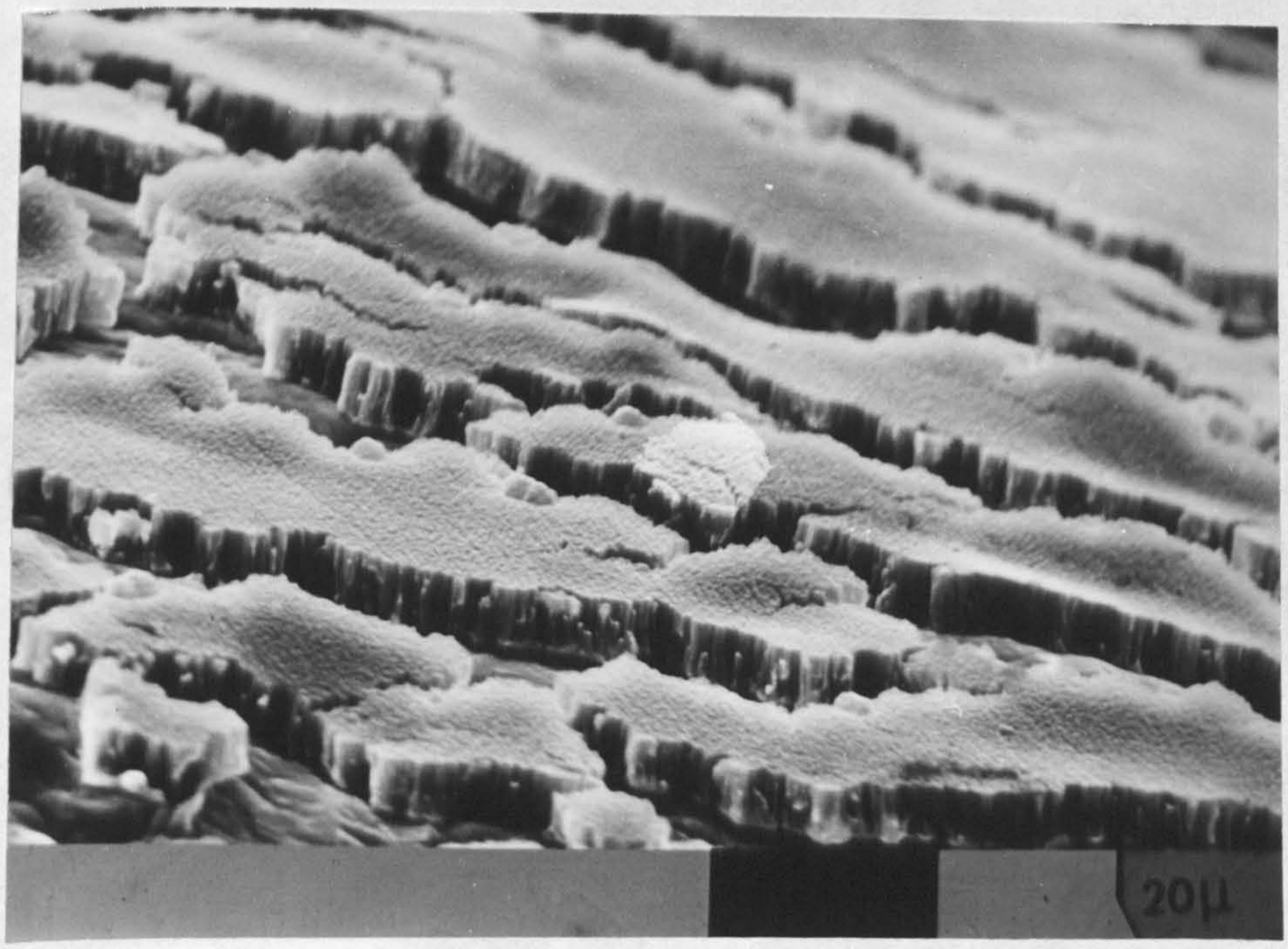

a. 3kV ; 10 mtorr

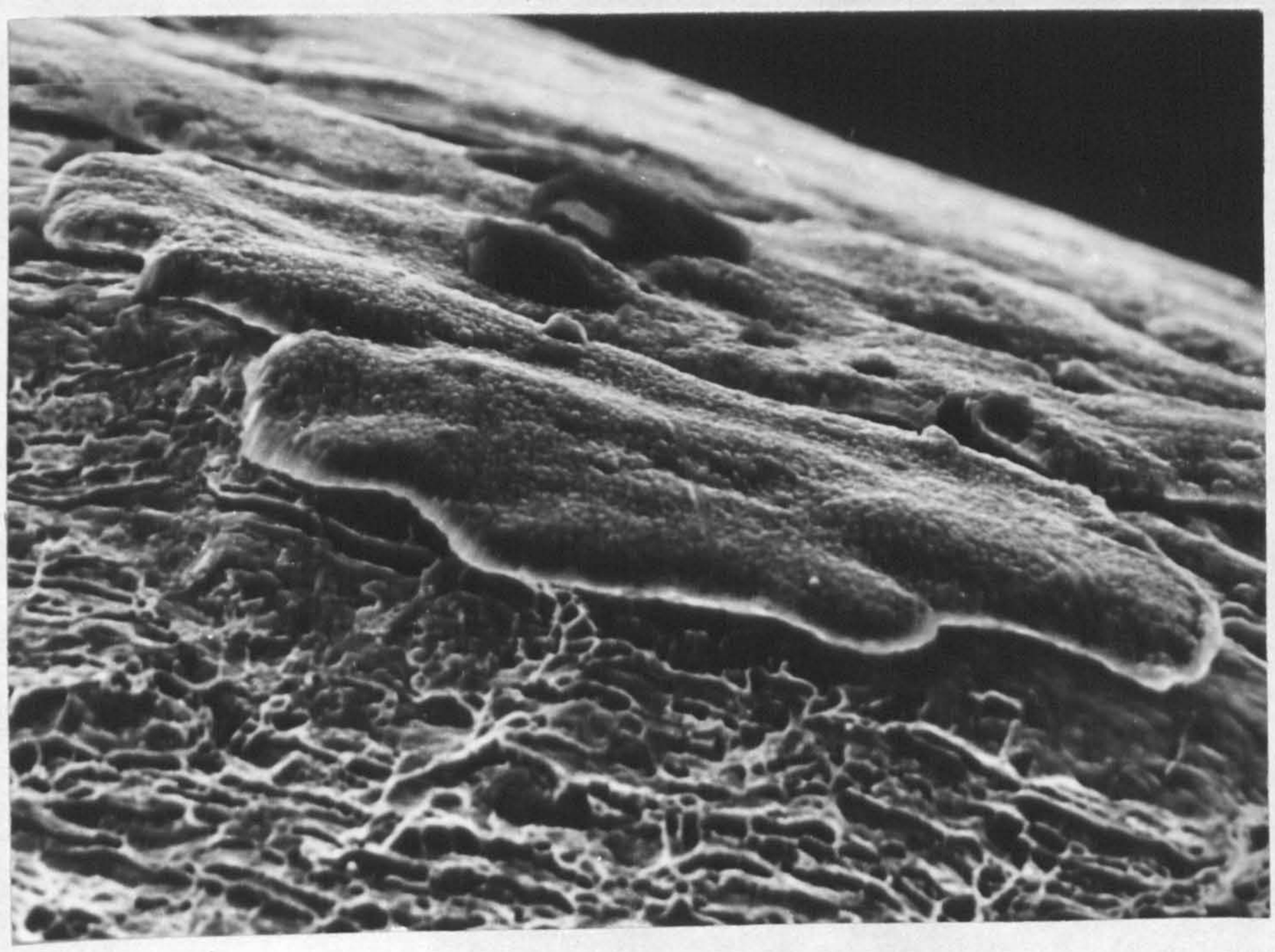

b. 3kV ; 10 mtorr - $3I_i$

Figure 5.3.1.11

Aluminium

5.3.2. Throwing Power

The throwing power of the ion plating technique is defined as being the capability of the process to coat out of sight parts of the substrate. A method of quantitatively determining the throwing power is to coat a flat substrate and then to determine the ratio between the thicknesses on the back (out of sight) and the front surfaces.

The throwing power is :

$$T_p = \frac{d_{fB}}{d_{fF}}$$

where d_{fB} = film thickness on the back surface

d_{fF} = film thickness on the front surface

In ideal conditions, $T_p = 1$ which means uniform thickness on the front and the back.

However, for copper films ion plated on flat nickel substrates under different conditions, the throwing power is plotted versus parameters in Figure 5.3.2.1 and 5.3.2.2.

It can be noticed that the increase in voltage and argon pressure leads to improvement of the throwing power which however remains below 0.7. The explanation is that as the voltage increases, the electric field increases as well and therefore, the collisions that take place at discreet angles with the field lines induce a stronger orrientation of the neutrals

towards the cathode area and thus, more neutrals will go to the out of sight back surface.
The increase in argon pressure leads to an increase in the gas scattering effect which however is the main factor responsible for the throwing power.
The activation of the positive probe had a negligible effect upon the throwing power (Figure 5.3.2.2.).

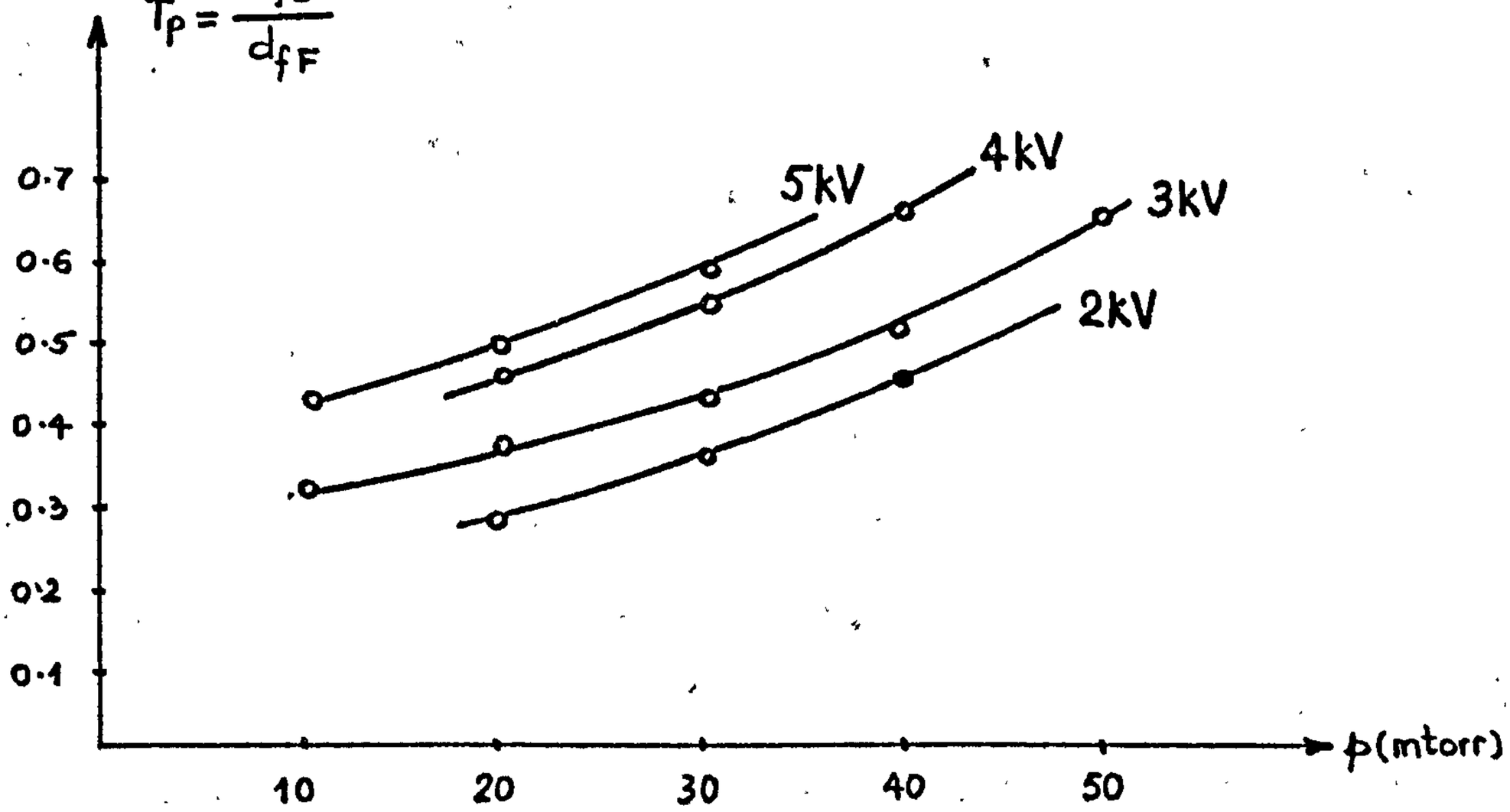

Figure 5.3.2.1

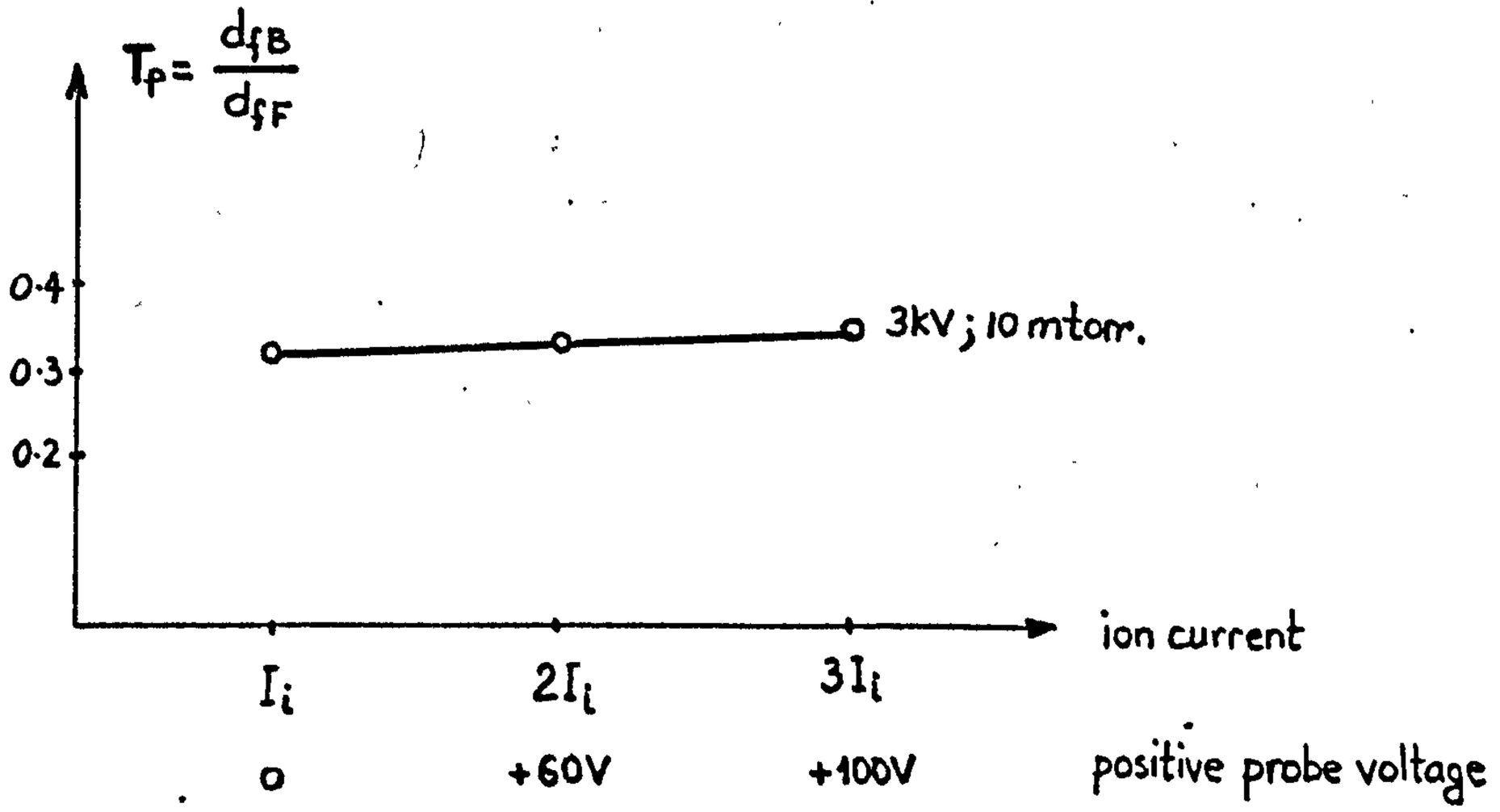

Figure 5.3.2.2

5.3.3. Internal Strain

The internal strain of thin ion plated films was measured using the integral breadths method applied to the line broadening of the x - ray diffraction pattern as previously described. The variation of strain with process parameters is presented in Figures 5.3.3.1. and 5.3.3.2.
As it can be noticed, the increase in voltage, pressure and ion current leads to reduction of the strain value 'e', and stress free films (e = o) are produced for 4 and 5 kV and argon pressures higher than 20 mtorr.

Using the positive probe, the films produced at 3 kV, 10 mtorr & 3 I_i and at 3 kV, 20 mtorr & 2 I_i are also stress free.
One explanation could be that the increase in the value of these parameters produces an increase in the local temperature leading to a relief of the internal stress.
The value σ of the stress can be calculated using:

$$\sigma = eE \qquad (5.3.3.3)$$

where E is Young's modulus.
For copper:

$$E = 17 \times 10^6 \text{ psi}$$

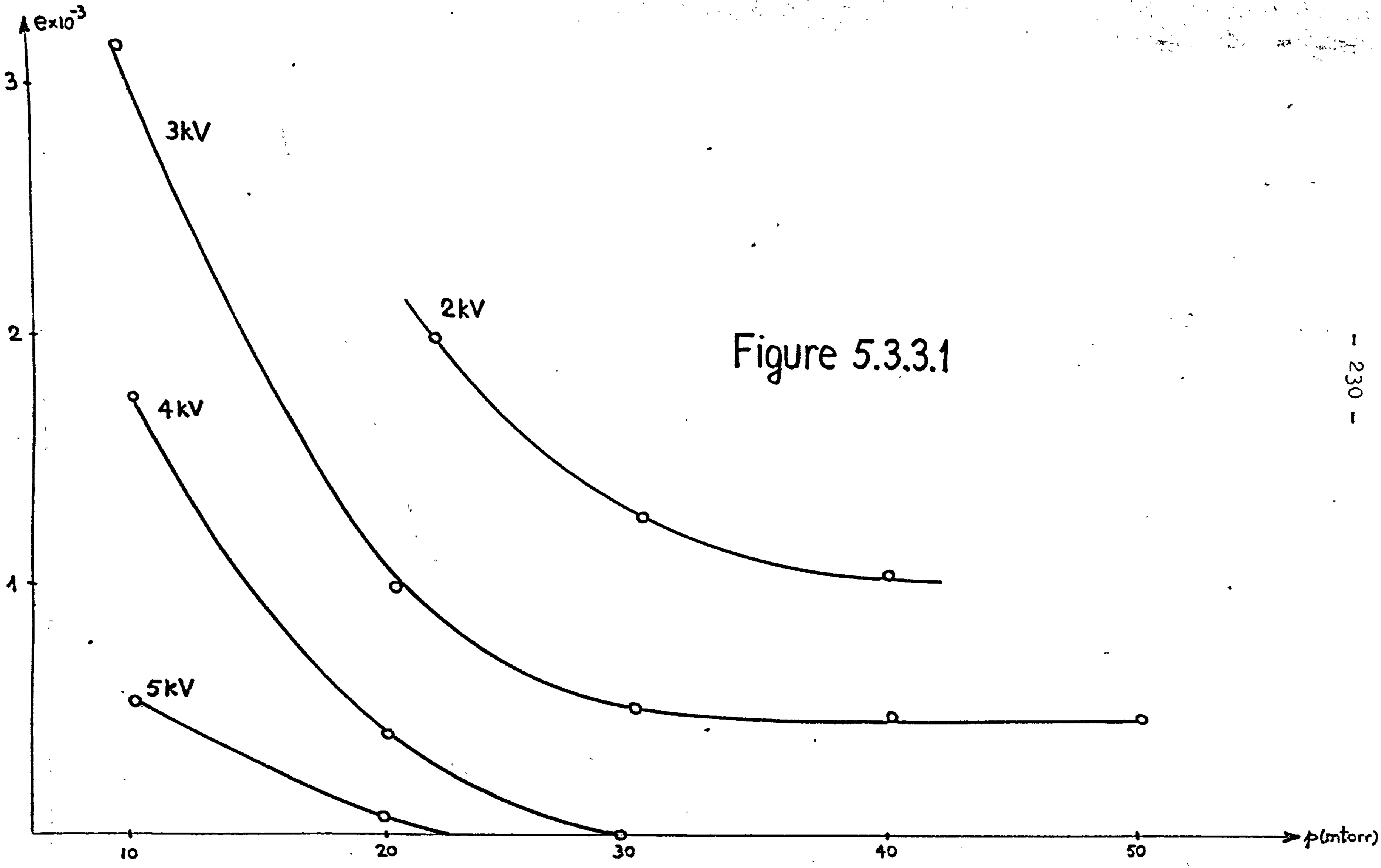

Figure 5.3.3.1

Figure 5.3.2
Positive probe-activated

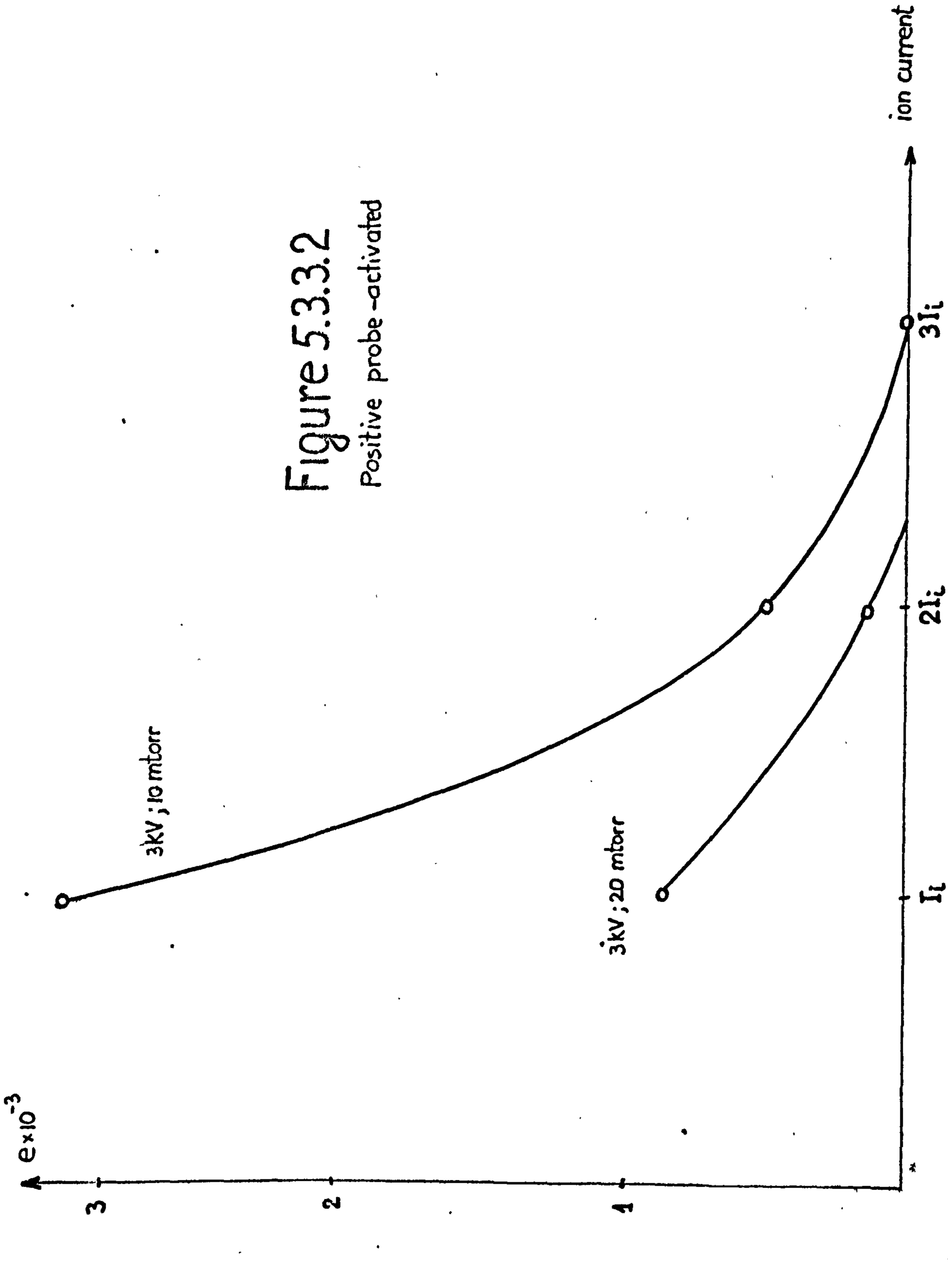

5.3.4. Conclusions

As a general conclusion, the introduction of a positive probe proves to be very useful in producing films with a dense structure, very adhesive and cohesive, having no internal stress. The two main factors thought to be responsible for the results are :

- The ratio between the sputtering rate and the deposition rate (ψ) which depends upon the ion current and the evaporation rate, for p and V constant. A well balanced ψ results in the peaks (that appear during the film growth) being erroded and the valleys being filled and also results in the removal through sputtering, of all nonadhesive film particles on the surface.

- The temperature is important since a high surface temperature leads to some recrystallization to take place and also leads to the reduction of the internal stress value.

It remains for further research to determine the optimum ion plating conditions for each metal or group of metals, since the sputtering yield and the melting point temperature vary extensively from metal to metal.

General Conclusions

1. Energetical neutrals are found to play a major part in the ion plating mechanism and experiments proved that coating on an earthed substrate behind a mesh, have characteristics typical for ion plating films.

2. The ionization efficiency is found to have extremely low values of about 0.1 % for various plating conditions

3. Neutral energy spectrum obtained using a heat imput simulation method, as well as a thoretical method, indicate that the energetical neutrals carry approximately 60% of the energy of the depositing particles. The neutrals can have energies up to the acceleration voltage but their avèrage energy is found to be arqund 150 eV for 3 kV bias.

4. The ion energy spectrum is also determined experimentally and found that although a small number of ions can have the full acceleration energy of 3 KeV for 3 kV bias voltage, their average energy is found to be of about 300 eV.

5. Experiments on the nucleation of ion plated films indicated that the process parameters have a major effect upon the density of the nuclei and that higher pressures, bias voltages and ion current density lead to dense and relatively uniform distributed nuclei with major effects upon the resulting film microstructure.

6. The AUGER analysis of the interface of the ion plated films indicated that the physical processes responsable for the deep graded interface are the thermal diffusion (for compatible pairs) and the atomistic mixture and redeposition (for incompatible pairs).

7. Copper films were ion plated in a diode system and also using a triode arrangement aimed at controlling

the ion current density independent of pressure and bias voltage.
A set of microstructures ranging from tapered crystallites to very unusually dense structures was obtained at relatively low substrate temperatures. The continuous and enhanced energetic bombardment, as well as a high local temperature, are thought to be responsible for the very dense structures and also for the relief in the internal stress.

Recommendations for Future Research

In order to better understand the effect of a third electrode upon the plating mechanisms, it is recommended to determine the neutral and ion energy spectrum for these case .
It is also necessary to separate the effect of ion bombardment and substrate temperature in obtaining the dense structures in order to understand the mechanisms of removing the Columnar structure .

APPENDIX

Calculation of the coefficient ' ψ '

$$\psi = \frac{D_R}{S_{pR}} \qquad (1)$$

where D_R = deposition rate ($\frac{\text{deposited atoms}}{cm^2 \text{ sec.}}$)

S_{pR} = sputtering rate ($\frac{\text{sputtered atoms}}{cm^2 \text{ sec.}}$)

S_{pR} could be calculated from the sputtering yield[29,30,49] S(E)

$$S(E) = \frac{3\alpha\lambda E}{4\pi^2 u_o} \quad \left(\frac{\text{atoms}}{\text{ion/neutral}} \right) \qquad (2)$$

The incident particle having the energy E_i:

$$E = \frac{4M_1M_2}{(M_1+M_2)^2} \quad E_i \qquad (3)$$

where E = energy transferred

E_i = energy of incidence

M_1, M_2 = masses of the incident and static atoms

S(E) can be written :

$$S(E) = 0.042 \frac{\alpha S_n(E)}{u_o} \qquad (4)$$

u_o is the surface barrier energy which can be taken as the heat of sublimation

$S_n(E)$ is tabulated[49]

$$S_{pR} = S(E) \left[N_{i(s)} + N_{n\bar{e}(s)} \right] \quad \left(\frac{\text{sputtred atoms}}{cm^2 \text{ sec.}} \right) \qquad (5)$$

where $N_{i(s)}$ and $N_{n\bar{e}(s)}$ are the number of ions and neutrals having energies higher than the sputtering threshold and can be calculated using (5.1.2.)

$$N_{i(s)} + N_{n\bar{e}(s)} = \frac{A_{ef_{sp}} \times N_{np}}{100} \quad \left(\frac{\text{particles}}{cm^2 \text{ sec.}} \right) \qquad (6)$$

where $A_{ef_{sp}}$ is the percentage of particles capable of producing sputtering.

An average sputtering rate could be determined if $A_{ef_{sp}}$ and S(E) are calculated for the average ion and neutral energies.

S(E) is tabulated for different (E) in Table 1[49].

The deposition rate could be calculated after depositing the same amount of material in similar geometrical and pressure conditions, as follows :

$$D_R = \frac{N_a}{S\ t} \qquad (7)$$

$$N_a = \frac{M}{m_a} = \frac{\rho S d_f}{m_a} \qquad (8)$$

where t = total deposition time (sec)

M = mass of the film

ρ = film density

S = total surface area

d_f = film thickness

m_a = mass of a film atom or molecule

Substituting in (7), it results :

$$D_R = \frac{\rho d_f}{m_a t} \quad \left(\frac{\text{deposited atoms}}{cm^2 \text{ sec.}} \right) \qquad (9)$$

If 'p' is the partial pressure of the film vapours, $N_{np}\left(\frac{\text{atoms}}{cm^2 \text{ sec.}} \right)$ could be calculated using the method described in Section 2.8.

D_R could be taken as being approximately equal to N_{np}

$$D_R = N_{np} \left(\frac{\text{atoms}}{cm^2 \text{ sec,}} \right) \qquad (10)$$

Substituting (6) and (10) into (1), it results :

$$\psi = \frac{N_{np}}{A_{ef_{sp}} \times N_{np}} \times 100 \qquad (11)$$

or :

$$\psi = \frac{100}{A_{ef_{sp}}} \qquad (12)$$

MISSING

PAGES

NOT

AVAILABLE

TABLE 1

Sputtering Yield of Argon Ions Incident on Various Materials.

Target Voltage	200	600	1,000	2,000	5,000	10,000
	Sputtering Yields, Atoms/Ion					
Ag	1.6	3.4				8.8
Al	0.35	1.2			2.0	
Au	1.1	2.8	3.6	5.6	7.9	
C	0.05*	0.2*				
Cr	0.7	1.3				
Cu	1.1	2.3	3.2	4.3	5.5	6.6
Fe	0.5	1.3	1.4	2.0	2.5	
Ge	0.5	1.2	1.5	2.0	3.0	
Mo	0.4	0.9	1.1		1.5	2.2
Nb	0.25	0.65				
Ni	0.7	1.5	2.1			
Pd	1.0	2.4				
Pt	0.6	1.6				
Si	0.2	0.5	0.6	0.9	1.4	
Ta	0.3	0.6			1.05	
Ti	0.2	0.6		1.1	1.7	2.1
W	0.3	0.6			1.1	
Zr	0.3	0.75				
	Sputtering Yields, Molecules/Ion					
SiC(0001)	0.45					
SiO_2			0.13	0.4		
Al_2O_3			0.04	0.11		

*Kr^+ ions

REFERENCES

1. TAKAGI, T., YAMADA,I., SASAKI,A., Proceedings of Ion Plating and Allied Techniques International Conference - Edinburgh 1977

2. MATTOX,D., Sandia Corp. - Report SC - DR - 281 - 63, 1963

3. BLACK LLAN,A., and SELBO, HARRY, - J. Electrochem. Soc., Vol. 113, 1966

4. MATTOX,D., Sandia Corp. - Report No SC - R - 65 - 852, 1965

5. BUCKLEY,D.H., JOHNSON,R.L., BRISSON,E.E., - Proceedings of the Conference of Ion Plating NASA - Lewis Research Center, XI, 149 (1972)

6. SHERBINEY,M. - Ph.D Thesis - University of Salford 1975

7. BLAND,P., KOMINIAK,G.J. and MATTOX,D.M. - J. Vac. Sci.Technol., vol.11, No 4 (1974) pg671

8. MATTOX,D.M. - J.Vac.Sci.Technol. vol.10, No.1 1973

9. BELENSKII,V.P. and KOPTENKO,V.M. - Prib.Tech. Eksp. 4, 188 (1970)

10. MORLEY,J.R. - U.S. Patent No.3,562,141, Febr.

9, 1971

11. HOLLAND,L. - The properties of Glass surfaces, Wiley, 1964 p.310

12. BUTLER,H.S. - 'Plasma Sheath formation by R.F. fields', Stanford University M.L.Report No.820, 1961

13. DAVIDSE,P.D., - SCP and Solid State Technol.1966

14. MATTOX,D.M. - Sputter Deposition and Ion Plating Technology - Thin film division - 5526 - Sandia Laboratories - Albuquerque,N.M. 8 7115 (1973)

15. DAVIS,W.D. and VANDERSLICE,T.A. - Phys.Rev. 131, 219 (1963)

16. CHOPRA,R.L. and RANDLETT,T.A. - Rev.Sci.Instr. 38, 1147 (1967)

17. AISENBERG,S. and CHABOT,R. - J.Appl.Phys. 42, 2953 (1971)

18. SCHMIDT,P.H., CASTELLANA,R.N. and SPENCER,E.G. - Solid State Technol. July 1972

19. MATTOX,D.M. - Proceedings of the 12th Natinal Vacuum Symposium of A.V.S. (A.V.S. - New York 1965)

20. TEER,D.G. - J.Adhesion, Vol. 8 (1977) p289-300

21. SWAROOP,B. and ADLER,I. - J.Vac.Sci.Technol. 10, 503 (1973)

22. CARTER,G. and COLLIGON,J.S. - The Ion Bombardment of Solids - (William Heinemann - London 1968)

23. TEER,D.G., DELCEA,B.L. and KIRKHAM,A.J. - J. Adhesion Vol.8, 1976 p.171 - 178

24. Conference on Sputtering and Ion Plating - March 16, 1972 NASA - SP 5111 p.154

25. AISENBERG,S. and CHABOT,R.W. - J.Vac.Sci.TechnoL 10, 104, 1973

26. AHMED,N.A.G. - M.Sc.Disertation, University of Salford - 1974

27. TEER,D.G., WALLS,J.M. and DELCEA,B.L. - to be published in Thin Solid Films

28. PALMBERG,P.W., RIACH,G.E., WEBER,R.E. and MACDONALD,N.C. - Handbook of Auger Electron Spectroscopy , 1972

29. ALMEN,O.and BRUCE,G. - Nucl.Instr.Methods, 11, 279 (1961)

30. LAEGREID,N. and WEHNER,G.K. - J.Appl.Phys. 32, 365 (1961)

31. MOVCHAN,B.A. and DEMCHISHIN,A.V. -.Fiz.Met.

Metalloved 28, 653 (1969)

32. THORNTON,J.A. - J.Vac.Sci.Technol. 11, 666 (1974)

33. BUNSHAH,R.F. and JUNTS,R.S. - J.Vac.Sci.Technol. Vol.9, No.6, Nov.- Dec. 1972

34. BAILEY,F.W.J. - Fundamentals of Engineering Metallurgy

35. BUNSHAH,R.F. - Physical Deposition of Metals, Alloys and Ceramics - private report - University of Calif., Los Angeles.

36. KLUG,H & ALEXANDER,L. - X - Ray Diffraction Procedures (1967)

37. COHEN,J.B. - Diffraction Methods in Materials Science - MacMillan

38. MMMETT F. KAELBLE (editor) - Handbook of x-Rays J. Willey 1974

39. JONES,F.W. - The Measurement of Particle Size by X - Ray Methods - Proc.Ray.Soc. (London), 166 A, 16 (1938)

40. KOCHENDORFER,A. - The Determination of Particle Size and Lattice Distorsions in Crystalline Materials from the Breadth of x - Ray Lines - Z.Krist. 105, 393 (1944)

41. RACHINGER,W.A. - J.Sci.Instrum., 25, 254 (1948)

42. CAMPBELL,D.S. - Internal Stresses in Thin Films - Basic Problems in Thin Films - edited by R. Niedermayer & M. Mayer - 1966 (p 223)

43. RACHINGER,W.A. - J.Sci.Instrum. 26, 423 (1955)

44. WILSON,A.J.R. - X-Ray Optics (1949)

45. HALDER,N.C. and WAGNER.C.N.J., Acta Crystallogr. 20, 312 (1966)

46. JEFFERY,J.W. - Methods in x-Ray Crystallography

47. CLARK,G.L., PISH,G. and WEEG,L.E. - J.Appl. Phys. 15, 193 (1944)

48. FRIEDMAN,H. and BIRKS,L.S. - Rev.Sci.Instr. 17, 99 (1946)

49. Handbook of Thin Film Technology - edited by Maissel,L.I. and Glang,R. part one, p.1-97

50. WAN,C.T., CHAMBERS,D.L. and CARMICHAEL,D.C. - invited paper at the International Conference on Vacuum Technology - Tokyo, June 1973

51. THORNTON,J.A. - J.Vac.Sci.Technol. Vol.11, No.4, 1974

52. SPALVINS,T. and BUCKLEY,D. - Amer.Vac.Soc., 10th vacuum metallurgy conference, Ney York, June 1967

53. FAWZIA,S - Ph.D. Thesis - University of Salford 1977

54. HUGHES,G.D. - Proceedings of Ion Plating and Allied Techniques International Conference - - Edinburgh, June 1977.

55. BUNSHAH,R.F. - Proceedings of Ion Plating and Allied Techniques International Conference - - Edinburgh, June 1977.